ADDRESSING THE CHALLENGES OF ANTIBIOTIC RESISTANCE, DEREPLICATION, AND BIOSYNTHESIS

ADDRESSING THE CHALLENGES OF ANTIBIOTIC RESISTANCE, DEREPLICATION, AND BIOSYNTHESIS

By HALEY L. ZUBYK, BHSc

A Thesis Submitted to the School of Graduate Studies in Partial Fulfilment of the Requirements for the Degree Doctor of Philosophy

DESCRIPTIVE NOTE

McMaster University DOCTOR OF PHILOSOPHY (2024) Hamilton, Ontario
(Biochemistry and Biomedical Sciences)

TITLE: Addressing the challenges of antibiotic resistance, dereplication, and biosynthesis

AUTHOR: Haley L. Zubyk, BHSc (McMaster University)

SUPERVISOR: Gerard D. Wright, PhD

NUMBER OF PAGES: xix, 217

LAY ABSTRACT

Antibiotics used in medical treatments today often originate from natural sources like environmental bacteria and are known as natural product antibiotics. These natural product antibiotics are essential for treating bacterial infections and play a crucial role in modern medicine, including surgery and cancer treatment. However, the increasing problem of antimicrobial resistance and the lack of new drugs being discovered threatens the effectiveness of these life-saving medicines. To combat antibiotic resistance and protect the use of antibiotics, we need to understand how bacteria resist antibiotics, develop better methods for discovering new antibiotics, and gain insights into how bacteria produce natural product antibiotics. This thesis addresses these challenges by trying to find bacteria that can break down antibiotics, improving a tool for drug discovery, and understanding how bacteria make the antibiotic known as edeine. These efforts advance our understanding of antibiotic resistance and pave the way for developing new and effective antibiotics.

ABSTRACT

Antibiotics form the cornerstone of modern medicine, facilitating advancements in numerous healthcare fields and contributing to unprecedented increases in human life expectancy. However, the efficacy of these life-saving drugs is now jeopardized by the rise of antimicrobial resistance. This growing threat is exacerbated by the slow pace of new antibiotic discoveries. The drug discovery process is both time-consuming and costly, and efforts to identify novel antibiotics often result in the rediscovery of known antibiotics, further hindering progress. To combat antibiotic resistance and facilitate the discovery of novel drugs, several approaches can be employed. First, understanding the mechanisms of resistance found in environmental bacteria is crucial for preparing against the potential mobilization of these resistance mechanisms into pathogenic bacteria. Second, developing tools that make the drug discovery process less costly and time-consuming can accelerate the discovery rate and broaden participation in drug discovery efforts. Finally, understanding how bacteria synthesize natural product antibiotics provides invaluable information that can be leveraged in drug discovery efforts, including synthetic biology approaches. This thesis addresses efforts and challenges in the various aspects of drug discovery. To enhance our understanding of environmental resistance mechanisms, I conducted a screen for ciprofloxacin-inactivating enzymes and characterized the activity of a previously reported ciprofloxacin-inactivating enzyme, CrpP. These findings highlight the difficulties associated with discovering synthetic antibiotic-inactivating enzymes. To contribute to drug discovery, I expanded the Antibiotic Resistance Platform and developed a streamlined version to improve antibiotic dereplication efforts, thereby accelerating the natural product discovery process. Additionally, I investigated the mechanism of β-serine biosynthesis, a nonproteinogenic amino acid found in the antibiotic edeine. By elucidating how β-serine is synthesized, this information can be applied to synthetic biology approaches for drug discovery.

ACKNOWLEDGEMENTS

I have been a part of the McMaster community for the past 11 years, and for 8 of those years, I have been lucky enough to call the Wright lab home. I came for the science, and I stayed for the friendships.

First and foremost, I need to thank Gerry Wright for taking a chance on me. I snuck my way into your lab one summer years ago, and your support as my supervisor and mentor has gotten me to where I am today. No words can express the gratitude that I have for you, but thank you for all your guidance, phrases, references that go over my head, and chalk talks. I have enjoyed every moment.

To my amazing committee members, Sara Andres and Fred Capretta, thank you for your scientific contributions to my projects and for being part of the team. Not many graduate students get to say that they've played in a band with their committee, and I am one of the lucky few.

To the Wright lab, past and present, thank you for being you and for making the graduate student experience all anyone could hope it would be. To the past crew – Arthur, Dan, Matt, Emily, AP, Nick, Beth, Allison, Caitlyn, Vishwas, Drew, Jarrod, Venky, Ricardo, George, Grace, Li-Jun, Min, Adam, Dave, Christian, and Andy. You've each imparted your own lessons to me, and I am so thankful for all the friendship and memories. To the current crew – Alex, Sommer, Dirk, Maya, Amna, Akos, Jacob, Divya, Mike, Linda, Kalinka, Wen (big man), Fei, Manoj, and Manpreet. It makes me so happy to know that the future of the Wright lab looks amazing with all of you in it. Thank you for seeing me through until the end.

Kalinka, my buddy, I am so grateful for our connection and for all the time we have had together. Thank you for being my lab mom—checking my math, teaching me how to make paper funnel snowflakes, catching all my mistakes, and for all the laughs. You have been a huge part of this journey, and I couldn't have done it without you.

Matt, my amazing partner. Thank you for all your love and support over the years, being there for the highs and lows, and making getting a PhD together an incredible experience. I am so proud of you, and I cannot wait to start this next chapter together.

Willow, my beloved dog, you are perfect in every way. Thank you for your silent support throughout the years and during the writing of this thesis. You have no clue how helpful you've been.

To the amazingly close friendships that have bloomed over the years in ways that only come out of grad school – Ken, you're my day 1. We made BDC proud. Nathan, we're officially the last stragglers. Wouldn't have it any other way. Andrea, I'm so lucky to have someone as pure and supportive as you in my life. Amna, I cannot wait to see what Nobel Prize you go on to win. You are so caring, and you're going to be amazing at whatever you choose to

do in the future. Dirk, I'm going to miss our unspoken desk-buddy relationship. Only a real friend would come up on stage alone and dance to All-Star with me. Rodion, I'm going to miss all your antics and crazy stories. Dave, I have never been more excited to see someone go through life's milestones. You're going to be an amazing professor. Mike – thank you for all the coffee chats and life chats. Julia – we became close very fast. Probably the only good thing that came out of your Canadian softball experience. Jacob – I can't wait to see what you get up to in northern BC. I'm so proud to know all of you amazing people.

I also need to thank those who were involved in my journey to become an educator. Celeste Suart, you are an amazing friend and so talented in all things education. Thank you for all your guidance and for helping me get my footing. Felicia Vulcu, you are my teaching inspiration. Thank you for all the compassion you showed me years ago as an undergraduate. Caitlin Mullarkey, you are such an incredible role model. I aspire to be a powerhouse like you one day. Marie Elliot, thank you for taking a chance on me for Microbial Genetics. It was my golden ticket. Dawn Bowdish, thank you so much for supporting all my goals and looking out for me. I am incredibly lucky to have such a strong group of women in science in my corner.

Lastly, thank you so much to my family and friends. You have shown me so much love and patience over the years and thank you for always staying by my side.

My time in the Wright lab has been **unforgettable**.

TABLE OF CONTENTS

LIST OF FIGURES

LIST OF TABLES

LIST OF ABBREVIATIONS AND SYMBOLS

α	alpha
Å	angstrom
β	beta
γ	gamma
ε	epsilon
λ	lambda (wavelength)
(+) EIC	positive mode extracted ion chromatogram
A domain	adenylation domain
AAT	aspartate aminotransferase
Ac-CIP	acetyl-ciprofloxacin
ACC	1-aminocyclopropane-1-carboxylate synthase
AME	aminoglycoside-modifying enzymes
APH	aminoglycoside phosphotransferase
ARGs	antibiotic-resistance genes
ARP	Antibiotic Resistance Platform
AUC	area under the curve
BGC	biosynthetic gene cluster
BLAST	Basic Local Alignment Search Tool
C domain	condensation domain
CI36	Ciprofloxacin Inactivator 36
CIP	ciprofloxacin
CLS	Canadian Light Source
COSY	correlated spectroscopy
DAHAA	2,6-diamino-7-hydroxyazeleic acid
DAPA	2,3-diaminopropionic acid
DCs	decarboxylase
DEPT	distortionless enhancement by polarization transfer
DHPS	dihydropteroate synthase
DMSO	dimethyl sulfoxide
E site	exit site
EMSA	electrophoretic mobility shift assay
erm	erythromycin ribosome methylase
ESBL	extended-spectrum-β-lactamase
f-met	formylmethionyl
FDA	Food and Drug Administration
GAD	glutamate decarboxylase

GE	GE23077
GSK	GlaxoSmithKline
HGT	horizontal gene transfer
HMBC	heteronuclear multiple bond correlation/coherence
HPAT	histidinol-phosphate aminotransferase
HPLC	high-performance liquid chromatography
HRMS	high-resolution mass spectrometry
HSQC	heteronuclear single quantum correlation
IDT	Integrated DNA Technologies
IPTG	isopropyl-β-d-thiogalactopyranoside
JoVE	Journal of Visualized Experiments
LAM	lysine 2,3-aminomutase
LB	lysogeny broth
LPS	lipopolysaccharide
Marfey's reagent	Nα-(2,4-dinitro-5-fluorophenyl)-L-valinamide
MARP	Minimal Antibiotic Resistance Platform
mAU	milli-absorbance units
MBLs	metallo-β-lactamases
MDR	multidrug resistance
MHB	Mueller Hinton broth
MIO	4-methylideneimidazole-5-one
MMCE	methylmalonyl-CoA epimerase
MOA	mechanism of action
MRSA	methicillin-resistant Staphylococcus aureus
NMR	nuclear magnetic resonance spectroscopy
NRPSs	nonribosomal peptide synthetases
ORFs	open reading frames
OrnDC	ornithine decarboxylase
P site	peptidyl site
PAM	phenylalanine 2,3-aminomutase
PBP	penicillin-binding protein
PCP domain	peptidyl carrier protein domain
PDB	Protein Data Bank
PKSs	polyketide synthases
PLP	pyridoxal 5' phosphate
PLP-DE	pyridoxal 5' phosphate-dependent enzyme
PLR	reduced pyridoxal 5’ phosphate
PPD	pyridoxal 5' phosphate-bound aspartate

PRPs	pentapeptide repeat proteins
RMSD	root mean square deviation
SAD	single-wavelength anomalous diffraction
SAM	S-adenosyl-L-methionine
SAM	*Streptomyces* antibiotic medium
SAR	structure-activity-relationship
SBLs	serine β-lactamases
TAT	tyrosine aminotransferase
TCEP	tris-(2-carboxyethyl)-phosphine
TE domain	thioesterase domain
TPDC	L-threonine-O-3-phosphate decarboxylases
VOC	vicinal oxygen chelate
VRE	vancomycin-resistant enterococci

DECLARATION OF ACADEMIC ACHIEVEMENT

I, Haley L. Zubyk, have performed all of the research in this body of work except where indicated in the preface of each chapter.

CHAPTER 1: Introduction

Introduction

Since the introduction of antibiotics in clinical settings during the 1940s, humanity has relied on their antimicrobial properties to combat bacterial infections. Perhaps most famously, Alexander Fleming's serendipitous discovery of penicillin kick-started the Golden Era of antibiotic discovery, forever changing our approach to treating infectious bacterial diseases (Lobanovska & Pilla, 2017). For the first time in history, humans are now more susceptible to succumbing to chronic diseases of old age than to infectious ones (Cook & Wright, 2022).

Antibiotics have laid the foundation for modern medicine, as their success enables invasive and immunosuppressive procedures such as surgery and chemotherapy. For decades, however, scientists have warned that pathogenic bacteria are rapidly becoming antibiotic-resistant (Neu, 1992; Viswanathan, 2014). Antimicrobial resistance is a natural occurrence in environmental bacteria, providing defence against bioactive natural products, but human activities, particularly the widespread use of antibiotics, have greatly accelerated its prevalence in clinical settings (Surette & Wright, 2017). This increase in resistance is primarily due to two key factors: the overuse and misuse of antibiotics. Examples of such scenarios include prescribing antibiotics for nonbacterial infections, such as viral infections, and unregulated usage, including over-the-counter availability of antibiotics in developing countries, which can expose bacteria to sublethal doses of antibiotics that fuel the spread of resistance (Ayukekbong et al., 2017; Ventola, 2015). As a result, it is estimated that 0.9-1.7 million deaths per year are attributed to antibiotic-resistant infections, with

numbers continuing to rise (Hegemann et al., 2023). By diminishing the efficacy of these drugs, we risk returning to a pre-antibiotic era.

Understanding the genetic and mechanistic diversity that underlies resistance is crucial for the appropriate use of our existing antimicrobials and the discovery or design of novel compounds that can evade prevalent resistance mechanisms.

Mechanisms of Antibiotic Resistance

Mechanisms of antibiotic resistance can be categorized as intrinsic or acquired. Intrinsic resistance refers to methods inherent to a microorganism that are encoded within the genome and are independent of antibiotic selective pressure (Cox & Wright, 2013). Comparatively, bacteria can acquire genetic material encoding resistance mechanisms through horizontal gene transfer (HGT) via various methods of DNA transfer, including transformation, conjugation, and transduction (Larsson & Flach, 2022; Waglechner et al., 2021). These antibiotic-resistance genes (ARGs) are typically acquired through mobile genetic elements, such as plasmids, and transferred between bacteria via transformation or conjugation. Transduction, a bacteriophage-mediated process of HGT, is rarely associated with the spread of resistance genes (Reygaert, 2018).

Intrinsic Resistance

A common theme in intrinsic resistance mechanisms is the prevention of antibiotic access to its target. This can occur by reducing bacterial cell permeability to impede antibiotic entry and increasing the efflux of antibiotics that enter the cell (**Figure 1**).

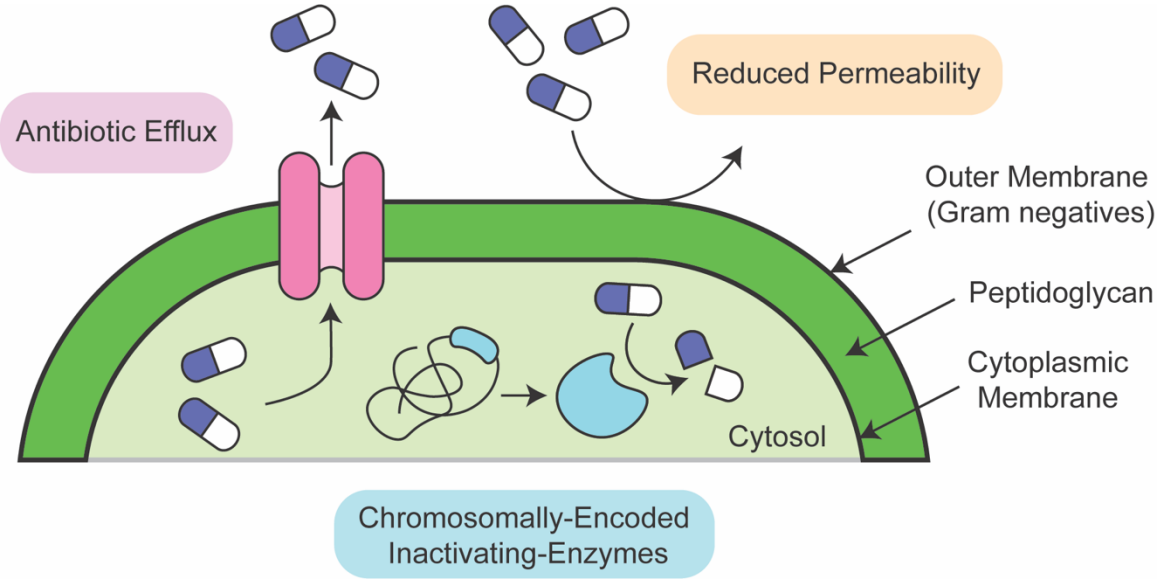

FIGURE 1. Mechanisms of intrinsic resistance.

Compared to Gram-positive bacteria, Gram-negative bacteria are intrinsically resistant to many antibiotic classes because their outer membrane is a permeability barrier that obstructs the entry of antibiotics (Reygaert, 2018). For example, the glycopeptide antibiotic vancomycin binds to target the D-ala-D-ala moiety on peptidoglycan precursors to inhibit crosslinking and block cell wall biosynthesis. However, vancomycin cannot penetrate the outer membrane of Gram-negative bacteria and fails to access its peptidoglycan target in the periplasm (Tsuchido & Takano, 1988).

Efflux pumps also play a significant role in intrinsic resistance. They can rapidly decrease intracellular antibiotic concentrations by expelling drugs into the extracellular space (Reygaert, 2018). While some efflux pumps exhibit narrow substrate specificity and are plasmid-encoded (e.g., the tetracycline efflux pump, TetA) (Sreejith et al., 2022), many pumps are encoded on bacterial chromosomes and efflux a broad range of substrates to

facilitate intrinsic resistance (e.g., multidrug resistance (MDR) efflux pumps) (Blair et al., 2015).

Additionally, certain bacteria have chromosomally encoded enzymes that can inactivate antibiotics. AmpC β-lactamases serve as a key example. Naturally occurring in many Enterobacteriaceae, these enzymes confer resistance to a variety of β-lactam antibiotics, including broad-spectrum cephalosporins. The expression of AmpC enzymes can be induced in various bacterial species and may be expressed at elevated levels due to mutations, leading to resistance during treatment even when a bacterium was initially susceptible (Jacoby, 2009). Moreover, several chromosomally encoded aminoglycoside resistance enzymes have been identified. For example, the novel aminoglycoside phosphotransferase APH(3')-IId, found in a multidrug-resistant *Brucella intermedia* isolate, confers resistance to various aminoglycosides (Lu et al., 2021). Additionally, *Enterococcus faecium* commonly harbours the aminoglycoside acetyltransferase AAC(6')-Ii and the *efmM*-encoded methyltransferase that modifies 16S rRNA to obstruct antibiotic binding at the ribosomal target site (Hollenbeck & Rice, 2012).

Some organisms, such as *Pseudomonas aeruginosa,* possess the deadly combination of a highly impermeable outer membrane, an extensive repertoire of efflux pumps, and chromosomally encoded resistance enzymes. In these cases, intrinsic resistance mechanisms severely limit the pool of effective antimicrobial agents (Pang et al., 2019; Torrens et al., 2019). Such challenges underscore the need for continuous innovation in antimicrobial strategies.

Acquired Resistance

In contrast to intrinsic resistance, acquired resistance mechanisms generally entail alterations to the antibiotic target or the antibiotic itself (**Figure 2A**), such as mutating, modifying, or physically protecting the antibiotic target to prevent antibiotics from binding or enzymatically inactivating the antibiotic (**Figure 2B**) (Schaenzer & Wright, 2020; Wright, 2005).

Target Mutation

Many antibiotics disrupt cell function by binding to their targets with high affinity, leading to detrimental effects (Blair et al., 2015). For antibiotics with protein targets, non-synonymous mutations in the gene encoding the target can confer resistance by altering its structure, reducing drug binding efficiency and thereby conferring resistance (Blair et al., 2015). A notable example of target mutation is associated with the antibiotic rifampin (RIF), which binds to RpoB, the β-subunit of prokaryotic RNA polymerase (Campbell et al., 2001; Li et al., 2021). Despite being a crucial anti-tuberculosis drug, mutations in *rpoB* can lead to high-level resistance to RIF in *Mycobacterium tuberculosis*. Even single amino acid substitutions can significantly diminish drug binding affinity, rendering RIF ineffective (Swain et al., 2020).

Acquisition of a Drug-Resistant Target

While bacteria can acquire mutations in their drug targets that make the target insensitive to drugs, they can also acquire genes that encode alternative drug-resistant

variants of their target. For instance, clinical resistance to sulfonamides in Gram-negative bacteria involves plasmid-borne genes, *sul1* and *sul2*, which encode variants of dihydropteroate synthase (DHPS), the sulfonamide drug target (Sköld, 2000). These variants allow bacteria to resist sulfonamides by performing DHPS's normal function in the folic acid pathway, even though the chromosomal copy is inhibited (Sköld, 2000).

Another pathway for acquiring drug-resistant targets is DNA uptake from the environment, leading to the formation of "mosaic genes." In this process, intragenic recombination occurs between an acquired allele and the host allele, altering the target gene (Hollingshead et al., 2000). *Streptococcus pneumoniae,* for example, develops penicillin resistance through mosaic penicillin-binding protein (PBP) genes, which encode penicillin-insensitive enzymes. These mosaic alleles form via recombination with DNA from closely related species like *Streptococcus mitis* (Unemo et al., 2012).

Target Modification

Aside from mutations in the antibiotic target, resistance can be conferred by chemically modifying the target to reduce antibiotic affinity. A common method of target modification involves the deployment of methyltransferases, which modify residues in or near the antibiotic binding pocket. For instance, the erythromycin ribosome methylase (*erm*) family of genes methylate 23S rRNA to alter the drug binding site, thereby inhibiting the binding of macrolides, lincosamides, and streptogramins (Kumar et al., 2014).

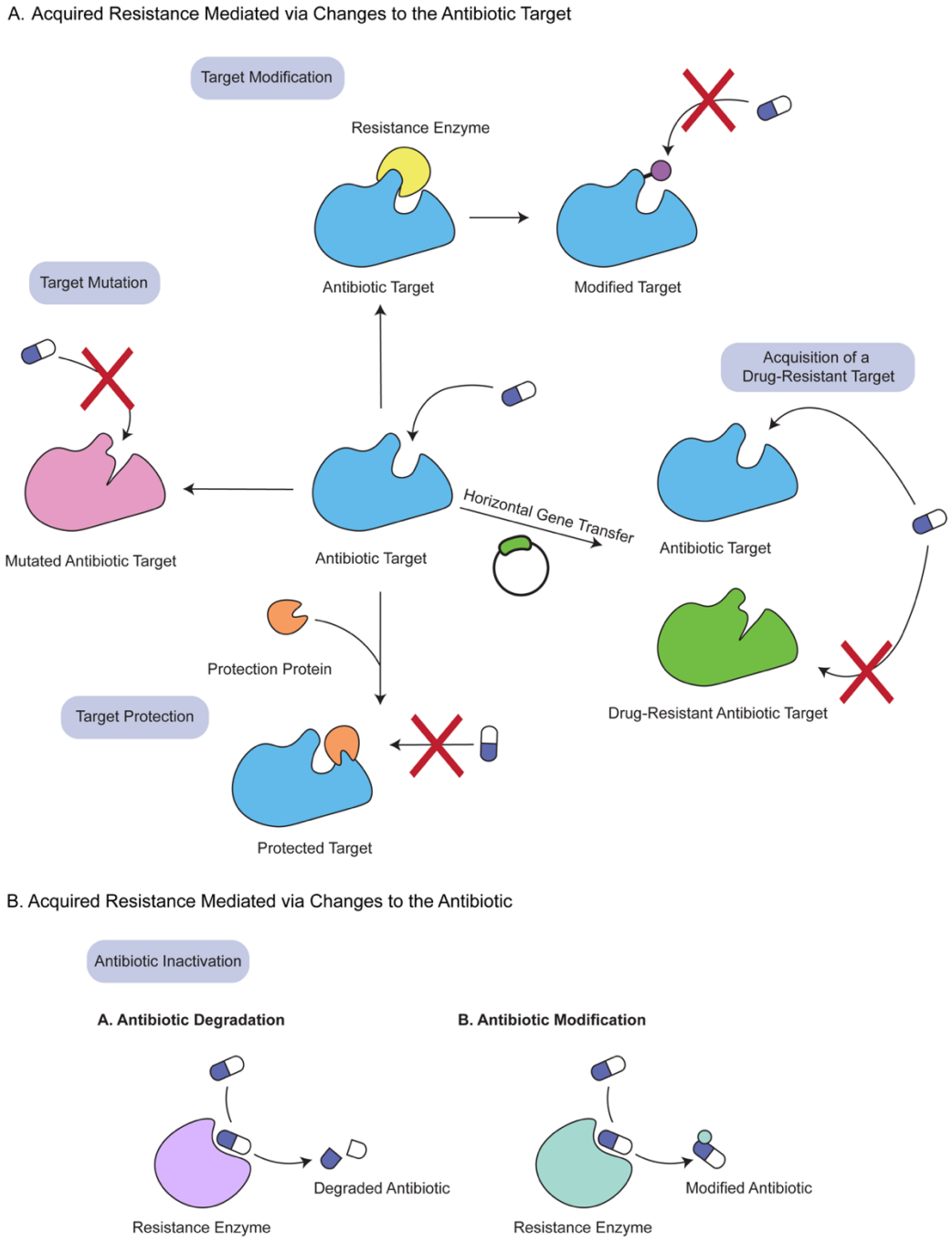

FIGURE 2. **Mechanisms of acquired resistance. A.** Resistance mechanisms involving changes to the antibiotic targets (mutation, modification, protection, acquisition of a resistant target). **B.** Resistance mechanisms involving changes to the antibiotic (antibiotic inactivation via degradation or modification).

Another example of target modification can be seen in polymyxin resistance. Polymyxins are cyclic cationic heptapeptide antibiotics that target lipopolysaccharide (LPS) on the outer membrane of Gram-negative bacteria (Schaenzer & Wright, 2020). However, bacteria can develop resistance to these antibiotics through enzymes that add basic primary amino functional groups to the Lipid A region of LPS (Schaenzer & Wright, 2020). These modifications effectively mask Lipid A with positive charges, repelling the cationic polymyxins and preventing their antibiotic activity (Schaenzer & Wright, 2020).

Target Protection

Resistance can arise through protection proteins that bind to the target and prevent effective drug interactions. The utilization of protection mechanisms occurs for numerous clinically relevant antibiotics, including macrolides, rifamycins, lincosamides, oxazolidinones, aminoglycosides, and fluoroquinolones (Fritsche Thomas R. et al., 2008; Kumar et al., 2014; Long et al., 2006; Surette et al., 2022; Vetting et al., 2011). For example, the *qnr* family of quinolone resistance genes encode pentapeptide repeat proteins (PRPs) that bind to and safeguard topoisomerase IV and DNA gyrase from antibiotic activity (Blair et al., 2015). Based on structural data for QnrB1, these PRPs interact with the target-drug complex after drug binding, releasing the antibiotic and enabling topoisomerase to resume its regular activity (Vetting et al., 2011). Similarly, Tet(O) and Tet(M) are ribosomal protection proteins that confer resistance to tetracyclines by displacing tetracyclines from the ribosome, thereby freeing it from the drugs' inhibitory effects and enabling protein synthesis to continue (Connell et al., 2003).

Antibiotic Inactivation

Lastly, in addition to altering their targets, bacteria can confer antibiotic resistance by directly destroying or modifying the antibiotic using inactivating enzymes. Thousands of such enzymes have been identified, enabling resistance to various antibiotic classes, including β-lactams, rifamycins, aminoglycosides, phenicols, and macrolides (Blair et al., 2015).

Inactivation via Degradation

Among the inactivating enzymes that destroy their antibiotic substrate, β-lactamases are extremely prevalent and confer resistance by hydrolyzing the pharmacophore of β-lactams, irreversibly destroying the antibiotic (Tooke et al., 2019). Multiple subclasses of β-lactamases exist and can hydrolyze different antibiotics within the same class, such as penicillins, cephalosporins, clavams, carbapenems, and monobactams (Livermore, 2008). As of the writing of this thesis, there are over 8,000 β-lactamases cataloged in the β-lactamases database (http://www.bldb.eu/) that have been characterized to varying degrees.

There are two distinct types of β-lactamase resistance mechanisms: the active-site serine enzymes (serine β-lactamases; SBLs) and the zinc metalloenzymes (metallo-β-lactamases; MBLs). SBLs utilize an active site serine residue as a nucleophile, hydrolyzing β-lactams at the β-lactam ring via a covalent acyl-enzyme intermediate. In contrast, MBLs employ a metal-activated water nucleophile to drive the hydrolytic reaction (Tooke et al., 2019). Both types of β-lactam resistance mechanisms have been widely disseminated

across important bacterial pathogens, making β-lactamases a significant healthcare concern (Tooke et al., 2019).

Additional examples of inactivating enzymes that function by degrading their antibiotic target include TetX and Rox. Both enzymes are flavin-dependent monooxygenases that degrade tetracyclines and rifamycins, respectively (W. Yang et al. 2004; Koteva et al. 2018). TetX hydroxylates tetracycline antibiotics, significantly reducing their antimicrobial properties due to an increased rate of degradation enabled by the unstable hydroxylated product (W. Yang et al. 2004; Volkers et al. 2011). In comparison, Rox hydroxylates several rifamycin antibiotics, resulting in ring opening and linearization of these macrocyclic antibiotics to eliminate their antimicrobial activity (Koteva et al., 2018).

Inactivation via Modification

Diverse families of enzymes exist that attach chemical groups to susceptible sites on antibiotics, blocking their ability to bind to their cellular target due to steric hindrance (Blair et al., 2015; Wright, 2005). Bacteria employ a variety of modifications to confer resistance, such as *O*-phosphorylation, *O*-nucleotidylylation, and *O*- and *N*-acetylation (**Figure 3**) (De Pascale and Wright 2010).

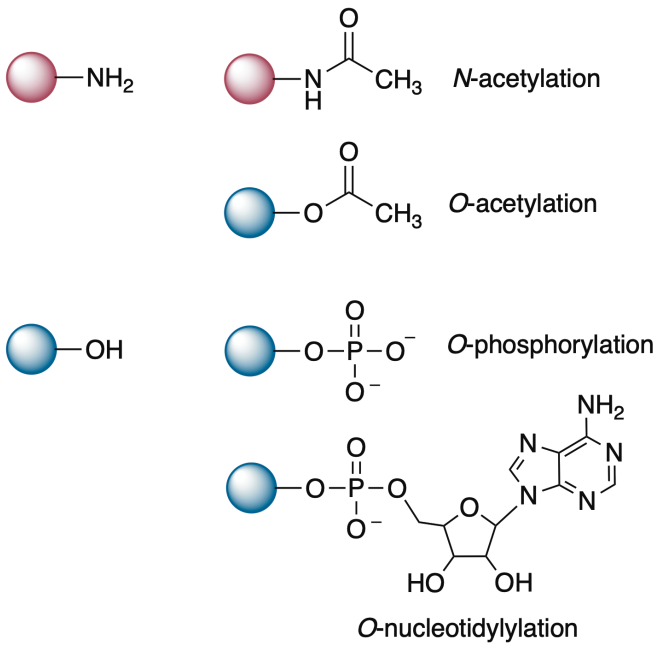

FIGURE 3. Inactivation via modification. Examples of chemical modifications catalyzed by antibiotic-inactivating enzymes. Modified amines are shown in red, and modified hydroxyl groups are shown in blue.

One class of antibiotics highly susceptible to modification is the aminoglycosides, primarily due to their large size and numerous exposed hydroxyl (-OH) and amine groups ($-NH_2$) (Blair et al., 2015). Aminoglycoside-modifying enzymes (AMEs) transfer bulky substrates to these exposed groups at various sites of the 2-deoxystreptamine core or sugar moieties, obstructing the interaction between aminoglycosides and their target, the ribosome (Ramirez & Tolmasky, 2010). Modified aminoglycosides are effectively detoxified, enabling these enzymes to confer high levels of resistance. Notably, AMEs exhibit a remarkable diversity of modifications, including phosphorylation, acetylation, and nucleotidylylation (Norris & Serpersu, 2013; Ramirez & Tolmasky, 2010).

Origins of Resistance

Antibiotic resistance has emerged and spread to human pathogens since the introduction of antibiotics like penicillin and prontosil into the clinic (Stekel, 2018). While it was previously apparent that antibiotics fueled the selection of resistant strains, over time, it became clear that human pathogens had acquired sophisticated and specific ARGs. In 1973, a pivotal discovery indicated that antibiotic resistance extends beyond pathogenic bacteria, as ARGs were identified in environmental bacteria (Benveniste & Davies, 1973). These environmental ARGs exhibited genetic similarities to clinical variants, hinting at a shared ancestry with ARGs found in pathogens (Benveniste & Davies, 1973). Extensive research has since revealed that non-pathogenic environmental microbes are often multidrug-resistant, possess levels of resistance surpassing bacterial strains associated with diseases, and harbour both known resistance mechanisms utilized by pathogens and novel ones (Allen et al., 2010; D'Costa et al., 2006). There is now substantial evidence supporting the notion that some ARGs commonly found in pathogens stem from gene families originating in the environment. One direct example includes the emergence of the fluoroquinolone ARG *qnr* in pathogenic bacteria (Surette & Wright, 2017). While this gene likely originated in an environmental *Shewanella* species, it is now commonly found on mobile genetic elements in plasmids and can be shared among bacteria (Poirel et al., 2005). These findings infer that environmental bacterial genomes are the primary reservoir for antibiotic resistance (Surette & Wright, 2017).

Furthermore, antibiotic resistance is ancient and predates the human discovery and use of these drugs. Evidence for this includes the discovery of a penicillin-resistant strain

of *Escherichia coli* in the 1940s, well before penicillin was commonly used in medicine (Abraham & Chain, 1940). More recently, a study by D'Costa et al. (2011) employed a targeted metagenomic analysis of a 30,000-year-old Beringian permafrost sample, finding a diverse collection of ARGs. This study confirmed that such genes existed long before the clinical use of antibiotics, demonstrating that antibiotic resistance is naturally occurring and widespread (D'Costa et al., 2011).

Another approach to understanding ancient antibiotic resistance involves studying isolated ecosystems with minimal human impact., such as isolated caves. Bhullar et al. (2012) examined culturable bacteria from Lechuguilla Cave in New Mexico, which had been isolated from the surface for about 4 million years. Many strains exhibited multidrug resistance. Notably, *Paenibacillus* sp. C231 was identified as resistant to 14 antibiotic classes, with seven instances of resistance attributed to enzymatic inactivation (Pawlowski et al., 2016). This research revealed a remarkable conservation of resistance mechanisms over millions of years in the absence of antibiotic pressure exerted by humans. It identified five novel resistance mechanisms with potential environmental origins, raising concerns about their transfer to pathogens in clinical settings (Pawlowski et al., 2016).

These studies collectively underscore the depth and complexity of antibiotic resistance as a natural phenomenon and stress the importance of considering environmental reservoirs in our understanding of modern antibiotic resistance.

The Evolution of Inactivating Enzymes

Inactivating enzymes represent one of the most successful resistance mechanisms in bacteria (Munita & Arias, 2016). Their potency in causing resistance stems partly from their high degree of substrate specificity, which makes them adept antibiotic antagonists. This specificity is believed to have evolved over millennia through a process of co-evolution between environmental bacteria producing natural product antibiotics and neighbouring bacteria occupying the same ecological niche (Marshall et al., 1998; Wright, 2005).

The evolution of inactivating enzymes stems from a pool of housekeeping genes in bacteria that possess the potential to evolve into resistance elements. Nature has repurposed fundamental bacterial metabolic reactions, such as phosphorylation and acetylation, as templates for resistance mechanisms. These genes, with the capacity to evolve and be repurposed into resistance enzymes, are termed proto-resistance genes (Morar & Wright, 2010).

An excellent example of inactivating enzymes evolving from proto-resistance genes is the β-lactamases, which confer resistance to β-lactams. β-lactams bind covalently to an active site serine residue found on PBPs, which crosslink peptide stems of newly synthesized peptidoglycan to impart rigidity and stability to the bacterial cell wall (Massova & Mobashery, 1998).

As previously mentioned, β-lactamases inactivate β-lactams by hydrolyzing and opening the lactam ring. The two primary mechanisms of β-lactamases are well understood: SBLs utilize an active site serine residue to catalyze a nucleophilic attack at the lactam

carbonyl carbon, forming a covalent enzyme intermediate resembling the inactivation step of PBPs. In contrast, MBLs use Zn^{2+}-dependent activation of a hydrolytic water molecule to hydrolyze β-lactams through a mechanism akin to that observed in metallo-peptidases (Morar & Wright, 2010).

Previous studies comparing the 3D structure of SBLs and PBPs hinted at a relationship between these enzyme groups, illustrating that β-lactamases share both structure and function with enzymes associated with cell wall metabolism and general peptidase activities (Kelly et al., 1986; Massova & Mobashery, 1998). Moreover, phylogenetic evidence suggests that some SBLs emerged 2.4 billion years ago from a common ancestor of PBPs (Hall & Barlow, 2004). Supporting this divergence, it is notable that β-lactamases have retained no peptidoglycan biosynthetic activity but have gained the ability to inactivate β-lactams (Morar & Wright, 2010).

As Morar and Wright exhibit, numerous other examples demonstrate the evolutionary connection between resistance enzymes and proto-resistance genes (2010). By examining antibiotic resistance from the perspective of genomic enzymology—which focuses on the relationships between protein structure and function within their genetic contexts and evolutionary history—it becomes clear that resistance enzymes have gradually evolved. Over millennia, these enzymes have adapted existing metabolic processes to neutralize antibiotics.

Inactivating Enzymes and Synthetic Antibiotics

Given the extended timescale required for housekeeping genes to evolve into resistance enzymes targeting natural product antibiotics, it is unsurprising that the emergence of drug-specific inactivating enzymes targeting synthetic antibiotics, used in clinical practice for only a few decades, is exceptionally rare. In a comprehensive study on antibiotic resistance prevalence in environmental *Streptomyces*, 480 strains were screened against 21 antibiotics, including natural products, semisynthetic derivatives, and synthetic antibiotics like ciprofloxacin and linezolid (D'Costa et al., 2006). Despite lacking prior exposure to synthetic antibiotics, 52 strains exhibited ciprofloxacin resistance, yet none displayed enzymatic inactivation of the drug, suggesting that such activity is unlikely (D'Costa et al., 2006). Since this study, a bi-functional aminoglycoside-modifying enzyme known as AAC(6')-Ib-cr, which confers resistance to some fluoroquinolones, has been identified (Rodríguez-Martínez et al., 2011). With two unique substitutions (Trp102Arg and Asp179Tyr) compared to the original aminoglycoside-acetylating variant AAC(6')-Ib, AAC(6')-Ib-cr can acetylate and confer low levels of resistance against ciprofloxacin and norfloxacin (Vetting et al. 2008). Only one other example of a synthetic antibiotic-inactivating enzyme has also been identified, involving the monooxygenase-mediated inactivation of sulfonamides by environmental bacteria (Kim et al. 2019).

The limited discovery of inactivating enzymes capable of providing high levels of resistance to synthetic antibiotics suggests that while these drugs are susceptible to resistance development, they benefit from the absence of dedicated resistance mechanisms upon their introduction into clinical practice. Unfortunately, the discovery of novel

synthetic antibiotics has proven largely unsuccessful, which will be discussed in the following section.

Drug Discovery and Phenotypic Screening

The Golden Era

Antibiosis is the antagonistic relationship between two organisms wherein one is adversely affected. Louis Pasteur was among the first scientists to propose the existence of antibiosis between microbes, suggesting that certain bacteria could produce and release compounds that kill other bacteria (Brunel, 1951). The discovery of penicillin, alongside numerous reports of other microorganisms producing antimicrobial compounds, prompted Selman Waksman to initiate investigations into microbes as potential producers of such compounds in the late 1930s (Hutchings et al., 2019). Waksman described antibiotics as "compounds made by microbes to destroy other microbes" and identified soil-dwelling Actinomycetes as prolific producers of antimicrobial natural products (Hutchings et al., 2019; Valiquette & Laupland, 2015). He unearthed several life-saving antibiotics, such as streptomycin and neomycin, using a systematic approach – the Waksman Platform- that involved looking for zones of growth inhibition around single colonies of isolated soil bacteria grown under various culture conditions (Lewis, 2012). Once identified, the inhibition was tested against targeted pathogenic bacteria (Kresge et al., 2004). This screening platform was subsequently adopted by pharmaceutical companies, heralding the Golden Era of antibiotic discovery, which saw the discovery of almost all known classes of antibiotics. However, this discovery pipeline has since been depleted due to the frequent

rediscovery of known compounds and the escalating challenge of identifying novel or unrelated compounds (Lewis, 2013; Valiquette & Laupland, 2015).

Synthetic Antibiotics

In response to the lack of novel natural product antibiotics being discovered, researchers and pharmaceutical companies began screening vast synthetic compound libraries in tandem with genome-based target identification, which involves analyzing genomic information to identify essential genes that make ideal candidates as drug targets. However, this approach proved unproductive (Tommasi et al., 2015). For example, GlaxoSmithKline (GSK) conducted 70 high-throughput screening campaigns over seven years with approximately 500,000 synthetic compounds (Hutchings et al., 2019; Payne et al., 2015). This approach yielded very few leads and failed to identify a single candidate for drug development (Hutchings et al., 2019; Tommasi et al., 2015). Only a few synthetic antibiotic classes have been successfully introduced throughout the history of antibiotic discovery, including fluoroquinolones, sulfonamides, oxazolidinones, and nitroimidazoles (Lewis, 2017; Wright, 2014). Pharmaceutical companies found that while it was relatively simple to pinpoint inhibitors of various drug targets *in vitro*, these compounds exhibited poor efficacy as safe drugs capable of penetrating bacterial cells. Subsequently, diverse, innovative strategies were explored in the quest for new drugs. These included the development of small molecules and antibodies to counteract pathogenicity factors, the design of strain-specific antibiotics, the investigation into bacteriophages, and advancements in vaccination. Nevertheless, most of these approaches necessitated

combination treatment with antibiotics or failed to demonstrate clinical proof-of-concept. These findings ultimately changed the focus of drug discovery, with some researchers turning towards the modern use of artificial intelligence for drug discovery and development and others turning back to nature in the search for novel antibiotics derived from microbial sources (Hegemann et al., 2023; Paul et al., 2021).

Antibiotic Dereplication

It is crucial to acknowledge that antibiotic dereplication remains essential in phenotypic screening. The term "dereplication" was first introduced in the inaugural CRC Handbook of Antibiotic Compounds in 1980 to underscore the importance of identifying and eliminating previously discovered active compounds at the early stages of screening (Langlykke, 1980; Van Middlesworth & Cannell, 1998). Typically, screening procedures involve exploring natural product production by bacteria through crude extract mixtures in primary screening. If activity is detected, the compound of interest undergoes isolation via activity-guided purification (Ito and Masubuchi 2014). Crude extracts are often laden with numerous compounds, making detecting a target compound labour-intensive and time-consuming (Takagi & Shin-Ya, 2012).

Due to the extensive efforts put into compound purification, it is essential to avoid wasting time isolating previously identified antibiotics from these crude mixtures. Some antibiotics are commonly rediscovered. It is estimated that among Actinomycetes, 4% of strains produce streptothricin, 5% produce streptomycin, and 1.6% produce tetracycline (Chevrette & Handelsman, 2021). Therefore, ruling out known drugs from the discovery

process in the initial steps of the drug discovery pipeline is crucial. However, this process frequently necessitates highly specialized equipment such as high-performance liquid-chromatography systems and high-resolution mass spectrometers, making dereplication financially burdensome. Despite these challenges posing a bottleneck in the drug discovery pipeline, antibiotic dereplication remains indispensable. It serves as a vital step following the preliminary screening of crude extracts, aiding in identifying extracts harbouring novel metabolites worthy of prioritization (Ito and Masubuchi 2014).

To overcome the gruelling process of dereplication and make antibiotic discovery more accessible, Cox et al. (2017) developed the Antibiotic Resistance Platform (ARP). The ARP serves a dual purpose: identifying antibiotic adjuvants and facilitating antibiotic dereplication. It consists of a library of resistance genes individually cloned into the pGDP plasmid series, allowing for fine-tuned levels of expression. These constructs are then transformed into wild-type *E. coli* BW25113 and the efflux deficient, hyper-permeable *E. coli* BW25113 Δ*bamB* Δ*tolC* strains. To dereplicate known antibiotics, antibiotic producing microorganisms, such as *Streptomyces*, are grown on Petri dishes to allow secondary metabolites to be excreted into the surrounding media. Strains from the *E. coli* library of resistance genes are then spotted on the surface of the secondary metabolite-containing media and left to grow. When available, inactivating enzymes are used during dereplication due to their high specificity and levels of resistance. If the microorganism being dereplicated is producing an antibiotic that any of the *E. coli* strains can resist, the *E. coli* strain expressing a resistance gene with activity against that antibiotic will grow on the surface of the Petri dish media. By correlating which resistance gene is expressed in the

growing *E. coli* strain, it can be determined which antibiotic is being made by the producing bacteria. Using this approach, the ARP enables rapid, cost-effective identification of commonly rediscovered antibiotics without requiring prior compound purification. The development of such a platform is pivotal in circumventing the bottleneck of antibiotic discovery posed by the dereplication process, rendering it an invaluable asset in the fight against antibiotic resistance (Cox et al. 2017; Zubyk, Cox, and Wright 2019).

Revisiting Discarded Compounds

As the field of antibiotic discovery advances, exploring the possibility of revisiting previously disregarded compounds is imperative. Bérdy (2005) estimated that by 2002, around 16,500 antibiotic natural products had already been identified. Despite recognizing the potential of natural products as valuable sources of antibiotics, only a fraction of their chemical structures have made it to clinical application (Bérdy, 2005; Wright, 2014). It is essential to note that despite their prior dismissal, a wealth of data is already available for these compounds. While significant progress is being made in antibiotic discovery through innovative screening methods, discovering and characterizing novel antibiotics remains time-consuming and costly. An alternative approach could involve re-evaluating the approximately 16,500 previously disregarded antimicrobial compounds to uncover new antibiotic candidates. Within this pool, it is reasonable to expect that some may offer the potential for optimization and eventual clinical use (Bérdy, 2012). Notably, two of the most recently approved antibiotics—linezolid (2000) and daptomycin (2003)—were initially

discovered in 1978 and 1987 but were shelved for many years before entering clinical practice.

Linezolid belongs to the oxazolidinone class of synthetic antibiotics, inhibiting translation by binding to the 50S subunit of the prokaryotic ribosome and preventing complex formation with the 30S subunit, mRNA, initiation factors, and formylmethionyl (f-met)-tRNA (Swaney et al., 1998). Initially discovered in the late 1980s by DuPont Pharmaceuticals, the first lead analogues (DuP 105 and DuP 721) proved unsuitable for pharmaceutical development due to liver toxicity observed in early clinical trials (Slee et al., 1987). However, research was resumed in the early 1990s by the then UpJohn Corporation, leading to the synthesis of non-toxic analogues through a series of structure-activity relationship studies, eventually resulting in the development of linezolid (Ford et al., 1997). Today, linezolid is utilized in the clinic to treat drug-resistant skin infections and pneumonia, exhibiting activity against vancomycin-resistant enterococci (VRE) and methicillin-resistant *Staphylococcus aureus* (MRSA) (Birmingham et al., 2003).

In comparison, daptomycin is a cyclic lipopeptide natural product antibiotic produced by *Streptomyces roseosporus*, which binds to the cell membrane of susceptible microorganisms, inducing rapid depolarization of membrane potential resulting in cell death (Taylor & Palmer, 2016). Discovered by scientists at Eli Lilly, daptomycin was initially discarded in the 1980s due to high-dose therapy-related toxicity affecting the musculoskeletal system (Tally et al., 1999). However, it was revisited in 1997 by Cubist Pharmaceuticals and successfully approved for clinical use by the U.S. Food and Drug Administration (FDA) in 2003 after realizing that adverse effects could be mitigated with

a lower dose regimen (Eisenstein et al., 2010). Daptomycin is now widely used to treat various infections caused by Gram-positive bacteria, including the previously mentioned VRE and MRSA (Tally et al., 1999).

Given these examples, it is reasonable to speculate that many more discarded or forgotten antimicrobials exist with the potential for clinical application. Among these overlooked compounds lies edeine, a linear peptide discovered in the 1960s but never pursued due to its toxicity against eukaryotic cells (Westman et al. 2013).

Revisiting the Peptide Antibiotic, Edeine

Edeine antibiotics display broad-spectrum activity against various organisms, including Gram-positive and Gram-negative bacteria, mycoplasmas, fungi, and certain mammalian cell types (Z. Kurylo-Borowska 1975). Although edeine binds to eukaryotic ribosomes, rendering it unsuitable for human or animal use, its binding site and conformation differ between eukaryotic and prokaryotic ribosomes. Therefore, revisiting and developing analogues devoid of human toxicity is possible. Furthermore, reports of edeine resistance are limited because it has never been used in the clinic. The only known edeine-specific resistance mechanism is the self-resistance enzyme EdeQ, which acetylates the drug to inactivate it. Homologs of EdeQ are relatively rare in microbial genomes. When present, they are found in the chromosomes of environmental bacteria, minimizing concerns about resistance mobilizing into the clinic (Westman et al. 2013). These characteristics make edeine an appealing candidate for optimization, leveraging its properties and biosynthetic pathway to develop safe analogues for human use.

Edeine Structure

During edeine biosynthesis, four biologically active molecules are generated: edeine A, B, D, and F, with edeine A and B being the major products and edeine D and F being minor products (Borowski et al., 1966; Czerwinski et al., 1983). These compounds have a distinctive core structure consisting of four non-proteinogenic amino acids, a glycine residue, and a polyamine tail. Each compound comprises β-serine, 2,3-diaminopropionic acid (DAPA), 2,6-diamino-7-hydroxyazeleic acid (DAHAA), and glycine. Differentiation among edeine A, B, D, and F is determined by the R1 and R2 groups at both termini, which may be either β-tyrosine or β-phenylalanine (R1) or spermidine or guanylspermidine (R2) (**Figure 4A**) (Westman et al. 2013).

Interestingly, each edeine compound exists as a mixture of two isomeric peptides: the active α isomer (e.g., edeine A1) and the inactive β isomer (e.g., edeine A2). The difference in activity between isomers results from the linkage of β-serine to DAPA. Active isomers feature the linkage of isoserine with the α-amino group of DAPA, while inactive isomers have the linkage to the β-amino group (**Figure 4B**). Only the α isomers have been identified as active antibiotics (Czerwinski et al., 1983)

Edeine Mode of Action

The mechanism of action (MOA) of edeines is known to be concentration-dependent, inhibiting DNA synthesis at low concentrations and protein synthesis at higher concentrations (Cozzarelli, 1977; Z. Kurylo-Borowska & Szer, 1972)**.** However, recent

research has mainly focused on edeine as a translation inhibitor, with the last significant studies on its effects on DNA synthesis conducted in the 1960s (Z. Kurylo-Borowska &

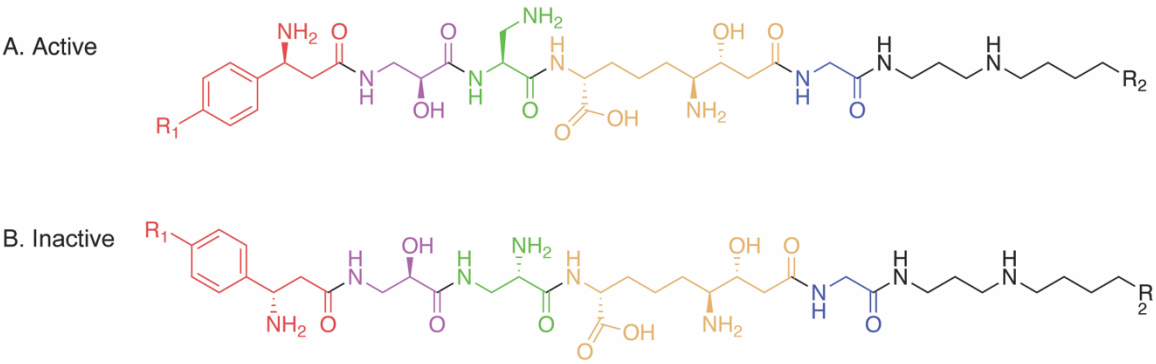

Edeine	R1	R2
A	OH	NH_2
B	OH	$NHC(NH)NH_2$
D	H	NH_2
F	H	$NHC(NH)NH_2$

DAPA: 2,3-diaminopropionic acid

DAHAA: 2,6-diamino-7-hydroxyazaelic acid

FIGURE 4. Chemical structure of edeines. A. The backbone of active edeine molecules are comprised of β-tyrosine or β-phenylalanine (R1), β-serine, 2,3-diaminopropionic acid (DAPA), 2,6-diamino-7-hydroxyazaelic acid (DAHAA), glycine, and either a spermidine or guanylspermidine polyamine chain (R2). **B.** Inactive edeine isomers have the same R groups as active edeines. Their backbone differs by the linkage of the β-serine residue to the β-amino group of 2,3-diaminopropionic acid (DAPA) rather than the α-amino group.

Szer, 1972; Zofia Kurylo-Borowska, 1964). Moreover, no mechanistic studies have been conducted to elucidate how edeine targets DNA synthesis. Nonetheless, several reports suggest that inhibiting translation can also suppress DNA synthesis (McClary et al., 2017). Based on this, I hypothesize that edeine primarily functions as a translation inhibitor, with any effects on DNA synthesis likely being secondary consequences of its principal activity.

Edeine effectively inhibits protein synthesis across all phylogenetic domains (Szer & Kurylo-Borowska, 1970). In prokaryotes, it specifically prevents the binding of initiation factor fMet-tRNA to the peptidyl (P) site of the 30S ribosomal subunit by occupying the space between the P and exit (E) sites (Dinos et al., 2004). It remains unclear whether edeine inhibition of P-site binding is due to direct steric hindrance or indirect conformational changes affecting mRNA positioning (Dinos et al., 2004). Conversely, in eukaryotic ribosomes, edeine predominantly binds to the E site (Garreau De Loubresse et al., 2014), where it forms a binding pocket with 18S rRNA nucleotides along the mRNA path, disrupting start codon recognition and preventing subunit joining by promoting continuous scanning of the 40S subunit (Kozak & Shatkin, 1978).

Structural analysis shows significant differences in edeine's binding conformations between prokaryotic and eukaryotic ribosomes. In eukaryotic ribosomes, edeine adopts an S-shaped conformation (PDB 4U4N) (Garreau De Loubresse et al., 2014), whereas in prokaryotic ribosomes, it takes a U-shaped conformation (PDB 1I95) (Pioletti et al., 2001) (**Figure 5**). This variation highlights the structural differences between the ribosomes of these two groups, offering potential targets for structure-activity-relationship (SAR) studies aimed at developing prokaryotic-specific derivatives of edeine.

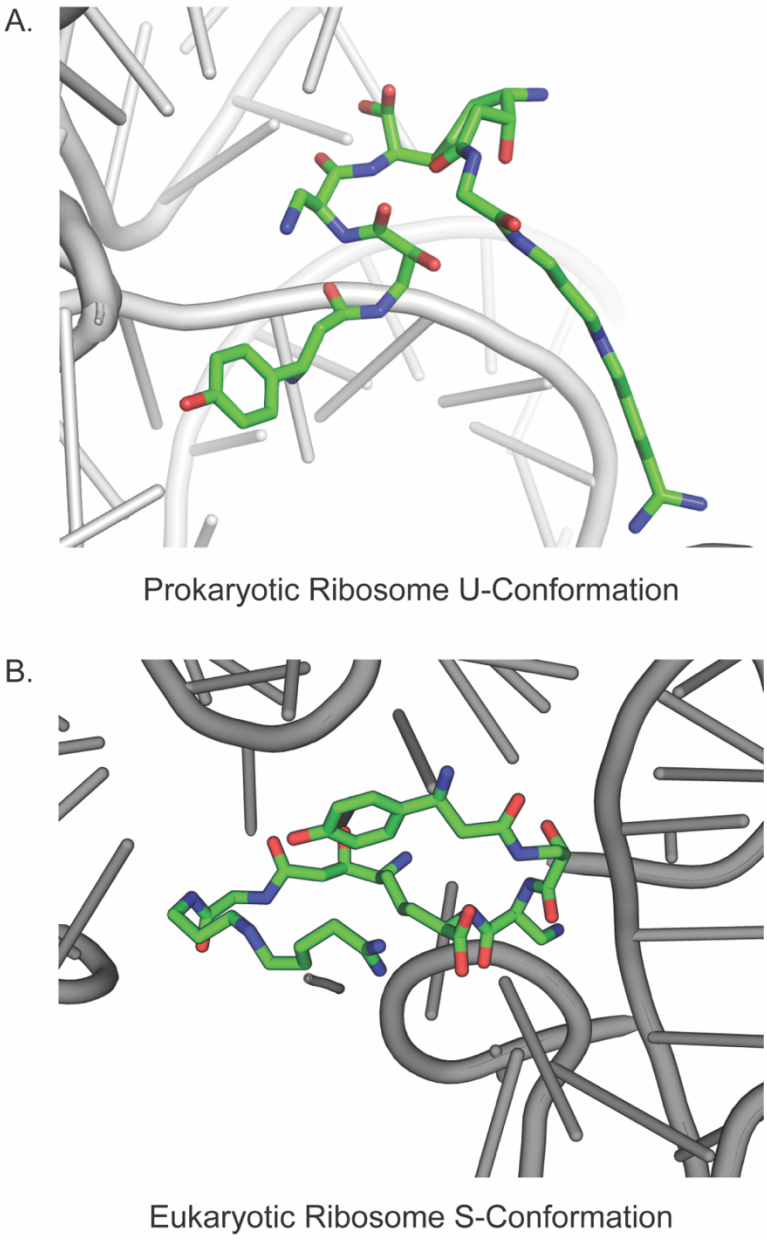

FIGURE 5. Conformation of edeine bound to the ribosome. A. Edeine bound to the 30S subunit of T. thermophilus (PDB 1I95). Edeine adapts a U-conformation. **B.** Edeine bound to the 80S subunit of Saccharomyces cerevisiae (PDB 4U4N). Edeine adapts a S-conformation.

Elucidating the Biosynthetic Pathway of Edeine

Introduction to Peptide Antibiotics & Biosynthesis

Peptide antibiotics constitute a diverse category of linear and cyclic antibiotics that can contain standard and non-proteinogenic amino acids (Koehbach & Craik, 2019). Throughout history, various peptide antibiotics, such as cyclopeptides (e.g., lysobactin), glycopeptides (e.g., vancomycin), and lipopeptides (e.g., daptomycin and colistin), have undergone clinical evaluation or approval for therapeutic purposes (Meng & Kumar, 2007). Nonetheless, incorporating α-amino acids in their structures often leads to inadequate protease stability, significantly constraining their clinical utility (Latham, 1999; Meng & Kumar, 2007). Strategies to enhance peptide resistance against proteases encompass N- and C-termini protection, backbone modification, cyclization, and integration of non-proteinogenic amino acids like β-amino acids (Khatri, Nuthakki, and Chatterjee 2019; Patočka 2011). β-amino acids are unique molecular constituents that are less common in nature compared to standard α-amino acids. Structurally, they differ by linking the amino group to the β-carbon rather than the α-carbon (**Figure 6**) (Patočka 2011). Many natural products, such as the anticancer agents taxol and bleomycin, incorporate β-amino acids or related moieties (Kudo, Miyanaga, and Eguchi 2014)

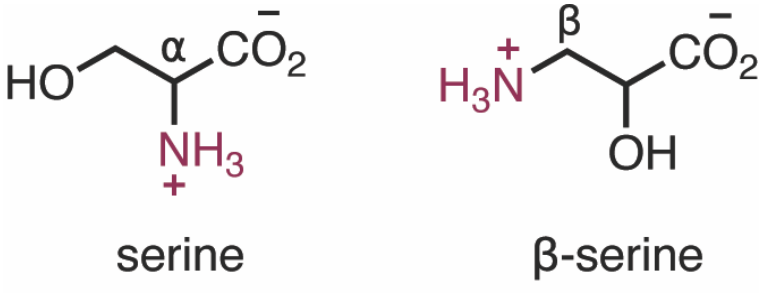

FIGURE 6. Structural comparison of α-amino acids and β-amino acids. β-amino acids (β-serine) differ structurally from α-amino acids (serine) due to the linkage of their amino group to the β-carbon rather than the α-carbon.

Nonribosomal peptide synthetases (NRPSs) are modular enzymes that catalyze the synthesis of peptide antibiotics from both standard and non-proteinogenic amino acid substrates (Miller & Gulick, 2016). The assembly of a nonribosomal peptide by an NRPS involves an assembly line of repeating steps facilitated by modules that contain three core catalytic domains (adenylation, thiolation (or peptidyl carrier protein), and condensation) (Miller & Gulick, 2016). Adenylation (A) domains catalyze the ATP-dependant binding to a specific amino acid substrate (standard or non-proteinogenic). Next, the amino acid residue is transferred to a peptidyl carrier protein (PCP) domain, which is bound as a thioester. The PCP-domain then shuttles the covalently bound amino acid to different domain active sites. The condensation (C) domain features donor and acceptor binding sites for upstream and downstream PCP-bound substrates. It is essential for catalyzing the formation of peptide bonds to elongate the growing peptide (Felnagle et al., 2008). Together, these three core domains comprise a minimal NRPS module. A fourth domain known as a thioesterase (TE) domain is often found at the C-terminus of the NRPS and catalyzes the release of the peptide from the NRPS. Other additional tailoring domains,

such as epimerization, methylation, and heterocylization domains, may be present in an NRPS module to introduce additional structural complexity (**Figure 7**) (Felnagle et al., 2008). A similar group of modular enzymes known as polyketide synthases (PKSs) exist that are responsible for the biosynthesis of secondary metabolites that produce polyketides, such as macrolide and tetracycline antibiotics (Nivina et al., 2019; Walsh, 2016). It is also possible for secondary metabolites to be synthesized using a combination of NRPS/PKS enzymes (Walsh, 2016). For an extensive overview of NRPS and PKS machinery and assembly, please refer to Walsh (2016), Felnagle et al. (2008), and Nivina et al. (2019).

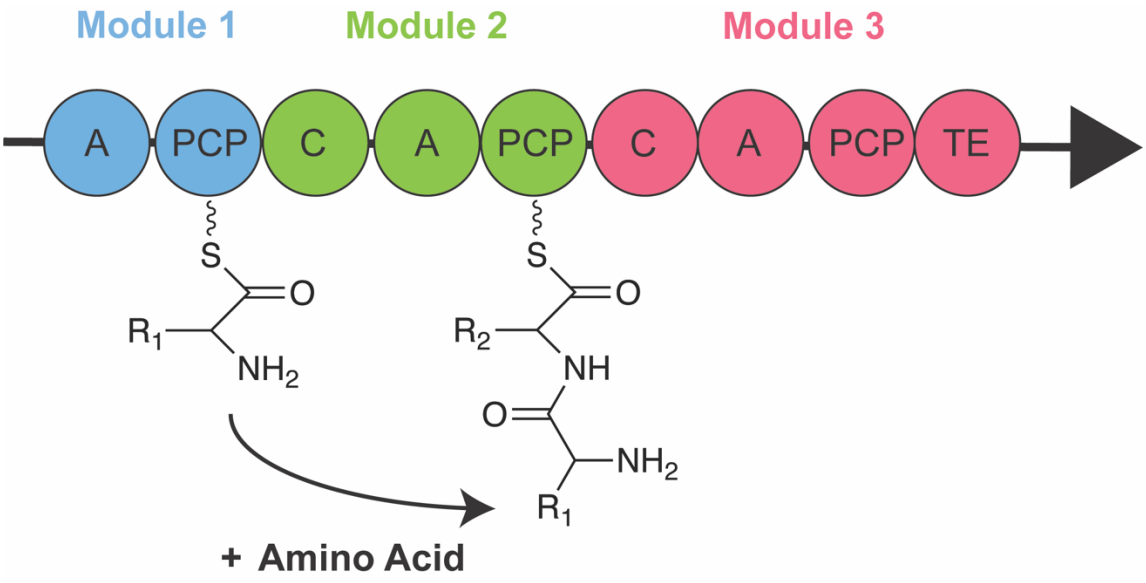

FIGURE 7. Schematic of a non-ribosomal peptide synthetase (NRPS). NRPS are modular enzymes that catalyze the synthesis of peptide antibiotics. A minimal module contains an adenylation (A) domain that catalyzes the binding of a specific amino acid, a peptidyl-carrier protein (PCP) domain that transfers bound amino acids between domains, and a condensation (C) domain that forms peptide bonds to elongate the growing peptide. Thioester (TE) domains catalyze the release of peptides from the NRPS.

Edeine Biosynthesis

The edeine family of antibiotics is a prime example of peptide antibiotics incorporating multiple non-proteinogenic amino acids. Understanding edeine biosynthesis may provide crucial insights into the mechanisms behind synthesizing these unconventional amino acids.

In 1966, it was established that edeine production remains unaffected by protein synthesis inhibitors, such as chloramphenicol, suggesting its synthesis through NRPSs rather than involving ribosomes or RNA templates (Borowska & Tatum, 1966). Over 40 years later, when studying the edeine self-resistance acetyltransferase EdeQ, Westman et al. (2013) assembled a draft genome for the edeine producer *B. brevis* Vm4, confirming the nonribosomal synthesis hypothesis.

Given the pentapeptide structure of edeine, researchers anticipated the presence of a biosynthetic gene cluster (BGC) housing enough NRPS modules to construct such a molecule. A BGC is a group of two or more genes physically clustered in a genome and encodes a biosynthetic pathway for producing a specialized metabolite (Medema et al., 2015). Five distinct BGCs in the *B. brevis* genome were revealed using BLAST. After excluding two clusters for not containing enough NRPS adenylation domains and identifying two clusters associated with gramicidin and tyrocidine production, the focus turned to a 45.1 kb cluster with 17 open reading frames (ORFs) (**Figure 8**) flanked by tRNA genes, emerging as the prime candidate for edeine biosynthesis (Westman et al. 2013).

Further analysis via the AntiSMASH pipeline uncovered four NRPSs (EdeK, L, N, and P), one hybrid polyketide synthetase (PKS)-NRPS (EdeI), and two PKS/NRPS-like

proteins harbouring PCP domains but lacking other NRPS-specific domains (EdeG and EdeJ) (Westman et al. 2013). Due to the higher proportion of domains than expected for pure peptide assembly, it is predicted that some may be inactive or involved in serving other functions (Westman et al. 2013).

Our current understanding of edeine biosynthesis remains limited. Although not formally investigated, it is hypothesized that EdeC and EdeD are responsible for DAPA biosynthesis in edeine, based on their similarity to SbnB and SbnA, which are required for DAPA synthesis in *Staphylococcus aureus* (Beasley, Cheung, and Heinrichs 2011). Furthermore, previous work on edeine suggests that β-tyrosine biosynthesis is facilitated by an unusual tyrosine 2,3-aminomutase (Parry and Kurylo-Borowska 1980). Analysis of the edeine BGC shows that only *edeO* shares similarity with aminomutases, with the protein sequence containing conserved domains found in the radical S-adenosyl-L-methionine (SAM) superfamily known to include aminomutases, indicating that this gene is likely responsible for edeine β-tyrosine biosynthesis (Westman et al. 2013).

More recently, *edeB* has been studied for its role in regulating edeine biosynthesis (Du et al., 2022). Bioinformatic analysis revealed that EdeB belongs to the ParB family of proteins, which function as transcription factors in various biological processes (Khare et al., 2004). It was shown that overexpression of EdeB in *B. brevis* X23 increased edeine production by 92.3%, and *edeB*-deletion mutants exhibited less antibacterial activity. Additionally, RT-qPCR results show a decrease in the expression of *edeA, edeQ, and edeK* when *edeB* is deleted. Lastly, it is reported that an electrophoretic mobility shift assay (EMSA) revealed direct binding of EdeB to the promoter region of the edeine BGC in *B.*

brevis, indicating its role in enhancing edeine production through direct interaction with the cluster (Du et al., 2022).

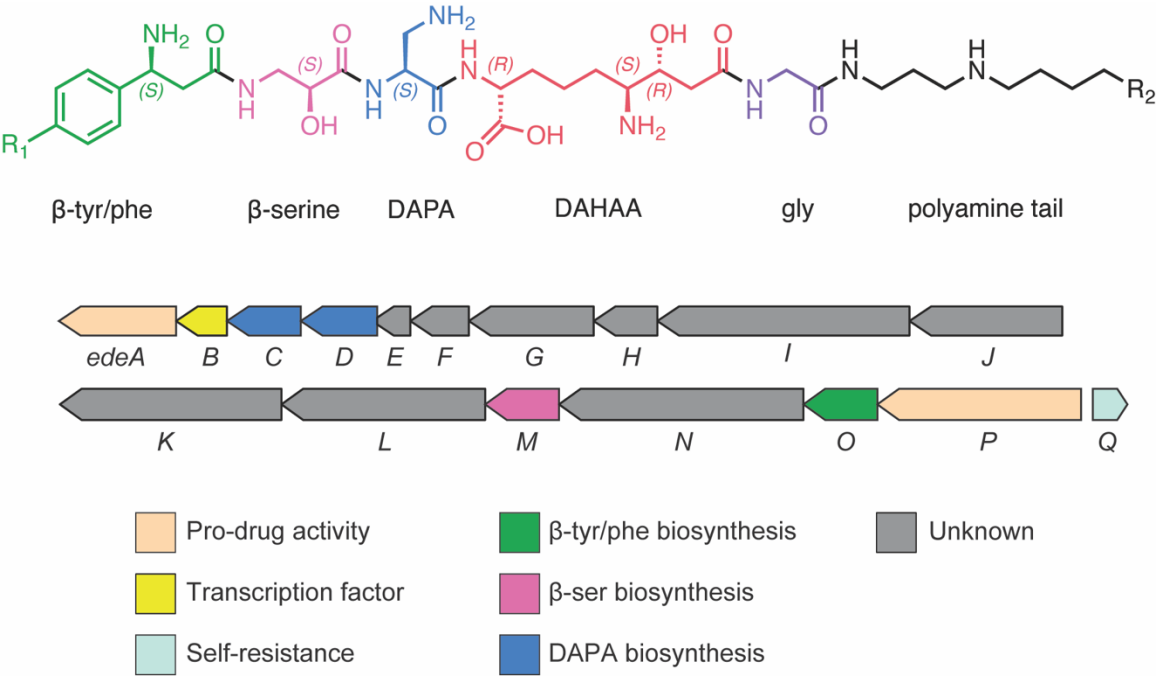

FIGURE 8. Edeine biosynthetic gene cluster and known gene functions (Westman et al., 2013; Volpe et al., 2023, Du et al., 2022).

EdeA has been investigated for activity as a type II prodrug-activating peptidase (Velilla et al. 2023; Volpe et al. 2023). Research suggests that EdeA shares homology with ClbP, an inner-membrane peptidase responsible for converting the prodrug pre-colibactin into its active form, colibactin. While edeine production has not been associated with a prodrug resistance mechanism previously, Volpe et al. (2023) have identified so-called "pre-edeines" with an acyl-D-asparagine prodrug moiety on the C-terminus of the molecule, implying a prodrug activation strategy in edeine biosynthesis. EdeP is

hypothesized to play a role in the biosynthesis of the acyl-D-asparagine moiety, based on the homology of its condensation domain with equivalent modules found in the BGCs colibactin, an adenylation domain predicted to have specificity for asparagine, and an epimerase domain capable of producing D-asparagine (Volpe et al. 2023). These findings conflict with the previously suggested role of EdeP being involved in DAHAA biosynthesis due to its epimerization domain and DAHAA being the only amino acid with D-configuration in edeine, as suggested by Westman et al. (2013). Overall, the investigation into EdeA and EdeP unveils potential prodrug activation mechanisms within edeine biosynthesis, challenging prior assumptions and urging further exploration.

A significant knowledge gap remains in understanding the biosynthesis of the edeine building blocks DAHAA and β-serine. The latter has been detected in some natural products produced by marine sponges, but documented research on its production primarily involves synthetic synthesis rather than elucidating the biosynthetic pathway (Westman et al. 2013; K. Yang et al. 2012). Homology searches of the edeine BGC revealed that among the unassigned genes, aspartate aminotransferase (AAT) shared sequence similarity to EdeM (71% I.D.). AAT is a well-known transaminase capable of transferring amino groups, suggesting that EdeM has the potential to be the putative β-serine biosynthesis enzyme (McPhalen, Vincent, and Jansonius 1992). In contrast, DAHAA is considered unique to edeines, and no predictions exist for its biosynthesis. However, this lack of information underscores the importance of investigating the chemical biology and mechanistic enzymology underlying its biosynthesis.

Ultimately, delving deeper into β-amino acid biosynthesis in edeine could yield novel antibiotic scaffolds and enhance applications involving β-amino acids, spanning agriculture, peptide mimetics, and combinatorial chemistry.

Aims of This Work

As the number of drug-resistant bacteria rises and the discovery of novel antibiotics slows, understanding the multitude of environmental resistance elements becomes crucial for anticipating future clinical challenges. Moreover, enhancing antibiotic discovery requires removing obstacles and exploring various approaches, including revisiting previously overlooked antibiotics, and delving into antibiotic biosynthesis pathways, which may lead to new compounds of interest. The work presented in this thesis addresses challenges related to understanding antibiotic resistance, dereplication, and biosynthesis.

In **Chapter 1**, I investigated the possibility of an inactivating enzyme evolving to have specific activity against the fluoroquinolone synthetic antibiotic class. This inquiry stemmed from a recently published article by Chávez-Jacobo et al. (2018), which reported a novel ciprofloxacin-modifying enzyme encoded on a plasmid in *P. aeruginosa*. However, upon analyzing the data, doubts arose regarding the authenticity of this discovery. In response, I began systematically analyzing the presented data and repeated previously reported experimental methods that concluded that this enzyme did not modify ciprofloxacin. Subsequent work involved screening over 200 ciprofloxacin-resistant soil isolates for drug inactivation, yielding no significant results.

Chapter 2 focuses on improving the drug discovery pipeline, emphasizing antibiotic dereplication for phenotypic screening. Expanding on the original ARP

developed in the Wright lab, the minimal ARP was created to streamline the dereplication process using fewer strains covering more antibiotic classes. Additionally, efforts were made to enhance the accessibility of the ARP, resulting in its deposit in the Addgene plasmid repository for global access. By making this platform more accessible, we aim to facilitate antibiotic discovery. Moreover, to accommodate a high demand for requests to learn how to use the platform, this chapter is associated with a step-by-step video published in the Journal of Visualized Experiments, providing accurate instructions on dereplicating with the minimal ARP.

In **Chapter 3**, I began elucidating the mechanism of β-serine biosynthesis in edeines. This work involved extensive research on the structure, mechanism, characteristics, and properties of EdeM, the β-serine biosynthesis enzyme. I present in this chapter the first reports of β-serine biosynthesis in any organism and introduce the discovery of a pyridoxal 5' phosphate (PLP)-dependent enzyme class with unprecedented mechanistic chemistry and interactions with the PLP cofactor.

Lastly, **Chapter 4** will discuss this work's implications and future directions.

References

Abraham, E. P., & Chain, E. (1940). An Enzyme from Bacteria able to Destroy Penicillin. *Nature*, *146*(3713), 837–837.

Allen, H. K., Donato, J., Wang, H. H., Cloud-Hansen, K. A., Davies, J., & Handelsman, J. (2010). Call of the wild: antibiotic resistance genes in natural environments. *Nature Reviews. Microbiology*, *8*(4), 251–259.

Ayukekbong, J. A., Ntemgwa, M., & Atabe, A. N. (2017). The threat of antimicrobial resistance in developing countries: causes and control strategies. *Antimicrobial Resistance and Infection Control*, *6*, 47.

Beasley, F. C., Cheung, J., & Heinrichs, D. E. (2011). Mutation of L-2,3-diaminopropionic acid synthase genes blocks staphyloferrin B synthesis in Staphylococcus aureus. *BMC Microbiology*, *11*. https://doi.org/10.1186/1471-2180-11-199

Benveniste, R., & Davies, J. (1973). Aminoglycoside Antibiotic-Inactivating Enzymes in Actinomycetes Similar to Those Present in Clinical Isolates of Antibiotic-Resistant Bacteria. *Proceedings of the National Academy of Sciences*, *70*(8), 2276–2280.

Bérdy, J. (2005). Bioactive microbial metabolites. *The Journal of Antibiotics*, *58*(1), 1–26.

Bérdy, J. (2012). Thoughts and facts about antibiotics: Where we are now and where we are heading. *The Journal of Antibiotics*, *65*(8), 385–395.

Bhullar, K., Waglechner, N., Pawlowski, A., Koteva, K., Banks, E. D., Johnston, M. D., Barton, H. A., & Wright, G. D. (2012). Antibiotic resistance is prevalent in an isolated cave microbiome. *PloS One*, *7*(4), e34953.

Birmingham, M. C., Rayner, C. R., Meagher, A. K., Flavin, S. M., Batts, D. H., & Schentag, J. J. (2003). Linezolid for the treatment of multidrug-resistant, gram-positive infections: experience from a compassionate-use program. *Clinical Infectious Diseases: An Official Publication of the Infectious Diseases Society of America*, *36*(2), 159–168.

Blair, J. M. A., Webber, M. A., Baylay, A. J., Ogbolu, D. O., & Piddock, L. J. V. (2015). Molecular mechanisms of antibiotic resistance. *Nature Reviews. Microbiology*, *13*(1), 42–51.

Borowska, Z. K., & Tatum, E. L. (1966). Biosynthesis of edeine by Bacillus brevis Vm4 in vivo and in vitro. *BBA Section Nucleic Acids And Protein Synthesis*, *114*(1), 206–209.

Borowski, E., Chmara, H., & Jareczek-Morawska, E. (1966). The antibiotic edeine. VI. Paper and thin-layer chromatography of components of the edeine complex. *Biochimica et Biophysica Acta*, *130*(2), 560–563.

Brunel, J. (1951). Antibiosis from Pasteur to Fleming. *Journal of the History of Medicine and Allied Sciences*, *6*(3), 287–301.

Campbell, E. A., Korzheva, N., Mustaev, A., Murakami, K., Nair, S., Goldfarb, A., & Darst, S. A. (2001). Structural mechanism for rifampicin inhibition of bacterial rna polymerase. *Cell*, *104*(6), 901–912.

Chávez-jacobo, V. M., Hernández-ramírez, K. C., Romo-rodríguez, P., & Pérez-gallardo, R. V. (2018). *CrpP Is a Novel Ciprofloxacin-Modifying Enzyme Encoded by the Pseudomonas aeruginosa pUM505 Plasmid*. *62*(6), 1–11.

Chevrette, M. G., & Handelsman, J. (2021). Needles in haystacks: reevaluating old paradigms for the discovery of bacterial secondary metabolites. *Natural Product Reports*, *38*(11), 2083–2099.

Connell, S. R., Tracz, D. M., Nierhaus, K. H., & Taylor, D. E. (2003). Ribosomal protection proteins and their mechanism of tetracycline resistance. *Antimicrobial Agents and Chemotherapy*, *47*(12), 3675–3681.

Cook, M. A., & Wright, G. D. (2022). The past, present, and future of antibiotics. *Science Translational Medicine*, *14*(657), eabo7793.

Cox, G., Sieron, A., King, A. M., De Pascale, G., Pawlowski, A. C., Koteva, K., & Wright, G. D. (2017). A Common Platform for Antibiotic Dereplication and Adjuvant Discovery. *Cell Chemical Biology*, *24*(1), 98–109.

Cox, G., & Wright, G. D. (2013). Intrinsic antibiotic resistance: mechanisms, origins, challenges and solutions. *International Journal of Medical Microbiology: IJMM*, *303*(6–7), 287–292.

Cozzarelli, N. R. (1977). The mechanism of action of inhibitors of DNA synthesis. *Annual Review of Biochemistry*, *46*(c), 641–668.

Czerwinski, A., Wojciechowskra, H., Andruszkiewicz, R., Grzybowska, J., Gumieniak, J., & Borowski, E. (1983). Total synthesis of edeine D. *The Journal of Antibiotics*, *36*(8), 1001–1006.

D'Costa, V. M., King, C. E., Kalan, L., Morar, M., Sung, W. W. L., Schwarz, C., Froese, D., Zazula, G., Calmels, F., Debruyne, R., Golding, G. B., Poinar, H. N., & Wright, G. D. (2011). Antibiotic resistance is ancient. *Nature*, *477*(7365), 457–461.

D'Costa, V. M., McGrann, K. M., Hughes, D. W., & Wright, G. D. (2006). Sampling the antibiotic resistome. *Science*, *311*(5759), 374–377.

De Pascale, G., & Wright, G. D. (2010). Antibiotic resistance by enzyme inactivation: from mechanisms to solutions. *Chembiochem: A European Journal of Chemical Biology*, *11*(10), 1325–1334.

Dinos, G., Wilson, D. N., Teraoka, Y., Szaflarski, W., Fucini, P., Kalpaxis, D., & Nierhaus, K. H. (2004). Dissecting the ribosomal inhibition mechanisms of edeine and pactamycin: the universally conserved residues G693 and C795 regulate P-site RNA binding. *Molecular Cell*, *13*(1), 113–124.

Du, J., Zhang, C., Long, Q., Zhang, L., Chen, W., & Liu, Q. (2022). Characterization of a pathway-specific activator of edeine biosynthesis and improved edeine production by its overexpression in Brevibacillus brevis. *Frontiers in Plant Science*, *13*, 1022476.

Eisenstein, B. I., Oleson, F. B., Jr, & Baltz, R. H. (2010). Daptomycin: from the mountain to the clinic, with essential help from Francis Tally, MD. *Clinical Infectious Diseases: An Official Publication of the Infectious Diseases Society of America*, *50 Suppl 1*, S10-5.

Felnagle, E. A., Jackson, E. E., Chan, Y. A., Podevels, A. M., Berti, A. D., McMahon, M. D., & Thomas, M. G. (2008). Nonribosomal peptide synthetases involved in the production of medically relevant natural products. *Molecular Pharmaceutics*, *5*(2), 191–211.

Ford, C. W., Hamel, J. C., Stapert, D., Moerman, J. K., Hutchinson, D. K., Barbachyn, M. R., & Zurenko, G. E. (1997). Oxazolidinones: new antibacterial agents. *Trends in Microbiology*, *5*(5), 196–200.

Fritsche Thomas R., Castanheira Mariana, Miller George H., Jones Ronald N., & Armstrong Eliana S. (2008). Detection of Methyltransferases Conferring High-Level Resistance to Aminoglycosides in Enterobacteriaceae from Europe, North America, and Latin America. *Antimicrobial Agents and Chemotherapy*, *52*(5), 1843–1845.

Garreau De Loubresse, N., Prokhorova, I., Holtkamp, W., Rodnina, M. V., Yusupova, G., & Yusupov, M. (2014). Structural basis for the inhibition of the eukaryotic ribosome. *Nature*, *513*(7519), 517–522.

Hall, B. G., & Barlow, M. (2004). Evolution of the serine β-lactamases: past, present and future. *Drug Resistance Updates: Reviews and Commentaries in Antimicrobial and Anticancer Chemotherapy*, *7*(2), 111–123.

Hegemann, J. D., Birkelbach, J., Walesch, S., & Müller, R. (2023). Current developments in antibiotic discovery: Global microbial diversity as a source for evolutionary optimized anti-bacterials: Global microbial diversity as a source for evolutionary optimized anti-bacterials. *EMBO Reports*, *24*(1), e56184.

Hollenbeck, B. L., & Rice, L. B. (2012). Intrinsic and acquired resistance mechanisms in enterococcus. *Virulence*, *3*(5), 421–433.

Hollingshead, S. K., Becker, R., & Briles, D. E. (2000). Diversity of PspA: mosaic genes and evidence for past recombination in Streptococcus pneumoniae. *Infection and Immunity*, *68*(10), 5889–5900.

Hutchings, M. I., Truman, A. W., & Wilkinson, B. (2019). Antibiotics: past, present and future. *Current Opinion in Microbiology*, *51*, 72–80.

Ito, T., & Masubuchi, M. (2014). Dereplication of microbial extracts and related analytical technologies. *The Journal of Antibiotics*, *67*(5), 353–360.

Jacoby, G. A. (2009). AmpC beta-lactamases. *Clinical Microbiology Reviews*, *22*(1), 161–182, Table of Contents.

Kelly, J. A., Dideberg, O., Charlier, P., Wery, J. P., Libert, M., Moews, P. C., Knox, J. R., Duez, C., Fraipont, C., Joris, B., Dusart, J., Frère, J. M., & Ghuysen, J. M. (1986). On the Origin of Bacterial Resistance to Penicillin: Comparison of a β-Lactamase and a Penicillin Target. *Science*, *231*(4744), 1429–1431.

Khare, D., Ziegelin, G., Lanka, E., & Heinemann, U. (2004). Sequence-specific DNA binding determined by contacts outside the helix-turn-helix motif of the ParB homolog KorB. *Nature Structural & Molecular Biology*, *11*(7), 656–663.

Khatri, B., Nuthakki, V. R., & Chatterjee, J. (2019). Strategies to Enhance Metabolic Stabilities. *Methods in Molecular Biology* , *2001*, 17–40.

Kim, D.-W., Thawng, C. N., Lee, K., Wellington, E. M. H., & Cha, C.-J. (2019). A novel sulfonamide resistance mechanism by two-component flavin-dependent monooxygenase system in sulfonamide-degrading actinobacteria. *Environment International*, *127*, 206–215.

Koehbach, J., & Craik, D. J. (2019). The Vast Structural Diversity of Antimicrobial Peptides. *Trends in Pharmacological Sciences*, *40*(7), 517–528.

Koteva, K., Cox, G., Kelso, J. K., Surette, M. D., Zubyk, H. L., Ejim, L., Stogios, P., Savchenko, A., Sørensen, D., & Wright, G. D. (2018). Rox, a Rifamycin Resistance Enzyme with an Unprecedented Mechanism of Action. *Cell Chemical Biology*, *25*(4), 403-412.e5.

Kozak, M., & Shatkin, A. J. (1978). Migration of 40 S ribosomal subunits on messenger RNA in the presence of edeine. *The Journal of Biological Chemistry*, *253*(18), 6568–6577.

Kresge, N., Simoni, R. D., & Hill, R. L. (2004). Selman Waksman: the Father of Antibiotics. *The Journal of Biological Chemistry*, *279*(48), e7–e8.

Kudo, F., Miyanaga, A., & Eguchi, T. (2014). Biosynthesis of natural products containing β-amino acids. *Natural Product Reports*, *31*(8), 1056–1073.

Kumar, N., Radhakrishnan, A., Wright, C. C., Chou, T.-H., Lei, H.-T., Bolla, J. R., Tringides, M. L., Rajashankar, K. R., Su, C.-C., Purdy, G. E., & Yu, E. W. (2014). Crystal structure of the transcriptional regulator Rv1219c of Mycobacterium tuberculosis. *Protein Science: A Publication of the Protein Society*, *23*(4), 423–432.

Kurylo-Borowska, Z. (1975). Biosynthesis of eideine:: II. Localization of edeine synthetase within Bacillus brevis Vm4. *Biochimica et Biophysica Acta (BBA) - General Subjects*, *399*(1), 31–41.

Kurylo-Borowska, Z., & Szer, W. (1972). Inhibition of bacterial DNA synthesis by edeine. Effect on Escherichia coli mutants lacking DNA polymerase I. *Biochimica et Biophysica Acta*, *287*(2), 236–245.

Kurylo-Borowska, Zofia. (1964). On the mode of action of edeine effect of edeine on the bacterial DNA. *Biochimica et Biophysica Acta (BBA) - Specialized Section on Nucleic Acids and Related Subjects*, *87*(2), 305–313.

Langlykke, A. (1980). CRC Handbook of antibiotic compound (IV), Edited by Bardy J et al. *CRC, Boca Raton, FL*.

Larsson, D. G. J., & Flach, C.-F. (2022). Antibiotic resistance in the environment. *Nature Reviews. Microbiology*, *20*(5), 257–269.

Latham, P. W. (1999). Therapeutic peptides revisited. *Nature Biotechnology*, *17*(8), 755–757.

Lewis, K. (2012). Antibiotics: Recover the lost art of drug discovery. *Nature*, *485*(7399), 439–440.

Lewis, K. (2013). Platforms for antibiotic discovery. *Nature Reviews. Drug Discovery*, *12*(5), 371–387.

Lewis, K. (2017). New approaches to antimicrobial discovery. *Biochemical Pharmacology*, *134*, 87–98.

Li, M.-C., Lu, J., Lu, Y., Xiao, T.-Y., Liu, H.-C., Lin, S.-Q., Xu, D., Li, G.-L., Zhao, X.-Q., Liu, Z.-G., Zhao, L.-L., & Wan, K.-L. (2021). rpoB Mutations and Effects on Rifampin Resistance in Mycobacterium tuberculosis. *Infection and Drug Resistance*, *14*, 4119–4128.

Livermore, D. M. (2008). Defining an extended-spectrum beta-lactamase. *Clinical Microbiology and Infection: The Official Publication of the European Society of Clinical Microbiology and Infectious Diseases*, *14 Suppl 1*, 3–10.

Lobanovska, M., & Pilla, G. (2017). Penicillin's Discovery and Antibiotic Resistance: Lessons for the Future? *The Yale Journal of Biology and Medicine*, *90*(1), 135–145.

Long, K. S., Poehlsgaard, J., Kehrenberg, C., Schwarz, S., & Vester, B. (2006). The Cfr rRNA methyltransferase confers resistance to phenicols, Lincosamides, oxazolidinones, pleuromutilins, and streptogramin A antibiotics. *Antimicrobial Agents and Chemotherapy*, *50*(7), 2500–2505.

Lu, W., Li, K., Huang, J., Sun, Z., Li, A., Liu, H., Zhou, D., Lin, H., Zhang, X., Li, Q., Lu, J., Lin, X., Li, P., Zhang, H., Xu, T., & Bao, Q. (2021). Identification and characteristics of a novel aminoglycoside phosphotransferase, APH(3')-IId, from an MDR clinical isolate of Brucella intermedia. *The Journal of Antimicrobial Chemotherapy*, *76*(11), 2787–2794.

Marshall, C. G., Lessard, I. A., Park, I., & Wright, G. D. (1998). Glycopeptide antibiotic resistance genes in glycopeptide-producing organisms. *Antimicrobial Agents and Chemotherapy*, *42*(9), 2215–2220.

Massova, I., & Mobashery, S. (1998). Kinship and diversification of bacterial penicillin-binding proteins and beta-lactamases. *Antimicrobial Agents and Chemotherapy*, *42*(1), 1–17.

McClary, B., Zinshteyn, B., Meyer, M., Jouanneau, M., Pellegrino, S., Yusupova, G., Schuller, A., Reyes, J. C. P., Lu, J., Guo, Z., Ayinde, S., Luo, C., Dang, Y., Romo, D., Yusupov, M., Green, R., & Liu, J. O. (2017). Inhibition of Eukaryotic Translation by the Antitumor Natural Product Agelastatin A. *Cell Chemical Biology*, *24*(5), 605-613.e5.

McPhalen, C. A., Vincent, M. G., & Jansonius, J. N. (1992). X-ray structure refinement and comparison of three forms of mitochondrial aspartate aminotransferase. *Journal of Molecular Biology*, *225*(2), 495–517.

Medema, M. H., Kottmann, R., Yilmaz, P., Cummings, M., Biggins, J. B., Blin, K., de Bruijn, I., Chooi, Y. H., Claesen, J., Coates, R. C., Cruz-Morales, P., Duddela, S., Düsterhus, S., Edwards, D. J., Fewer, D. P., Garg, N., Geiger, C., Gomez-Escribano, J. P., Greule, A., … Glöckner, F. O. (2015). Minimum Information about a Biosynthetic Gene cluster. *Nature Chemical Biology*, *11*(9), 625–631.

Meng, H., & Kumar, K. (2007). Antimicrobial activity and protease stability of peptides containing fluorinated amino acids. *Journal of the American Chemical Society*, *129*(50), 15615–15622.

Miller, B. R., & Gulick, A. M. (2016). Structural Biology of Nonribosomal Peptide Synthetases. *Methods in Molecular Biology* , *1401*, 3–29.

Morar, M., & Wright, G. D. (2010). The genomic enzymology of antibiotic resistance. *Annual Review of Genetics*, *44*, 25–51.

Munita, J. M., & Arias, C. A. (2016). Mechanisms of Antibiotic Resistance. *Microbiology Spectrum*, *4*(2). https://doi.org/10.1128/microbiolspec.VMBF-0016-2015

Neu, H. C. (1992). The crisis in antibiotic resistance. *Science*, *257*(5073), 1064–1073.

Nivina, A., Yuet, K. P., Hsu, J., & Khosla, C. (2019). Evolution and Diversity of Assembly-Line Polyketide Synthases. *Chemical Reviews*, *119*(24), 12524–12547.

Norris, A. L., & Serpersu, E. H. (2013). Ligand promiscuity through the eyes of the aminoglycoside N3 acetyltransferase IIa. *Protein Science: A Publication of the Protein Society*, *22*(7), 916–928.

Pang, Z., Raudonis, R., Glick, B. R., Lin, T.-J., & Cheng, Z. (2019). Antibiotic resistance in Pseudomonas aeruginosa: mechanisms and alternative therapeutic strategies. *Biotechnology Advances*, *37*(1), 177–192.

Parry, R. J., & Kurylo-Borowska, Z. (1980). Biosynthesis of amino acids. Investigation of the mechanism of .beta.-tyrosine formation. *Journal of the American Chemical Society*, *102*(2), 836–837.

Patočka, J. (2011). B-Amino Acids and Their Natural Biologically Active Derivatives. 5. Derivatives of Unusual Alicyclic and Heterocyclic B-Amimo. *Military Medical Science*, *80*(44), 2–11.

Paul, D., Sanap, G., Shenoy, S., Kalyane, D., Kalia, K., & Tekade, R. K. (2021). Artificial intelligence in drug discovery and development. *Drug Discovery Today*, *26*(1), 80–93.

Pawlowski, A. C., Wang, W., Koteva, K., Barton, H. A., McArthur, A. G., & Wright, G. D. (2016). A diverse intrinsic antibiotic resistome from a cave bacterium. *Nature Communications*, *7*, 13803.

Payne, D. J., Miller, L. F., Findlay, D., Anderson, J., & Marks, L. (2015). Time for a change: addressing R&D and commercialization challenges for antibacterials. *Philosophical Transactions of the Royal Society of London. Series B, Biological Sciences*, *370*(1670), 20140086.

Pioletti, M., Schlünzen, F., Harms, J., Zarivach, R., Glühmann, M., Avila, H., Bashan, A., Bartels, H., Auerbach, T., Jacobi, C., Hartsch, T., Yonath, A., & Franceschi, F. (2001). Crystal structures of complexes of the small ribosomal subunit with tetracycline, edeine and IF3. *The EMBO Journal*, *20*(8), 1829–1839.

Poirel, L., Rodriguez-Martinez, J.-M., Mammeri, H., Liard, A., & Nordmann, P. (2005). Origin of plasmid-mediated quinolone resistance determinant QnrA. *Antimicrobial Agents and Chemotherapy*, *49*(8), 3523–3525.

Ramirez, M. S., & Tolmasky, M. E. (2010). Aminoglycoside modifying enzymes. *Drug Resistance Updates: Reviews and Commentaries in Antimicrobial and Anticancer Chemotherapy*, *13*(6), 151–171.

Reygaert, W. C. (2018). An overview of the antimicrobial resistance mechanisms of bacteria. *AIMS Microbiology*, *4*(3), 482–501.

Rodríguez-Martínez, J. M., Cano, M. E., Velasco, C., Martínez-Martínez, L., & Pascual, A. (2011). Plasmid-mediated quinolone resistance: an update. *Journal of Infection and Chemotherapy: Official Journal of the Japan Society of Chemotherapy*, *17*(2), 149–182.

Schaenzer, A. J., & Wright, G. D. (2020). Antibiotic Resistance by Enzymatic Modification of Antibiotic Targets. *Trends in Molecular Medicine*, *26*(8), 768–782.

Sköld, O. (2000). Sulfonamide resistance: mechanisms and trends. *Drug Resistance Updates: Reviews and Commentaries in Antimicrobial and Anticancer Chemotherapy*, *3*(3), 155–160.

Slee A M, Wuonola M A, McRipley R J, Zajac I, Zawada M J, Bartholomew P T, Gregory W A, & Forbes M. (1987). Oxazolidinones, a new class of synthetic antibacterial agents: in vitro and in vivo activities of DuP 105 and DuP 721. *Antimicrobial Agents and Chemotherapy*, *31*(11), 1791–1797.

Sreejith, S., Shajahan, S., Prathiush, P. R., Anjana, V. M., Mathew, J., Aparna, S., Abraham, S. S., & Radhakrishnan, E. K. (2022). Rapid detection of mobile resistance genes tetA and tetB from metaplasmid isolated from healthy broiler feces. *Microbial Pathogenesis*, *166*, 105504.

Stekel, D. (2018). First report of antimicrobial resistance pre-dates penicillin. *Nature*, *562*(7726), 192.

Surette, M. D., Waglechner, N., Koteva, K., & Wright, G. D. (2022). HelR is a helicase-like protein that protects RNA polymerase from rifamycin antibiotics. *Molecular Cell*, *82*(17), 3151-3165.e9.

Surette, M. D., & Wright, G. D. (2017). Lessons from the Environmental Antibiotic Resistome. *Annual Review of Microbiology*, *71*, 309–329.

Swain, S. S., Sharma, D., Hussain, T., & Pati, S. (2020). Molecular mechanisms of underlying genetic factors and associated mutations for drug resistance in Mycobacterium tuberculosis. *Emerging Microbes & Infections*, *9*(1), 1651–1663.

Swaney Steve M., Aoki Hiroyuki, Ganoza M. Clelia, & Shinabarger Dean L. (1998). The Oxazolidinone Linezolid Inhibits Initiation of Protein Synthesis in Bacteria. *Antimicrobial Agents and Chemotherapy*, *42*(12), 3251–3255.

Szer, W., & Kurylo-Borowska, Z. (1970). Effect of edeine on aminoacyl-tRNA binding to ribosomes and its relationship to ribosomal binding sites. *BBA Section Nucleic Acids And Protein Synthesis*, *224*(2), 477–486.

Takagi, M., & Shin-Ya, K. (2012). Construction of a natural product library containing secondary metabolites produced by actinomycetes. *The Journal of Antibiotics*, *65*(9), 443–447.

Tally, F. P., Zeckel, M., Wasilewski, M. M., Carini, C., Berman, C. L., Drusano, G. L., & Oleson, F. B., Jr. (1999). Daptomycin: a novel agent for Gram-positive infections. *Expert Opinion on Investigational Drugs*, *8*(8), 1223–1238.

Taylor, S. D., & Palmer, M. (2016). The action mechanism of daptomycin. *Bioorganic & Medicinal Chemistry*, *24*(24), 6253–6268.

Tommasi, R., Brown, D. G., Walkup, G. K., Manchester, J. I., & Miller, A. A. (2015). ESKAPEing the labyrinth of antibacterial discovery. *Nature Reviews. Drug Discovery*, *14*(8), 529–542.

Tooke, C. L., Hinchliffe, P., Bragginton, E. C., Colenso, C. K., Hirvonen, V. H. A., Takebayashi, Y., & Spencer, J. (2019). β-Lactamases and β-Lactamase Inhibitors in the 21st Century. *Journal of Molecular Biology*, *431*(18), 3472–3500.

Torrens, G., Hernández, S. B., Ayala, J. A., Moya, B., Juan, C., Cava, F., & Oliver, A. (2019). Regulation of AmpC-Driven β-Lactam Resistance in Pseudomonas aeruginosa: Different Pathways, Different Signaling. *MSystems*, *4*(6). https://doi.org/10.1128/mSystems.00524-19

Tsuchido, T., & Takano, M. (1988). Sensitization by heat treatment of Escherichia coli K-12 cells to hydrophobic antibacterial compounds. *Antimicrobial Agents and Chemotherapy*, *32*(11), 1680–1683.

Unemo, M., Golparian, D., Nicholas, R., Ohnishi, M., Gallay, A., & Sednaoui, P. (2012). High-level cefixime- and ceftriaxone-resistant Neisseria gonorrhoeae in France: novel penA mosaic allele in a successful international clone causes treatment failure. *Antimicrobial Agents and Chemotherapy*, *56*(3), 1273–1280.

Valiquette, L., & Laupland, K. B. (2015). Digging for new solutions. *The Canadian Journal of Infectious Diseases & Medical Microbiology = Journal Canadien Des Maladies Infectieuses et de La Microbiologie Medicale / AMMI Canada*, *26*(6), 289–290.

Van Middlesworth, F., & Cannell, R. J. P. (1998). Dereplication and Partial Identification of Natural Products. In R. J. P. Cannell (Ed.), *Natural Products Isolation* (pp. 279–327). Humana Press.

Velilla, J. A., Volpe, M. R., Kenney, G. E., Walsh, R. M., Jr, Balskus, E. P., & Gaudet, R. (2023). Structural basis of colibactin activation by the ClbP peptidase. *Nature Chemical Biology*, *19*(2), 151–158.

Ventola, C. L. (2015). The antibiotic resistance crisis: part 1: causes and threats. *P & T: A Peer-Reviewed Journal for Formulary Management*, *40*(4), 277–283.

Vetting, M. W., Chi, H. P., Hegde, S. S., Jacoby, G. A., Hooper, D. C., & Blanchard, J. S. (2008). Mechanistic and structural analysis of aminoglycoside N-acetyltransferase AAC(6′)-Ib and its bifunctional, fluoroquinolone-active AAC(6′)-Ib-cr variant. *Biochemistry*, *47*(37), 9825–9835.

Vetting, M. W., Hegde, S. S., Wang, M., Jacoby, G. A., Hooper, D. C., & Blanchard, J. S. (2011). Structure of QnrB1, a plasmid-mediated fluoroquinolone resistance factor. *The Journal of Biological Chemistry*, *286*(28), 25265–25273.

Viswanathan, V. K. (2014). Off-label abuse of antibiotics by bacteria. *Gut Microbes*, *5*(1), 3–4.

Volkers, G., Palm, G. J., Weiss, M. S., Wright, G. D., & Hinrichs, W. (2011). Structural basis for a new tetracycline resistance mechanism relying on the TetX monooxygenase. *FEBS Letters*, *585*(7), 1061–1066.

Volpe, M. R., Velilla, J. A., Daniel-Ivad, M., Yao, J. J., Stornetta, A., Villalta, P. W., Huang, H.-C., Bachovchin, D. A., Balbo, S., Gaudet, R., & Balskus, E. P. (2023). A small molecule inhibitor prevents gut bacterial genotoxin production. *Nature Chemical Biology*, *19*(2), 159–167.

Waglechner, N., Culp, E. J., & Wright, G. D. (2021). Ancient Antibiotics, Ancient Resistance. *EcoSal Plus*, *9*(2). https://doi.org/10.1128/ecosalplus.ESP-0027-2020

Walsh, C. T. (2016). Insights into the chemical logic and enzymatic machinery of NRPS assembly lines. *Natural Product Reports*, *33*(2), 127–135.

Westman, E. L., Yan, M., Waglechner, N., Koteva, K., & Wright, G. D. (2013). Self Resistance to the Atypical Cationic Antimicrobial Peptide Edeine of Brevibacillus brevis Vm4 by the N-Acetyltransferase EdeQ. *Chemistry & Biology*, *20*(8), 983–990.

Wright, G. D. (2005). Bacterial resistance to antibiotics: enzymatic degradation and modification. *Advanced Drug Delivery Reviews*, *57*(10), 1451–1470.

Wright, G. D. (2014). Something old, something new: revisiting natural products in antibiotic drug discovery. *Canadian Journal of Microbiology*, *60*(3), 147–154.

Yang, K., Fen, J., Fang, H., Zhang, L., Gong, J., & Xu, W. (2012). Synthesis of a novel series of L-isoserine derivatives as aminopeptidase N inhibitors. *Journal of Enzyme Inhibition and Medicinal Chemistry*, *27*(2), 302–310.

Yang, W., Moore, I. F., Koteva, K. P., Bareich, D. C., Hughes, D. W., & Wright, G. D. (2004). TetX is a flavin-dependent monooxygenase conferring resistance to tetracycline antibiotics. *The Journal of Biological Chemistry*, *279*(50), 52346–52352.

Zubyk, H. L., Cox, G., & Wright, G. D. (2019). Antibiotic Dereplication Using the Antibiotic Resistance Platform. *Journal of Visualized Experiments: JoVE*, *152*. https://doi.org/10.3791/60536

CHAPTER 2: Ciprofloxacin-Inactivating Enzymes

Preface

The work presented in this chapter was previously published in:

Zubyk HL, Wright GD. (2021). CrpP Is Not a Fluoroquinolone-Inactivating Enzyme. *Antimicrob Agents Chemother*. 65(8):e0077321. doi: 10.1128/AAC.00773-21.

The publisher has granted permission to reproduce the material herein.

H.L.Z. performed all experiments. H.L.Z. and G.D.W. conceived the experiments and wrote the manuscript.

Note: While not a part of the published manuscript, a materials and methods section has been added to this chapter to complete scientific records.

Approximately one year into my graduate studies, Chávez-Jacobo et al. (2018) published an article titled "CrpP is a Novel Ciprofloxacin-Modifying Enzyme Encoded by the *Pseudomonas aeruginosa* pUM505 Plasmid". In this publication, the authors claim to have identified a new ciprofloxacin phosphotransferase. As detailed in the introduction chapter of this thesis, enzyme-mediated inactivation of synthetic antibiotics is considered exceptionally rare, making this publication particularly intriguing due to its novelty. However, upon reviewing the article, it became evident that the presented data did not support the unprecedented claims. Several subsequent publications building upon the findings of the initial paper by Chávez-Jacobo et al. (2018) were later identified, indicating the rapid dissemination of this claim, which we considered to be based on weak evidence. Given the unprecedented report of ciprofloxacin phosphorylation, we set out to rigorously analyze this enzyme. Initially conceived as a side project, investigating this narrative posed a significant challenge, requiring approximately three years of effort to amass sufficient evidence to demonstrate unequivocally that CrpP has no ciprofloxacin inactivation activity.

While the publication featured in this chapter is complete, it underscores the challenges inherent in understanding antibiotic resistance and working with negative data. Although we were confident in our findings, convincing others that a previously reported resistance enzyme did not, in fact, confer resistance proved to be challenging, needing to mitigate any doubts that could be raised regarding the adequacy of our experimental procedures. It is important to note that several experiments were omitted from this narrative due to obstacles associated with working with CrpP. Nonetheless, the publication of this narrative has effectively corrected the propagation of CrpP misinformation and rectified the prevailing scientific literature.

I initiated efforts to identify a genuine ciprofloxacin-inactivating enzyme to expand on this research. Working with soil samples collected from various locations, including Nova Scotia, California, the Ugbawka village in Nigeria, and Cancun and Acapulco, Mexico, I prepared soil dilution plates supplemented with antifungals and varying concentrations of ciprofloxacin. These plates were then incubated at 30°C, and bacterial colonies were periodically selected over a week to isolate both fast-growing and slow-growing bacteria. Using this method, I successfully isolated over 200 ciprofloxacin-resistant soil bacteria.

Each isolate was subjected to an agar plug assay (**Schematic 1**) to identify strains conferring ciprofloxacin resistance through inactivation rather than other mechanisms. Initially, resistant isolates were cultured on solid media containing ciprofloxacin for a week. Subsequently, plugs from these isolates' plates were transferred onto solid media plates streaked with the indicator strain *Staphylococcus epidermidis*. The ability of a resistant

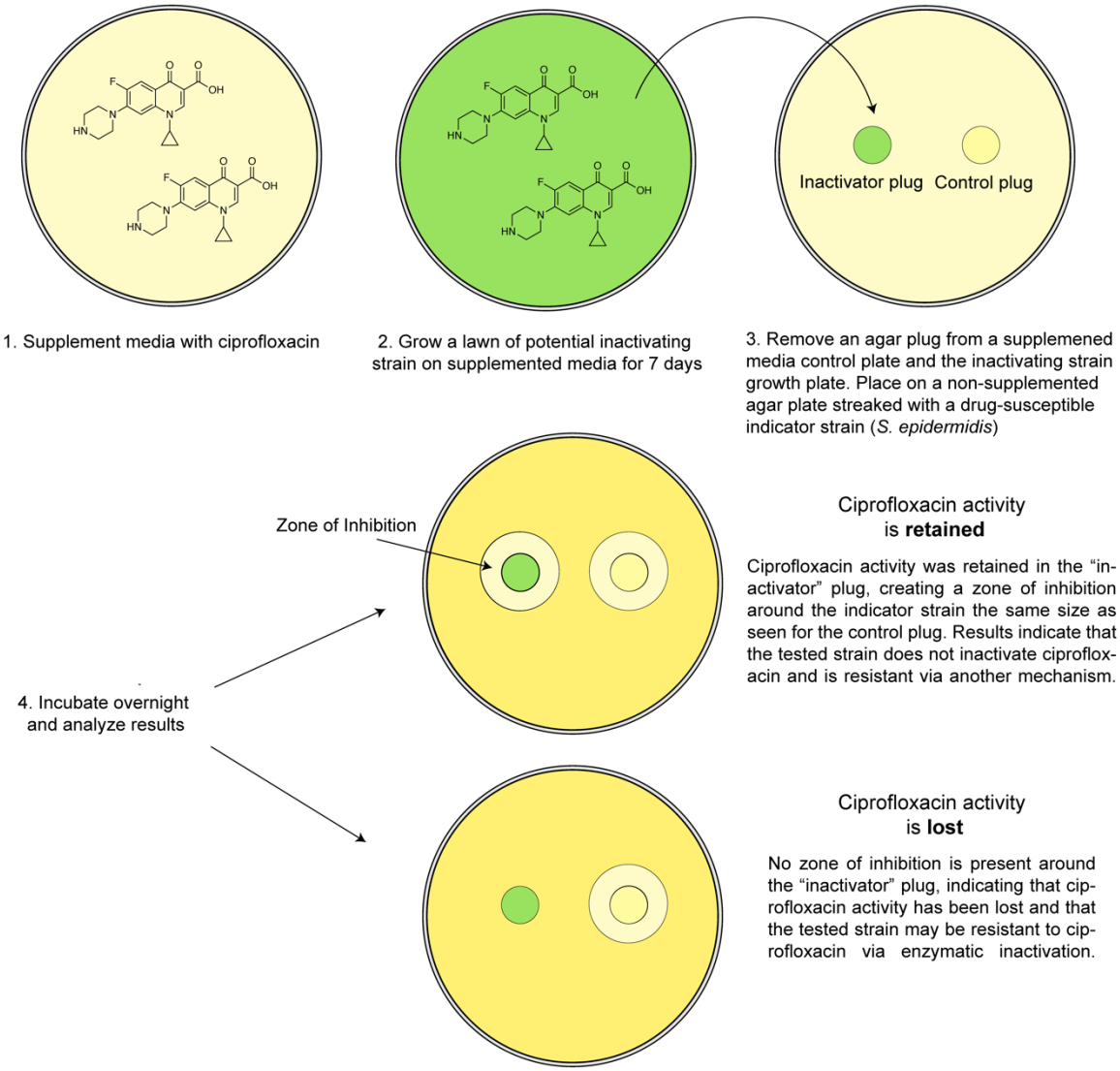

SCHEMATIC 2. Agar plug assays. Schematic of the agar plug assay method used to identify strains capable of inactivating ciprofloxacin.

strain to inactivate ciprofloxacin was gauged by its capacity to nullify the antimicrobial activity of ciprofloxacin in the media on which it initially grew and, consequently, the agar plug placed on *S. epidermidis*. Agar plugs containing potentially inactivated ciprofloxacin yielded either zones of inhibition on the indicator strain with a smaller diameter than control plugs containing unmodified ciprofloxacin or no zone of inhibition at all. Reduced inhibition zone sizes suggested a lower concentration of ciprofloxacin in the agar plug, indicating that the resistant isolate owed its activity to drug inactivation rather than other mechanisms, like antibiotic efflux or target protection, that would not remove the drug from the media.

Following this protocol, one promising strain was identified – Ciprofloxacin Inactivator 36 (CI36). CI36 demonstrated the ability to eliminate ciprofloxacin from solid and liquid media up to 50 μg/mL. Through 16S sequencing, this strain was identified as a *Streptomyces viridochromogenes* sp. from Acapulco, Mexico. To identify the gene(s) responsible for this activity, I constructed a genomic library from CI36 in *E. coli* to isolate ciprofloxacin-resistant clones that could be sequenced to uncover the novel ciprofloxacin-inactivating enzyme. Despite extensive efforts, this approach yielded only clones overexpressing broad-spectrum efflux pumps that conferred low-level resistance, proving unsuccessful in identifying the target gene(s).

In a newly devised approach to identify the genes responsible for inactivation, we employed activity-guided purification of the inactivating enzyme using ammonium sulfate to generate various lysate fractions of CI36. These fractions were subsequently evaluated for activity by introducing ciprofloxacin and analyzing the reaction contents via high-

performance liquid chromatography (HPLC). While a decrease in ciprofloxacin concentration was observed in whole-cell lysate fractions, this activity was lost upon removing insoluble material from the lysate. Moreover, HPLC analysis of the active whole-cell lysate fraction did not reveal the appearance of any new peaks, which would typically indicate drug modification or breakdown of ciprofloxacin into new fragments. Consequently, these results made it unclear what was happening to the antibiotic.

Given that only cell-based experiments, such as the agar plug assay and whole-cell lysate reactions, showed a complete loss of activity without any detectable traces of modified ciprofloxacin, our next hypothesis was that ciprofloxacin might be either binding to the cell or becoming trapped inside it. To test this hypothesis, we conducted a final experiment involving the growth of CI36 in liquid media supplemented with ciprofloxacin. After overnight incubation, we separated the supernatant from the pellet through centrifugation. Subsequent disk diffusion assays again confirmed the absence of antibiotic activity in the supernatant. However, we then extracted the cell pellet with dimethyl sulfoxide (DMSO) to recover all metabolites that might be bound inside or to the cell, including any possible modified ciprofloxacin species insoluble in water. The cell pellet DMSO extract was then tested for activity via disk diffusion assay, revealing the restoration of ciprofloxacin activity. We analyzed both the supernatant and the cell pellet extract via high-resolution mass spectrometry, confirming the absence of ciprofloxacin in the supernatant and the presence of concentrated, unmodified ciprofloxacin in the cell pellet extract.

Disappointingly, these findings revealed that while CI36 seemed to nullify ciprofloxacin activity in both liquid and solid media, this effect was not attributable to drug inactivation but rather to the cell acting akin to a ciprofloxacin ‘sponge’, eliminating all drug activity from cell culture supernatant and solid media. Though this phenotype was intriguing, no further exploration was pursued into this mechanism of ciprofloxacin retention and resistance. These outcomes underscore the improbability of identifying synthetic antibiotic-inactivating enzymes and affirm our initial doubts regarding CrpP's role as a ciprofloxacin-modifying enzyme.

CrpP is Not a Fluoroquinolone-Inactivating Enzyme

Enzyme-mediated antibiotic inactivation is a common mechanism of drug resistance in bacteria (De Pascale and Wright 2010). The genes encoding these resistance proteins are frequently associated with mobile elements, making them particularly concerning due to their propensity for horizontal transfer through bacterial populations. Given the specificity of enzymes for their substrates, which has often coevolved with antibiotic production over millennia (Waglechner, McArthur, and Wright 2019), it is not surprising that natural-product antibiotics and their semisynthetic derivatives are particularly vulnerable to enzymatic inactivation. Various hydrolases (β-lactams), kinases (aminoglycosides and macrolides), nucleotidyltransferases (lincosamides and aminoglycosides), acyltransferases (chloramphenicol and aminoglycosides), oxygenases (tetracyclines and rifamycins), and many others are known. In contrast, enzyme-mediated inactivation of synthetic antibiotics is rare. Examples include monooxygenase-mediated inactivation of sulfonamides by soil bacteria (Kim et al. 2019) and coopting of an aminoglycoside acetyltransferase, AAC(6′)-Ib-cr, for the modification of fluoroquinolone antibiotics containing a piperazine moiety with a free secondary amine, such as ciprofloxacin (CIP) and norfloxacin (Robicsek et al. 2006; Vetting et al. 2008).

The 2018 report of a novel ciprofloxacin-inactivating enzyme, CrpP, encoded by a gene located on plasmid pUM505 in *Pseudomonas aeruginosa* (Chávez-jacobo et al. 2018), is therefore highly unusual. The *crpP* gene is predicted to encode a small, 65-amino-acid protein sharing sequence similarity with a short region of an aminoglycoside phosphotransferase (APH) from *Mycobacterium smegmatis* and an APH(3′)-IIb from *P.*

aeruginosa M18. CrpP possesses Gly7 and Ile26, conserved residues in APH enzymes with roles in catalysis and ATP binding, respectively. This similarity prompted the hypothesis that CrpP was a fluoroquinolone phosphotransferase. Purification of the protein followed by enzyme assays using the canonical coupled pyruvate kinase/lactate dehydrogenase assay for ADP release showed concentration-dependent saturable activity with ciprofloxacin and ATP, consistent with enzyme activity. Mass spectrometry of CrpP-inactivated ciprofloxacin identified many signals interpreted as being the initial formation of a ciprofloxacin-ATP adduct (covalently linked through the carboxyl of ciprofloxacin and the γ-phosphate of ATP). The plasmid pUM505 harboring *crpP* confers a 2-fold (levofloxacin) to 8-fold (moxifloxacin) increase in the fluoroquinolone MIC in *P. aeruginosa* PAO1 compared to *P. aeruginosa* ATCC 27853. The MICs for ciprofloxacin and norfloxacin were increased 4-fold (0.5 to 2.0 μg/ml). Paradoxically, the expression of *crpP* on the high-copy-number plasmid pUCP20 in *P. aeruginosa* PAO1 had either no effect (ciprofloxacin and norfloxacin) or a 2-fold increase (levofloxacin and moxifloxacin) in the MIC compared to *P. aeruginosa* ATCC 27853. The expression of pUC:*crpP* in *Escherichia coli* did not affect the MICs of some fluoroquinolones (norfloxacin, levofloxacin, and moxifloxacin) and had a modest 2-fold effect (0.004 μg/ml increased to 0.008 μg/ml) for ciprofloxacin.

We were intrigued by this discovery given the rarity of enzymes inactivating synthetic antibiotics, especially in clinical strains. We did, however, have questions about the initial hypothesis. The region of protein similarity between CrpP and the *M. smegmatis* kinase shown by those authors is in a part of APH enzymes that has some minor overlap with the Mg^{2+} binding site but is not directly involved in catalysis or ATP binding.

Those authors also noted that CrpP shows similarity to a 79-amino-acid APH(3)-IIb from *P. aeruginosa* M18 (Wu et al. 2011). However, this protein (GenBank accession no. AEO73307.1) lacks the requisite amino acid residues for phosphotransfer (Wright and Thompson 1999) and is likely a pseudogene. Indeed, the authors of the *P. aeruginosa* M18 genome sequence report noted that the isolate was more susceptible to kanamycin than other strains (Wu et al. 2011). A second APH in this genome (GenBank accession no. AEO75667.1) shows homology to the APH(3′) streptomycin/spectinomycin kinase family, has the necessary active-site residues for kinase activity, and is likely responsible for the spectinomycin resistance phenotype of *P. aeruginosa* M18. The similarity of CrpP with APHs is therefore tenuous.

Similarly, the mass spectrometry results in Fig. 4 of the original CrpP publication (Chávez-jacobo et al. 2018) are challenging to interpret. The transfer of a phosphate from ATP to antibiotics or other substrates such as proteins generally occurs through nucleophilic attack of the phosphate acceptor on the γ-phosphate (or occasionally on the β-phosphate via the transfer of pyrophosphate followed by hydrolysis to generate the monophosphorylated product (Wright and Thompson 1999)). The mass spectrum interpretation reported a chemically unprecedented ciprofloxacin-ATP adduct linked by the carboxyl of the antibiotic and the γ-phosphate of ATP, which is highly unlikely. Those authors suggest that this adduct decomposes to the ciprofloxacin acyl-phosphate. Again, this compound is predicted to be highly chemically unstable and may not be detectable in the mass spectrum. Indeed, we have attempted to synthesize this molecule, even under anhydrous conditions, without success.

Since the discovery of CrpP, Chavez-Jacobo et al. have delved deeper into understanding this novel resistance element. In 2018, they began by searching for homologous *crpP* genes in extended-spectrum-β-lactamase (ESBL)-producing transconjugants and clinical isolates of *Enterobacteriaceae* in Mexican hospitals (Hernández-Ramírez et al. 2018). Sequence analysis of the homologs revealed that *crpP*-like genes contain the conserved residues Gly7, Thr8, Asp9, Lys33, Gly34, and Cys40. Mutagenesis experiments later confirmed that Gly7, Asp9, and Lys33 are involved in ATP binding in the N-terminal region and that Cys40 is a CrpP-specific conserved C-terminal residue essential for activity (Chávez-jacobo et al. 2018). Comparatively, Ortiz de la Rosa et al. (2020) identified four CrpP homologs (CrpP2, CrpP3, CrpP4, and CrpP5) across *P. aeruginosa* clinical isolates from Europe, and sequence analysis revealed that each of these proteins has a missense mutation in the previously reported "essential catalytic residue" Gly7. To measure the activity of these homologs compared to CrpP, each gene was cloned into the shuttle vector pUCp24 and transformed into *Escherichia coli* TOP10. All homologs were found to modestly decrease ciprofloxacin susceptibility except for CrpP1 (the original CrpP), which had no activity against the drug (Ortiz de la Rosa, Nordmann, and Poirel 2020). No such effect was detected in *P. aeruginosa* PAO1. These conflicting results suggest that Gly7 is, in fact, nonessential for enzymatic activity and that CrpP may utilize a different mechanism of action than previously reported. To further complicate the CrpP literature, Hernandez-Garcia et al. (2021) recently reported two additional homologs (CrpP6 and CrpP7) in *P. aeruginosa* clinical isolates from Spain and Portugal. Susceptibility assays against a number of clinical isolates expressing the

various *crpP* genes determined that CrpP7 is the only homolog associated with a decrease in ciprofloxacin susceptibility. It was hypothesized that this result reflected the presence of a missense mutation in the catalytic residue Gly7 in CrpP2 to CrpP6 that is absent in CrpP and CrpP7. Those authors concluded that the presence of *crpP* genes is not always associated with ciprofloxacin resistance, but the central hypothesis that CrpP is a ciprofloxacin kinase remains unchallenged.

Drug and Strain	Presence of 0.5 mM IPTG	MIC (μg/mL)
Moxifloxacin		
E. coli BL21(DE3)/pET28a:*crpP*	+	0.0156
E. coli BL21(DE3)/pET28a:*crpP*	-	0.0156-0.0312
E. coli BL21(DE3)/pET28a	+	0.0156
E. coli BL21(DE3)/pET28a	-	0.0156
Levofloxacin		
E. coli BL21(DE3)/pET28a:*crpP*	+	0.0156
E. coli BL21(DE3)/pET28a:*crpP*	-	0.0156
E. coli BL21(DE3)/pET28a	+	0.0156
E. coli BL21(DE3)/pET28a	-	0.0078
Norfloxacin		
E. coli BL21(DE3)/pET28a:*crpP*	+	0.0312
E. coli BL21(DE3)/pET28a:*crpP*	-	0.0312
E. coli BL21(DE3)/pET28a	+	0.0312
E. coli BL21(DE3)/pET28a	-	0.0312

Ciprofloxacin		
E. coli BL21(DE3)/pET28a:*crpP*	+	0.0039
E. coli BL21(DE3)/pET28a:*crpP*	-	0.0039-0.0078
E. coli BL21(DE3)/pET28a	+	0.0039
E. coli BL21(DE3)/pET28a	-	0.0039-0.0078

TABLE 1. MICs for *E. coli* BL21(DE3)/pET28a:*crpP* and *E. coli* BL21(DE3)/pET28a in the presence and absence of 0.5 mM IPTG

Given the conflicting results and questions associated with these reports, we revisited the analysis of CrpP. We synthesized the original gene for expression in *E. coli*. Several cloning attempts into our standard pGDP vectors (constitutive *lac* and *bla* promoters) used to express resistance genes (Cox et al. 2017) resulted in the selection for *crpP* alleles with various mutations, suggesting that the gene product may be toxic. We successfully overexpressed the protein in *E. coli* BL21(DE3)/pET28a:*crpP* to suppress expression in the absence of isopropyl-β-d-thiogalactopyranoside (IPTG). We measured the susceptibility to ciprofloxacin, levofloxacin, norfloxacin, and moxifloxacin in the presence of 0.5 mM IPTG by broth microdilution studies but could not detect resistance (**Table 1**). We also measured ciprofloxacin resistance by an Etest, with the same result (not shown). We next overexpressed the protein for purification using *E. coli* BL21(DE3)/pET28a:*crpP*. This construct generated a soluble His_6-tagged protein (**Fig. 1A**). Using the purified sample, we attempted to measure kinase activity using the coupled pyruvate kinase/lactate

dehydrogenase ADP release assay. However, we could not detect ADP release activity (the highest concentrations tested were 2 mM ATP, 0.1 mM ciprofloxacin, and 5 µg/ml CrpP).

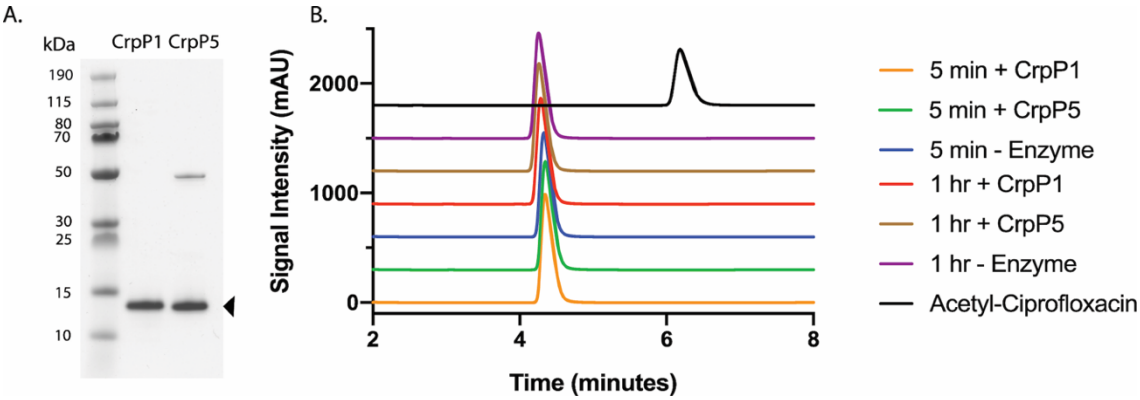

FIGURE 1. Purification and characterization of recombinant CrpP and CrpP5. A. SDS-polyacrylamide gel of His6-tagged CrpP and CrpP5 purified from *E. coli* BL21(DE3)/pET28a:*crpP* and *E. coli* BL21(DE3)/pET28a:*crpP5*, respectively, demonstrating the purity of the protein used in these studies. A minor immobilized metal affinity chromatography contaminant is present at ~50 kDa in the CrpP5 sample. The gel was stained with Coomassie brilliant blue. **B.** HPLC trace of ciprofloxacin (1mM) following incubation with ATP (2mM) in the presence and absence of purified CrpP or CrpP5 (5mg/ml). Reaction mixtures were incubated for both 5 min and 1 h. Acetyl-ciprofloxacin was used as a positive control to demonstrate that the HPLC method can detect modified drugs. No modified ciprofloxacin was detected in the enzyme reactions. Signal intensity was measured in milliabsorbance units (mAU).

We then established a high-performance liquid chromatography (HPLC) assay to measure any phosphorylation of ciprofloxacin catalyzed by CrpP (2 mM ATP, 1 mM ciprofloxacin, and 5 µg/ml CrpP) (the HPLC limit of detection for CIP is 1.6 ng, with ~1,655 ng injected per sample). Incubations over 5 to 60 min showed no change in the ciprofloxacin peak (**Fig. 1B**). High-resolution mass spectrometry analysis of the reaction

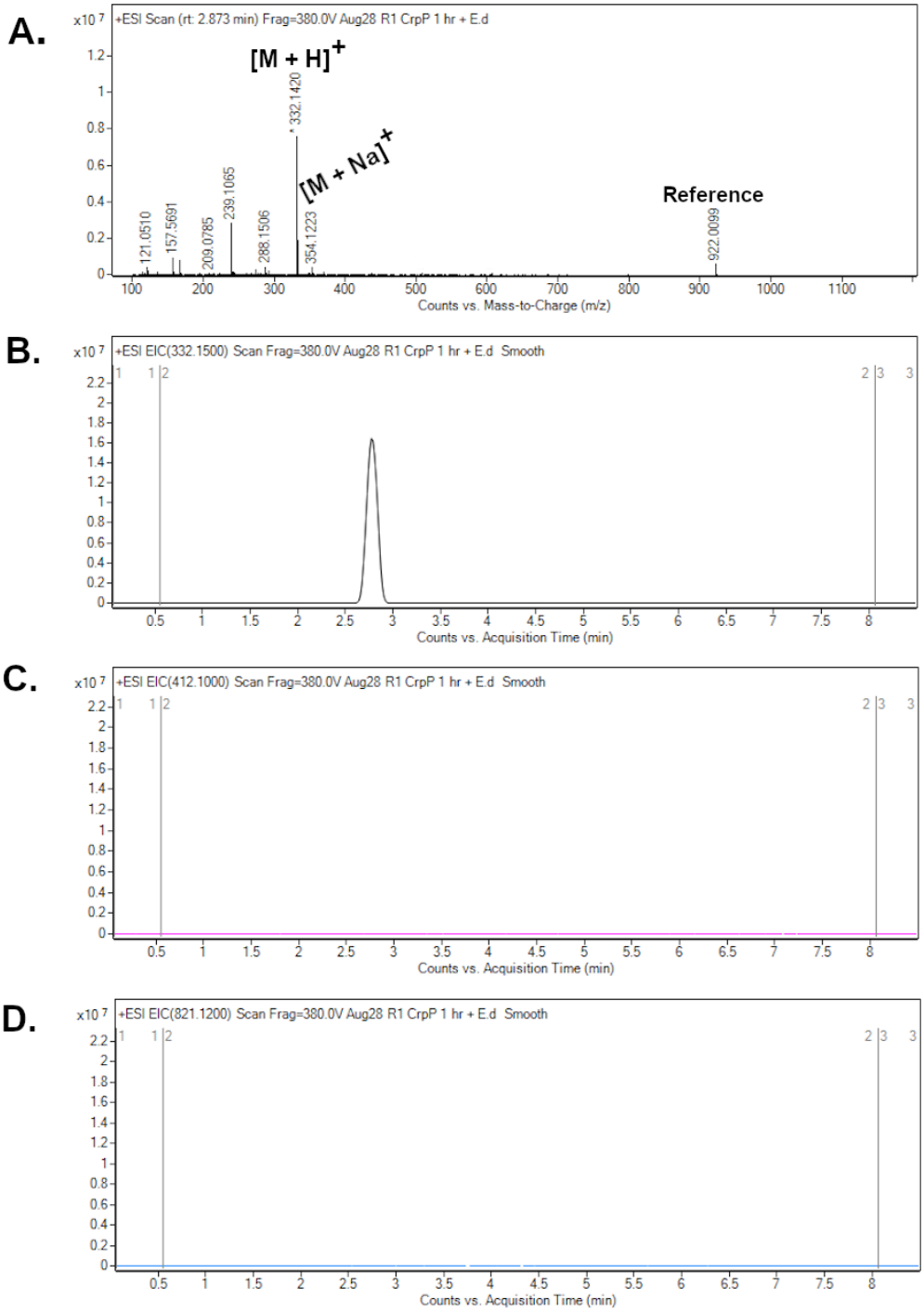
A.
x10 7
+ESI Scan (rt: 2.873 min) Frag=380.0V Aug28 R1 CrpP 1 hr + E.d
[M + H]+
[M + Na]+
Reference
121.0510
157.5691
209.0785
239.1065
288.1506
332.1420
354.1223
922.0099
Counts vs. Mass-to-Charge (m/z)
B.
+ESI EIC(332.1500) Scan Frag=380.0V Aug28 R1 CrpP 1 hr + E.d Smooth
Counts vs. Acquisition Time (min)
C.
+ESI EIC(412.1000) Scan Frag=380.0V Aug28 R1 CrpP 1 hr + E.d Smooth
Counts vs. Acquisition Time (min)
D.
+ESI EIC(821.1200) Scan Frag=380.0V Aug28 R1 CrpP 1 hr + E.d Smooth
Counts vs. Acquisition Time (min)

FIGURE 2. High-resolution mass spectrometry (HRMS) analysis of CrpP reactions. HRMS analysis of ciprofloxacin (1mM) following incubation with ATP (2mM) in the presence of purified CrpP (5mg/ml) after reacting for 1h. **A.** Positive electrospray ionization (1ESI) spectra at a retention time (Rt) of 2.873 min (the Rt for ciprofloxacin). Ciprofloxacin can be detected as [M 1 H]1 at m/z 332.1420 and [M 1 Na]1 at m/z 354.1223. Note that the signal at m/z 288.1506 is a result of losing the carboxyl group during the mass spectrometry analysis and is representative of [M 2 CO2H 1 H]1. The protonated form of HEPES buffer is detected at m/z 239.1065. No phosphorylated ciprofloxacin is present (expected m/z 412.10), nor is there evidence of the previously reported ATP-ciprofloxacin adduct (m/z 820.12). * indicates that the signal for [M 1 H]1 is oversaturated. The reference compound used is HP-0921 (m/z 922.0099). **B.** 1ESI extracted-ion chromatogram (EIC) at m/z 332.15 for [M 1 H]1. Note that due to the oversaturated signal, the EIC was obtained for m/z 332.15 rather than m/z 332.14 as seen in panel A. A high-intensity signal with the same Rt as [M 1 H]1 in panel A is detected (Rt = 2.8 min). **C and D.** 1ESI EIC at m/z 412.10 and m/z 821.12 for ciprofloxacin acyl-phosphate (calculated exact mass, m/z 412.1068) **C.** and the proposed ATP-ciprofloxacin adduct (calculated exact mass, m/z 812.1257) **D.** There is no signal for either compound.

mixture showed no evidence of ciprofloxacin modification (the limit of detection for CIP is 1.5 ng, with ~165.5 ng injected per sample) (**Fig. 2**). Due to the unavailability of standard phosphorylated ciprofloxacin, acetyl-ciprofloxacin, the product of AAC(6′)-Ib-cr, was used as a positive control to demonstrate the ability of our HPLC method to detect inactive modified fluoroquinolones. To address the activity of CrpP homologs, we overexpressed and purified CrpP5 using *E. coli* BL21(DE3)/pET28a:*crpP5* (**Fig. 1A**). The activity of CrpP5 was measured by HPLC under the same conditions as the ones described above for CrpP, and the results showed that CrpP5 does not modify ciprofloxacin (**Fig. 1B**).

Given these rigorous experimental results together with the protein sequence analysis, we show that CrpP alone is not a ciprofloxacin kinase, nor is it responsible for ciprofloxacin resistance in *E. coli*. We cannot rule out that CrpP, perhaps combined with other gene products, may be involved in the low-level fluoroquinolone resistance detected

by others. However, the cumulative data are consistent with the position that CrpP is not an enzyme that confers clinically relevant antibiotic resistance.

Acknowledgements

We thank Laurent Poirel and José Manuel Ortiz de la Rosa for their valuable discussions. This research was funded by a Canadian Institutes of Health Research grant (FRN-148463), an Ontario graduate scholarship (to H.L.Z.), an Alexander Graham Bell Canada graduate scholarship (to H.L.Z.), and a Canada research chair in antibiotic biochemistry (to G.D.W.).

(Beginning of unpublished data)

Materials and Methods

Cloning and Susceptibility Assays

To clone *crpP* and *crpP5* into pET28a, synthetic gBlock gene fragments were ordered from Integrated DNA Technologies (IDT) using the NCBI Reference Sequences deposited by Chávez-Jacobo et al. (2018) (NC_016138.1) and Ortiz de la Rosa et al. (2020) (WP_071580329.1). gBlocks were designed with *Nde*I and *Xho*I restriction enzyme sites and ATG start codons to optimize expression in *E. coli*. Both genes were digested with *Nde*I and *Xho*I (Thermo Scientific FastDigest Restriction Enzymes) and ligated into pET28a (Thermo Scientific T4 DNA ligase 5U/μL) according to manufacturer instructions. Following transformation into *E. coli* TOP10, plasmids were isolated for each construct and sent to the MOBIX sequencing facility at McMaster University for sequence

verification before transformation into *E. coli* BL21 (DE3). Using CLSI guidelines, susceptibility assays were performed for *E. coli* BL21 (DE3) pET28a:*crpP* (published) and *E. coli* BL21 (DE3) pET28a:*crpP5* (unpublished) against moxifloxacin, levofloxacin, ciprofloxacin, and norfloxacin in the presence and absence of 0.5 mM isopropyl ß-D-1-thiogalactopyranoside (IPTG). *E. coli* BL21 (DE3) pET28a was used as a control. No resistance could be detected for either construct.

Overexpression and Purification

Both CrpP and CrpP5 were overexpressed in *E. coli* BL21 (DE3) pET28a:*crpP* and *E. coli* BL21 (DE3) pET28a:*crpP5*, respectively. Overnight cultures of both strains were prepared before inoculating 1L of LB media per strain with a 1:50 inoculum. Cultures were then incubated at 37°C until reaching an OD_{600} of 0.5-0.6, followed by cooling flasks in an ice bath for 30 minutes. Protein overexpression was induced using 0.5 mM IPTG, and cultures were grown at 16°C for 18 hours. Once induction was complete, cells were harvested by centrifugation at 6000 x g for 25 minutes. Each pellet was resuspended in buffer A (25 mM HEPES [pH 7.5], 300 mM NaCl, 10 mM imidazole) and lysed using a continuous cell disrupter (Constant Systems Limited, Daventry UK) at 20,000 psi. Crude lysate was collected in a beaker containing DNAase, lysozyme, and an EDTA-free Pierce protease inhibitor tablet (Thermo Scientific) before centrifugation at 30,000 x g for 25 minutes at 4°C. Clarified lysate was collected in a 500 mL Erlenmeyer flask and incubated with 0.5 mL of HisPur Cobalt Resin (Thermo Scientific) resin that was pre-equilibrated with buffer A for 30 minutes at 4°C. The mixtures were loaded onto gravity flow columns

and washed with three full column volumes each (100 mL CV) of buffer B (25 mM HEPES [pH 7.5], 300 mM NaCl, 25 mM imidazole). The protein was eluted using a step-wise (25% increments) gradient of 0-100% buffer C (25 mM HEPES [pH 7.5], 300 mM NaCl, 250 mM imidazole). Elutions were dialyzed at 4°C for 18 hours against buffer D (25 mM HEPES [pH 7.5], 300 mM NaCl) before analyzing the samples using SDS-PAGE (Tris-Glycine 15%) with Coomassie staining. Elutions containing protein were pooled, concentrated (Amicon Ultra Centrifugal Filter, 3 kDA MWCO), and stored at 4°C.

Enzyme Assays

Purified CrpP and CrpP5 (5 μg/mL) were tested for their ability to modify ciprofloxacin via phosphorylation after 5-minute and 1-hour incubation periods with ciprofloxacin (1 mM) and Mg-ATP (2 mM) at 37°C in buffer containing 50 mM HEPES (pH 7.0), 40 mM KCl, 10 mM $MgCl_2$ in a 1 mL reaction volume. Negative controls contained the same reagents minus the presence of CrpP or CrpP5. Reactions were quenched using a 1:1 volume of glacial acetic acid.

High-Performance Liquid Chromatography

Enzyme reactions were analyzed via HPLC to monitor the formation of a phosphorylated ciprofloxacin peak catalyzed by CrpP and CrpP5. A total of 5 μL of each reaction was injected onto an XSelect CSH C18 column (5 μm, 4.6x100 mm) and eluted using an isocratic mobile phase of 8:92 acetonitrile: water with 2% acetic acid over ten minutes at a flow rate of 1 mL/min. Acetyl-ciprofloxacin (Ac-CIP) was used as a positive control to

demonstrate that the HPLC method used can detect a modified drug. Signal intensity was measured in milli-absorbance units (mAU). Please refer to **Figure 1** for details regarding data analysis.

Mass Spectrometry

Enzyme reactions were analyzed via high-resolution mass spectrometry (HRMS) to analyze ciprofloxacin following incubation with ATP and CrpP. Samples were injected on the Q-TOF LC/MS (Agilent Technologies 6550 iFunnel) using an Agilent Eclipse XDB-C8 column (3.5 μm, 2.1 x 100 mm. The LC/MS was run at 0.2 ml/min using the following gradient: 1 min, 5% B; 7 min, 95% B; 7.5 min, 95% B; 8 min, 95% B. Solvents A and B were H_2O and CH_3CN 0.1% formic acid, respectively. Please refer to **Figure 2** for details regarding data analysis.

References

Chávez-jacobo, Víctor M., Karen C. Hernández-ramírez, Pamela Romo-rodríguez, and Rocío Viridiana Pérez-gallardo. 2018. "CrpP Is a Novel Ciprofloxacin-Modifying Enzyme Encoded by the Pseudomonas Aeruginosa PUM505 Plasmid" 62 (6): 1–11.

Cox, Georgina, Arthur Sieron, Andrew M. King, Gianfranco De Pascale, Andrew C. Pawlowski, Kalinka Koteva, and Gerard D. Wright. 2017. "A Common Platform for Antibiotic Dereplication and Adjuvant Discovery." *Cell Chemical Biology* 24 (1): 98–109.

De Pascale, Gianfranco, and Gerard D. Wright. 2010. "Antibiotic Resistance by Enzyme Inactivation: From Mechanisms to Solutions." *Chembiochem: A European Journal of Chemical Biology* 11 (10): 1325–34.

Hernández-García, Marta, María García-Castillo, Sergio García-Fernández, Diego López-Mendoza, Jazmín Díaz-Regañón, João Romano, Leonor Pássaro, Laura Paixão, and Rafael Cantón. 2021. "Presence of Chromosomal CrpP-like Genes Is Not Always Associated with Ciprofloxacin Resistance in Pseudomonas Aeruginosa Clinical Isolates Recovered in ICU Patients from Portugal and Spain." *Microorganisms* 9 (2). https://doi.org/10.3390/microorganisms9020388.

Hernández-Ramírez, Karen C., Rosa I. Reyes-Gallegos, Víctor M. Chávez-Jacobo, Amada Díaz-Magaña, Víctor Meza-Carmen, and Martha I. Ramírez-Díaz. 2018. "A Plasmid-Encoded Mobile Genetic Element from Pseudomonas Aeruginosa That Confers Heavy Metal Resistance and Virulence." *Plasmid* 98 (May): 15–21.

Kim, Dae-Wi, Cung Nawl Thawng, Kihyun Lee, Elizabeth M. H. Wellington, and Chang-Jun Cha. 2019. "A Novel Sulfonamide Resistance Mechanism by Two-Component Flavin-Dependent Monooxygenase System in Sulfonamide-Degrading Actinobacteria." *Environment International* 127 (June): 206–15.

Ortiz de la Rosa, José Manuel, Patrice Nordmann, and Laurent Poirel. 2020. "Pathogenicity Genomic Island-Associated CrpP-Like Fluoroquinolone-Modifying Enzymes among Pseudomonas Aeruginosa Clinical Isolates in Europe." *Antimicrobial Agents and Chemotherapy* 64 (7). https://doi.org/10.1128/AAC.00489-20.

Robicsek, Ari, Jacob Strahilevitz, George A. Jacoby, Mark Macielag, Darren Abbanat, Chi Hye Park, Karen Bush, and David C. Hooper. 2006. "Fluoroquinolone-Modifying Enzyme: A New Adaptation of a Common Aminoglycoside Acetyltransferase." *Nature Medicine* 12 (1): 83–88.

Vetting, Matthew W., Hye Park Chi, Subray S. Hegde, George A. Jacoby, David C. Hooper, and John S. Blanchard. 2008. "Mechanistic and Structural Analysis of Aminoglycoside N-Acetyltransferase AAC(6′)-Ib and Its Bifunctional, Fluoroquinolone-Active AAC(6′)-Ib-Cr Variant." *Biochemistry* 47 (37): 9825–35.

Waglechner, Nicholas, Andrew G. McArthur, and Gerard D. Wright. 2019. "Phylogenetic Reconciliation Reveals the Natural History of Glycopeptide Antibiotic Biosynthesis and Resistance." *Nature Microbiology* 4 (11): 1862–71.

Wright, G. D., and P. R. Thompson. 1999. "Aminoglycoside Phosphotransferases: Proteins, Structure, and Mechanism." *Frontiers in Bioscience: A Journal and Virtual Library* 4 (January): D9-21.

Wu, Da-Qiang, Jing Ye, Hong-Yu Ou, Xue Wei, Xianqing Huang, Ya-Wen He, and Yuquan Xu. 2011. "Genomic Analysis and Temperature-Dependent Transcriptome Profiles of the Rhizosphere Originating Strain Pseudomonas Aeruginosa M18." *BMC Genomics* 12 (August): 438.

CHAPTER 3: Antibiotic Dereplication for Natural Product Drug Discovery

Preface

The work presented in this chapter was previously published in:

Zubyk HL, Cox G, Wright GD. (2019) Antibiotic Dereplication Using the Antibiotic Resistance Platform. *J Vis Exp*. (152), e60536, doi: 10.3791/60536.

The publisher has granted permission to reproduce the material herein.

H.L.Z. performed all experiments. G.C. and G.D.W. developed the original Antibiotic Resistance Platform. H.L.Z. and G.D.W. developed the minimal Antibiotic Resistance Platform. H.L.Z., G.C., and G.D.W. wrote and edited the manuscript.

The Antibiotic Resistance Platform (ARP), initially developed by Cox et al. (2017), serves multiple purposes: facilitating the discovery of antibiotic adjuvants, testing novel antimicrobials against known resistance mechanisms, and aiding in antibiotic dereplication. The ARP consists of a library of resistance genes individually cloned into the pGDP plasmid series, then transformed into either *E. coli* BW25113 or the hyper-permeable *E. coli* BW25113 Δ*bamB*Δ*tolC*. Each gene undergoes experimental validation through susceptibility assays to determine its minimum inhibitory concentration in the respective strain. Initially comprising 42 genes, each cloned into a combination of plasmids resulting in 96 individual constructs, the ARP now includes 131 individual resistance genes across 251 constructs.

During my tenure in the Wright lab, I've been tasked with maintaining and expanding the ARP to ensure its relevance and comprehensiveness in covering a wide range of known antibiotics. To facilitate effective dereplication, the ARP must include newly discovered genes and those that confer resistance to commonly encountered antibiotics. This philosophy drew our attention to the *crpP* story discussed in Chapter 2. As of 2023,

my contributions have led to the design, cloning, sequencing, and experimental validation of 48% of the ARP, encompassing 61 antibiotic resistance genes and 120 constructs.

In addition to expanding the ARP, I've focused on enhancing its accessibility. As outlined in the introduction chapter of this thesis, antibiotic dereplication is both time and resource-intensive. However, the ARP offers a cost-effective and efficient solution, lowering the barriers to drug discovery and dereplication. To further streamline the process and increase its utility, I developed the "Minimal Antibiotic Resistance Platform" (MARP), which eliminates gene redundancy and assesses a compound's ability to penetrate the Gram-negative outer membrane.

Recognizing the significant interest in the platform, I've made the MARP available through Addgene (Kit #1000000143), a non-profit plasmid repository aimed at improving access to research materials. This process involved depositing the plasmids, providing protocols, gene-related information, and collaborating with Addgene to create an informative webpage for the kit. Since May 2023, 104 purchases have been made by researchers in 29 different countries.

To further support the utilization of this platform and facilitate drug discovery, I've authored a protocol-based manuscript for publication in the *Journal of Visualized Experiments* (JoVE). Given the substantial interest from researchers at McMaster University and beyond in learning this technique, I initiated the manuscript submission process with JoVE for its ability to present experimental methods in both written and video formats. This publication and the coinciding video provide a step-by-step visual guide, making the dereplication platform easily replicable. Since its publication in 2019, this

article has been accessed over 9,700 times by 200 individual academic institutions. By disseminating the ARP/MARP dereplication platform, I aim to enhance accessibility to natural product drug discovery for researchers worldwide.

Antibiotic Dereplication Using the Antibiotic Resistance Platform

Abstract

One of the main challenges in the search for new antibiotics from natural product extracts is the re-discovery of common compounds. To address this challenge, dereplication, which is the process of identifying known compounds, is performed on samples of interest. Methods for dereplication such as analytical separation followed by mass spectrometry are time-consuming and resource-intensive. To improve the dereplication process, we have developed the antibiotic resistance platform (ARP). The ARP is a library of approximately 100 antibiotic resistance genes that have been individually cloned into *Escherichia coli.* This strain collection has many applications, including a cost- effective and facile method for antibiotic dereplication. The process involves the fermentation of antibiotic-producing microbes on the surface of rectangular Petri dishes containing solid medium, thereby allowing for the secretion and diffusion of secondary metabolites through the medium. After a 6-day fermentation period, the microbial biomass is removed, and a thin agar overlay is added to the Petri dish to create a smooth surface and enable the growth of the *E. coli* indicator strains. Our collection of ARP strains is then pinned onto the surface of the antibiotic- containing Petri dish. The plate is next incubated overnight to allow for *E. coli* growth on the surface of the overlay. Only strains containing resistance to a specific antibiotic (or class) grow on this surface enabling rapid identification of the produced compound. This method has been successfully used for the identification of producers of known antibiotics and as a means to identify those producing novel compounds.

Introduction

Since the discovery of penicillin in 1928, natural products derived from environmental microorganisms have proven to be a rich source of antimicrobial compounds (Lo Grasso et al. 2016). Approximately 80% of natural product antibiotics are derived from bacteria of the genus *Streptomyces* and other actinomycetes, while the remaining 20% is produced by fungal species (Lo Grasso et al. 2016). Some of the most common antibiotic scaffolds used in the clinic such as the β-lactams, tetracyclines, rifamycins, and aminoglycosides, were originally isolated from microbes (Thaker et al. 2013). However, due to the rise of multidrug resistant (MDR) bacteria, our current panel of antibiotics has become less effective in treatment (Gajdács 2019a; Boucher et al. 2009). These include the "ESKAPE" pathogens (i.e., vancomycin-resistant enterococci and β-lactam-resistant *Staphylococcus aureus*, *Klebsiella pneumoniae*, *Pseudomonas aeruginosa*, *Acinetobacter baumannii*, and *Enterobacter* sp.), which are a subset of bacteria deemed to be associated with the highest risk by a number of major public health authorities such as the World Health Organization (Gajdács 2019a; Boucher et al. 2009; Gajdács 2019b). The emergence and global spread of these MDR pathogens results in a constant need for novel antibiotics (Gajdács 2019a; Boucher et al. 2009; Gajdács 2019b). Regrettably, the past two decades have demonstrated that the discovery of novel antibiotics from microbial sources is increasingly difficult (Gaudêncio and Pereira 2015). Current approaches to drug discovery include the high-throughput screening of bioactive compounds, including natural product extract libraries, allowing for thousands of extracts to be tested at a given time (Thaker et al. 2013). However, once antimicrobial activity is detected, the next step is to analyze the

contents of the crude extract to identify the active component and eliminate those containing known or redundant compounds (Ito and Masubuchi 2014; Van Middlesworth and Cannell 2008). This process, referred to as dereplication, is vital to prevent and/or significantly reduce the time spent on the re-discovery of known antibiotics (Ito and Masubuchi 2014; Tawfike, Viegelmann, and Edrada-Ebel 2013). Although a necessary step in natural product drug discovery, dereplication is notoriously laborious and resource-intensive (Cox et al. 2017).

Ever since Beutler et al. first coined the term "dereplication", extensive efforts have been made to develop innovative strategies for the rapid identification of known antibiotics (Hubert et al. 2017; Beutler 1990). Today the most common tools used for dereplication include analytical chromatographic systems such as high-performance liquid chromatography, mass spectrometry, and nuclear magnetic resonance-based detection methods (Hubert et al. 2017; Mohimani et al. 2018). Unfortunately, each of these methods requires the use of expensive analytical equipment and sophisticated data interpretation.

In an attempt to develop a dereplication method that can be rapidly performed without specialized equipment, we established the antibiotic resistance platform (ARP) (Cox et al. 2017). The ARP can be used for the discovery of antibiotic adjuvants, the profiling of new antibiotic compounds against known resistance mechanisms, and the dereplication of known antibiotics in extracts derived from actinobacteria and other microbes. Here, we focus on its application in antibiotic dereplication. The ARP utilizes a library of isogenic *Escherichia coli* strains expressing individual resistance genes that are effective against the most commonly re-discovered antibiotics (Baltz 2006; Baltz 2005).

When the *E. coli* library is grown in the presence of a secondary metabolite-producing organism, the identity of the compound can be deduced by the growth of *E. coli* strains that express its associated resistance gene (Cox et al. 2017). When the ARP was first reported, the library consisted of >40 genes conferring resistance to 16 antibiotic classes. The original dereplication template was designed to encompass a subset of resistance genes per antibiotic class to provide information regarding antibiotic subclass during the dereplication process. Today, the ARP is comprised of >90 genes that confer resistance to 18 antibiotic classes. Using our extensive collection of resistance genes, a secondary dereplication template has been developed and is known as the minimal antibiotic resistance platform (MARP). This template was created to eliminate gene redundancy and to simply provide information regarding the general antibiotic class that a dereplicated metabolite is related to. Additionally, the MARP template possesses both wildtype and a hyperpermeable/efflux deficient strain of *E. coli* BW25113 (*E. coli* BW25113 Δ*bamB*Δ*tolC)*, compared to the original incarnation of the ARP, which only utilizes the hyperpermeable strain. This unique aspect creates additional phenotypes during dereplication, indicating a compounds ability to cross the outer membrane of Gram-negative bacteria. Here, we describe a robust protocol to be followed when dereplicating with either the ARP and/or MARP, highlight the most critical steps to be followed, and discuss the various possible outcomes.

Protocol

1. Preparation of E. coli Library Glycerol Stocks (from Agar Slants)

1. Streak the ARP/MARP *E. coli* strains from lysogeny broth (LB) agar slants onto Petri dishes containing LB agar and the appropriate selectable marker (**Table 1**).
2. Prepare cultures for each of the *E. coli* strains by inoculating 3 mL of LB containing the appropriate selectable marker with a single colony. Grow overnight at 37 °C with aeration (250 rpm).
3. Combine 800 µL of culture and 200 µL of sterile 80% glycerol in a 1.8 mL cryovial. Mix by inverting the tubes 3−4 times, and store at -80 °C.

2. ARP/MARP Frozen Stock Library Plate Preparation

1. Streak the ARP/MARP strains from the glycerol stocks prepared in section 1 onto a new set of Petri dishes containing LB agar and the appropriate selectable marker. Grow overnight at 37 °C.
2. Using aseptic technique, pipette 500 µL of cation adjusted Mueller Hinton broth (MHB) from a sterile reservoir into each well of a sterile 96 deep well plate.
3. With the plates prepared in step 2.1, use an applicator stick to inoculate the 96 deep well plate in accordance with the ARP/MARP map (**Supplemental Figure 1** and **Supplemental Figure 2**). Ensure that the appropriate selectable marker is added to each well. Place a breathable sealing membrane over the surface of the deep well plate and incubate overnight at 37 °C (250 rpm).

4. Ensure that there are no contaminated wells by referring to the ARP/MARP map. Repeat if contaminated. Using a multi-channel pipettor, transfer 100 µL from each well of the deep well plate to a sterile 96-well round bottom plate. Repeat this step to create multiple frozen stock library plates.

   NOTE: It is best to prepare at least 5 library plates at a time to keep from repeating steps 2.1−2.4 in the event of frozen stock library plate contamination.

5. Finish making the ARP/MARP frozen stock library plates by pipetting 100 µL of sterile 50% glycerol into each well and mix by gently pipetting up and down.
6. Cover the plates with sterile aluminum seals and ensure that each well is individually sealed.
7. Number the plates and dedicate only one frozen stock library plate for inoculating new templates at a given time. Keep the remainder as back-ups in the event of frozen stock library plate contamination.
8. Place the plate lid on top of the aluminum seal and store at -80 °C.

3. Seed Culture and Dereplication Plate Preparation

1. Using an applicator stick, inoculate 3 mL of *Streptomyces* antibiotic medium (SAM) (or other appropriate medium for the organism being tested) in a test tube containing one sterile glass bead (to break up the mycelium) with the producing strain that is

to be dereplicated. For *Streptomyces,* gently scrape spores from the surface of a colony.

2. Using the same wooden applicator stick, streak a sterility control on a Petri dish containing Bennett's agar.
3. Incubate the seed culture at 30 °C with aeration for 6 days (250 rpm) and incubate the sterility control plate at 30 °C for 6 days.

NOTE: Refer to **Table 2** for SAM and Bennett's media recipes. The above instructions are suitable for most actinomycetes. Alter growth media as necessary for other bacteria and fungi.

4. Prepare dereplication plates by aspirating 23 mL of warm Bennett's agar into a serological pipette and dispense 20 mL evenly across the surface of a rectangular Petri dish (**Table of Materials**), leaving the remainder of the medium in the pipette to prevent air bubble formation. **NOTE:** Ensure that the surface being used to pour plates is level and perform this step before the agar has cooled too much; a flat surface is imperative for library pinning in the next stages.
5. Gently rotate the plate until the medium covers all areas of the plate and do not disturb it until the agar has set completely.
6. Prepare nitrocellulose membrane sheets (**Table of Materials**) by using a rectangular Petri dish lid as a tracing template so that the sheets fit the surface of the dereplication plate. Cut the sheets and autoclave them in a sterile pouch.

NOTE: This membrane allows for organisms to sporulate on its surface, while secondary metabolites may be excreted into the medium below. Once grown, the membrane is removed to provide a clean surface for dereplication. The closer fit that the membrane paper has on the surface of the Bennett's agar, the cleaner the dereplication result.

7. Check the sterility control plate to ensure that no contaminants are present after 6 days of incubation. If contamination-free, remove the lid of the rectangular Petri dish and pipette 200 µL of seed culture onto the surface of the Bennett's agar.
8. Evenly spread the culture across the surface of the entire plate using a sterile cotton swab.
9. Place the nitrocellulose membrane prepared in step 3.6 over top of the culture on the surface of the Petri dish. Begin by aligning the bottom edge of the membrane to the bottom edge of the Petri dish, and slowly apply the membrane from the bottom edge to the top edge of the plate.
10. Use a sterile cotton swab to smooth out any air bubbles that may have formed between the membrane-agar interface, ensuring that the membrane is flush to the agar.
11. Put the lid back on the rectangular Petri dish and place it upside down in a sealed plastic bag. Incubate at 30 °C for 6 days.

4. Dereplication Plate MHB Overlay and ARP/MARP Library Plate Preparation

1. After 6 days, remove the dereplication plate from the 30 °C incubator. Using sterile tweezers (autoclaved or sprayed thoroughly with 70% ethanol), carefully remove the nitrocellulose membrane from the surface of the Bennett's agar.

   NOTE: This step will remove the hydrophobic spores and mycelia grown on the surface of the membrane to provide a clean surface for dereplication, facilitating step 4.2.

2. As described for step 3.4, ensure the work surface is level and use a serological pipette to aspirate 23 mL of warm cation adjusted MHB agar. Create an overlay by dispensing 20 mL evenly across the surface of the dereplication plate, leaving the remainder of the medium in the pipette to prevent air bubble formation.
3. Gently rotate the plate until the medium covers all areas and do not disturb it until the agar has set completely. Once cooled and solidified, return the dereplication plate to the sealed plastic bag and store it upside down at 4 °C overnight.

   NOTE: This step allows for diffusion of secondary metabolites from the fermented Bennett's medium into the MHB agar overlay. If the nitrocellulose membrane was not prepared properly there will be spore growth around the edges of the plate, which have hydrophobic properties that repel the MHB agar. Do not pour the overlay on top of these spores because it can result in contamination of the overlay.

4. On the same day that the overlay is poured, inoculate a fresh ARP/MARP template by pipetting 100 µL of cation adjusted MHB into each well of a 96-well plate.

   NOTE: To reduce the chance of spreading contamination during dereplication, use a single ARP/MARP library plate to only dereplicate 2−3 dereplication plates. Therefore, inoculate enough 96-well ARP/MARP plates based on the number of strains that will be dereplicated.

5. Take the frozen stock ARP/MARP library plate out of the -80 °C freezer. Remove the aluminum seal before condensation begins to form on its underside, thereby decreasing the chance of contaminating neighboring wells in the library plate.
6. Using sterile 96-well pinning tools (or other forms of inoculation equipment), carefully pin from the frozen stock ARP/MARP library plate and inoculate the fresh MHB-containing 96-well plates. To minimize contamination during dereplication, prepare as many ARP or MARP library plates needed to only dereplicate 2−3 dereplication plates per library plate. Sterilize pinning tools between inoculating each plate.
7. Put a new sterile aluminum seal on the frozen template once complete and return it to the -80 °C freezer. Place the inoculated 96-well plates inside of a sealed plastic bag and incubate at 37 °C with aeration (250 rpm) for 18 h.

   NOTE: New frozen stock library plates can be prepared from this step after

ensuring that no contamination is present. Add glycerol to the plate before storing at -80 °C as described in step 2.5.

5. Dereplicating Using the ARP/MARP

1. Remove the ARP/MARP template from the incubator and ensure that no contaminants are present. Always dereplicate using a template that is freshly prepared and not directly from the frozen stock.
2. Remove the dereplication plates from 4 °C and allow to equilibrate to room temperature. If there is condensation, open the lids and allow to dry in a sterile environment.
3. Using sterile pinning tools (or other inoculation equipment), pin from the ARP/MARP library plate onto the surface of the MHB agar overlay of the dereplication plates. Be careful not to pierce the agar. Sterilize pinning tools in between inoculating each dereplication plate.
4. After pinning the template onto the surface of the dereplication plates, allow the template inoculum to dry for 3−5 min. Place the inoculated dereplication plates upside down in a sealed plastic bag and incubate overnight at 37 °C.
5. Analyze dereplication results the following day by comparing growth on the dereplication plate to wells that correspond to the ARP/MARP map (**Table 3** and **Table 4**).

Representative Results

The following results were obtained when a collection of antibiotic-producing strains of interest were dereplicated using the ARP and/or MARP.

A diagram of the ARP/MARP dereplication workflow is depicted in **Figure 1**, and library plate maps are shown in **Supplemental Figure 1** and **Supplemental Figure 2**. **Figure 2** demonstrates a positive dereplication result wherein the environmental extract WAC 8921 is identified as a chloramphenicol producer. **Figure 3** shows a lack of ARP growth entirely, which indicates the presence of either an unknown antibiotic or a less commonly found antibiotic that is not accounted for in the ARP/MARP library plate. **Figure 4** demonstrates a growth pattern that is unique to the MARP because of its utilization of both wildtype *E. coli* BW25113 and a hyperpermeable and efflux deficient mutant *E. coli* BW25113 Δ*bamB*Δ*tolC.* This result suggests the presence of a compound with antimicrobial activity that is unable to surpass an intact outer membrane. **Figure 5** shows an *E. coli* growth pattern that suggests the improper sterilization of pinning tools and **Figure 6** shows an example of ARP/MARP frozen stock library plate contamination. **Figure 7** demonstrates what happens if the agar overlay is pierced during dereplication. Lastly, **Figure 8** shows MHB overlay related contamination that can occur during the dereplication process.

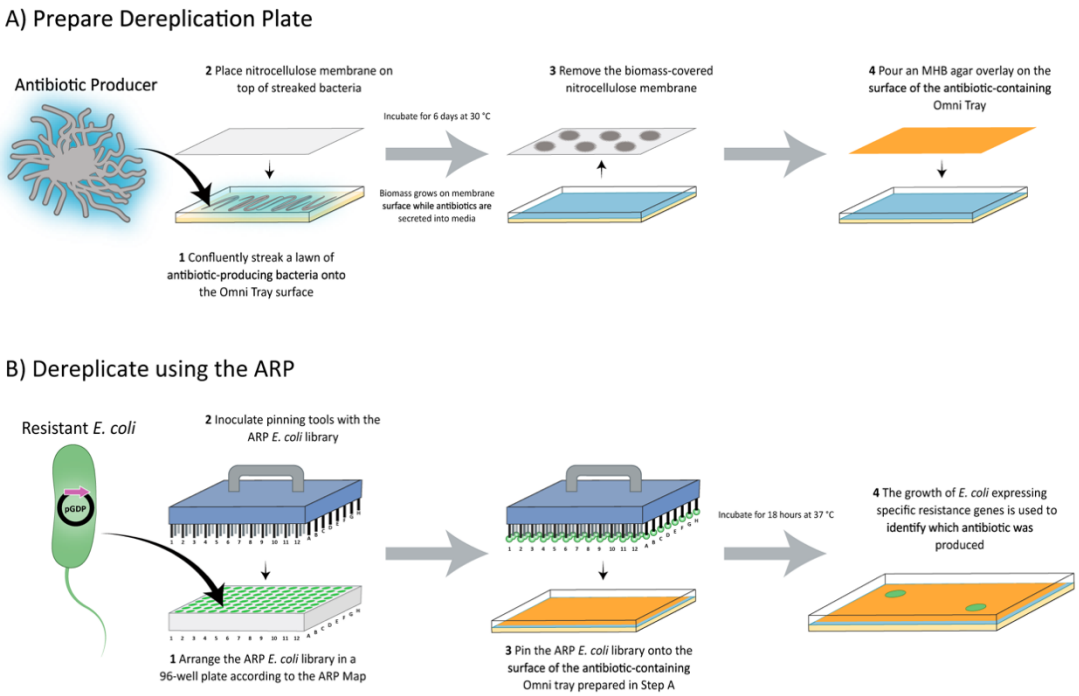

FIGURE 1. A schematic of the dereplication process. The producing strain to be dereplicated is streaked onto a rectangular Petri dish as a lawn and a nitrocellulose membrane is placed on top. The plate is then incubated for 6 days wherein the producing-strain related biomass grows on the surface of the membrane while and secondary metabolites produced are secreted into the Petri dish media. After a 6-day fermentation period, the membrane is removed and an MHB overlay is added to the surface of the antibiotic-containing media to provide a smooth surface for pinning. The ARP/MARP *E. coli* library, which is arranged in a 96-well plate format according to the ARP/MARP Maps, is then pinned onto the surface of the overlay. After incubating the tray overnight at 37 °C, the growth of *E. coli* strains expressing specific resistance genes indicates the identity of the compound produced.

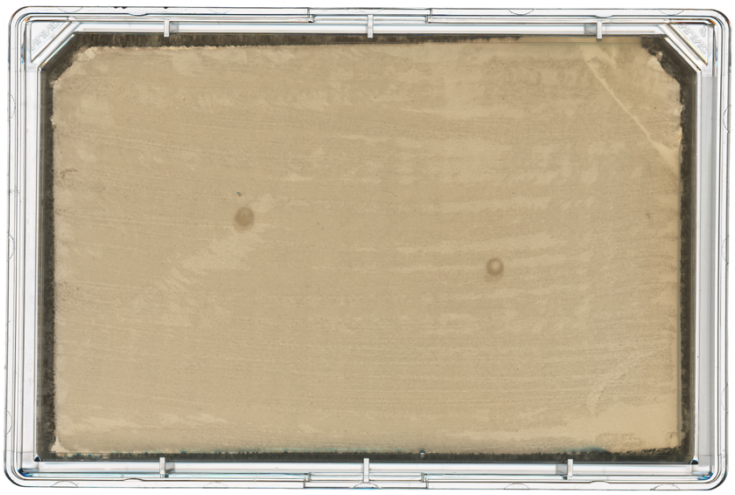

FIGURE 2. Dereplication of a known antibiotic. The producing strain WAC 8921 was dereplicated using the ARP template. Growth of *E. coli* BW25113 Δ*bamB*Δ*tolC* pGDP1:*CAT* on the surface of the MHB agar overlay indicates that WAC 8921 is a chloramphenicol producer.

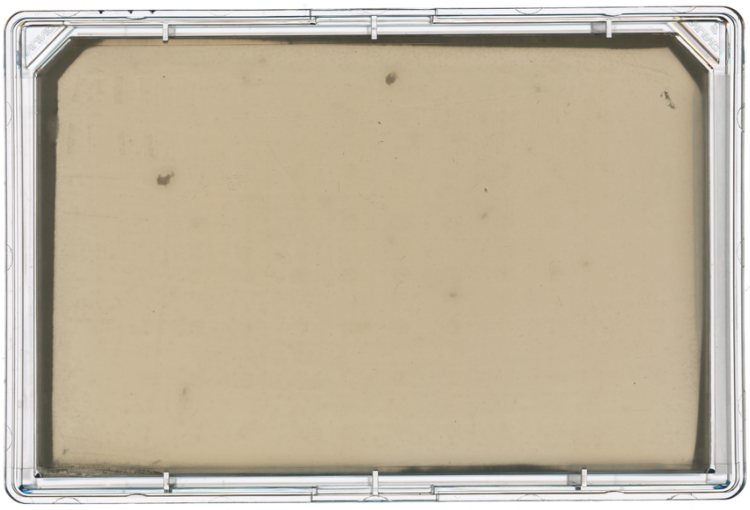

FIGURE 3. Dereplication of an unknown antibiotic. The producing strain WAC 9941 was dereplicated using the ARP template. A lack of *E. coli* library growth was seen on the surface of the rectangular Petri dish, indicating that either WAC 9441 is producing an unknown antimicrobial compound or a rare antibiotic that is not accounted for in the ARP.

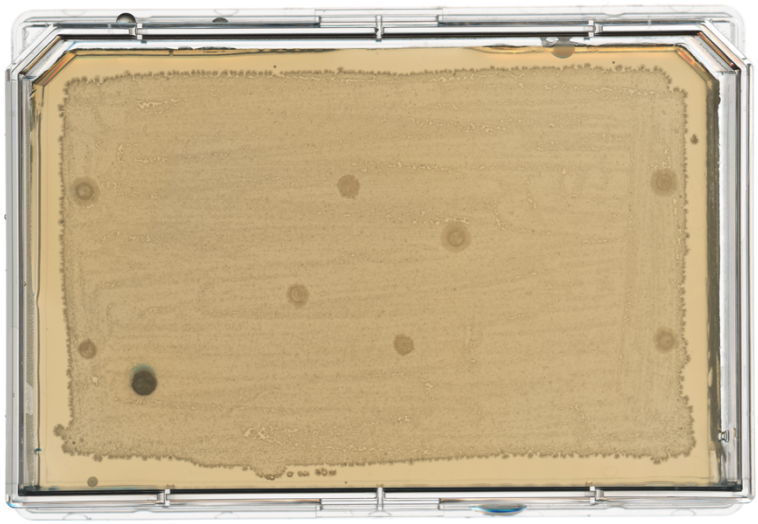

FIGURE 4. Identification of an antimicrobial compound that cannot traverse an intact outer membrane. The producing strain WAC 4178 was dereplicated using the MARP template. Strains of *E. coli* BW25113 are capable of growing on the surface of the secondary metabolite-containing media, whereas all strains of *E. coli* BW25113 Δ*bamB*Δ*tolC* cannot grow. This suggests that WAC 4178 is producing an antimicrobial compound that cannot traverse an intact outer membrane.

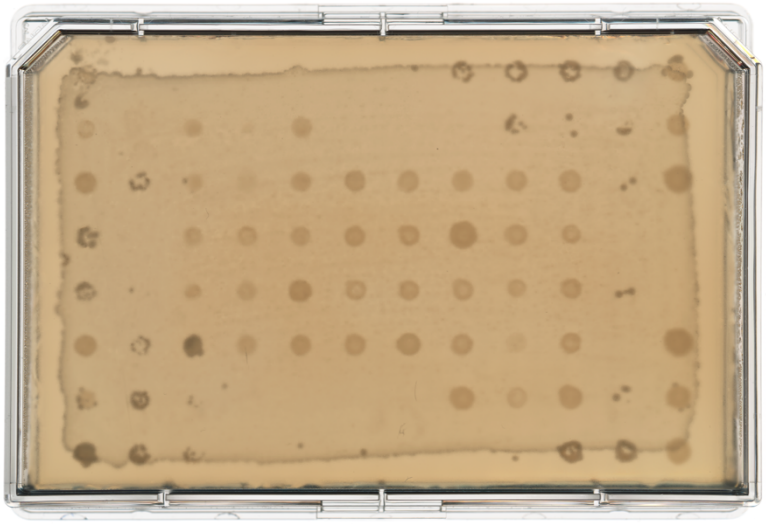

FIGURE 5. Contamination due to non-sterile pinning tools. The producing strain WAC 7094 was dereplicated using the ARP template. The presence of *E. coli* library growth in areas that did not have an assigned *E. coli* strain suggests that the pinning tools used to inoculate the MHB agar overlay of the rectangular Petri dish were not properly sterilized. This results in the transfer of unknown *E. coli* strains across the overlay.

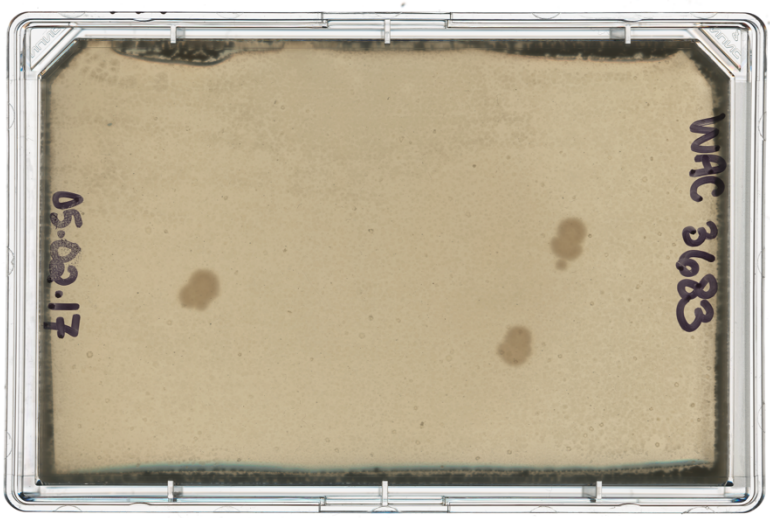

FIGURE 6. Contamination due to a contaminated frozen stock ARP/MARP template. The producing strain WAC 3683 was dereplicated using the ARP template. Three distinct *E. coli* colonies grew on the rectangular Petri dish surface: two correspond with *E. coli* BW25113 Δ*bamB*Δ*tolC* expressing STAT, a streptothricin resistance enzyme, and the other corresponds to *E. coli* BW25113 Δ*bamB*Δ*tolC* expressing VIM-2_{SS}, a β- lactam resistance enzyme. Due to a lack of replicating *bla*VIM2ss colony growth, in addition to the lack of cross-resistance known to occur between these two antibiotic classes, it can be assumed that a strain other than *E. coli* Δ*bamB*Δ*tolC* pGDP1: *bla*VIM2ss is growing in the respective frozen library plate well.

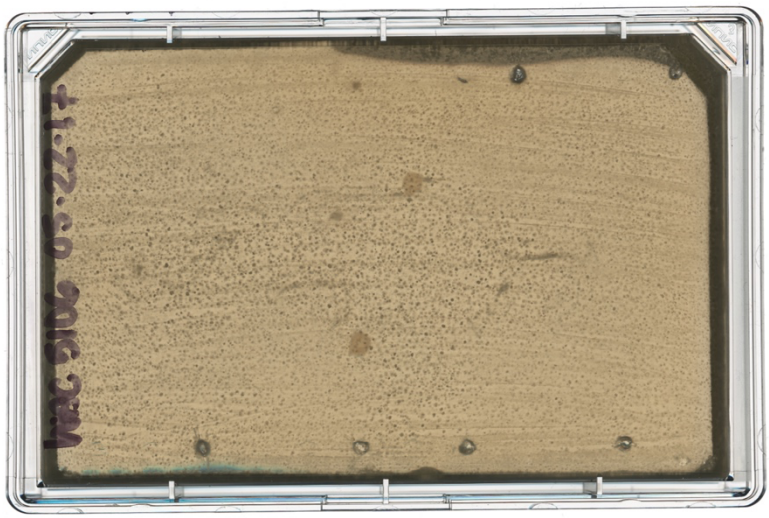

FIGURE 7. Pierced MHB agar overlay. The producing strain WAC 5106 was dereplicated using the ARP template. This strain was found to be a streptomycin producer, as indicated by the growth of *E. coli* BW25113 Δ*bamB*Δ*tolC* pGDP3:*aph(6)-Ia.* Puncture holes can be seen on the surface of the MHB agar overlay along the perimeter of the plate. While this does not affect the dereplication results, it can make the data difficult to interpret at first glance.

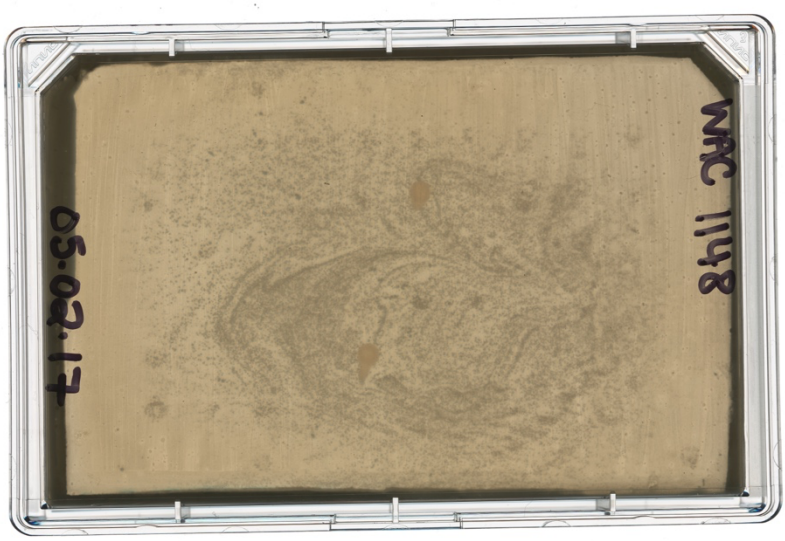

FIGURE 8. Contamination of the MHB agar overlay. Contaminated MHB agar produces an irregular growth pattern on the surface of the overlay that becomes visible after incubating the plate overnight at 37 °C. Although *E. coli* growth may still be visible through the contamination, it is advised to repeat the experiment before extrapolating data from the plate.

Plasmid	Selectable Marker
pGDP1	Kanamycin 50 μg/mL
pGDP2	
pGDP3	Ampicillin 100 μg/mL
pGDP4	
None	-

TABLE 1. Selectable markers used in the pGDP plasmid series. Streak the ARP/MARP *E. coli* strains onto LB agar Petri dishes containing the appropriate selectable marker at the right concentration for each plasmid.

Media	Ingredient	Amount
SAM	Glucose	15 g
	Soya peptone	15 g
	NaCl	5 g
	Yeast Extract	1 g
	$CaCO_3$	1 g
	Glycerol	2.5 mL
	ddH_2O	To 1 L
Bennett's	Potato starch	10 g
	Casamino acids	2 g

	Yeast extract	1.8 g
	Czapek mineral mix	2 mL
	Agar (optional)	15 g
	ddH_2O	To 1 L
Czapek mineral mix	KCl	10 g
	$MgSO_4 \bullet 7H_2O$	10 g
	$NaNO_3$	12 g
	$FeSO_4 \bullet 7H_2O$	0.2 g
	Concentrated HCl	200 µL
	ddH_2O	To 100 mL

TABLE 2. Recipes for SAM and Bennett's media, and Czapek mineral mix. Adjust SAM and Bennett's to pH 6.8 before autoclaving, and filter sterilize the Czapek mineral mix.

Antibiotic Class	**Antibiotic**	**Resistance Gene**	***E. coli* Strain**	**Well Position**
Aminoglycosides	Streptomycin	*aph(3'')-Ia*	Δ*bamB*Δ*tolC* BW25113	B3, G10
	2-Deoxystreptamine	*rmtB*	Δ*bamB*Δ*tolC* BW25113	F3, C10
	Apramycin	*apmA*	Δ*bamB*Δ*tolC* BW25113	C5, F8
	Spectinomycin	*aph(9)-Ia*	Δ*bamB*Δ*tolC* BW25113	B5, G8
β-lactams	Penicillin	*NDM-1*		B4, G9

	Cephalosporin		Δ*bamB*Δ*tolC* BW25113	
	Carbapenem			
Lincosamides	Lincosamides	*ermC*	Δ*bamB*Δ*tolC* BW25113	D4, E9
Macrolides	Macrolides			
Type B Streptogramins	Type B Streptogramins			
Type A Streptogramins	Type A Streptogramins	*vatD*	Δ*bamB*Δ*tolC* BW25113	C3, F10
Streptothricin	Streptothricin	*STAT*	Δ*bamB*Δ*tolC* BW25113	D3, E10
Tetracyclines	Tetracycline	*tet*(A)	Δ*bamB*Δ*tolC* BW25113	D5, E8
Chloramphenicols	Chloramphenicols	*CAT*	Δ*bamB*Δ*tolC* BW25113	E4, D9
Fosfomycins	Fosfomycins	*fosA*	Δ*bamB*Δ*tolC* BW25113	F6, C7
Rifamycins	Rifamycins	*arr*	Δ*bamB*Δ*tolC* BW25113	E3, D10
Polymyxins	Polymyxins	*mcr-1*	wild-type BW25113	C6, F7
Echinomycins	Echinomycins	*uvrA*	Δ*bamB*Δ*tolC* BW25113	F4, C9
Sideromycins	Albomycin	*fhuB* mutant	Δ*bamB*Δ*tolC* BW25113	C4, F9
Tuberactinomycins	Viomycin	*vph*	Δ*bamB*Δ*tolC* BW25113	F5, C8
N/A	N/A	N/A	wild-type BW25113	C1, C12, F1, F12, E5, D8
N/A	N/A	N/A	Δ*bamB*Δ*tolC* BW25113	A1, A12, B1, B12, D6, D7, E6, E7, G1,

				G12, H1, H12

TABLE 3. Well designation table for the minimal ARP strains. This table indicates which well of a 96-well plate that each of the minimal ARP strains can be found in according to the minimal ARP library plate map. The table also lists which antibiotic class each gene confers resistance to. Please note that some genes may confer resistance to more than one antibiotic within the given antibiotic class.

Antibiotic Class	**Antibiotic**	**Resistance Gene**	***E. coli* Strain**	**Well Position**
Aminoglycosides	Streptomycin	*aph(3'')-Ia*	Δ*bamB*Δ*tolC* BW25113	B2, G11
		aph(6)-Ia	Δ*bamB*Δ*tolC* BW25113	C6,F7
	Spectinomycin	*aph(9)-Ia*	Δ*bamB*Δ*tolC* BW25113	A2, H11
	Gentamicin	*aac(3)-Ia*	Δ*bamB*Δ*tolC* BW25113	A3,H10
		ant(2'')-Ia	Δ*bamB*Δ*tolC* BW25113	A5, H8
		aph(2'')-Id	Δ*bamB*Δ*tolC* BW25113	A4, H9
		armA	Δ*bamB*Δ*tolC* BW25113	A6, H7
		aac(6')-aph(2'')-Ia	Δ*bamB*Δ*tolC* BW25113	B5,G8
	Kanamycin	*aph(3')-Ia*	Δ*bamB*Δ*tolC* BW25113	B4, G9
		aph(3')-Illa	Δ*bamB*Δ*tolC* BW25113	B3, G10

	Hygromycin	*aph(4)-Ia*	Δ*bamB*Δ*tolC* BW25113	B6,G7
β-lactams	Amoxicillin	*TEM-1*	Δ*bamB*Δ*tolC* BW25113	F6, C7
	Ceftazidime	*CTX-M-15*	Δ*bamB*Δ*tolC* BW25113	F5, C8
	Oxacillin	*OXA-10*	Δ*bamB*Δ*tolC* BW25113	G5, B8
		OXA-48	Δ*bamB*Δ*tolC* BW25113	H5, A8
	Meropenem	*IMP-7ss*	Δ*bamB*Δ*tolC* BW25113	G4, B9
		KPC-2	Δ*bamB*Δ*tolC* BW25113	G6, B7
		NDM-1	Δ*bamB*Δ*tolC* BW25113	H6, A7
	Imipenem	*VIM-2*	Δ*bamB*Δ*tolC* BW25113	F4, C9
Lincosamides	Lincosamides	*ermC*	Δ*bamB*Δ*tolC* BW25113	C4, F9
		lnu(A)	Δ*bamB*Δ*tolC* BW25113	C5, F8
Macrolides	Macrolides	*ermC*	Δ*bamB*Δ*tolC* BW25113	C4, F9
		mphA	Δ*bamB*Δ*tolC* BW25113	C3, F10
		mphB	Δ*bamB*Δ*tolC* BW25113	C2, F11
Type B Streptogramins	Type B Streptogramins	*ermC*	Δ*bamB*Δ*tolC* BW25113	C4, F9
		Vgb	Δ*bamB*Δ*tolC* BW25113	D4, E9
Type A Streptogramins	Type A Streptogramins	*vatD*	Δ*bamB*Δ*tolC* BW25113	D5, E8

Streptothricin	Streptothricin	*STAT*	Δ*bamB*Δ*tolC* BW25113	D3, E10
Tetracyclines	Tetracycline	*tet*(M)	Δ*bamB*Δ*tolC* BW25113	E5, D8
Chloramphenicols	Chloramphenicols	*CAT*	Δ*bamB*Δ*tolC* BW25113	E4, D9
Fosfomycins	Fosfomycins	*fosA*	Δ*bamB*Δ*tolC* BW25113	H4, A9
Rifamycins	Rifamycins	*arr*	Δ*bamB*Δ*tolC* BW25113	E3, D10
N/A	N/A	N/A	Δ*bamB*Δ*tolC* BW25113	A1, A12, B1, B12, D6, D7, E6, E7, G1, G12, H1, H12

TABLE 4. Well designation table for the ARP strains. This table indicates which well of a 96-well plate that each of the ARP strains can be found in according to the ARP library plate map. The table also lists which antibiotic class each gene confers resistance to. Please note that some genes may confer resistance to more than one antibiotic within the given antibiotic class.

SUPPLEMENTAL FIGURE 1. Library plate map used for the original antibiotic resistance platform (ARP) template. Organize the respective *E. coli* strains in a 96-well plate using this format to ensure that all necessary controls and duplicates are included. This figure has been modified from Cox et al. (2017).

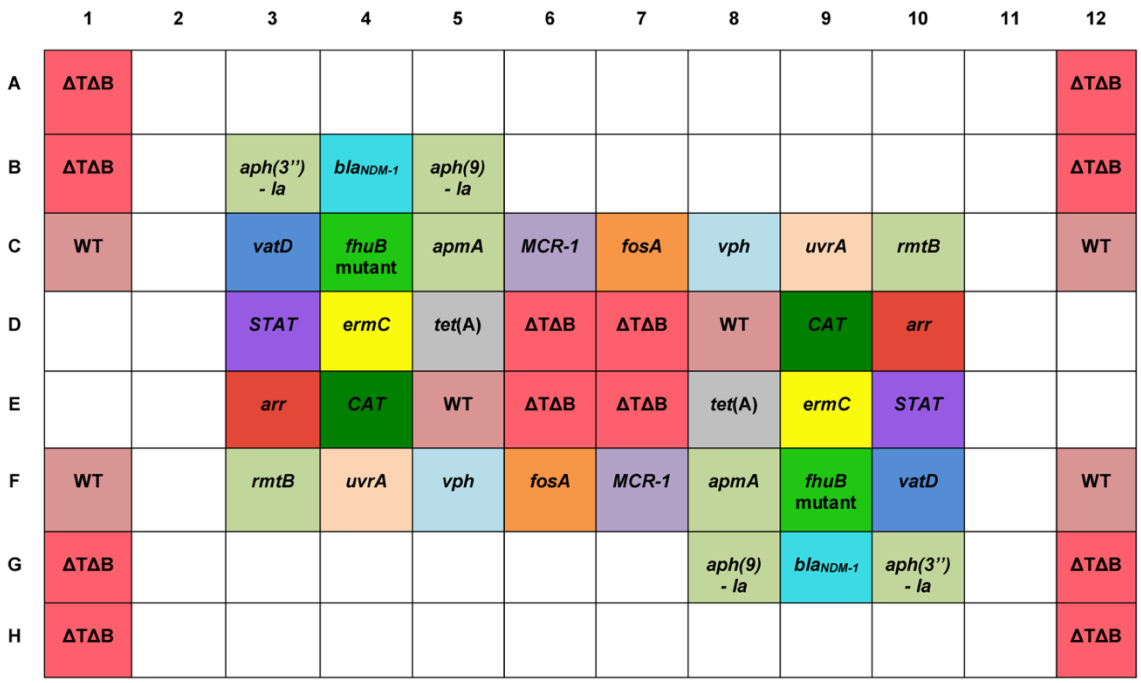

SUPPLEMENTAL FIGURE 2. Library plate map used for the minimal antibiotic resistance platform (MARP) template. Organize the respective *E. coli* strains in a 96-well plate using this format to ensure that all necessary controls and duplicates are included.

Discussion

The protocol described above can be applied to both the discovery of novel antimicrobial compounds and adjuvants that can be used in conjunction with existing antibiotics to rescue their activity. The platform takes advantage of the high substrate specificity of resistance mechanisms and their cognate antibiotics, to dereplicate compounds within crude natural product extracts. Although the time required for dereplication plates to be prepared is lengthy (~2 weeks), the dereplication process itself is complete after a single overnight incubation period, which is rapid in comparison to the time it can take to isolate and characterize a compound from crude extracts. Additionally, no expensive or highly specialized equipment is required, making this platform accessible and cost-effective.

Another major benefit of this platform is its flexibility. The ARP can be expanded to contain resistance genes that encompass more antibiotic classes. This is achieved by monitoring literature for the emergence of novel resistance enzymes and using basic molecular cloning techniques to add the genes to the *E. coli* library. Furthermore, the dereplication template is customizable based on the desired level of broad or narrow range substrate specificity that an individual wants to use when dereplicating. Any combination of genes in the *E. coli* library can be used to make novel library plates with the ability to detect compounds with different profiles. For example, a β-lactamase expressing *E. coli* template could be developed to allow for the highly specific dereplication of β-lactams and their different subclasses.

While this platform was initially designed to dereplicate compounds on solid media, it also works in liquid media. This is useful when working with compounds that have already been purified, wherein only a limited amount is available for testing, or when working with compounds that do not diffuse easily or consistently in solid media. Lastly, while this protocol was described using the *E. coli* strains BW25113 and BW25113 Δ*bamB*Δ*tolC,* the platform can be used with the resistance gene library expressed in different strains of *E. coli* (dereplication phenotypes may vary). Ultimately, the Antibiotic Resistance Platform is flexible, has many applications, and is advantageous over other dereplication methods.

To ensure that reproducible and non-contaminated results are obtained, it is critical to follow appropriate sterilization and aseptic techniques. Failure to do so will result in contamination of the pinning tools, library plate, or the dereplication plate itself. While selectable markers are present in the *E. coli* library, which can help prevent contamination caused by bacteria missing the marker, it does not prevent the cross- contamination of strains using the same marker. To reduce the risk of this happening it is essential to carefully sterilize the bacterial pinning tools before pinning from the library plate. Each library plate should only be pinned from 3−4 times maximum before discarding for a new template. This prevents the spread of contamination across all dereplication plates if a library plate becomes contaminated during the pinning process. Additionally, no antibiotics are used when inoculating the dereplication plate and so great care must be taken to prevent contamination before it is left to ferment for six days. Another possible source of contamination is in the MHB agar overlay of the dereplication plate. If the overlay media

is contaminated, growth will only appear after the overnight incubation at 37 °C post-pinning. Overlay contamination can make it extremely difficult to analyze the growth of the *E. coli* library on the overlay surface. To reduce the chances of overlay contamination, prepare MHB agar fresh before pouring the overlay. It is recommended that until an individual is comfortable with this method, dereplication plates should always be prepared in duplicate or triplicate such that in the event of contamination of one plate, data can still be extracted from the hopefully non- contaminated plates.

Lastly, it is important to note that the ARP/MARP has limitations. This protocol is not suitable for the dereplication of producing-strains that produce more than one bioactive compound. Each strain in the *E. coli* library has been designed to express a single resistance gene. If two antibiotics are being produced by an organism, neither resistance gene will confer resistance to the second antibiotic, thereby resulting in cell death of both strains. Thus, this possibility must be considered when dereplication results suggest the presence of a novel antibiotic because the production of multiple antibiotics cannot be detected by the current single construct *E. coli* library. One approach that can be taken to combat the challenge of dereplicating strains that produce more than one antibiotic involves using the agar-plug procedure described in the original ARP paper by Cox et al. (2017). In this method, a portion of a fermented solid medium is removed from an antibiotic-producer containing plate and placed onto a lawn of indicator ARP strain. The indicator strain can be any of the resistant *E. coli* strains in the ARP library. Zones of inhibition are then used to compare the bioactivity of a producing-strain against the ARP strains and a wild-type strain. ARP strains that form an inhibitory zone of decreased size compared to the wild-

type strain can resist the compound being produced. This method has proven to be effective at identifying strains capable of producing multiple antibiotics (Cox et al. 2017).

In summary, for obtaining the best results when dereplicating with the ARP/MARP it is recommended that dereplication plates are prepared in duplicate or triplicate. Other critical steps in the protocol include pinning from a fresh library plate (never frozen) and removing as much biomass as possible from the producing-strain during the membrane removal stage. If all necessary steps are followed, one should have successful dereplication results for a producing-strain of interest within a two-week time frame.

Disclosures

The authors have nothing to disclose.

Acknowledgements

Research in the Wright lab pertaining to the ARP/MARP was supported by the Ontario Research Fund and Canadian Institutes of Health Research grant (FRN-148463). We would like to acknowledge Sommer Chou for assisting in the expansion and organization of the ARP library.

References

Baltz, R. H. 2005. "Antibiotic Discovery from Actinomycetes: Will a Renaissance Follow the Decline and Fall?" *Archives of MicrobiologyArchives of Microbiology*. (55): 186-196

Baltz, Richard H. 2006. "Marcel Faber Roundtable: Is Our Antibiotic Pipeline Unproductive Because of Starvation, Constipation or Lack of Inspiration?" *Journal of Industrial Microbiology & Biotechnology* 33 (7): 507–13.

Beutler, J. A. 1990. "Dereplication of Phorbol Bioactives: Lyngbya Majuscula and Croton Cuneatus." *Journal of Natural Products* 53 (4): 867–74.

Boucher, Helen W., George H. Talbot, John S. Bradley, John E. Edwards, David Gilbert, Louis B. Rice, Michael Scheld, Brad Spellberg, and John Bartlett. 2009. "Bad Bugs, No Drugs: No ESKAPE! An Update from the Infectious Diseases Society of America." *Clinical Infectious Diseases: An Official Publication of the Infectious Diseases Society of America* 48 (1): 1–12.

Cox, Georgina, Arthur Sieron, Andrew M. King, Gianfranco De Pascale, Andrew C. Pawlowski, Kalinka Koteva, and Gerard D. Wright. 2017. "A Common Platform for Antibiotic Dereplication and Adjuvant Discovery." *Cell Chemical Biology* 24 (1): 98–109.

Gajdács, Mário. 2019a. "The Concept of an Ideal Antibiotic: Implications for Drug Design." *Molecules* 24 (5): 892.

Gajdács, Mário. 2019b. "The Continuing Threat of Methicillin-Resistant Staphylococcus Aureus." *Antibiotics* 8 (2): 52.

Gaudêncio, Susana P., and Florbela Pereira. 2015. "Dereplication: Racing to Speed up the Natural Products Discovery Process." *Natural Product Reports* 32 (6): 779–810.

Hubert, Jane, Jean Marc Nuzillard, and Jean Hugues Renault. 2017. "Dereplication Strategies in Natural Product Research: How Many Tools and Methodologies behind the Same Concept?" *Phytochemistry Reviews* 16 (1): 55–95.

Ito, Tatsuya, and Miyako Masubuchi. 2014. "Dereplication of Microbial Extracts and Related Analytical Technologies." *The Journal of Antibiotics* 67 (5): 353–60.

Lo Grasso, Letizia, Delia Chillura Martino, and Rosa Alduina. 2016. *Production of Antibacterial Compounds from Actinomycetes*. Edited by Dharumadurai (intechopen) Dhanasekaran. IntechOpen.

Mohimani, Hosein, Alexey Gurevich, Alexander Shlemov, Alla Mikheenko, Anton Korobeynikov, Liu Cao, Egor Shcherbin, Louis Felix Nothias, Pieter C. Dorrestein, and

Pavel A. Pevzner. 2018. “Dereplication of Microbial Metabolites through Database Search of Mass Spectra.” *Nature Communications* 9 (1): 1–12.

Tawfike, Ahmed Fares, Christina Viegelmann, and Ruangelie Edrada-Ebel. 2013. “Metabolomics and Dereplication Strategies in Natural Products.” In *Metabolomics Tools for Natural Product Discovery: Methods and Protocols*, edited by Ute Roessner and Daniel Anthony Dias, 227–44. Totowa, NJ: Humana Press.

Thaker, Maulik N., Wenliang Wang, Peter Spanogiannopoulos, Nicholas Waglechner, Andrew M. King, Ricardo Medina, and Gerard D. Wright. 2013. “Identifying Producers of Antibacterial Compounds by Screening for Antibiotic Resistance.” *Nature Biotechnology* 31 (10): 922–27.

Van Middlesworth, Frank, and Richard J. P. Cannell. 2008. “Dereplication and Partial Identification of Natural Products.” In *Methods in Biotechnology*.

CHAPTER 4: Elucidating the Mechanism of β-serine Biosynthesis in Edeine

Preface

The work presented in Chapter 4 has not been published.

Haley L. Zubyk, Kalinka Koteva, Jacob P. Walsh, Erin L. Westman, Sara N. Andres, Gerard D. Wright

HLZ designed and performed experiments, completed data analysis, made figures, and wrote and edited the manuscript. KK performed the NMR analysis. JPW purified edeine. ELW collected preliminary data for this project. SNA assisted with EdeM crystallization and edited the manuscript. GDW designed experiments and wrote and edited the manuscript.

Introduction

Microorganisms are adept chemical engineers capable of constructing and utilizing various molecular substrates, including β-amino acids. Unlike the more commonly known α-amino acids, which connect the amino group to the α-carbon, β-amino acids amino groups are linked to the β-carbon (Patočka 2011). These unique non-proteinogenic amino acids and their derivatives are crucial in many bioactive natural products. They not only enhance reactivity and structural diversity but also exhibit increased resistance to proteolysis, thereby stabilizing the natural products in which they are found (Patočka 2011).

A notable example is edeine, a basic linear pentapeptide antibiotic produced by the soil bacterium *Brevibacillus brevis*. The biosynthesis of edeine is orchestrated by a 45.1 kb gene cluster containing 17 open reading frames (**Figure 1**) (Westman et al. 2013). Structurally, edeine is remarkable for containing four non-proteinogenic amino acids: β-tyrosine/β-phenylalanine, β-serine, 2,3-diaminopropionic acid (DAPA), and 2,6-diamino-7-hydroxyazeleic acid (DAHAA) (**Figure 1**) (Z. Kurylo-Borowska 1975; Westman et al. 2013). Research on β-tyrosine/β-phenylalanine and DAPA biosynthetic pathways in other contexts has been elucidated (Beasley, Cheung, and Heinrichs 2011; Parry and Kurylo-Borowska 1980; Kobylarz et al. 2014). However, the biosynthesis of β-serine and DAHAA remains less understood, with DAHAA being unique to edeine and β-serine found in various nonribosomal peptides produced by marine sponges and antimicrobials like the RNA polymerase inhibitor GE23077 (Westman et al. 2013; Zhang et al. 2014; Fernández et al. 2020).

This study focuses on elucidating the biosynthesis of β-serine in edeine. By deepening our understanding of naturally occurring β-amino acids in the synthesis of edeine, this research could inform future synthetic biology applications aimed at developing novel antibiotic scaffolds to combat antibiotic resistance and enhance uses in agriculture, peptide mimetics, and combinatorial chemistry.

Several enzyme families are known to synthesize β-amino acids, including aminomutases such as lysine 2,3-aminomutase (LAM), a radical S-adenosylmethionine (SAM) enzyme. LAM uses three cofactors and a 5' deoxyadenosyl radical, produced in a SAM-activated radical reaction pathway, to transfer an amino group, converting lysine into β-lysine (Frey 1993; Pflüger et al. 2003), Another example is the 4-methylideneimidazole-5-one (MIO)-dependent enzymes like phenylalanine 2,3-aminomutase (PAM), which converts phenylalanine to β-phenylalanine (Kudo, Miyanaga, and Eguchi 2014).

In our search for a putative β-serine biosynthesis enzyme within the edeine BGC, we began by excluding genes known to produce β-tyrosine/β-phenylalanine and DAPA, narrowing our focus. Further homology searches among the remaining genes showed that aspartate aminotransferase (AAT), a pyridoxal 5' phosphate (PLP)-dependent enzyme known to react with α-amino groups when catalyzing the reversible transfer of an α-amino group from aspartate to α-ketoglutarate to form glutamate and oxaloacetate , was the closest protein homolog to EdeM, with 71% identity (**Figure 1**) (Kirsch et al. 1984). This similarity suggested the hypothesis that EdeM has the potential to be the β-serine biosynthesis enzyme.

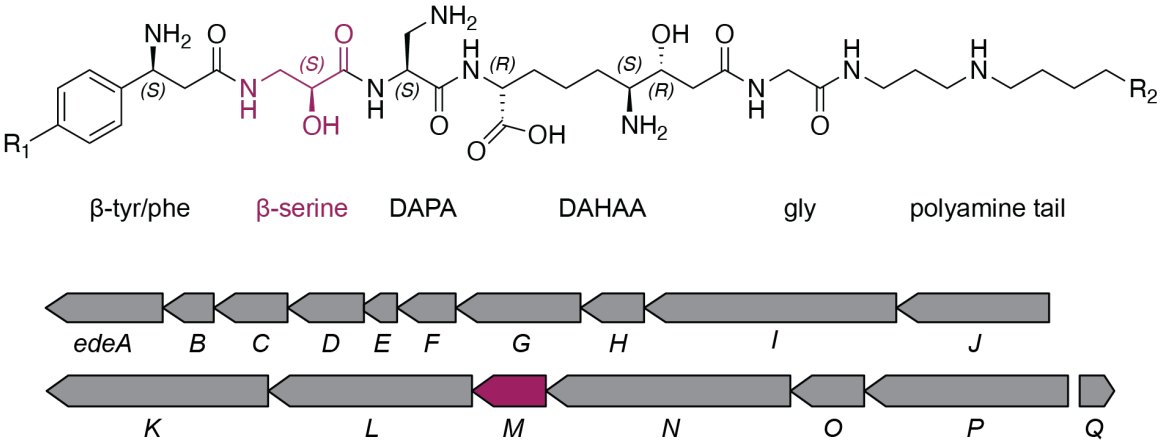

Gene	Proposed Function	Protein Homolog	% Identity
edeM	β-serine biosynthesis	aspartate aminotransferase	71

FIGURE 1. *edeM* encodes a putative β-serine synthase. The peptide antibiotic edeine is produced by *Brevibacillus brevis sp.*, and possesses four β-amino acids, including β-serine. Using the edeine biosynthetic gene cluster identified by Westman et al (2013), *edeM* was annotated as the putative gene encoding a β-serine synthase. The closest protein homolog for EdeM is aspartate aminotransferase, which belongs to a family of pyridoxal 5' phosphate-dependant enzymes known as transaminases, which can transfer amino groups between substrates.

To explore whether EdeM is responsible for β-serine biosynthesis in edeine, the gene was cloned, and the resulting protein was overexpressed and purified. X-ray crystallography confirmed that EdeM shares structural characteristics with fold-type I, class I aminotransferases. Several experiments were conducted to determine the substrate specificity of EdeM, revealing that only a single substrate, serine, is required for the formation of β-serine. Stable isotope labelling further revealed that EdeM catalyzes a reaction mechanism that is unprecedented amongst PLP-dependent enzymes. This finding underscores EdeM's distinctive role as a novel biosynthesis enzyme, making it a subject of significant interest for further research.

Materials and Methods

Molecular Cloning

Genomic DNA from *Brevibacillus brevis* Vm4 was isolated and used as the DNA template to amplify *edeM* (GenBank ID: AHH86047.1) using Phusion DNA polymerase (Thermo Scientific) according to the manufacturer's instructions. Oligonucleotide primers encoding *Nde*I and *Hind*III restriction sites were used to amplify the gene and allow insertion into the pET28a overexpression vector. The PCR product was purified and digested with the respective restriction enzymes (Thermo Scientific FastDigest Enzymes) and ligated into similarly digested pET28a before transformation into *Escherichia coli* TOP10 chemically competent cells. EdeM mutants (K40A, K235A, Y126F, Y205F, Y240F, Y320F) were prepared using site-directed mutagenesis. The sequences of all constructs were verified by Sanger sequencing (MOBIX Lab, McMaster University) before transformation into *E. coli* BL21 (DE3).

Overexpression and Purification

Overexpression strains were grown in 1L of autoinduction media (autoclaved 1% yeast extract and 2% tryptone in ddH_2O supplemented with 0.2% 1M $MgSO_4$, 4%50X LAC [25 g glycerol, 2.5 g glucose, 10 g lactose per 100 mL ddH_2O], 5% 20X NPSC [53.5 g NH_4Cl, 32.23 g Na_2SO_4, 66 g KH_2PO_4, 71 g Na_2HPO_4 per 1L ddH_2O], 0.1% trace elements [1 g $FeSO_4 \cdot 7H_2O$, 8.8 g $ZnSO_4 \cdot 7H_2O$, 0.4 g $CuSO_4 \cdot 7H_2O$, 0.15 g $MnSO_4 \cdot 4H_2O$, 0.1 g $Na_2B_4O_7 \cdot 10H_2O$, 0.05g $(NH_4)_6MO_7O_{24} \cdot 4H_2O$ in 1L ddH_2O]) supplemented with

kanamycin (50 μg/mL) and one 250 mg vitamin B6 tablet (Jamieson) as a source of PLP precursor for 3 days at 25 °C and 180 rpm. Cells were harvested by centrifugation at 6,400 × g, 4 °C, and resuspended in lysis buffer (25 mM HEPES [pH 7.5], 300 mM NaCl, and 10 mM imidazole). Resuspended cells were lysed using a continuous cell disrupter (Constant Systems Limited, Daventry UK) at 20,000 psi, 4°C in the presence of lysozyme (Bioshop), deoxyribonuclease (Sigma Aldrich), and Pierce EDTA-free protease inhibitor tablets (Thermo Scientific). Whole-cell lysate was centrifuged at 30,000 × *g* to remove cell debris before incubating clarified lysate with 1 mL of Ni-NTA resin (Qiagen) equilibrated in lysis buffer for 30 minutes on ice. The lysate-resin slurry was then loaded onto an Econo-Pac chromatography column (1.5 x 12 cm) (Bio-Rad) with a 20 mL bed volume, and the resin was washed with wash buffer (25 mM HEPES [pH 7.5], 300 mM NaCl, and 25 mM imidazole). Proteins were eluted using elution buffer (25 mM HEPES [pH 7.5], 300 mM NaCl, and 250 mM imidazole) before overnight dialysis at 4 °C against 2 L of dialysis buffer per protein (25 mM HEPES [pH 7.5], 300 mM NaCl, 0.25 mM tris-(2-carboxyethyl)-phosphine (TCEP)). Sample purity was assessed by running the elution on a 12% SDS-PAGE and visualizing the gel with Coomassie Blue R-250 staining solution before concentrating via a centrifugal filter column (Amicon Ultra-15, 30,000 NMWL) and storage at 4 °C. All samples prepared using this method were used in downstream assays. Samples used for native EdeM crystallization were further purified by anion exchange (HiTrap Q HP 5 mL, GE Healthcare) on the FPLC system (ÄKTAexplorer 100 Air; GE Healthcare) using a low to high salt gradient (low salt buffer: 25 mM HEPES [pH 7.5], 50 mM NaCl, high salt buffer: 25 mM HEPES [pH 7.5], 300 mM NaCl). Samples containing

EdeM were detected at 280 nm and analyzed using SDS-PAGE before concentration and storage at 4 °C. For seleno-methionine incorporated EdeM, pET28a:*edeM* was transformed into *E. coli* B834 before expression in M9 minimal media supplemented with amino acids (no methionine) and L-selenomethionine. Media was inoculated with a starter culture (1:250) and grown to OD_{600} = 0.5 at 37 °C, 250 rpm before inducing expression with 1 mM isopropyl β-D-1-thiogalactopyranoside (IPTG) for 20 h at 16 °C. The same purification methods were followed as those used for native EdeM crystallization.

In Vitro Assay Conditions

EdeM assays were carried out in 100 μL reactions containing 100 mM HEPES [pH 7.5], 150 mM NaCl, 1 mM L-serine, 30 μM of EdeM, and 30 μM of PLP. Reactions were incubated at 25 °C for 1 h before pre-column derivatization. Derivatization reactions contained 10 μL enzyme reaction, 10 μL 1M $NaHCO_3$, and 50 uL of 1% Marfey's reagent (N_α-(2,4-dinitro-5-fluorophenyl)-L-valinamide) solubilized in acetone. These reactions were incubated at 40 °C for 1 h before being terminated with 10 mL of 1M HCl, followed by dilution with 420 mL MeOH.

High-Performance Liquid Chromatography (HPLC)

Derivatized enzyme reactions were filtered, and 15 μL was injected onto an Agilent Eclipse XDB-C8 column (3.5 μm, 2.1 x 100 mm) and analyzed by HPLC (Agilent 1260 Infinity, Agilent Technologies). The run method was optimized to separate the L-serine starting

material and D-β-serine product (Rt = 16 min and 17 min). The HPLC separation was performed at 0.4 ml/min using the following gradient: 0 min, 10% B; 1 min, 20% B; 20 min, 30% B; 21 min, 90% B; 22 min, 10% B; 28 min, 10% B. Solvents A and B were H_2O 0.1% formic acid and CH_3CN 0.1% formic acid, respectively. Absorbance was monitored at 340 nm.

Steady-State Kinetics

Steady-state kinetics parameters of EdeM were determined using a non-continuous HPLC-based assay, following the *in vitro* assay conditions and HPLC analysis methods previously described. Standard curves for L-serine and D-β-serine were developed in the absence of the enzyme. The area under the curve (AUC) for each concentration of L-serine and D-β-serine was plotted using GraphPad Prism. Simple linear regression was applied to establish the equation of the line, which was then used to calculate the concentration of D-β-serine produced by EdeM. The enzyme was assayed across various concentrations of L-serine: 0, 0.05, 0.1, 0.25, 0.5, 1, and 2 mM, with each concentration tested in duplicate. Reactions were quenched after 15 minutes—a timeframe determined to be within the linear range of the reaction— by directly adding the sample to Marfey's derivatization reagents and initiating derivatization. The samples were subsequently analyzed by HPLC as described above. The AUC values for D-β-serine were converted to concentrations for each L-serine concentration tested. These results were analyzed using GraphPad Prism by nonlinear regression fit to the Michaelis-Menten equation (**1**).

(1) $v = (k_{cat}*E_t)S/(K_M + S)$

Mass Spectrometry

Derivatized enzyme reactions were filtered, and 0.5 mL was injected on the Q-TOF LC/MS (Agilent Technologies 6550 iFunnel) using an Agilent Eclipse XDB-C8 column (3.5 µm, 2.1 x 100 mm). The run method was optimized to separate the L-serine starting material and D-β-serine product (Rt = 12.5 min and 13.5 min). The LC/MS was run at 0.2 ml/min using the following gradient: 0.5 min, 10% B; 1 min, 20% B; 20 min, 30% B; 21 min, 90% B; 22 min, 10% B. Solvents A and B were H_2O and ACN 0.1% formic acid, respectively.

Apo-EdeM Crystallization

Crystals were grown at 23 °C using the vapour diffusion hanging drop method with 1 mL of protein solution (1.83 mg/mL) combined with 1 uL of each condition from the PEGS II precipitant libraries and 500 µL of 1.5 M ammonium sulphate in each reservoir. Crystals grew in the precipitant condition containing 0.1 M Tris [pH 8.5] and 8% PEG 8000. Crystals were flash frozen in liquid nitrogen prior to diffraction data collection. Diffraction data were collected at the McMaster University home source before collecting at the Canadian Light Source (CLS). Crystals had a strong diffraction signal of 2.5 Å with weak spots at 2.2-2.3 Å using the home source and an improved diffraction signal of 1.8 Å at the CLS; however, the crystal phase could not be determined. Selenomethionine derivatized EdeM (1.83 mg/mL) was then used to set up crystal trays with a matrix of the initial

crystallization condition (0.1 M Tris at [pH 7.5], [pH 8.0], [pH 8.5], [pH 9.0] and 6%, 8%, 10%, 12% PEG 8000). Crystals formed in 0.1 M Tris [pH 7.5] with 10% PEG 8000 at 23 °C. Crystals were flash frozen in liquid nitrogen before diffraction data collection. Diffraction data were collected at the CLS, with a diffraction signal of 2.3 Å. The apo-EdeM structure was solved using the single-wavelength anomalous diffraction (SAD) method in Phenix.solve, which identified 10 out of 11 selenium sites in the asymmetric unit. An initial model of the protein was built using Phenix.autobuild, and used to solve the structure of the apo-EdeM crystal using molecular replacement in Phenix.phaser (Liebschner et al. 2019). The structure was refined using Phenix.refine (Liebschner et al. 2019) and Coot (Emsley et al. 2010).

EdeM-PLR Crystallization

EdeM sample supplemented with PLP was reduced using 1M $NaBH_3CN$ for 1 h in the dark before washing the sample with buffer to remove the reducing agent and excess PLP. Crystals were grown at 23 °C using the vapour diffusion hanging drop method with 1 μL of protein solution (1.83 mg/mL) combined with 1 μL of reservoir solution using each condition from the MCSG X library. Crystals grew in 0.1 M MES [pH 5.5], 10% PEG 8000, and 0.2 M calcium acetate. Crystals were cryoprotected using mother liquor mixed with 25% PEG 8000 before flash freezing prior to diffraction data collection. Diffraction data were collected at the CLS, with a diffraction signal of 2.2 Å. The structure was solved using Phenix.phaser and the apo-EdeM structure for molecular replacement. Refinement was completed using Phenix.refine and coot. Reduced PLP (PLR) and acetate (co-crystallized

in the active site from the 0.2 M calcium acetate crystallization condition) were modelled into the Fo-Fc difference in density at RMSD 1 Å sigma level after initial rounds of refinement.

Labelling with $^{18}OH_2$

Reactions were set up using 100 mM HEPES [pH 7.5], 150 mM NaCl, 30 μM EdeM, and 1 mM L-serine solubilized in $^{18}OH_2$, with 86% of the total volume (100 μL) comprised of pure $^{18}OH_2$. As a positive control for $^{18}OH_2$ incorporation, reactions containing the metallo-b-lactamase NDM-1 (1 μM) (King et al. 2014) and meropenem (0.5 mM) were prepared and treated the same. Controls for both EdeM and NDM-1 reactions were prepared in H_2O. Reactions were incubated at 30 °C for 1 h before derivatizing reaction contents with Marfey's reagent, as previously described. Derivatized samples were injected into the Q-TOF LC/MS (Agilent Technologies 6550 iFunnel) to detect $^{18}OH_2$ incorporation using the same method as previously described.

NMR Spectroscopy of ^{13}C-Serine Reaction Products

EdeM assays were carried out in 1 mL reactions containing 100 mM HEPES [pH 7.5], 150 mM NaCl, 150 μM of enzyme, and either 1 mg of L-serine-2-^{13}C or L-serine-1-^{13}C. Reactions were incubated at 30 °C for 1 h before derivatizing reaction contents with Marfey's reagent, as previously described. The derivatized samples were then lyophilized and resuspended in 1 mL of DMSO before loading the entire volume onto a 43 g C18

RediSep column for purification via flash chromatography (CombiFlash Rf 200) (solvent A: H_2O 0.1% formic acid, solvent B: can 0.1% formic acid). This method separated the ^{13}C-labelled starting material and the ^{13}C-labelled D-β-serine reaction product. No-enzyme control reactions containing 1 mg of L-serine-2-^{13}C or L-serine-1-13C were also prepared and purified using the same methods. The purified controls and ^{13}C-labelled D-β-serine reaction product were lyophilized and resuspended in DMSO-d_6 (Cambridge Isotopes) for NMR. Experiments were run on a Bruker 700 MHz spectrometer (Center for Microbial Chemical Biology, McMaster University) to determine the position of the D-β-serine ^{13}C labels.

Edeine Purification

Starter cultures of *B. brevis* Vm4 were grown in a 500 mL baffled Erlenmeyer flask containing 100 mL of PY media (in 1L ddH_2O: 10 g peptone from casein, 5 g yeast extract, 5 g NaCl, and after autoclaving, add $MgCl_2$ 50 μg/mL and $MnCl_2$ 30 μg/mL) at 30 °C for 3 days at 250 rpm. The starter culture was used to inoculate 4L (1:50 inoculum) of yeast minimal media (in 1L ddH_2O: 15 g glycerol, 15 g yeast extract, 1.5 g $CaCO_3$, 10 mL of precursor solution 1 [in 50 mL ddH_2O: 200 mg each of arginine, ornithine, lysine, glutamic acid, phosphor-serine, serine, and glycine] and solution 2 [in 50 mL ddH_2O: 200 mg each of tyrosine and phenylalanine, pH adjusted to pH 8.0 with NaOH]). The bulk culture was pH adjusted to pH 7.0 and aliquoted into 50 mL volumes in separate 250 mL baffled Erlenmeyer flasks. Flasks were incubated at 30 °C overnight at 250 rpm. Following incubation, cells were harvested by centrifugation at 6,400 × g and supernatant was

combined with 5% v:v (wet) HP20 resin and incubated overnight at 4 °C with gentle rocking. Compounds were extracted from the resin via batch extraction using a MeOH:ddH_2O 20% v:v stepwise gradient from 0-100% MeOH (20, 40, 60, 80, 100% MeOH fractions), with a 4X volume-to-resin ratio for each fraction. Fractions were tested for edeine activity via Kirby Bauer disk diffusion assays against *E. coli* BW25113 Δ*bamB* Δ*tolC* (control, edeine^s) and *E. coli* BW25113 Δ*bamB* Δ*tolC* pGDP1:*edeQ* (test strain, edeine^r) on LB agar Petri dishes by spotting 20 µL of each fraction onto 6 mm thick antibiotic test disks (A.M.D. Manufacturing Inc). The 40, 60, and 80% fractions were found to possess activity against the edeine^s strain but not the edeine^r strain, indicating the presence of edeine. Active fractions were pooled, lyophilized, and resuspended in 200 mL of ddH_2O. Resuspended active fractions were next combined with preconditioned AG 50-X4 resin (20 mL of hydrated resin was washed with three 10X volumes of ddH_2O) (hydrogen-form, 50-100 mesh, Bio-Rad and gently agitated for 30 minutes at room temperature. The resin was applied into a glass column (2.5 x 25 cm) and washed with an additional 5X column volumes of ddH_2O. A 0.1-1M gradient of NH_4OH was used to elute edeine from the column. Following elution, the resin was washed with an additional 3X column volume of NH_4OH to remove any remaining edeine from the column. Fractions (10 mL) were collected throughout the elution and neutralized to pH 7.0 through dropwise titration of glacial acetic acid. Fractions were tested for antibiotic activity and positive fractions were pooled and lyophilized before the final purification step using a Sephadex G-50 size exclusion column (2.8 x 90 cm) in water with a flow rate of 60 mL/hour. Fractions (6 mL) were assessed for antibiotic activity, and the active fractions were lyophilized. The

presence of edeine B was confirmed via 700 MHz NMR (^{1}H, ^{13}C, COSY, HSQC, HMBC (Bruker AVIII)) and LC-MS (Agilent 6546 Q-ToF with a dual AJS electrospray ionization source). A total of 70 mg of edeine was obtained from 4 L of *B. brevis* Vm4 culture.

Edeine Hydrolysis and Mass Spectrometry

Purified edeine B was hydrolyzed by combining 2.6 mg of sample with 5 mL of 6N HCl and incubating the mixture at 90 °C for 24 h before evaporation under a stream of N_2. The hydrolyzed edeine sample was derivatized with Marfey's reagent as previously described. Samples were injected on the Q-TOF LC/MS (Agilent Technologies 6550 iFunnel) using an Agilent Eclipse XDB-C8 column (3.5 μm, 2.1 x 100 mm. The LC/MS was run at 0.2 ml/min using the following gradient: 1 min, 5% B; 7 min, 95% B; 7.5 min, 95% B; 8 min, 95% B. Solvents A and B were H_2O and CH_3CN 0.1% formic acid, respectively

Results

EdeM converts L-serine to D-β-serine without additional substrates

Transaminases play a crucial role in amino acid metabolism and require two substrates: an amino group donor (amino acid) and an amino group acceptor (α-keto acid) (Koper et al. 2022). AAT, a protein identified to share a similar sequence with EdeM as predicted using the Basic Local Alignment Search Tool (BLAST) (% ID = 71) (Camacho et al. 2009), catalyzes the conversion of aspartate (amino group donor) and α-ketoglutarate (amino group acceptor) into oxaloacetate and glutamate (**Figure 2a**). To investigate

whether EdeM functions similarly in producing β-serine from serine, we hypothesized that serine would be utilized by EdeM as the amino group donor and 2-hydroxy-3-oxopropionic acid as the amino group acceptor (**Figure 2b**).

To test this hypothesis, *edeM* was cloned, and the encoded enzyme was overexpressed and purified. An endpoint analytical assay was then employed to monitor reactions involving EdeM with various substrates. The results were analyzed via mass spectrometry and confirmed that EdeM can convert L-serine to D-β-serine independently, without requiring additional substrates (**Figure 2c**).

To investigate the amino acid substrate specificity of EdeM, assays were conducted using ten additional amino acids (alanine, valine, leucine, methionine, asparagine, aspartate, threonine, cysteine, phenylalanine, and tryptophan). None reacted with EdeM to form a product, indicating a specific interaction with L-serine. Following these specificity tests, the steady-state kinetic parameters of EdeM reacting with L-serine were determined using an HPLC-based assay to more comprehensively characterize the enzyme's activity (**Figure 3**). The measured values were consistent with literature reports indicating that enzymes involved in secondary metabolism are typically ~30-fold slower than those in central metabolism and shared similarities with those reported for AAT (Bar-Even et al. 2011; M. D. Toney and Kirsch 1991).

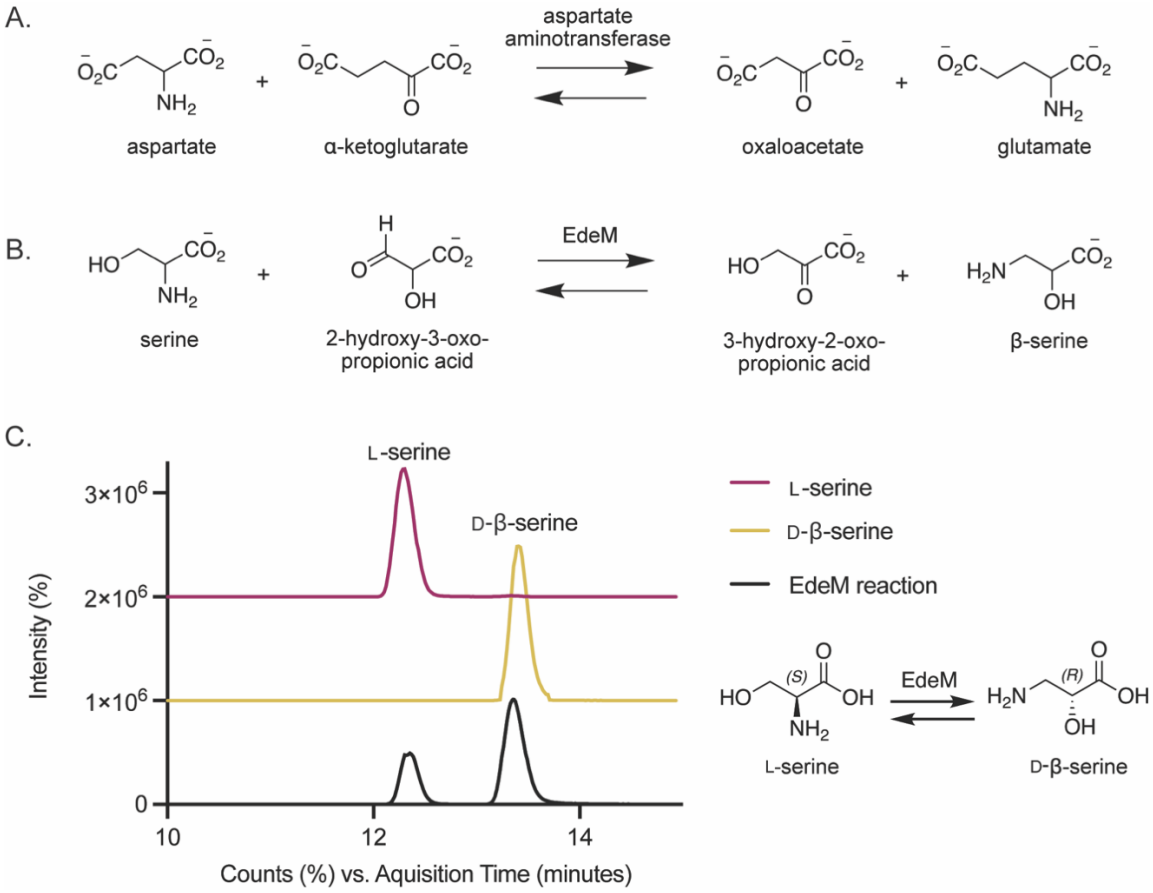

FIGURE 2. EdeM only requires one substrate. A. Aspartate aminotransferase (AAT) produces glutamate and oxaloacetate from aspartate and α-ketoglutarate. **B.** Modelled after an analogous reaction mechanism to AAT, it was hypothesized that EdeM produces β-serine and 3-hydroxy-2-oxo-propionic acid from serine and 2-hydroxy-3-oxo-propionic acid. **C.** Positive mode extracted ion chromatogram (+EIC) at 386.13 *m/z*. Standards for Marfey's derivatized L-serine and D-β-serine are shown in maroon and yellow, with 12.5- and 13.5-minute retention times. The contents of a 1-hour reaction containing EdeM and L-serine are shown in black. While the peak for L-serine is present, there is also the formation of a second peak that corresponds with D-β-serine. These data demonstrate that EdeM can convert L-serine to D-β-serine without additional substrates.

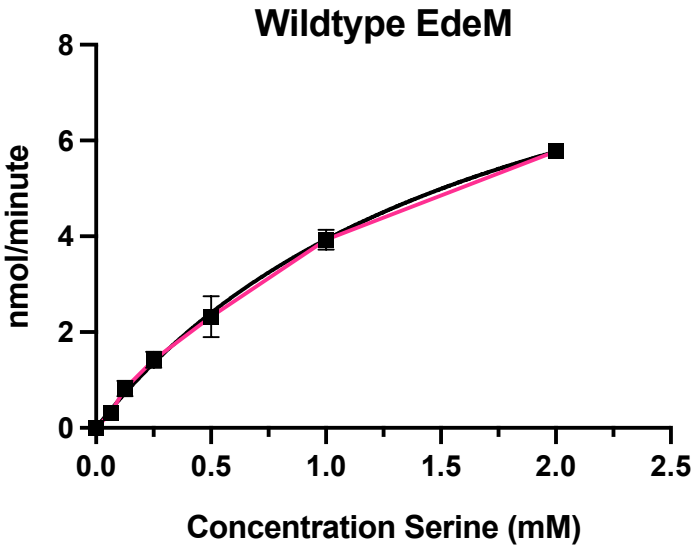

K_M (mM)	k_{cat} (s^{-1})	k_{cat}/K_M ($M^{-1}s^{-1}$)
1.75 ± 0.54	0.06	3.43×10^1

FIGURE 3. Steady-state kinetic parameters of EdeM at 25 °C

Comparing EdeM to aspartate aminotransferase

Given the unique mechanistic properties of EdeM compared to typical transaminases, we proceeded to crystallize EdeM and compare its 3D crystal structure with that of AAT (**statistics are shown in Supplementary Table 1**). Crystal structures for both apo-EdeM and EdeM-PLR (reduced PLP) with acetate co-crystallized in the active site were obtained (**Supplemental Figure 1**). This analysis aimed to identify structural differences that could elucidate how EdeM's mechanism is facilitated.

PLP-dependent enzymes can be divided into seven protein families based on the 3-dimensional fold of the proteins (fold-types I to VII) – all of which are structurally unrelated (Koper et al. 2022). Aminotransferases (ATs), also known as transaminases, are found in

fold-type families I and IV, and are further phylogenetically divided into four distinct classes: Class I, II, III, and IV (Koper et al. 2022). Classes I, II, and IV have evolved from an ancestral fold-type I enzyme, whereas class III has independently evolved from a fold-type IV enzyme (Mehta, Hale, and Christen 1993; Christen and Mehta 2001). Each class of transaminase forms distinct phylogenetic clades and utilizes similar substrates (Koper et al. 2022). Within these, class I is the largest and most functionally diverse class of transaminases and utilizes substrates such as aspartate, aromatic amino acids, histidinol phosphate, kynurenine, and diaminopimelate (Koper et al. 2022).

Fold-type I transaminases usually form homodimers or homotetramers, which are essential for enzymatic function since the active site is located at the interface between subunits (Milano et al. 2013). The active site is built mostly from one subunit but contains essential residues contributed from the dimer-related protomer (Cheong, Escalante-Semerena, and Rayment 2002). Each subunit is approximately 400 residues long and with a molecular weight of ~ 45 kDa. These subunits are organized into a large N-terminal domain (~ residues 48-325), a small C-terminal domain (~ residues 14-47 and 326-410), and a shorter linker domain (~ residues 3-14) (McPhalen, Vincent, and Jansonius 1992). The large domain, which interacts with the PLP cofactor, is referred to as the cofactor domain. The smaller domain is flexible, transitioning from an "open" to a "closed" conformation upon amino acid substrate binding, thereby enclosing the substrate within the active site (McPhalen, Vincent, and Jansonius 1992). The third domain, much shorter, contains just enough residues to form an extended strand contributing to the dimer's structural stability (McPhalen, Vincent, and Jansonius 1992).

AAT is one of the most thoroughly studied fold-type I, class I transaminases (Christen and Mehta 2001). Structural alignments performed in PyMol between EdeM and AAT from *Escherichia coli* (Protein Data Bank [PDB] ID 1ARG) (Graber et al. 1995) reveal considerable similarities between the two enzymes (**Figure 4a**) (Schrödinger, L., & DeLano, W. 2020). EdeM, like AAT, forms a homodimer and contains 387 residues, resulting in a molecular weight of 44.2 kDa, consistent with that of transaminases. Additionally, EdeM appears to have adopted a closed conformation in the EdeM-PLR crystal structure, with co-crystallization of acetate in the active site mimicking the binding of an amino acid substrate. A whole protein alignment of apo-EdeM and EdeM-PLR in Pymol results in a root-mean-square deviation (RMSD) of atomic position of 1.85 Å due to bulk movement of the small domain inward toward the active site (**Supplemental Figure 2**), resembling the changes seen between open and closed conformations in AAT (Kirsch et al. 1984). Although EdeM and AAT share only 16% sequence similarity, the widespread structural similarity across PLP-DE makes their similarity in folds and domains unsurprising (Hoegl et al. 2018). A pair-wise structural alignment using the DALI Protein Structure Comparison Server reveals an RMSD of 3.0 Å, indicating a reasonably significant structural alignment between the homodimers of both enzymes (Holm 2020).

Certain amino acid residues in the active site are highly conserved among transaminases to accommodate substrates and the PLP cofactor for efficient catalytic activity. To illustrate these residues, numbering taken from the *E. coli* class I aspartate aminotransferase (PDB 1ARG) (Graber et al. 1995) will be used. All transaminases must have an active-site lysine (K258) that forms a Schiff-base linkage with the cofactor PLP

(Koper et al. 2022). Additionally, an active-site aspartate (D222) is essential for maintaining protonation of the PLP pyridine ring nitrogen, crucial for the transamination reaction, and an arginine residue (R386) coordinates the α-carboxylate of the enzyme substrates (Michael D. Toney 2014). In class I transaminases, several additional residues are conserved, such as an asparagine (N194) and tyrosine (Y225) that interact with the pyridine ring and another arginine residue (R266), which stabilize the phosphate group of the PLP cofactor.

Furthermore, although not conserved across all transaminases, an aromatic tryptophan residue (W140) that facilitates pi stacking with the pyridine ring of PLP is present in many (Koper et al. 2022). These conserved residues are crucial for maintaining the proper conformation and functionality of the active site. When comparing the active site of EdeM with AAT, it becomes apparent that both enzymes share these conserved residues, except for tryptophan 140, which is replaced by a tyrosine residue in EdeM. Since both amino acids are aromatic and capable of facilitating pi stacking with PLP, this substitution does not appear to be significant. Alignment of the conserved active site residues and the PLP cofactor in Chain A of both enzymes yielded an RMSD value of 0.84 Å (**Figure 4b**). These results suggest that although EdeM only requires one substrate to convert L-serine to D-β-serine, the enzyme likely employs canonical PLP transaminase chemistry using the known conserved catalytic residues.

Proposed single-substrate transamination reaction

Fold-type I PLP-dependent enzymes share key mechanistic features, including the covalent linkage of PLP to the ε-amino group of an active-site lysine residue via a Schiff

base, forming an internal aldimine (Christen and Mehta 2001). When the enzyme encounters its amino acid substrate, the amino group of the substrate replaces the ε-amino group via a transaldimination reaction, forming an external aldimine common to all PLP-dependent enzyme reactions with amino (Christen and Mehta 2001). Regardless of the reaction type, PLP acts as an electron sink, stabilizing carbanionic intermediates by storing electrons from the cleaved substrate bonds and donating them for the formation of new bonds with incoming protons or additional substrates (Christen and Mehta 2001; Walsh 1979).

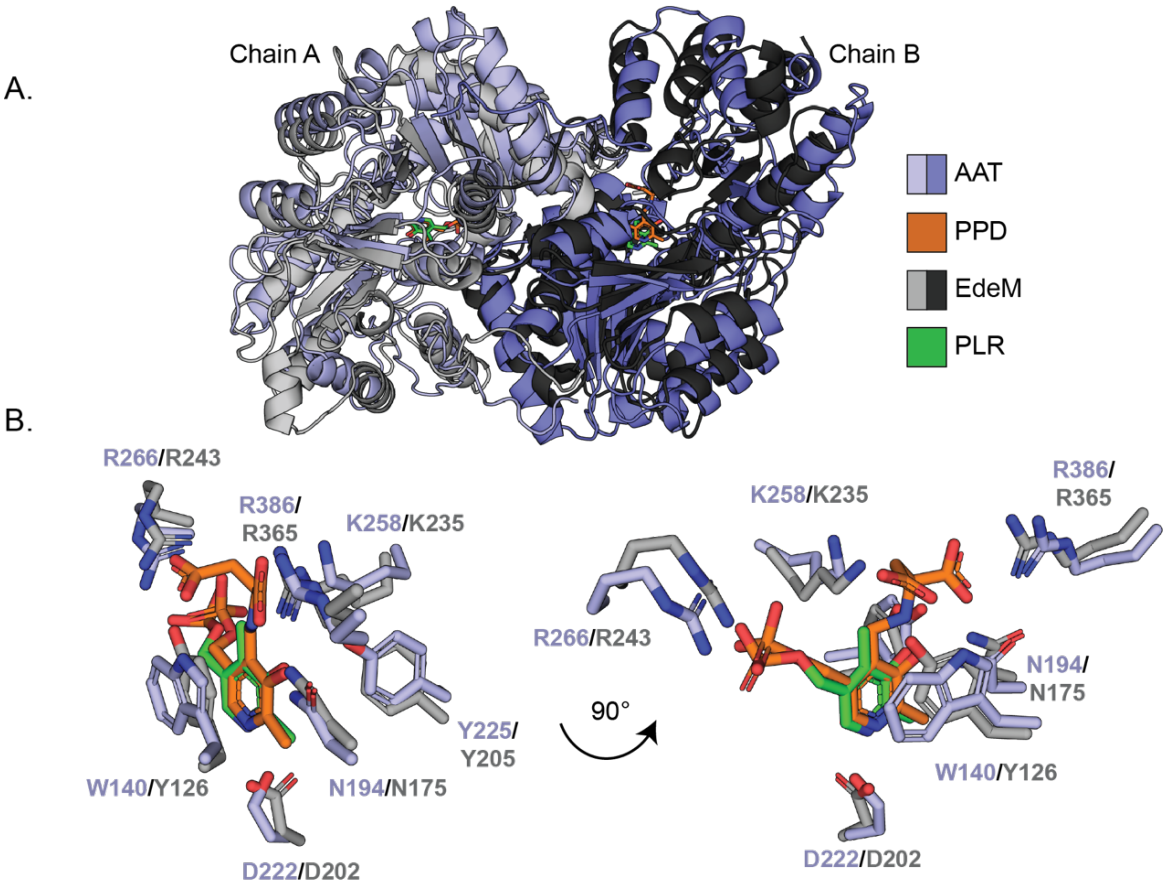

FIGURE 4. Structural comparison of EdeM and AAT. A. Alignment of EdeM (resolution 2.3 Å) (grey) and AAT from *E. coli* (PDB 1ARG, resolution 2.20 Å) (purple) crystal structures using PyMol. EdeM co-crystalized in the presence of reduced PLP (PLR), shown in green. AAT co-crystalized in the presence of PLP-bound aspartate (external aldimine) (PPD), shown in orange. Pairwise structural alignment of both proteins in DALI produces a Z score of 32.5, RMSD 2.8 Å, and % ID 16. **B.** Alignment of conserved active site residues and bound cofactors. RMSD 0.84 Å. Active site alignments were performed with Chain A of EdeM due to K235 being unbound to the cofactor and more structurally similar to the external aldimine (PPD) formed in AAT.

Transaminases utilize a "ping-pong bi-bi" kinetic mechanism to transfer amino groups (McPhalen, Vincent, and Jansonius 1992; Michael D. Toney 2014). In the first half-reaction, PLP forms an internal aldimine with the ε-amino group of a catalytic lysine residue in the active site. Upon contact with the amino acid substrate, a transaldimination reaction occurs, breaking the bond between PLP and the enzyme to form a Schiff base with the amino acid, creating an external aldimine. The external aldimine then forms a quinoid intermediate, which is converted to ketimine before being hydrolyzed to release its first product, an α-keto acid, and generate the PLP intermediate, pyridoxamine phosphate (PMP) (**Figure 5**). In the second half-reaction, the amino acceptor α-ketoglutarate reacts with PMP, reversing the initial reaction steps to regenerate PLP and release the 2nd product, an amino acid (Michael D. Toney 2014).

Given that EdeM requires only one substrate to convert L-serine to D-β-serine, and considering its strong structural resemblance to typical transaminases, a single-substrate transamination reaction was proposed, adhering to the established PLP transaminase chemistry.

We hypothesized that EdeM would follow the same steps as a typical transaminase in the first half-reaction, as previously described for AAT. This involves L-serine reacting with PLP to generate PMP and release the α-keto acid 3-hydroxy-2-oxo-propionic acid through hydrolysis. However, rather than discarding this newly generated α-keto acid to react with an incoming second substrate, an α-keto acid, amino group acceptor, 3-hydroxy-2-oxo-propinoic acid, participates in a keto-enol tautomerization to form 2-hydroxy-3-oxo-

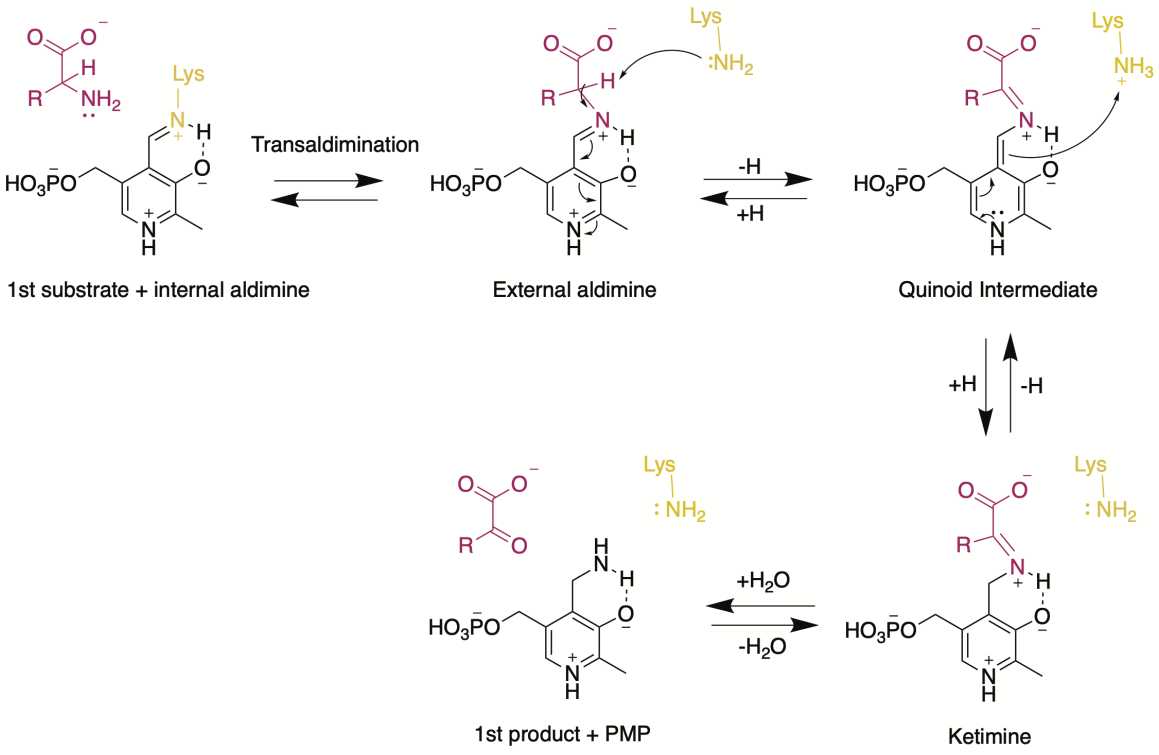

FIGURE 5. First half-reaction of fold type I transaminase catalyzed reactions. Typically, transaminases require two substrates: an amino-group donor (amino acid) and an amino-group acceptor (α-keto acid). In the first half-reaction of the bi-bi ping-pong, the internal aldimine formed between PLP and a catalytic lysine residue undergoes a transaldimination reaction with the amino acid substrate, forming the external aldimine. The α-carbon proton is then abstracted by an active site base (lysine), forming the quinoid intermediate. The nitrogen of the pyridine ring is then protonated, leading to formation of the ketimine intermediate that is readily hydrolyzed to release an α-keto acid and pyridoxamine phosphate (PMP).

propionic acid. This aldehyde could then act as the 'second substrate', which could react with the PMP intermediate, producing D-β-serine and regenerating PLP. To test this hypothesis, EdeM reactions were prepared in the presence of $^{18}OH_2$. If the proposed mechanism was correct, incorporation of ^{18}O into 3-hydroxy-2-oxo-propinoic acid upon hydrolysis would be expected and carried through to the D-β-serine final product (**Figure 6**). After derivatization with Marfey's reagent, the $^{18}OH_2$ reactions were analyzed by high-resolution mass spectrometry in an effort to detect a mass increase of 2 Da (388.14 *m/*z) compared to the $^{16}OH_2$ control (386.14 *m/*z), which would indicate successful ^{18}O incorporation. As a positive control for ^{18}O incorporation via hydrolysis, we used the well-characterized β-lactamase NDM-1 in an $^{18}OH_2$ reaction with its substrate, meropenem to confirm our ability to measure the expected 2Da increase in product (**Supplemental Figure 3**). When the experiment was repeated with EdeM and L-serine, the results showed a negligible increase in ^{18}O incorporation (< 1%) between the L-serine starting material and D-β-serine final product. This result is inconsistent with the involvement of a hydrolysis step in the EdeM reaction, suggesting that the enzyme does not employ a conventional two-substrate transamination mechanism to produce D-β-serine (**Figure 7**).

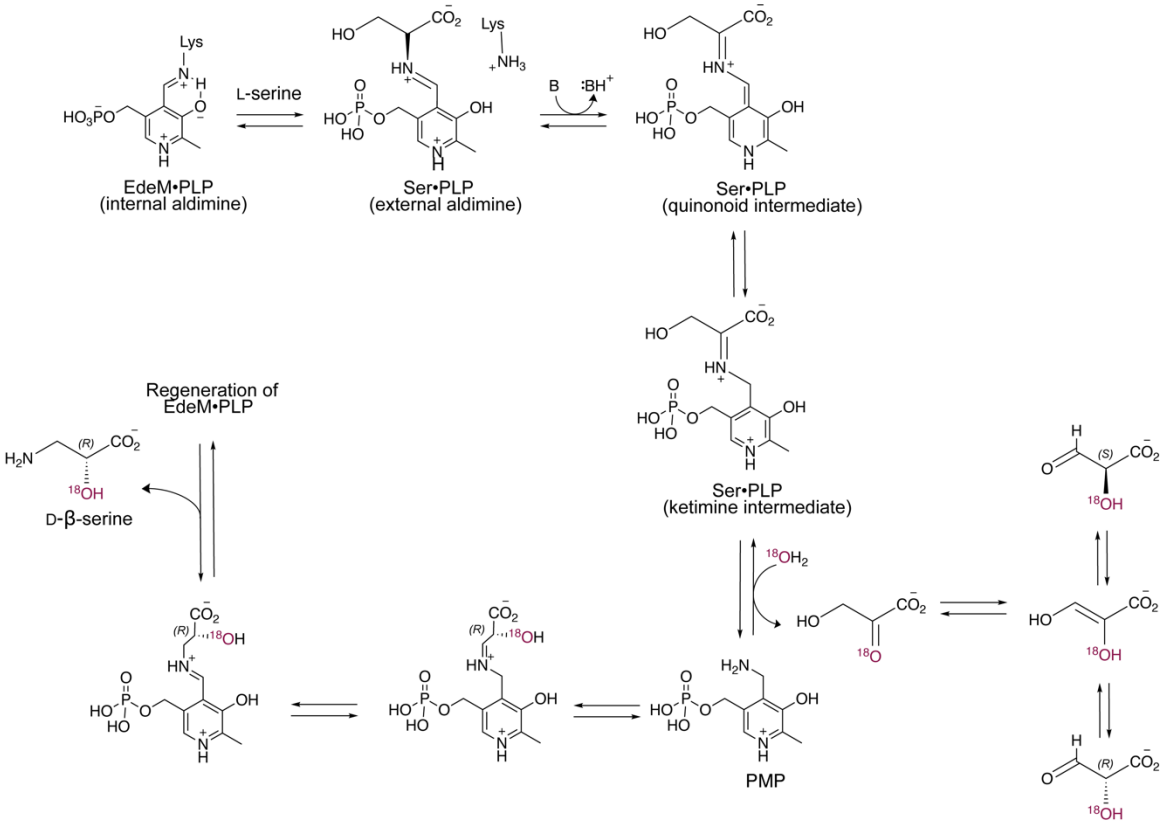

FIGURE 6. Proposed EdeM single-substrate transamination reaction. In the first half-reaction, L-serine reacts with PLP to generate PMP and release the α-keto acid 2-hydroxy-3-oxo-propionic acid through hydrolysis. In the second half-reaction, 2-hydroxy-3-oxo-propionic acid tautomerizes to form an aldehyde, which reacts with PMP to accept the amino group. This results in the production of D-β-serine and the regeneration of PLP. It is hypothesized that if EdeM catalyzes a transamination reaction in the presence of $^{18}OH_2$, ^{18}O should be incorporated into D-β-serine precursors during the hydrolysis reaction at the end of the first half-reaction, leading to the formation of ^{18}O-D-β-serine.

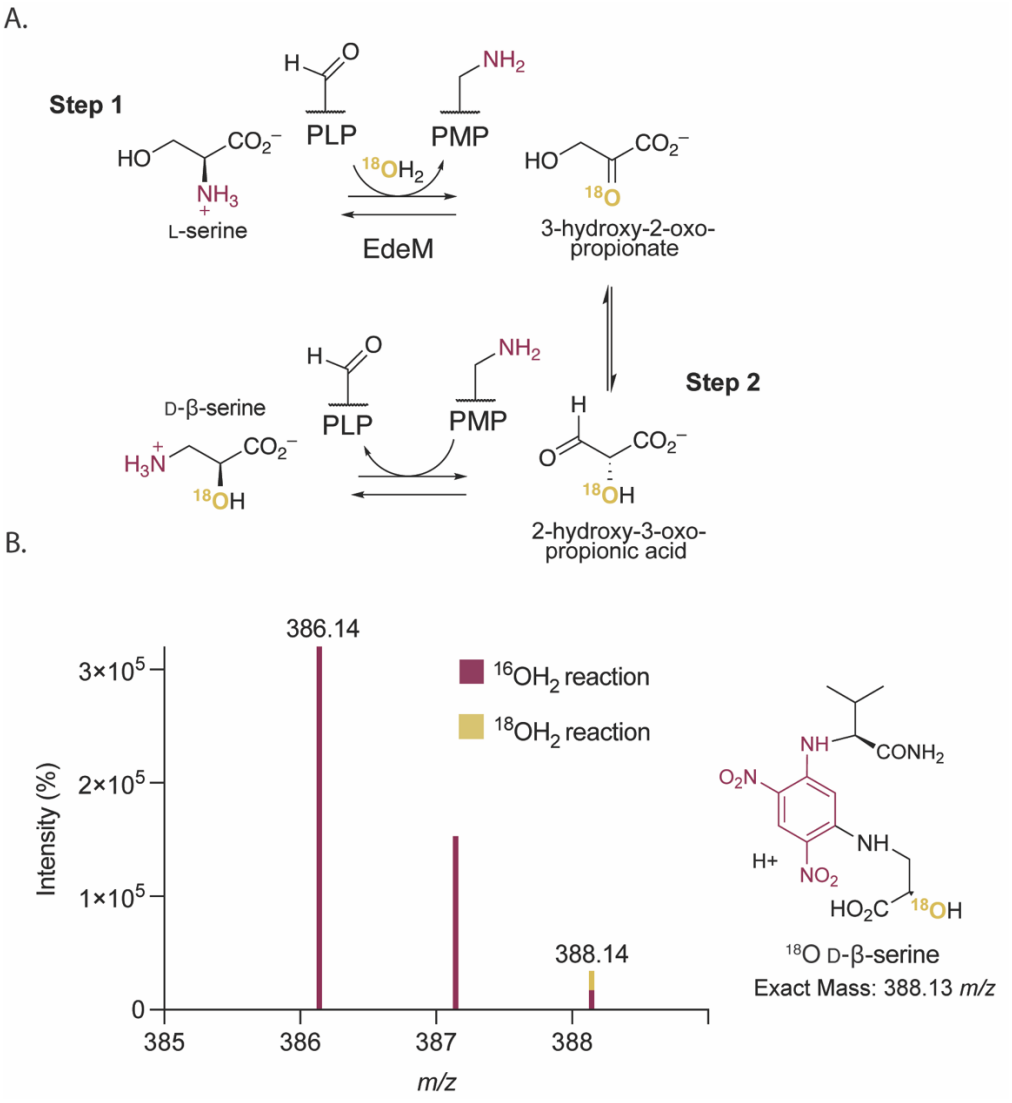

FIGURE 7. EdeM does not incorporate ^{18}O into D-β-serine. A. Simplified schematic of the proposed single-substrate transamination mechanism of EdeM. **B.** Positive-ion mode electrospray mass spectra of D-β-serine in EdeM reactions prepared in $^{16}OH_2$ (control) and $^{18}OH_2$. Samples were left for 1 hour at 37°C before derivatizing with Marfey's reagent and analyzing reaction products by high-resolution mass spectrometry. It is expected that if ^{18}O is incorporated into D-β-serine during the first half-reaction hydrolysis step, the final product will have a mass increase of 2 Da for a molecular weight of 388.13 *m/z* compared to reactions prepared in $^{16}OH_2$ (386.14 *m/z*). Compared to the control, there is a negligible difference between the signals produced for both reactions, indicating that EdeM, the proposed transamination reaction, is incorrect.

Investigating the molecular transformation of L-serine by EdeM

Discovering that the enzymatic mechanism of EdeM does not involve a hydrolysis step, which typically leads to the release of an initial product and PMP, prompted us to investigate whether EdeM catalyzes an unexpected rearrangement of L-serine to produce D-β-serine. The lack of evidence for a hydrolysis step suggests that serine may remain bound to PLP throughout the reaction.

To further explore this hypothesis, we conducted large-scale EdeM reactions (10X the volume used for *in vitro* assays) using two different L-serine samples labelled with ^{13}C at distinct positions (C2 – the α-carbon and C1 – the carboxy group carbon). After purifying the reaction product, we analyzed it using NMR to determine the fate of the isotopic label.

Results showed that compared to the L-serine-2-^{13}C control, the ^{13}C label of the product was observed at the β-position, forming D-β-serine-3-^{13}C, and reactions containing L-serine-1-^{13}C yielded D-β-serine-1-^{13}C (**Supplemental Figures 4-25, Supplemental Tables 2-3**). These products are consistent with a rearrangement involving the migration of CO_2 from the 'C-terminus' to the 'N-terminus of L-serine'. In this process, the carboxy group carbon (C1) forms a new C-C bond with the hydroxyl group carbon (C3) of L-serine, transforming C3 into C2. This creates a new chiral center at this newly formed C2 α-position. The amino group carbon (initially C2) then becomes C3 at the β-position, leading to the formation of D-β-serine (**Figure 8a**).

The detection of D-β-serine-1-^{13}C from L-serine-1-^{13}C suggests that the CO_2 involved in this rearrangement either originates from the serine molecule being rearranged or another molecule of serine within the active site rather than from an exogenous source

(**Figure 8b**). However, considering the limited space in the active site of EdeM and the improbability of accommodating a second serine molecule, it is likely that the transferred CO_2 originates from the same molecule undergoing rearrangement.

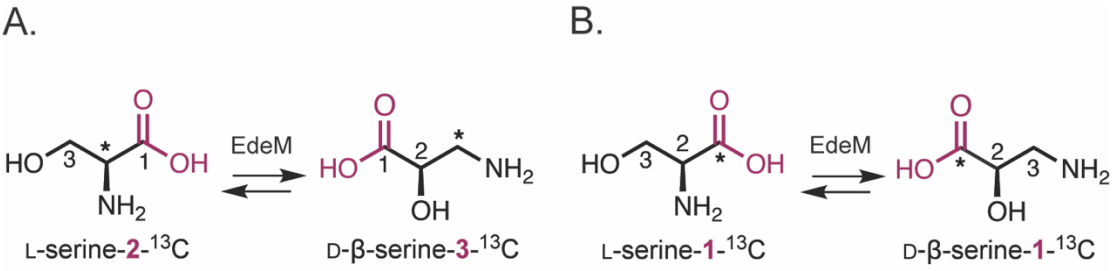

FIGURE 8. Schematic of the rearrangement of ^{13}C-labelled serine by EdeM. The position of the ^{13}C label is indicated by (*) **A.** In a reaction with L-serine-2-^{13}C, EdeM catalyzed the formation of D-β-serine-3-^{13}C, indicating that the ^{13}C label was moved from the C2 to C3 position. This likely occurs through the movement of the carboxy group, which includes C1. C1 forms a new C-C bond with C3, transforming C3 into C2. The amino group carbon (initially the C2 α-carbon) then becomes C3 at the β-position, leading to the formation of D-β-serine **B.** In a reaction with L-serine-1-^{13}C, EdeM catalyzed the formation of D-β-serine-1-^{13}C. This shows that the ^{13}C label moved with the rearrangement of CO_2 to form D-β-serine, indicating that the rearranged CO_2 originated from the labelled serine molecule itself rather than from an external source.

Comparing EdeM to PLP-dependent decarboxylases

Comparison to DC II and III subfamily decarboxylases

To gain insight into the molecular rearrangement of L-serine catalyzed by EdeM, we revisited the protein's crystal structure with the newfound understanding that it does not

function as a transaminase, which transfers an amino group to produce its final product but instead catalyzes the movement of CO_2. EdeM belongs to the fold-type I family of PLP-dependent enzymes, which is primarily composed of transaminases; however, it also includes amino acid decarboxylases (DCs), which are further divided into three subfamilies (DC I-III) (Christen and Mehta 2001).

The DC I subfamily contains more distantly related enzymes, such as glycine dehydrogenase and glycine hydroxymethyltransferase. DC II is comprised of glutamate, histidine, and tyrosine/L-3,4-dihydroxyphenylalanine decarboxylases, while DC III includes ornithine, arginine, and lysine decarboxylases. Although these enzymes all contain PLP-binding domains, their sizes vary significantly compared to aminotransferases (Cheong et al. 2002).

Hypothesizing that the first step in the EdeM reaction involves the decarboxylation of L-serine, we compared the structure of EdeM against decarboxylases from subfamilies DC II and III to identify similarities that could explain how EdeM decarboxylates L-serine. Glutamate DC (GAD) was selected from the DC II subfamily for structural comparison as it shares the highest substrate similarity with EdeM. GAD catalyzes the irreversible decarboxylation of L-glutamic acid to γ-aminobutyric acid (Yogeswara, Maneerat, and Haltrich 2020).

Extensive analysis of GAD from *Lactobacillus* sp. revealed a sequence of highly conserved residues in PLP-dependant DC (HVD[A/S]A[S/F]GG) (Yogeswara, Maneerat, and Haltrich 2020). Furthermore, analysis of the structure of *L. brevis* GAD (PDB 5GP4) identified a flexible loop, residues Tyr-308-Glu312, located near the substrate binding site.

This loop is important for the catalytic reaction, with the conserved Tyr residue being essential for facilitating decarboxylation (Yogeswara, Maneerat, and Haltrich 2020). Thr215 and Asp246 are two additional highly conserved catalytic residues that promote decarboxylation (Yogeswara, Maneerat, and Haltrich 2020). However, upon comparing this crystal structure with EdeM, it was determined that EdeM does not possess equivalent conserved residues.

Next, a structural comparison was conducted for EdeM and ornithine decarboxylase, which is representative of all DC III decarboxylases, including lysine and arginine DC (Momany et al. 1995). Analysis of critical active site residues in ornithine DC from *Lactobacillus* 30a (PDB 1ORD) (Momany et al. 1995) and AAT from *E. coli* (1ARG) (Graber et al. 1995) within EdeM revealed that while EdeM possesses all of the conserved AAT residues, it does not contain any of the DC residues uniquely utilized by ornithine DC (**Figure 9**) (**Table 1**). This includes the histidine residue stacked in front of the cofactor pyridine ring, which acts as a possible proton donor and is highly conserved among PLP-dependent decarboxylases (Burkhard et al. 2001). These results suggest that although EdeM is not a transaminase, its overall structure and active site are more similar to PLP-dependent transaminases than subfamily DC II or III decarboxylases.

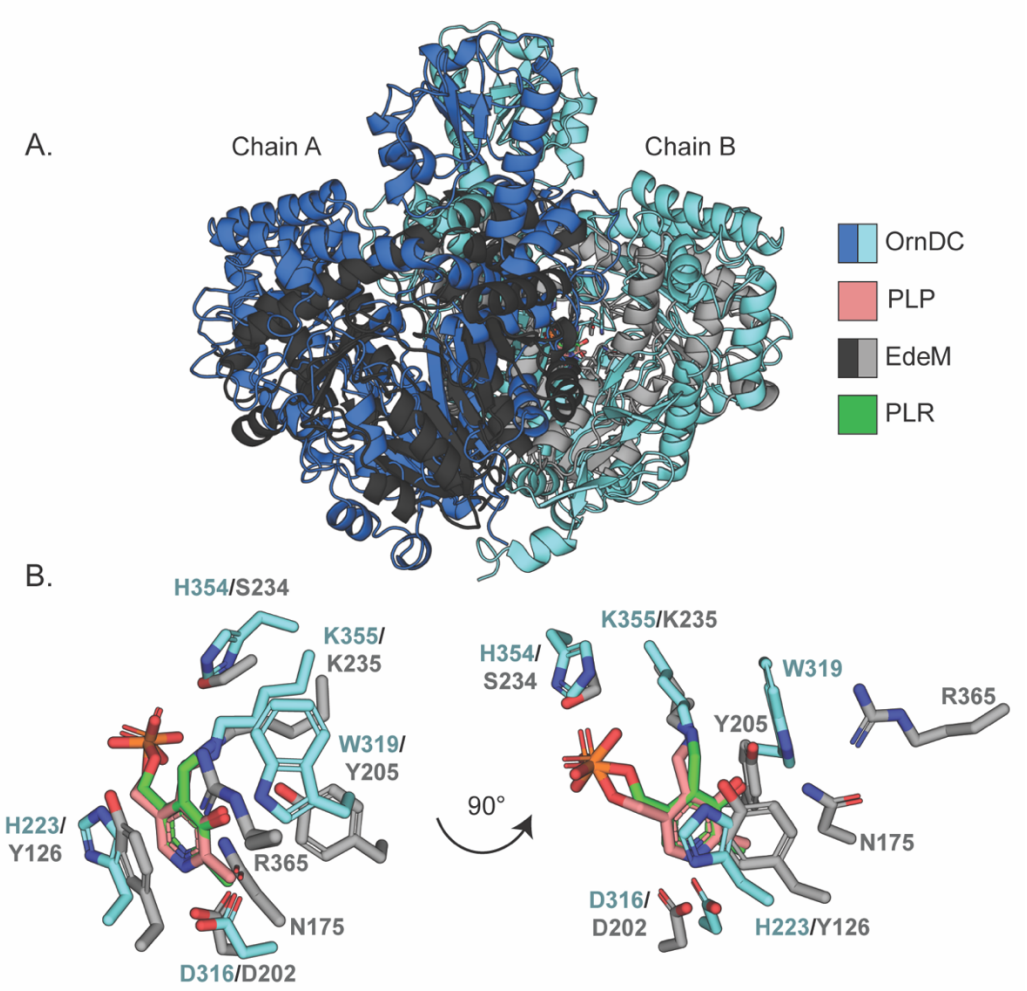

FIGURE 9. Structural comparison of EdeM and Ornithine DC. A. Alignment of EdeM (resolution 2.3 Å) (grey) and ornithine DC from *Lactobacillus* 30a (PDB 1ORD, resolution 3.0 Å) (blue) crystal structures using PyMol. EdeM co-crystalized in the presence of reduced PLP (PLR), shown in green. Ornithine DC co-crystalized in the presence of PLP (internal aldimine) (PLP), shown in pink. Pairwise structural alignment of both proteins in DALI produces a Z score of 16.3, RMSD 4.8 Å, and % ID 10. **B.** Alignment of conserved active site residues and bound cofactors. RMSD 1.15 Å. Active site alignments were performed with Chain B of EdeM due to K235 being bound to the cofactor and more structurally similar to the internal aldimine formed in ornithine DC.

Functional or structural role	OrnDC residue	AAT residue	EdeM residue
Schiff base with PLP	Lys355	Lys258	Lys235
Salt bridge/H-bond with α-carboxylate group of substrate	-	Arg386	Arg365
H-bond to OH of PLP	Trp319	Tyr225	Tyr205
Salt bridge/H-bond to N1 of PLP	Asp316	Asp222	Asp202
H-bond to O3' of PLP	-	Asn194	Asn175
H-bond to OP, possible proton donor in DC	His354	Ser257	Ser234
PLP binding, possible proton donor in DC	His223	Trp140	Y126

TABLE 1. Comparison of critical amino acid residues in ornithine decarboxylase (OrnDC), aspartate aminotransferase (AAT), and EdeM.

Comparison to an atypical PLP-dependent decarboxylase

With EdeM showing no structural similarity to known PLP-dependent DCs, we next searched for the most structurally similar DC compared to EdeM, regardless of the presence of PLP cofactor. Using the structural alignment tool DALI, it was determined that the most structurally similar decarboxylase to EdeM is L-threonine-*O*-3-phosphate decarboxylase from *Salmonella enterica* (PDB1LC7) (Cheong, Escalante-Semerena, and Rayment 2002), with a Z score of 35.5, RMSD 2.8 Å and % ID of 17, compared to the top hit aspartate aminotransferase from *Arabidopsis thaliana* (PDB 5WML) (Holland et al. 2018), with a Z score of 49.7, RMSD 1.8 Å, and % ID of 23 (Holm 2020).

L-threonine-*O*-3-phosphate decarboxylase, also known as CobD, is one of 25 enzymes in the cobalamin cofactor biosynthetic pathway. It decarboxylates L-threonine-*O*-3-phosphate to produce *R*-1-amino-2-propanol phosphate (Cheong, Escalante-Semerena, and Rayment 2002). Interestingly, this enzyme was initially believed to be a PLP-dependent

transaminase based on sequence similarity with the enzyme family; however, it was later shown to be a decarboxylase (Brushaber, O'Toole, and Escalante-Semerena 1998). This finding was unusual because transaminase activity is highly conserved among the AAT subfamily of PLP-dependent enzymes (Cheong, Escalante-Semerena, and Rayment 2002). CobD appears to have evolved from a transaminase rather than an amino acid decarboxylase, even though both types of enzymes are found within the fold type I family of PLP-DE (Cheong, Escalante-Semerena, and Rayment 2002). The only other report of a member from the AAT subfamily that does not behave like a transaminase is 1-aminocyclopropane-1-carboxylate synthase (ACC), which catalyzes the formation of ethylene from SAM in plants (Capitani et al. 1999). ACC shares low sequence similarity with ATT; however, the active sites are very similar despite having a completely different catalytic activity (Capitani et al. 1999).

CobD was crystallized in three different forms: apo-CobD (PDB 1LC5), apo-CobD with substrate (PDB 1LC7), and CobD with an external aldimine (L-threonine-*O*-3-phosphate bound to PLP) (PDB 1LC8). The apo-CobD structure revealed that the enzyme is a dimer with a large domain typical of PLP binding domains for enzymes in the AAT PLP-DE family. The only major difference found in the overall structure of CobD and typical transaminases was a short N-terminal extension, or linker domain, that does not interact with the neighbouring dimer. Instead, the N-terminal residues fold against the small domain of the same subunit (Cheong, Escalante-Semerena, and Rayment 2002).

Extensive crystallographic studies on the CobD external aldimine structure were conducted to understand how the enzyme facilitates decarboxylation while structurally

resembling a transaminase. Transamination reactions are heavily controlled by stereochemical positioning, where the bond to be broken lies orthogonal to the plane of the PLP Schiff base π system, allowing electrons to delocalize into the PLP electron sink (Dunathan 1971, 1966).

It was determined that CobD does not possess any radically different active site residues compared to typical transaminases. Instead, the enzyme facilitates decarboxylation by positioning the carboxylate moiety of L-threonine-*O*-3-phosphate out of the plane of the PLP pyridoxal ring and placing the α-hydrogen out of reach of the catalytic base provided by the active site lysine (Cheong, Escalante-Semerena, and Rayment 2002). This positioning favours decarboxylation over proton abstraction, leading to transamination (Cheong, Escalante-Semerena, and Rayment 2002).

Although the structure of CobD has not directly elucidated the mechanism of EdeM, the analysis demonstrates that EdeM is not the only aspartate aminotransferase-related enzyme that does not function as a typical transaminase but has evolved to facilitate decarboxylation. These studies highlight the importance of solving high-resolution crystal structures of substrate-bound enzymes to understand enzymatic mechanisms with minute structural differences. Understanding the stereochemical positioning of substrates and the geometry of the active site in the presence of substrates is crucial for such elucidation.

Understanding the EdeM active site

EdeM homologs from other systems

Protein homologs help identify conserved active site residues to elucidate enzyme mechanisms. Applying this approach, we searched for natural products containing D-β-serine and examined their BGCs for predicted transaminases, indicating a D-β-serine biosynthetic pathway similar to EdeM. This search led to the identification of the cyclic-peptide antibiotic GE23077 (GE), an inhibitor of bacterial RNA polymerase produced by *Actinomadura* sp. (Zhang et al. 2014). Like edeine, GE is produced nonribosomally and includes several unusual peptides, including D-β-serine (**Figure 10a**) (Zhang et al. 2014).

The GE BGC was obtained from the whole genome sequence of *A. citrea* DSM 43461 (NCBI Reference Sequence: NZ_JACCBT010000001.1). AntiSMASH analysis revealed a 69.3 kb BGC with an annotated fold type I aminotransferase (Blin et al. 2023). Alignment of the edeine and GE BGCs using c-linker showed that the only shared regions within the clusters corresponded to EdeM and the annotated aminotransferase (van den Belt et al. 2023) (**Figure 10a**). ClustalW analysis determined that the genes were 52% identical and 68% similar (Larkin et al. 2007). These results suggest that the putative aminotransferase in the GE BGC is most likely an EdeM homolog (GE-EdeM).

Several attempts were made to purify GE-EdeM from an overexpression strain to verify its activity. However, the protein remained insoluble in various expression and purification conditions.

Structural alignments with transaminases and decarboxylases

To identify conserved residues between EdeM and GE-EdeM, we developed a 3D model of GE-EdeM using AlphaFold 3 for sequence-based alignments in DALI

(**Supplemental Figure 26**) (Jumper et al. 2021; Holm 2020). Several fold-type I PLP-DE were selected as references for conserved residues in aminotransferases and decarboxylases (tyrosine aminotransferase [PDB 1BW0] (Blankenfeldt et al. 1999), L-threonine-*O*-3-phosphate decarboxylase [1LKC] (Cheong et al. 2002), aspartate aminotransferase [1ARG] (Graber et al. 1995), histidinol-phosphate aminotransferase [4RAE] (Nasir, N., Anant, A., Vyas, R., Biswal, B.K. 2015), glutamate decarboxylase [5GP4] (Huang et al. 2018), 2,2,-dialkylglycine decarboxylase [1M0N] (W. Liu et al. 2002), and ornithine decarboxylase [1ORD] (Momany et al. 1995)) (**Supplemental Figure 27**).

As expected, the results demonstrated that GE EdeM was the most structurally similar to EdeM, with a Z score of 46.3 and 56% ID (**Figure 10b**). The next four most structurally similar enzymes were tyrosine aminotransferase (Z=43, 21% ID), L-threonine-*O*-2-phosphate decarboxylase (Z=34.9, 14% ID), aspartate aminotransferase (Z=32.5, 16% ID), and histidinol-phosphate aminotransferase (Z=30.2, 18% ID).

Based on the evolutionary pedigree of fold type I PLP-DE as described by Christen and Mehta (2001), tyrosine aminotransferase (TAT) and AAT are closely related, with both enzymes belonging to the class I group of aminotransferases. It was surprising to see that TAT was more structurally similar to EdeM than AAT, given that TAT has not appeared in any previous structural analysis of EdeM.

As for L-threonine-*O*-3-phosphate decarboxylase (TPDC) and histidinol-phosphate aminotransferase (HPAT), previous studies have found these enzymes to be highly structurally similar despite their different mechanisms (Cheong, Escalante-Semerena, and Rayment 2002). HPAT is more distantly related to fold-type I, class I aminotransferase,

compared to AAT, and as described earlier, TPDC is an example of a decarboxylase that evolved from a folding type I transaminase.

Lastly, glutamate decarboxylase (Z=24.6, 11% ID), 2,2,-dialkylglycine decarboxylase (Z=20.5, 9% ID), and ornithine decarboxylase (Z=16.3, 10% ID), were the least structurally similar compared to EdeM. This is consistent with the fact that 2,2-dialkylglycine decarboxylase is categorized as a class III aminotransferase with a dual mechanism facilitating decarboxylation and transamination (Adachi et al. 2003). In contrast, glutamate decarboxylase and ornithine decarboxylase are DC II and DC III type enzymes, respectively, and are the most distantly related to class I aminotransferases (Christen and Mehta 2001).

These results further support the notion that while EdeM does not have typical transaminase activity, it structurally resembles a transaminase, much like TPDC.

Identification of potential catalytic active site tyrosine residues

When analyzing the structural alignment, we searched for residues conserved in both EdeM and GE-EdeM but not in the other enzymes. Focusing on residues found in the active site based on their 3D structures, we found that both EdeM and GE-EdeM have four tyrosine residues in their active sites, whereas the other enzymes have a maximum of two (**Figure 10b**). Based on EdeM numbering, these residues are Y126, Y205, Y240, and Y320.

The presence of aromatic amino acids in the active site of PLP-DE is common. For instance, class I aminotransferases typically have an aromatic amino acid positioned in front of PLP to facilitate pi stacking with the pyridine ring (Koper et al. 2022). In EdeM,

Y126 fulfills this role, and as shown in **Figure 10b**, most enzymes in the alignment possess an aromatic amino acid at this position (tyrosine (Y), phenylalanine (F), tryptophan (W), or histidine (H)) (Shao et al. 2022; Liao et al. 2013). Additionally, approximately 90% of class I ATs have a conserved tyrosine residue that interacts with PLP by hydrogen bonding to the 3'-hydroxyl group (EdeM Y205) (Koper et al. 2022; Jonathan M. Goldberg et al. 1993). In the structural alignment, this tyrosine residue is consistently present in all the aminotransferases and absent in the decarboxylases. These findings further support the idea that EdeM evolved from a class I aminotransferase but indicate that these tyrosine residues are not unique to EdeM and GE-EdeM.

Regarding the remaining two tyrosine residues in the EdeM active site, the structural alignment shows that Y240 is not highly conserved among transaminases. TAT possesses a proline at this position, HPAT lacks a residue at this site, and TPDC has a proline residue. The only transaminase with a tyrosine at this site is AAT. In class I ATs, this residue is known to contribute to the stability of PLP by interacting with the phosphate group via hydrogen bonds (Koper et al. 2022; M. D. Toney and Kirsch 1987). This residue is shown in **Figure 10c**, in an overlay of selected tyrosine residues from the structural alignment with the active site of EdeM.

In AAT (1ARG) (Graber et al. 1995), Y70 from chain B is found in the active site of Chain A, whereas Y240 of EdeM and Y255 of GE-EdeM both come from Chain A, which is atypical of previous reports. Additionally, AAT Y70 is positioned downward toward PLP, as expected of a residue that interacts with the cofactor, whereas Y240 and Y255 are positioned away from PLP, potentially toward the acetate that is co-crystallized

in the enzyme active site. We hypothesize that the carboxyl group of acetate represents that of an amino acid substrate in the active site of EdeM. These differences suggest that Y240 may be essential in facilitating the transfer of CO_2 in the active site of EdeM.

Lastly, Y320 is partially conserved across the ATs in the structural alignment. Those that lack tyrosine have an aromatic phenylalanine residue in its place, suggesting that an aromatic residue is essential in this position. No reports are currently available on the role of this residue; however, as shown in **Figure 10c**, these residues appear to be positioned toward the carboxyl group of acetate (except for Y299 of TPDC), with all hydroxyl groups within range of hydrogen bonding (2.4-2.8 Å). These results suggest that Y320 may also play a role in CO_2 transfer catalyzed by EdeM.

While not all of the listed tyrosine residues are unique to EdeM and its homolog, all four tyrosine residues in a single enzyme active site are unique. Based on the density of tyrosine residues in the active site, their functional OH groups, and the positioning of Y240 and Y320 suggesting possible interaction with the substrate, we hypothesized that these hydroxyl groups are essential in facilitating the EdeM reaction mechanism.

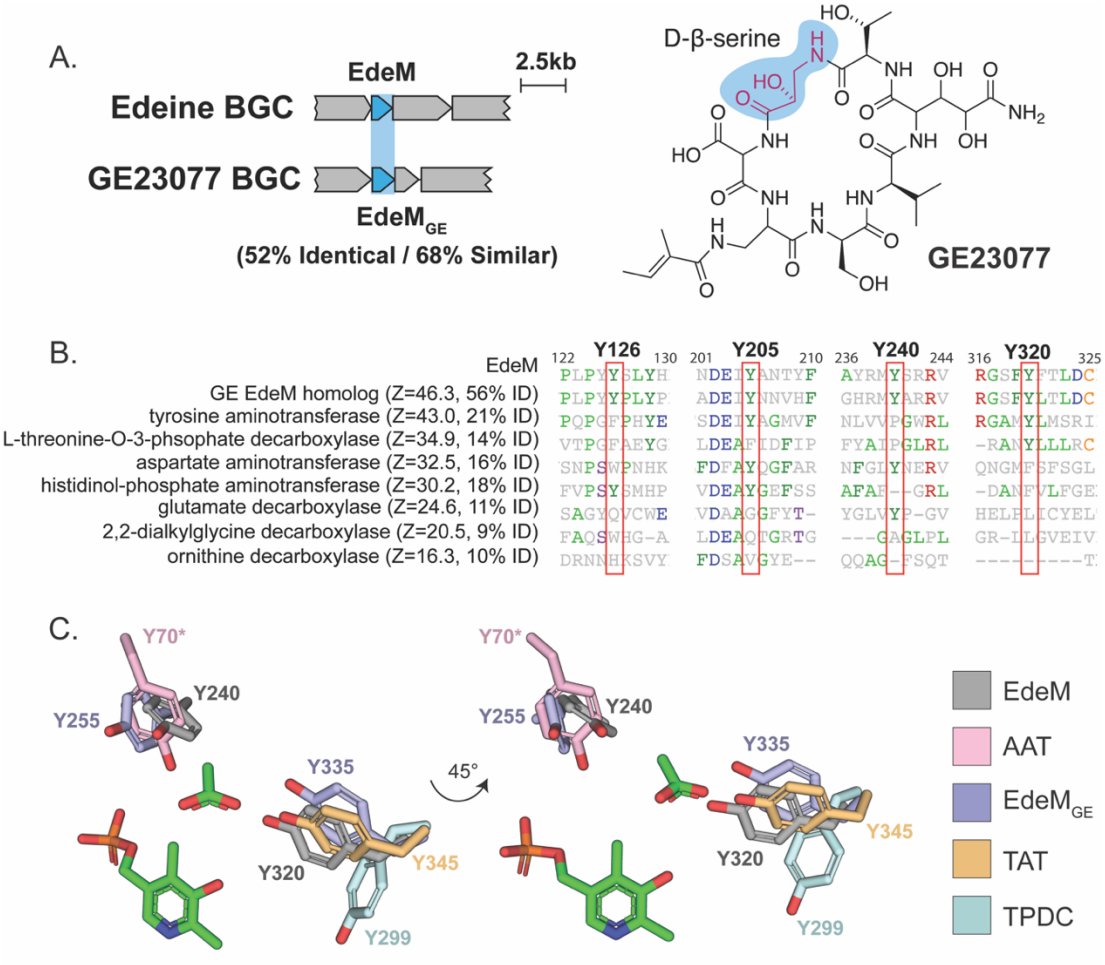

FIGURE 10. Alignment of EdeM with GE-EdeM, transaminases, and decarboxylases. A. The antibiotic GE23077 contains D-β-serine in its structure. Alignment of the GE BGC and the edeine BGC revealed a potential EdeM homolog, GE-EdeM. **B.** Structural alignments were conducted with EdeM (resolution 2.3 Å) against an AlphaFold 3 model of GE-EdeM, tyrosine aminotransferase [PDB 1BW0, resolution 2.50 Å], L-threonine-*O*-3-phosphate decarboxylase [1LKC, resolution 1.80 Å], aspartate aminotransferase [1ARG, resolution 2.20 Å], histidinol-phosphate aminotransferase [4RAE, resolution 2.59 Å], glutamate decarboxylase [5GP4, resolution 2.16 Å], 2,2,-dialkylglycine decarboxylase [1M0N, resolution 2.20 Å], and ornithine decarboxylase [1ORD, resolution 3.00 Å]. Results for Y126, Y205, Y240, and Y320 based on EdeM numbering are outlined in red. **C.** Overlay of select tyrosine residues from EdeM (gray), aspartate aminotransferase (AAT) (pink), GE-EdeM (purple), tyrosine aminotransferase (TAT) (orange), L-threonine-*O*-3-phosphate decarboxylase (TPDC) (blue). PLR and acetate from the EdeM crystal structure are down in green. All tyrosine's except for those marked with * are from chain A of their respective crystal structure.

EdeM tyrosine mutant steady-state kinetics

To investigate the importance of these hydroxyl groups, we created phenylalanine mutants for Y126, Y205, Y240, and Y320. Changes in protein stability relative to wildtype EdeM were determined via thermal shift assay (**Table 2**). Y126F and Y240F had the same melting temperature range as wildtype EdeM (44-46 °C), Y320F was slightly less stable (40 °C), and Y205F had increased stability (62 °C). We concluded that differences in the stability of the tyrosine-phenylalanine mutants were modest and would not significantly affect the enzyme structure. Therefore, we proceeded to measure their enzymatic activity.

Enzyme	Tm (°C) at pH 7.5
EdeM	44-45
Y126	44
Y205	62
Y240	46
Y320	40

TABLE 2. Thermal shift assay results for EdeM and EdeM tyrosine mutants.

Results showed that the Y240F and Y205 EdeM mutants were inactive. This contrasts with similar mutations in AAT, where these tyrosine residues are important but not essential for catalysis. In AAT, Y70 (corresponding to EdeM Y240) plays a subtle, fine-tuning role in the enzyme's overall catalytic efficiency. Mutating this residue to

phenylalanine results in an enzyme that binds substrates and the cofactor more weakly (M. D. Toney and Kirsch 1991). Similarly, Y225 in AAT (corresponding to EdeM Y205) increases the catalytic efficiency by destabilizing the enzyme-substrate complex (Jonathan M. Goldberg et al. 1991). These findings suggest that while these tyrosine residues are non-essential for the activity of typical aminotransferases, they are crucial for the activity of EdeM.

Furthermore, Y320F and Y126F mutants were significantly less active than wildtype enzymes, with specificity constants (k_{cat}/K_M) 47.5- and 135-fold lower than wildtype EdeM, respectively (**Table 3**). This result is particularly interesting for Y126F, as a tyrosine residue at this position does not appear essential in other transaminases, which can utilize other aromatic amino acids at this site to facilitate pi-stacking with PLP. For example, AAT uses tryptophan at this position, while TAT uses phenylalanine. This finding indicates that the hydroxyl group of tyrosine at this position may be essential for efficient EdeM catalysis.

Regarding Y320 in EdeM, little is known about its role. However, Moreno et al. (2014) speculate that the hydroxyl group of Y345 in TAT (corresponding to Y320 in EdeM), oriented toward the internal aldimine, may affect the reactivity of PLP with the amino group donor or acceptor when replaced with phenylalanine. Our results indicate that while Y320 is required for efficient catalytic activity, further investigation is needed to understand its role fully.

Overall, further studies on the roles of each tyrosine residue in the active site of EdeM are necessary to determine whether they are involved in the movement of CO_2 in the EdeM active site and, if not, to identify which residues are responsible.

Enzyme	$kcat/k_M$ ($M^{-1}sec^{-1}$)
Wildtype EdeM	3.43×10^{1}
EdeM Y126F	2.53×10^{-1}
EdeM Y205F	-
EdeM Y240F	-
EdeM Y320F	7.22×10^{-1}

TABLE 3. Specificity constants of wildtype EdeM and EdeM tyrosine mutants.

Edeine contains L-β-serine

Although we demonstrated that EdeM converts L-serine to D-β-serine, it is important to note that available crystal structures of edeine bound to ribosomes show the molecule contains L-β-serine (Pioletti et al. 2001). To verify that these crystal structures accurately represent the edeine produced by the biosynthetic gene cluster (BGC) from which EdeM was cloned, we purified edeine B from the Wright lab's working isolate of *B. brevis* Vm4 and re-examined the stereochemistry of β-serine.

After purification, edeine B was subjected to acid hydrolysis to separate the molecule into its individual components. The hydrolyzed mixture was then derivatized with Marfey's reagent and analyzed via high-resolution mass spectrometry. When comparing

the results to L- and D-β-serine standards, it was determined that edeine contains L-β-serine (**Supplemental Figure 28**). Given the extensive evidence that EdeM catalyzes the formation of D-β-serine, we believe that *B. brevis* Vm4 must possess an additional gene capable of epimerizing D-β-serine into L-β-serine before incorporation into edeine.

Discussion

The work completed in this chapter has significantly advanced our understanding of D-β-serine biosynthesis in edeine. We have identified *edeM* as the gene responsible for D-β-serine production. Previously studied mechanisms of β-amino acid biosynthesis involve MIO or SAM-dependent aminomutases. EdeM, however, is a novel pyridoxal phosphate-dependent enzyme that, while structurally resembling a transaminase, uses what appears to be unprecedented PLP chemistry to transfer CO_2 from the α-carbon to the β-carbon to form D-β-serine. Additionally, we identified a potential EdeM homolog and utilized the crystal structure of EdeM to perform several structural alignments and pinpoint active site residues essential for activity, subsequently determining their specificity constants. Furthermore, we now know that there must be an enzyme within *B. brevis* Vm4, either in the edeine biosynthetic gene cluster or elsewhere in the chromosome, that is responsible for converting D-β-serine to L-β-serine before its incorporation into the final structure of the peptide antibiotic. Despite these insights into the role of EdeM in producing D-β-serine, two significant questions remain regarding β-serine biosynthesis in edeine: What is the molecular mechanism of EdeM, and how is D-β-serine converted to L-β-serine before incorporation into edeine?

Understanding the molecular mechanism of EdeM

Summary of findings to date

Although the exact mechanism by which EdeM converts L-serine to D-β-serine remains unclear, we have gained significant insights into various aspects of the enzyme that will aid in elucidating its function. Notably, EdeM requires only a single substrate and demonstrates high substrate specificity for the conversion of L-serine to D-β-serine. Unlike many aminotransferases, which exhibit considerable substrate promiscuity due to mechanistic, functional, and structural constraints (Koper et al. 2022), EdeM's specificity suggests that its active site is fine-tuned for D-β-serine biosynthesis. This indicates that the enzyme's molecular mechanism and the catalytic residues have evolved to accommodate the chemical structure of its substrates.

Furthermore, the ^{18}O incorporation experiment revealed that EdeM's mechanism does not involve a hydrolysis step, implying that the conversion of L-serine to D-β-serine likely occurs entirely within the active site when the substrate is anchored to PLP. Lastly, the ^{13}C stable isotope experiments demonstrated a molecular rearrangement involving the transfer of the substrate's carboxyl group from the α-carbon to the β-carbon, creating a new chiral center and resulting in D-β-serine formation. These findings, combined with the ^{18}O incorporation study, have allowed us to propose a plausible mechanism for EdeM, although it has not yet been experimentally validated (**Figure 11**). We currently hypothesize that the active site tyrosine residues play a role in coordinating CO_2 to prevent its diffusion. While additional experiments will be required to validate our proposed mechanism, the current evidence provides a crucial foundation for directing the remainder of our study.

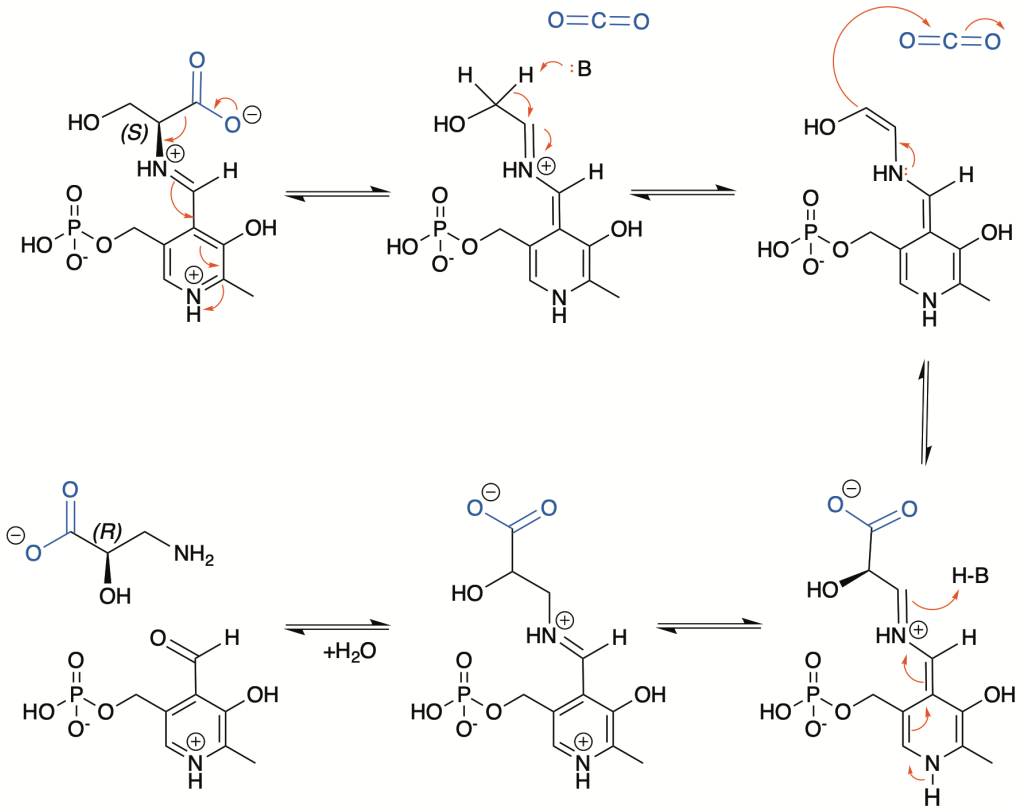

FIGURE 11. Proposed EdeM reaction mechanism. The proposed reaction mechanism of EdeM begins with the formation of an external aldimine between PLP and L-serine. Following this, L-serine undergoes decarboxylation, and the resulting carbanion is stabilized by the PLP electron sink. An active site base then abstracts a proton from the β-carbon of L-serine, generating a carbanion capable of forming a carbon-carbon bond with the transferred CO_2 group. Subsequently, the external aldimine Schiff base is reformed by proton abstraction from the active site base. Finally, D-β-serine is released from PLP via hydrolysis, regenerating free PLP.

Obtaining an EdeM-PLP·Substrate crystal structure

To elucidate the molecular mechanism of EdeM, obtaining a crystal structure of EdeM with a substrate bound to PLP is essential. Cheong et al. (2002) demonstrated that understanding the mechanism of an enzyme with an active site nearly identical to a typical transaminase requires analyzing subtle differences in the positioning of the substrate-bound cofactor. This analysis allows the prediction of which residues are involved in catalysis and how the reaction proceeds.

Numerous attempts have been made to crystallize EdeM with L-serine or D-β-serine in the active site. Over 6,000 crystallization conditions were tested with wildtype enzyme (± reduced PLP) and inactive K235A and Y205F mutants. Although it is uncertain why mutant EdeM has not yet been crystallized, one explanation for the difficulty in crystallizing wildtype EdeM with an external aldimine complex is that EdeM only requires a single substrate to produce D-β-serine.

For instance, the rate-determining step for wildtype AAT in the L-aspartate to oxaloacetate direction is ketimine hydrolysis, where oxaloacetate is released from PLP to produce PMP (J. M. Goldberg and Kirsch 1996). This limitation may increase the likelihood of obtaining a crystal structure with an intact internal aldimine. In contrast, EdeM's reaction requires only one substrate and lacks a hydrolysis step, potentially allowing the substrate to proceed at a rate that makes capturing the intermediate by crystal structure challenging.

To overcome this challenge, we sought to identify amino acid inhibitors of EdeM that would covalently bind to PLP and prevent the reaction from proceeding, making it easier to crystallize substrate-bound PLP. We identified L-alanine and 3-fluoro-DL-alanine

as reversible inhibitors of EdeM (**Supplemental Figure 29**). Presumably, both amino acids are competitive inhibitors of EdeM that bind to PLP via Schiff base formation and inhibit the reaction based on their structural differences to L-serine that prevent the transfer of CO_2. It is possible that while L-alanine and 3-fluoro-DL-alanine are an appropriate size to fit in the active site of EdeM, the molecular mechanism of EdeM is highly dependent on the hydroxyl side chain of L-serine. The changes in electronegativity at the site of CO_2 transfer in the presence of these inhibitors may prevent the formation of a predicted enamine needed to accept the incoming CO_2 group, allowing the reaction to proceed (**Figure 11**). Steady-state kinetics have yet to be performed to determine the inhibitor constants of these substrates. Several attempts have been made thus far to co-crystalize EdeM in the presence of an inhibitor to no avail.

Given the significance of obtaining an EdeM crystal structure with substrate-bound PLP, it is essential to continue our crystallization efforts. Several strategies can improve the crystallization properties of EdeM, including optimizing the crystallization setup (e.g., using different crystallization libraries, seeding techniques, and temperature variations) and modifying EdeM itself (e.g., creating truncation variants, removing the enzyme's HIS tag, and employing proteolysis).

Another approach involves working with EdeM homologs that may crystallize more readily. For instance, GE-EdeM, identified as a potential homolog in *Actinomadura* sp. for producing GE23077, was investigated. Numerous attempts were made to purify GE-EdeM and verify its activity as a D-β-serine producer. However, only insoluble protein could be purified, making crystallization with this sample impossible.

Therefore, additional efforts to identify an EdeM homolog that can be successfully purified may facilitate obtaining a crystal structure of EdeM in complex with substrate-bound PLP. This approach, combined with optimizing crystallization conditions and enzyme modifications, is crucial for advancing our understanding of EdeM's molecular mechanism.

Understanding the interaction between EdeM and PLP

Throughout our study of EdeM, we have worked to understand the interaction between enzyme and PLP cofactor, which has proven to be atypical. One significant difference between EdeM and typical PLP-dependent enzymes is the absence of the characteristic yellow color of the purified enzyme, which usually indicates the presence of a PLP-bound substrate (Beattie et al. 2013). Instead, EdeM is colorless when purified, suggesting a lack of bound PLP.

The Schiff base of internal aldimines is conjugated with the PLP π system, resulting in an absorption maxima of 420-430 nm when protonated and 360 nm when unprotonated, detectable by absorbance spectroscopy (Jonathan M. Goldberg et al. 1993). As expected from the lack of yellow colour, the UV spectrum of EdeM does not show a signal at 420 nm. Conversely, the enzyme exhibits an absorbance at 388 nm, which matches the absorbance maximum seen for free PLP in solution (**Supplemental Figure 30**) (Ahmed, McPhie, and Miles 1996). These results suggest that PLP exists in an unbound state in the active site of EdeM. This hypothesis is further supported by intact mass spectrometry analysis, which shows that approximately 50% of freshly purified EdeM lacks PLP.

Consequently, supplementing EdeM reactions with PLP is necessary to achieve maximal activity.

However, trypsin digest analysis (**Supplemental Figure 31**) and the PLP-bound crystal structure of EdeM confirm that a Schiff base can form between EdeM and its active site lysine residue, K235. Interestingly, studies by Goldberg et al. (1993) demonstrated that in a Y225F mutant of AAT (equivalent to Y205 in EdeM), the absorbance maxima of an unprotonated Schiff base shift to 386 nm, similar to the 388 nm observed with free PLP. Y225 typically hydrogen bonds with the 3' hydroxyl group of PLP, and removing this interaction destabilizes the ground state of the C3-O3' bond of PLP relative to the excited state, resulting in a red-shifted λmax (Jonathan M. Goldberg et al. 1993).

Interestingly, however, when the equivalent residue in EdeM is mutated, Y205, the enzyme turns a deep-yellow colour and exhibits absorbance at 420 nm, a phenomenon also observed with the K235A mutant despite the absence of a catalytic lysine residue capable of forming a Schiff base (**Supplemental Figure 32**). A similar colour change has been observed in a lysine-to-alanine mutant of NikK, a transaminase that incorporates an amino group into the ketohexuronic acid precursor of nikkomycins (Binter et al. 2011). In this study, Binter et al. (2011) note that the purified lysine mutant displays a deep yellow colour, however, with an absorbance maximum shifted to a lower wavelength (400 nm).

These observations, though not yet fully understood, suggest that PLP may exist in the active site of EdeM unbound to lysine in an internal aldimine or that the electrostatic interactions of PLP bound to EdeM affect the UV absorbance spectra of the enzyme and its mutants. Ultimately, EdeM interacts with its cofactor in an atypical manner, necessitating

extensive analysis of the PLP cofactor's protonation state and its interactions with the active site of EdeM to contribute to the proposal of a detailed enzymatic mechanism.

Understanding D- to L-β-serine conversion

It is fascinating that the edeine BGC contains an enzyme that produces D-β-serine and needs another enzyme to convert it into L-β-serine before incorporation into edeine, rather than having a single enzyme that creates the final product. This discovery opens an exciting avenue for understanding the biosynthetic pathways of both β-serine isomers.

To elucidate the D- to L-β-serine conversion in edeine, we are investigating two approaches: examining the role of EdeM in L-β-serine production and analyzing the edeine BGC to identify a gene that encodes an epimerase capable of converting D- to L-β-serine.

Deletion of edeM from the edeine BGC

To determine if EdeM is involved in L-β-serine production, we initiated an attempt to delete e*deM* from the edeine BGC in *B. brevis* Vm4. We hypothesized that that EdeM is not involved in the production of L-β-serine. By supplementing *B. brevis* Vm4 Δ*edeM* with D-β-serine in the absence of EdeM, we aimed to determine if another gene in the BGC could catalyze the conversion of D-β-serine to L-β-serine, thereby enabling its incorporation into edeine. This would prove that EdeM is solely responsible for D-β-serine formation.

To facilitate this, we developed a plasmid using a pUC19 backbone, which includes an apramycin resistance cassette flanked by e*deM* homology arms on either side, along with lox sites. This plasmid is designed to recombine with the homologous regions of *edeM* in the *B. brevis* chromosome, replacing *edeM* with the apramycin cassette. Additionally, we developed a temperature-sensitive helper plasmid using a pDR244 backbone, incorporating an erythromycin resistance cassette and Cre recombinase. This helper plasmid allows for the scarless deletion of *edeM* from the chromosome at the integrated lox sites and can be cured from *B. brevis* by growing the strain at a non-permissive temperature (Wozniak and Simmons 2022).

While the creation of both plasmids was successful, multiple attempts to transfer DNA into *B. brevis* Vm4 cells following protocols reported for other *B. brevis* strains were unsuccessful (Okamoto et al. 1997; Takahashi et al. 1983; Takagi et al. 1989). Interestingly, Takagi et al. (1989) demonstrated that transformation efficiency varies among *B. brevis* strains, with 15 out of 21 strains not producing transformants. *B. brevis* Vm4 may be another strain that cannot be transformed with DNA in a laboratory setting. Future directions for this approach include obtaining additional strains that produce edeine, such as *B. fortis* NRS-1210 or *B. brevis* X23 (Q. Liu et al. 2022; Johnson, Bowman, and Dunlap 2020). It is important to emphasize further investigation into the genetic tractability of *B. brevis* and other edeine-producing strains of *Brevibacillus*, not only for the successful deletion of EdeM from the edeine BGC for this study but to enable further investigation of edeine biosynthesis.

Analyzing the edeine BGC for an epimerase

The analysis of the edeine BGC using antiSMASH predicts the presence of a single epimerization domain within the NRPS EdeP. However, research by Volpe et al. (2023) has shown that edeine production is associated with a prodrug resistance mechanism, wherein an acyl-D-asparagine moiety is located at the C-terminus of the molecule, rendering the drug inactive within the cells of the producing organism. Volpe and colleagues hypothesized that EdeP synthesizes the acyl-D-asparagine moiety based on the homology of its condensation domain with related modules in the colibactin BGC. This includes an adenylation domain with predicted specificity for asparagine and an epimerization domain that can convert L-asparagine to D-asparagine (Volpe et al. 2023).

Our analysis of EdeP using antiSMASH confirms the presence of an adenylation domain with predicted substrate specificity for asparagine located downstream of a starter condensation domain. Although condensation domains are not typically the first module of an NRPS, they are responsible for acylating the first amino acid in the assembly line when present (Zhong et al. 2021). These findings support the proposed function of EdeP in prodrug moiety formation.

Despite the prediction of a single epimerization domain in the edeine BGC, we further examined the predicted domains of each NRPS module to identify any additional domains capable of converting D- to L-β-serine. This approach identified a vicinal oxygen chelate (VOC) superfamily domain in the NRPS EdeN. VOC domains are found in various structurally related metalloenzymes, and a conserved domain database search in NCBI (Wang et al. 2023) indicated that the VOC domain prediction in EdeN was based on a

structural alignment with the VOC superfamily member methylmalonyl-CoA epimerase (MMCE) (Mulako et al. 2008). Notably, MMCE is known to convert D-methylmalonyl-CoA to L-methylmalonyl-CoA (Diogo et al. 2023).

Although methylmalonyl-CoA is not structurally equivalent to β-serine, we hypothesize that the structural difference of D-β-serine compared to an α-amino acid, with the hydroxyl group on β-serine resembling a keto acid, paired with the lack of known D-β-serine biosynthesis pathways, and the specificity of MMCE for reacting with D-substrates, suggests that antiSMASH cannot accurately predict the substrate for the putative epimerization domain in EdeN. Consequently, it may be responsible for the conversion of D- to L-β-serine. This hypothesis has yet to be tested in a laboratory setting; however, it provides a rationale for the existence of an epimerase capable of facilitating the conversion of D- to L-β-serine before incorporation into edeine. Alternatively, the necessary epimerase may be located elsewhere in the chromosome.

Conclusion

PLP-dependent enzymes have been studied since the 1950s; over 70 years later, novel enzymatic mechanisms continue to be uncovered. To the best of our knowledge, EdeM represents the first report of a PLP-dependent enzyme catalyzing the intramolecular rearrangement of an amino acid to produce a β-amino acid, or any product, and is the first known enzyme responsible for D-β-serine biosynthesis. Despite this significant discovery, many questions remain unanswered before we can fully understand D-β-serine biosynthesis in edeine.

These findings have allowed us to prioritize the next steps in this project, including a detailed investigation of PLP interactions within the active site of EdeM, continued crystallization efforts, and elucidating the steps involved in the conversion of D- to L-β-serine. We hope this research emphasizes the importance of investigating β-amino acid biosynthesis enzymes and drives the discovery of other novel β-amino acid biosynthesis pathways. Such discoveries could advance various fields, including synthetic biology, drug discovery, peptide mimetics, and agriculture.

References

Adachi, Kiichi, Grant H. Nelson, Keith A. Peoples, Todd M. DeZwaan, Amy R. Skalchunes, Ryan W. Heiniger, Jeffrey R. Shuster, Lisbeth Hamer, and Matthew M. Tanzer. 2003. "Sequence Analysis and Functional Characterization of the Dialkylglycine Decarboxylase Gene DGD1 from Mycosphaerella Graminicola." *Current Genetics* 43 (5): 358–63.

Ahmed, S. A., P. McPhie, and E. W. Miles. 1996. "A Thermally Induced Reversible Conformational Transition of the Tryptophan Synthase Beta2 Subunit Probed by the Spectroscopic Properties of Pyridoxal Phosphate and by Enzymatic Activity." *The Journal of Biological Chemistry* 271 (15): 8612–17.

Bar-Even, Arren, Elad Noor, Yonatan Savir, Wolfram Liebermeister, Dan Davidi, Dan S. Tawfik, and Ron Milo. 2011. "The Moderately Efficient Enzyme: Evolutionary and Physicochemical Trends Shaping Enzyme Parameters." *Biochemistry* 50 (21): 4402–10.

Beasley, Federico C., Johnson Cheung, and David E. Heinrichs. 2011. "Mutation of L-2,3-Diaminopropionic Acid Synthase Genes Blocks Staphyloferrin B Synthesis in Staphylococcus Aureus." *BMC Microbiology* 11. https://doi.org/10.1186/1471-2180-11-199.

Beattie, Ashley E., Sita D. Gupta, Lenka Frankova, Agne Kazlauskaite, Jeffrey M. Harmon, Teresa M. Dunn, and Dominic J. Campopiano. 2013. "The Pyridoxal 5'-Phosphate (PLP)-Dependent Enzyme Serine Palmitoyltransferase (SPT): Effects of the Small Subunits and Insights from Bacterial Mimics of Human HLCB2a HSAN1 Mutations." *BioMed Research International* 2013 (September): 194371.

Belt, Matthias van den, Cameron Gilchrist, Thomas J. Booth, Yit-Heng Chooi, Marnix H. Medema, and Mohammad Alanjary. 2023. "CAGECAT: The CompArative GEne Cluster Analysis Toolbox for Rapid Search and Visualisation of Homologous Gene Clusters." *BMC Bioinformatics* 24 (1): 181.

Binter, Alexandra, Gustav Oberdorfer, Sebastian Hofzumahaus, Stefanie Nerstheimer, Georg Altenbacher, Karl Gruber, and Peter Macheroux. 2011. "Characterization of the PLP-Dependent Aminotransferase NikK from Streptomyces Tendae and Its Putative Role in Nikkomycin Biosynthesis." *The FEBS Journal* 278 (21): 4122–35.

Blankenfeldt, W., C. Nowicki, M. Montemartini-Kalisz, H. M. Kalisz, and H. J. Hecht. 1999. "Crystal Structure of Trypanosoma Cruzi Tyrosine Aminotransferase: Substrate Specificity Is Influenced by Cofactor Binding Mode." *Protein Science: A Publication of the Protein Society* 8 (11): 2406–17.

Blin, Kai, Simon Shaw, Hannah E. Augustijn, Zachary L. Reitz, Friederike Biermann, Mohammad Alanjary, Artem Fetter, et al. 2023. "AntiSMASH 7.0: New and Improved Predictions for Detection, Regulation, Chemical Structures and Visualisation." *Nucleic Acids Research* 51 (W1): W46–50.

Brushaber, K. R., G. A. O'Toole, and J. C. Escalante-Semerena. 1998. "CobD, a Novel Enzyme with L-Threonine-O-3-Phosphate Decarboxylase Activity, Is Responsible for the Synthesis of (R)-1-Amino-2-Propanol O-2-Phosphate, a Proposed New

Intermediate in Cobalamin Biosynthesis in Salmonella Typhimurium LT2." *The Journal of Biological Chemistry* 273 (5): 2684–91.

Burkhard, P., P. Dominici, C. Borri-Voltattorni, J. N. Jansonius, and V. N. Malashkevich. 2001. "Structural Insight into Parkinson's Disease Treatment from Drug-Inhibited DOPA Decarboxylase." *Nature Structural Biology* 8 (11): 963–67.

Camacho, Christiam, George Coulouris, Vahram Avagyan, Ning Ma, Jason Papadopoulos, Kevin Bealer, and Thomas L. Madden. 2009. "BLAST+: Architecture and Applications." *BMC Bioinformatics* 10 (December): 421.

Capitani, G., E. Hohenester, L. Feng, P. Storici, J. F. Kirsch, and J. N. Jansonius. 1999. "Structure of 1-Aminocyclopropane-1-Carboxylate Synthase, a Key Enzyme in the Biosynthesis of the Plant Hormone Ethylene." *Journal of Molecular Biology* 294 (3): 745–56.

Cheong, Cheom-Gil, Cary B. Bauer, Kevin R. Brushaber, Jorge C. Escalante-Semerena, and Ivan Rayment. 2002. "Three-Dimensional Structure of the l-Threonine-O-3-Phosphate Decarboxylase (CobD) Enzyme from Salmonella Enterica,." *Biochemistry* 41 (15): 4798–4808.

Cheong, Cheom-Gil, Jorge C. Escalante-Semerena, and Ivan Rayment. 2002. "Structural Studies of the L-Threonine-O-3-Phosphate Decarboxylase (CobD) Enzyme from Salmonella Enterica: The Apo, Substrate, and Product−Aldimine Complexes,." *Biochemistry* 41 (29): 9079–89.

Christen, P., and P. K. Mehta. 2001. "From Cofactor to Enzymes. The Molecular Evolution of Pyridoxal-5'-Phosphate-Dependent Enzymes." *Chemical Record* 1 (6): 436–47.

Diogo, Rui, Inês B. Rua, Sara Ferreira, Célia Nogueira, Cristina Pereira, Joana Rosmaninho-Salgado, and Luísa Diogo. 2023. "Methylmalonyl Coenzyme A (CoA) Epimerase Deficiency, an Ultra-Rare Cause of Isolated Methylmalonic Aciduria With Predominant Neurological Features." *Cureus* 15 (10): e48017.

Dunathan, H. C. 1966. "Conformation and Reaction Specificity in Pyridoxal Phosphate Enzymes." *Proceedings of the National Academy of Sciences of the United States of America* 55 (4): 712–16.

———. 1971. "Stereochemical Aspects of Pyridoxal Phosphate Catalysis." *Advances in Enzymology and Related Areas of Molecular Biology* 35: 79–134.

Emsley, P., B. Lohkamp, W. G. Scott, and K. Cowtan. 2010. "Features and Development of Coot." *Acta Crystallographica. Section D, Biological Crystallography* 66 (Pt 4): 486–501.

Fernández, Rogelio, Asep Bayu, Tri Aryono Hadi, Santiago Bueno, Marta Pérez, Carmen Cuevas, and Masteria Yunovilsa Putra. 2020. "Unique Polyhalogenated Peptides from the Marine Sponge Ircinia Sp." *Marine Drugs* 18 (8). https://doi.org/10.3390/md18080396.

Frey, P. A. 1993. "Lysine 2,3-Aminomutase: Is Adenosylmethionine a Poor Man's Adenosylcobalamin?" *FASEB Journal: Official Publication of the Federation of American Societies for Experimental Biology* 7 (8): 662–70.

Goldberg, J. M., and J. F. Kirsch. 1996. "The Reaction Catalyzed by Escherichia Coli Aspartate Aminotransferase Has Multiple Partially Rate-Determining Steps, While

That Catalyzed by the Y225F Mutant Is Dominated by Ketimine Hydrolysis." *Biochemistry* 35 (16): 5280–91.

Goldberg, Jonathan M., Ronald V. Swanson, Harris S. Goodman, and Jack F. Kirsch. 1991. "The Tyrosine-225 to Phenylalanine Mutation of Escherichia Coli Aspartate Aminotransferase Results in an Alkaline Transition in the Spectrophotometric and Kinetic PKa Values and Reduced Values of Both Kcat and Km." *Biochemistry* 30 (1): 305–12.

Goldberg, Jonathan M., Jie Zheng, Hua Deng, Yong Q. Chen, Robert Callender, and Jack F. Kirsch. 1993. "Structure of the Complex between Pyridoxal 5'-Phosphate and the Tyrosine 225 to Phenylalanine Mutant of Escherichia Coli Aspartate Aminotransferase Determined by Isotope-Edited Classical Raman Difference Spectroscopy." *Biochemistry* 32 (32): 8092–97.

Graber, Rachel, Patrik Kasper, Vladimir N. Malashkevich, Erika Sandmeier, Philipp Berger, Heinz Gehring, Johan N. Jansonius, and Philipp Christen. 1995. "Changing the Reaction Specificity of a Pyridoxal-5'-Phosphate-Dependent Enzyme." *European Journal of Biochemistry / FEBS* 232 (2): 686–90.

Hoegl, Annabelle, Matthew B. Nodwell, Volker C. Kirsch, Nina C. Bach, Martin Pfanzelt, Matthias Stahl, Sabine Schneider, and Stephan A. Sieber. 2018. "Mining the Cellular Inventory of Pyridoxal Phosphate-Dependent Enzymes with Functionalized Cofactor Mimics." *Nature Chemistry* 10 (12): 1234–45.

Holland, Cynthia K., Daniel A. Berkovich, Madeleine L. Kohn, Hiroshi Maeda, and Joseph M. Jez. 2018. "Structural Basis for Substrate Recognition and Inhibition of Prephenate Aminotransferase from Arabidopsis." *The Plant Journal: For Cell and Molecular Biology* 94 (2): 304–14.

Holm, Liisa. 2020. "DALI and the Persistence of Protein Shape." *Protein Science: A Publication of the Protein Society* 29 (1): 128–40.

Huang, Jun, Hui Fang, Zhong-Chao Gai, Jia-Qi Mei, Jia-Nan Li, Sheng Hu, Chang-Jiang Lv, Wei-Rui Zhao, and Le-He Mei. 2018. "Lactobacillus Brevis CGMCC 1306 Glutamate Decarboxylase: Crystal Structure and Functional Analysis." *Biochemical and Biophysical Research Communications* 503 (3): 1703–9.

Johnson, Eric T., Michael J. Bowman, and Christopher A. Dunlap. 2020. "Brevibacillus Fortis NRS-1210 Produces Edeines That Inhibit the in Vitro Growth of Conidia and Chlamydospores of the Onion Pathogen Fusarium Oxysporum f. Sp. Cepae." *Antonie van Leeuwenhoek* 113 (7): 973–87.

Jumper, John, Richard Evans, Alexander Pritzel, Tim Green, Michael Figurnov, Olaf Ronneberger, Kathryn Tunyasuvunakool, et al. 2021. "Highly Accurate Protein Structure Prediction with AlphaFold." *Nature* 596 (7873): 583–89.

King, Andrew M., Sarah A. Reid-Yu, Wenliang Wang, Dustin T. King, Gianfranco De Pascale, Natalie C. Strynadka, Timothy R. Walsh, Brian K. Coombes, and Gerard D. Wright. 2014. "Aspergillomarasmine A Overcomes Metallo-β-Lactamase Antibiotic Resistance." *Nature* 510 (7506): 503–6.

Kirsch, Jack F., Gregor Eichele, Geoffrey C. Ford, Michael G. Vincent, Johan N. Jansonius, Heinz Gehring, and Philipp Christen. 1984. "Mechanism of Action of

Aspartate Aminotransferase Proposed on the Basis of Its Spatial Structure." *Journal of Molecular Biology* 174 (3): 497–525.

Kobylarz, Marek J., Jason C. Grigg, Shin-Ichi J. Takayama, Dushyant K. Rai, David E. Heinrichs, and Michael E. P. Murphy. 2014. "Synthesis of L-2,3-Diaminopropionic Acid, a Siderophore and Antibiotic Precursor." *Chemistry & Biology* 21 (3): 379–88.

Koper, Kaan, Sang-Woo Han, Delia Casas Pastor, Yasuo Yoshikuni, and Hiroshi A. Maeda. 2022. "Evolutionary Origin and Functional Diversification of Aminotransferases." *The Journal of Biological Chemistry* 298 (8): 102122.

Kudo, Fumitaka, Akimasa Miyanaga, and Tadashi Eguchi. 2014. "Biosynthesis of Natural Products Containing β-Amino Acids." *Natural Product Reports* 31 (8): 1056–73.

Kurylo-Borowska, Z. 1975. "Biosynthesis of Eideine:: II. Localization of Edeine Synthetase within Bacillus Brevis Vm4." *Biochimica et Biophysica Acta (BBA) - General Subjects* 399 (1): 31–41.

Larkin, M. A., G. Blackshields, N. P. Brown, R. Chenna, P. A. McGettigan, H. McWilliam, F. Valentin, et al. 2007. "Clustal W and Clustal X Version 2.0." *Bioinformatics* 23 (21): 2947–48.

Liao, Si-Ming, Qi-Shi Du, Jian-Zong Meng, Zong-Wen Pang, and Ri-Bo Huang. 2013. "The Multiple Roles of Histidine in Protein Interactions." *Chemistry Central Journal* 7 (1): 44.

Liebschner, Dorothee, Pavel V. Afonine, Matthew L. Baker, Gábor Bunkóczi, Vincent B. Chen, Tristan I. Croll, Bradley Hintze, et al. 2019. "Macromolecular Structure Determination Using X-Rays, Neutrons and Electrons: Recent Developments in Phenix." *Acta Crystallographica. Section D, Structural Biology* 75 (Pt 10): 861–77.

Liu, Qingshu, Liang Zhang, Yunsheng Wang, Cuiyang Zhang, Tianbo Liu, Caichen Duan, Xiaoying Bian, et al. 2022. "Enhancement of Edeine Production in Brevibacillus Brevis X23 via in Situ Promoter Engineering." *Microbial Biotechnology* 15 (2): 577–89.

Liu, Wenshe, Claude J. Rogers, Andrew J. Fisher, and Michael D. Toney. 2002. "Aminophosphonate Inhibitors of Dialkylglycine Decarboxylase: Structural Basis for Slow Binding Inhibition." *Biochemistry* 41 (41): 12320–28.

McPhalen, C. A., M. G. Vincent, and J. N. Jansonius. 1992. "X-Ray Structure Refinement and Comparison of Three Forms of Mitochondrial Aspartate Aminotransferase." *Journal of Molecular Biology* 225 (2): 495–517.

Mehta, P. K., T. I. Hale, and P. Christen. 1993. "Aminotransferases: Demonstration of Homology and Division into Evolutionary Subgroups." *European Journal of Biochemistry / FEBS* 214 (2): 549–61.

Milano, Teresa, Alessandro Paiardini, Ingeborg Grgurina, and Stefano Pascarella. 2013. "Type I Pyridoxal 5'-Phosphate Dependent Enzymatic Domains Embedded within Multimodular Nonribosomal Peptide Synthetase and Polyketide Synthase Assembly Lines." *BMC Structural Biology* 13 (October): 26.

Momany, Cory, Stephen Ernst, Ratna Ghosh, Ning-Leh Chang, and Marvin L. Hackert. 1995. "Crystallographic Structure of a PLP-Dependent Ornithine Decarboxylase

FromLactobacillus30a to 3.0 Å Resolution." *Journal of Molecular Biology* 252 (5): 643–55.

Moreno, M. A., A. Abramov, J. Abendroth, A. Alonso, S. Zhang, P. J. Alcolea, T. Edwards, D. Lorimer, P. J. Myler, and V. Larraga. 2014. "Structure of Tyrosine Aminotransferase from Leishmania Infantum." *Acta Crystallographica. Section F, Structural Biology and Crystallization Communications* 70 (Pt 5): 583–87.

Mulako, I., J. M. Farrant, H. Collett, and N. Illing. 2008. "Expression of Xhdsi-1VOC, a Novel Member of the Vicinal Oxygen Chelate (VOC) Metalloenzyme Superfamily, Is up-Regulated in Leaves and Roots during Desiccation in the Resurrection Plant Xerophyta Humilis (Bak) Dur and Schinz." *Journal of Experimental Botany* 59 (14): 3885–3901.

Nasir, N., Anant, A., Vyas, R., Biswal, B.K. 2015. "WwPDB: 4RAE." 2015. https://www.wwpdb.org/pdb?id=pdb_00004rae.

Okamoto, A., A. Kosugi, Y. Koizumi, F. Yanagida, and S. Udaka. 1997. "High Efficiency Transformation of Bacillus Brevis by Electroporation." *Bioscience, Biotechnology, and Biochemistry* 61 (1): 202–3.

Parry, Ronald J., and Z. Kurylo-Borowska. 1980. "Biosynthesis of Amino Acids. Investigation of the Mechanism of .Beta.-Tyrosine Formation." *Journal of the American Chemical Society* 102 (2): 836–37.

Patočka, Jiří. 2011. "B-Amino Acids and Their Natural Biologically Active Derivatives. 5. Derivatives of Unusual Alicyclic and Heterocyclic B-Amimo." *Military Medical Science* 80 (44): 2–11.

Pflüger, K., S. Baumann, G. Gottschalk, W. Lin, H. Santos, and V. Müller. 2003. "Lysine-2,3-Aminomutase and Beta-Lysine Acetyltransferase Genes of Methanogenic Archaea Are Salt Induced and Are Essential for the Biosynthesis of Nepsilon-Acetyl-Beta-Lysine and Growth at High Salinity." *Applied and Environmental Microbiology* 69 (10): 6047–55.

Shao, Jinfeng, Bastiaan P. Kuiper, Andy-Mark W. H. Thunnissen, Robbert H. Cool, Liang Zhou, Chenxi Huang, Bauke W. Dijkstra, and Jaap Broos. 2022. "The Role of Tryptophan in π Interactions in Proteins: An Experimental Approach." *Journal of the American Chemical Society* 144 (30): 13815–22.

Takagi, Hiroaki, Shogo Kagiyama, Kiyoshi Kadowaki, Norihiro Tsukagoshi, and Shigezo Udaka. 1989. "Genetic Transformation of *Bacillus Brevis* with Plasmid DNA by Electroporation." *Agricultural and Biological Chemistry* 53 (11): 3099–3100.

Takahashi, W., H. Yamagata, K. Yamaguchi, N. Tsukagoshi, and S. Udaka. 1983. "Genetic Transformation of Bacillus Brevis 47, a Protein-Secreting Bacterium, by Plasmid DNA." *Journal of Bacteriology* 156 (3): 1130–34.

Toney, M. D., and J. F. Kirsch. 1987. "Tyrosine 70 Increases the Coenzyme Affinity of Aspartate Aminotransferase. A Site-Directed Mutagenesis Study." *The Journal of Biological Chemistry* 262 (26): 12403–5.

———. 1991. "Tyrosine 70 Fine-Tunes the Catalytic Efficiency of Aspartate Aminotransferase." *Biochemistry* 30 (30): 7456–61.

Toney, Michael D. 2014. "Aspartate Aminotransferase: An Old Dog Teaches New Tricks." *Archives of Biochemistry and Biophysics* 544 (February): 119–27.

Volpe, Matthew R., José A. Velilla, Martin Daniel-Ivad, Jenny J. Yao, Alessia Stornetta, Peter W. Villalta, Hsin-Che Huang, et al. 2023. "A Small Molecule Inhibitor Prevents Gut Bacterial Genotoxin Production." *Nature Chemical Biology* 19 (2): 159–67.

Walsh, Christopher. 1979. *Enzymatic Reaction Mechanisms*. W. H. Freeman.

Wang, Jiyao, Farideh Chitsaz, Myra K. Derbyshire, Noreen R. Gonzales, Marc Gwadz, Shennan Lu, Gabriele H. Marchler, et al. 2023. "The Conserved Domain Database in 2023." *Nucleic Acids Research* 51 (D1): D384–88.

Westman, Erin L., Marie Yan, Nicholas Waglechner, Kalinka Koteva, and Gerard D. Wright. 2013. "Self Resistance to the Atypical Cationic Antimicrobial Peptide Edeine of Brevibacillus Brevis Vm4 by the N-Acetyltransferase EdeQ." *Chemistry & Biology* 20 (8): 983–90.

Wozniak, Katherine J., and Lyle A. Simmons. 2022. "Genome Editing Methods for Bacillus Subtilis." *Methods in Molecular Biology* 2479: 159–74.

Yogeswara, Ida Bagus Agung, Suppasil Maneerat, and Dietmar Haltrich. 2020. "Glutamate Decarboxylase from Lactic Acid Bacteria—A Key Enzyme in GABA Synthesis." *Microorganisms* 8 (12): 1923.

Zhang, Yu, David Degen, Mary X. Ho, Elena Sineva, Katherine Y. Ebright, Yon W. Ebright, Vladimir Mekler, et al. 2014. "GE23077 Binds to the RNA Polymerase 'i' and 'I+1' Sites and Prevents the Binding of Initiating Nucleotides." *ELife* 3 (April): e02450.

Zhong, Lin, Xiaotong Diao, Na Zhang, Fengwei Li, Haibo Zhou, Hanna Chen, Xianping Bai, et al. 2021. "Engineering and Elucidation of the Lipoinitiation Process in Nonribosomal Peptide Biosynthesis." *Nature Communications* 12 (1): 1–15.

Supplemental Information

	EdeM-PLR	Apo-EdeM
Wavelength		
Resolution range	57.95 - 2.3 (2.382 - 2.3)	37.3 - 1.7 (1.761 - 1.7)
Space group	P 21 21 21	P 21 21 21
Unit cell	60.78 66.1 192.18 90 90 90	64.6608 92.6599 122.229 90 90 90
Unique reflections	33921 (3443)	80092
Completeness (%)	95.68 (99.77)	98.34 (97.12)
Wilson B-factor	25.79	11.87
Reflections used in refinement	33768 (3443)	80088 (7795)
Reflections used for R-free	1987 (201)	1998 (195)
R-work	0.1756 (0.1960)	0.1421 (0.1645)
R-free	0.2132 (0.2223)	0.1584 (0.2022)
Number of non-hydrogen atoms	6604	7265
macromolecules	6160	6157
ligands	41	0
solvent	406	1108

Protein residues	771	762
RMS(bonds)	0.016	0.008
RMS(angles)	1.21	1.08
Ramachandran favored (%)	95.94	96.17
Ramachandran allowed (%)	4.06	3.30
Ramachandran outliers (%)	0.00	0.53
Rotamer outliers (%)	5.08	1.03
Clashscore	5.53	5.05
Average B-factor	30.07	17.57
macromolecules	29.93	15.84
ligands	22.57	-
solvent	32.85	27.21
Number of TLS groups	10	9

SUPPLEMENTAL TABLE 1. X-ray diffraction data collection and refinement statistics. Statistics for the highest-resolution shell are shown in parentheses.

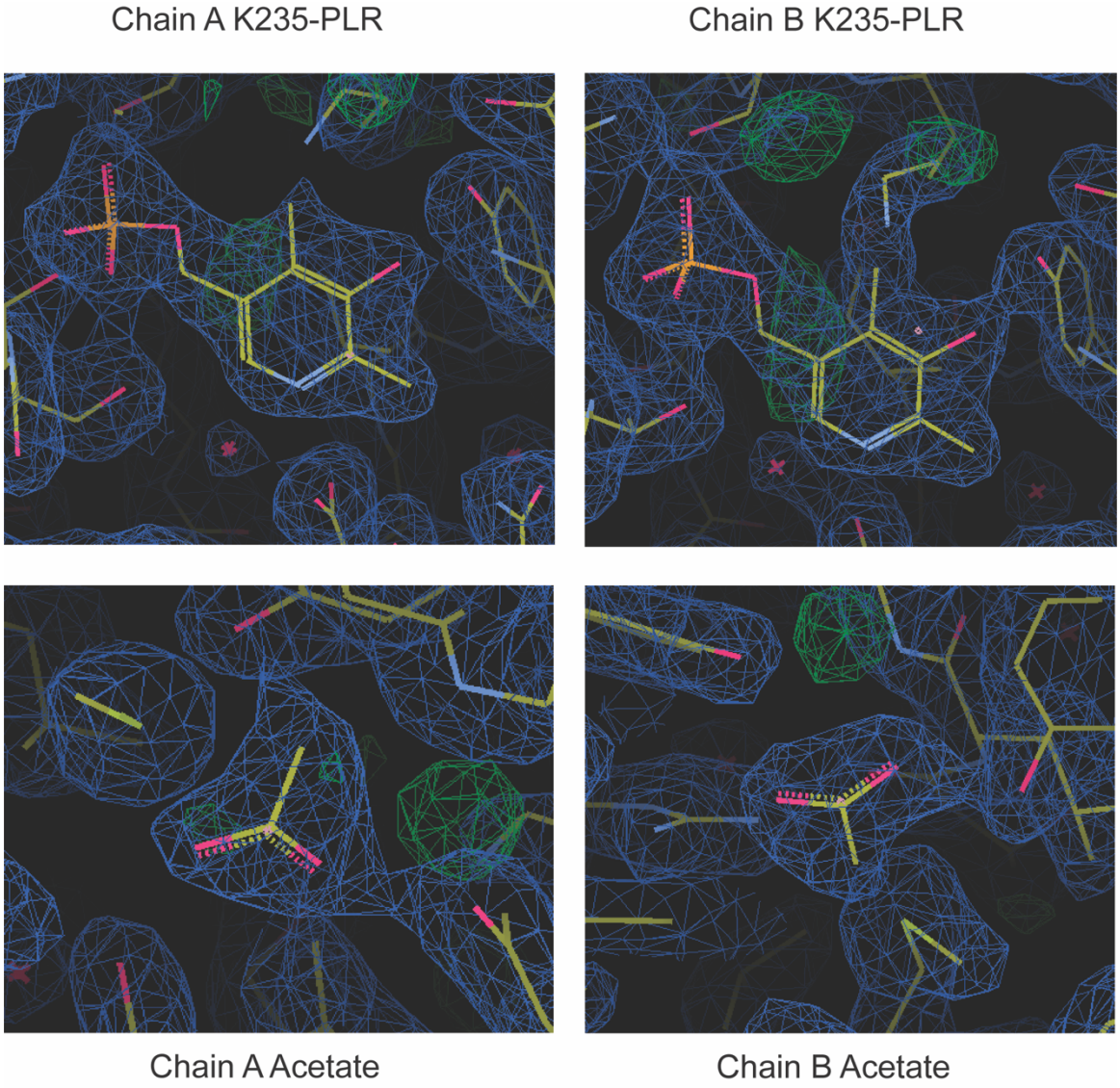

SUPPLEMENTAL FIGURE 1. Reduced PLP (PLR) and acetate crystallized in the active site of EdeM. Fo-Fc electron density map contoured at RMSD 1 Å sigma level for PLR and acetate in the active site of EdeM. Ligands are shown in Chain A and Chain B. Electron density surrounding the reduced Schiff base between K235 and PLR is partially complete in Chain A and complete in Chain B.

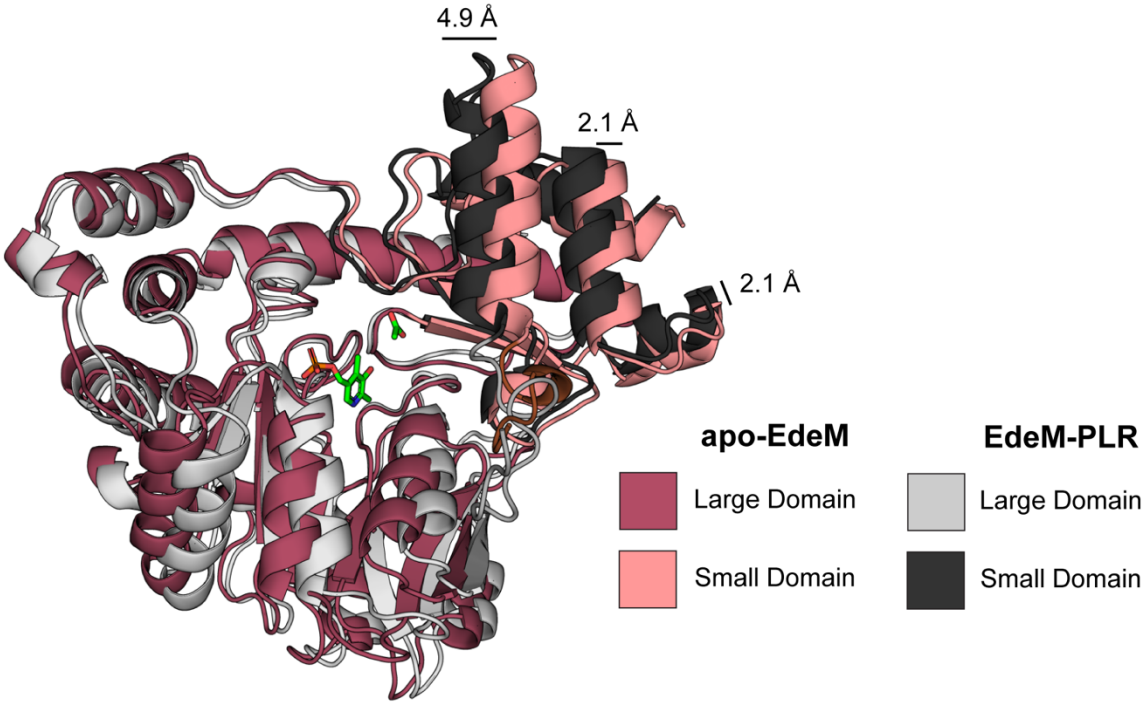

SUPPLEMENTAL FIGURE 2. Open and closed conformations of EdeM. Overlay of Chain B for apo-EdeM (open conformation) and EdeM-PLR (closed conformation) (RMSD 1.85 Å). The large and small domains of apo-EdeM are in dark pink and light pink, respectively. The large and small domains of EdeM-PLR are in black and grey, respectively. PLR and acetate are in green. The small domain of EdeM-PLR (grey) is positioned inwards toward the active site due to the presence of bound acetate. Distances between various α-helices of the small domain in both conformations are annotated.

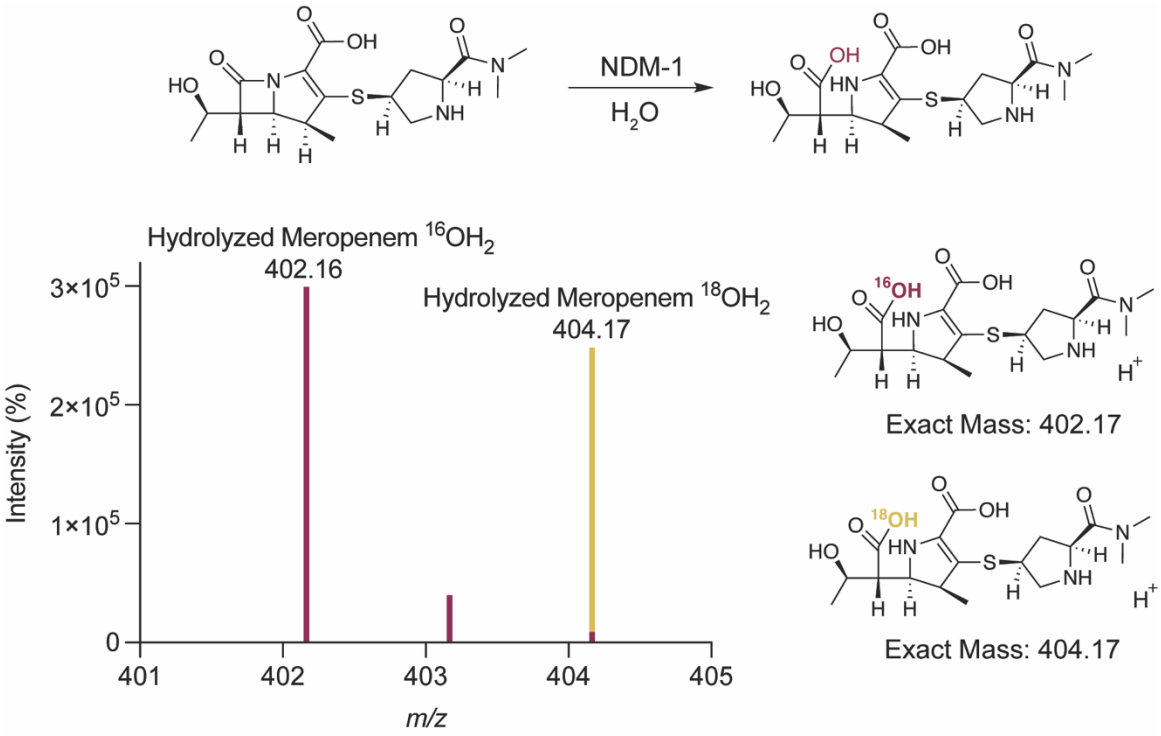

SUPPLEMENTAL FIGURE 3. NMD-1 and meropenem ^{18}O incorporation control. The incorporation of 2 Da is seen in the hydrolyzed meropenem reaction product when reactions are prepared in $^{18}OH_2$.

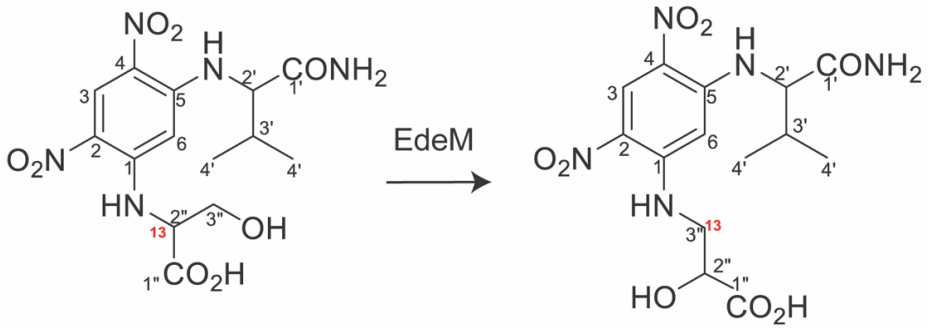

Atom #	^{1}H (L-serine)	^{13}C (L-serine)	Atom #	^{1}H (D-β-serine)	^{13}C (D-β-serine)
1	**-**	**147.66**	1	-	147.5
2	**-**	**123.84**	2	-	123.4
3	**9.00 (d, *J* = 7.7 Hz, 1H)**	**128.47**	3	**8.97 (s, 1H)**	128.31
4	**-**	**123.75**	4	-	123.4
5	**-**	**146.99**	5	-	148.03
6	**5.81 (s, 1H)**	**91.73**	6	**6.10 (s, 1H))**	92.05
L-Valinamide			L-Valinamide		
2’	4.07 (dd, *J* = 7.8, 6.1 Hz, 1H)	61.86	2’	4.16 (dd, *J* = 7.8, 5.5 Hz, 1H)	61.46
3’	2.29 – 2.06 (m, 1H)	30.17	3’	2.21 (dq, *J* = 13.5, 6.7 Hz, 1H)	31.17
CH_3 (4’)	1.05 – 0.96 (m, 7H)	19.1 18.2	CH3	0.99 (dd, *J* = 6.8, 2.3 Hz, 6H)	19.92 18.89
NH	8.51 (d, *J* = 7.8 Hz, 1H)	-	NH	8.52	-
$CONH_2$ (1’)	7.74 – 7.64 (m, 1H), 7.39 (dd, *J* = 8.0, 2.1 Hz, 1H)	171.7	CONH2	7.67 (dd, *J* = 33.0, 2.0 Hz, 1H), 7.45 – 7.18 (m, 1H)	171.60
L-Ser			D-Ise		
2”	4.57 (d, *J* = 7.6 Hz, 0.5H), 4.40 – 4.33 (m, 0.5H)	57.25	2”	4.21 (dt, *J* = 8.2, 4.2 Hz, 1H)	73.36
3”	3.93 – 3.74 (m, 2H)	60.08	3”	3.59 (dd, *J* = 12.0, 6.3 Hz, 1H) 3.22 (dd, *J* = 13.6, 7.0 Hz, 1H)	46.77
NH	8.91 (d, *J* = 6.8 Hz, 1H)	-	NH	8.59 (t, *J* = 4.8 Hz, 1H)	-
CO_2H (1”)		172.05	CO_2H	-	176.32

SUPPLEMENTAL TABLE 2. Complete NMR assignment of control L-serine-2-^{13}C and the reaction product D-β-serine-3-^{13}C after derivatization with Marfey's reagent and purification from large-scale EdeM reactions in dmso-d_6.

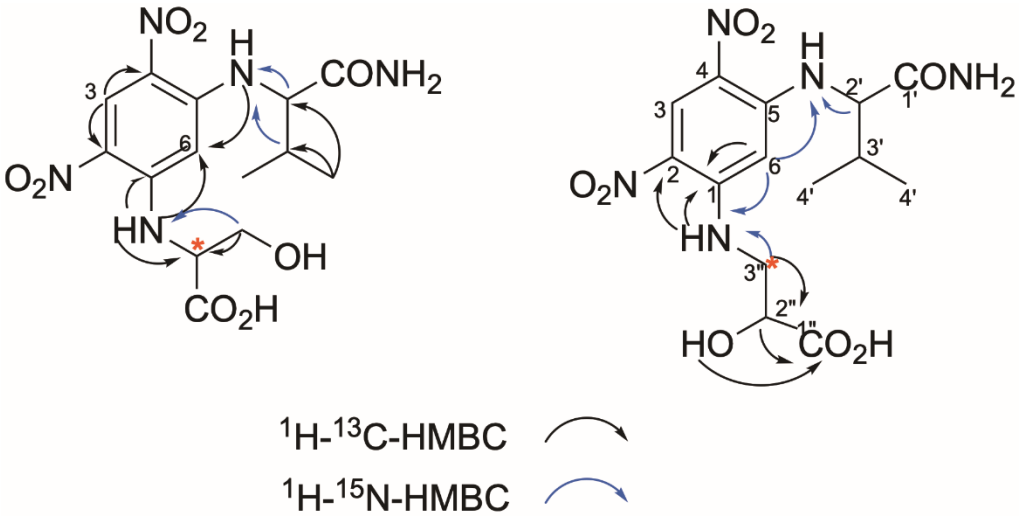

SUPPLEMENTAL FIGURE 4. HMBC diagram of Marfey's labelled L-serine-2-^{13}C control and D-β-serine-3-^{13}C reaction product.

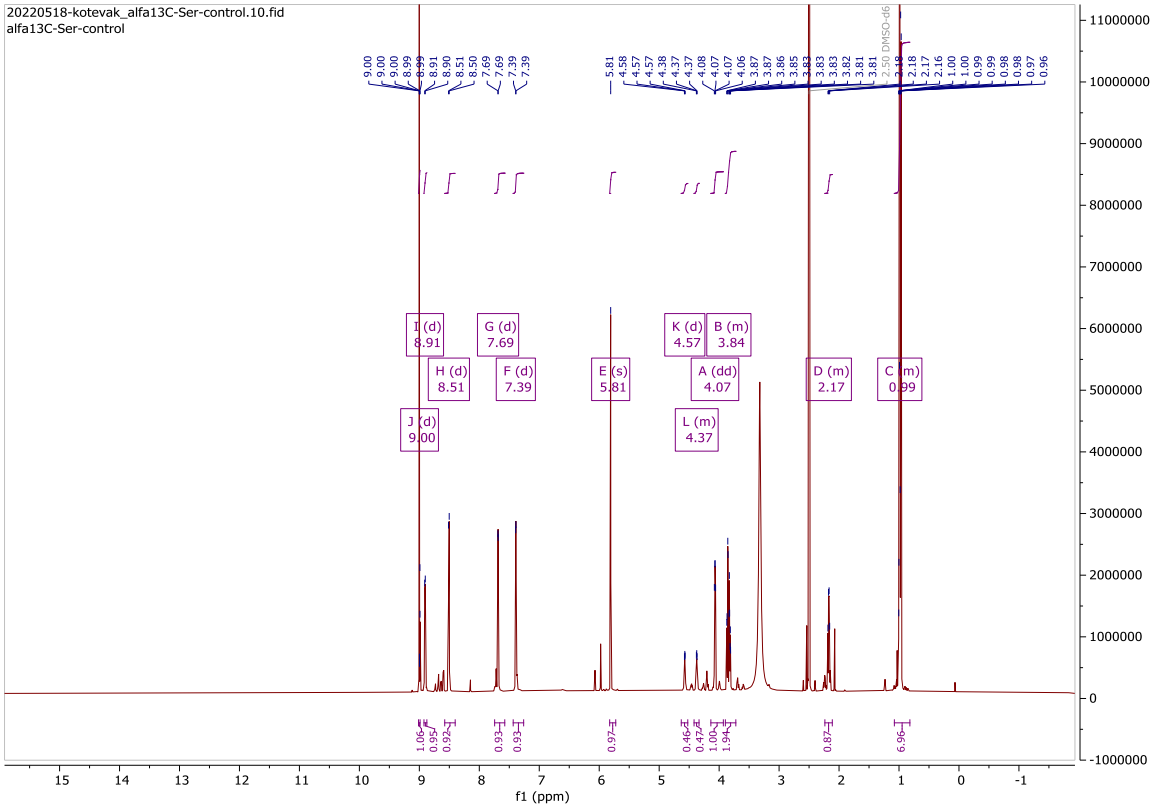

SUPPLEMENTAL FIGURE 5. ^{1}H-NMR spectra of Marfey's labelled L-serine-2-^{13}C in dmso-d_6. The proton attached to the α-carbon is split in two with chemical shifts of 4.47 and 4.57 ppm.

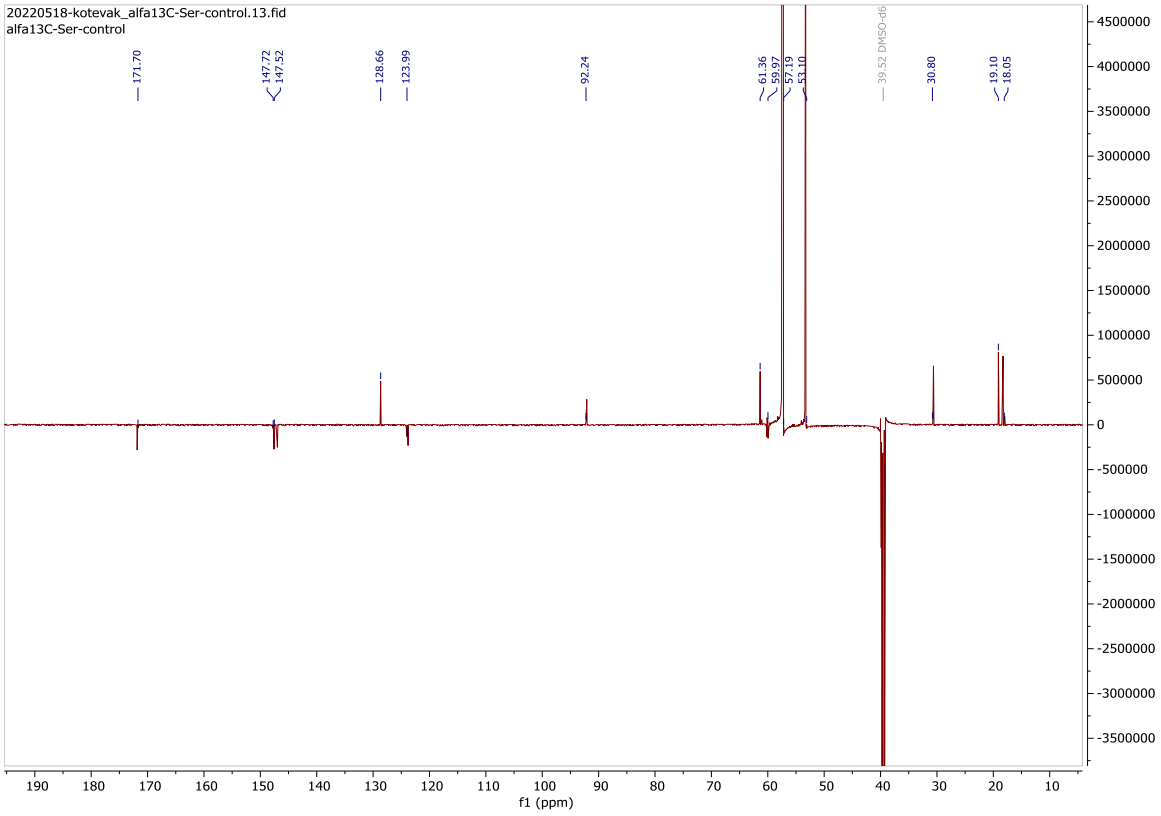

SUPPLEMENTAL FIGURE 6. ^{13}C NMR DEPTQ-135 spectra of Marfey's labelled L-serine-2-^{13}C in dmso-d_6. The CH α-carbon is in the same phase as the CH_3 groups of the Marfey's valinamide group. DEPTQ-135 shows CH/CH_3 (methine/methyl) with a positive phase and CH_2 with negative quaternary carbons.

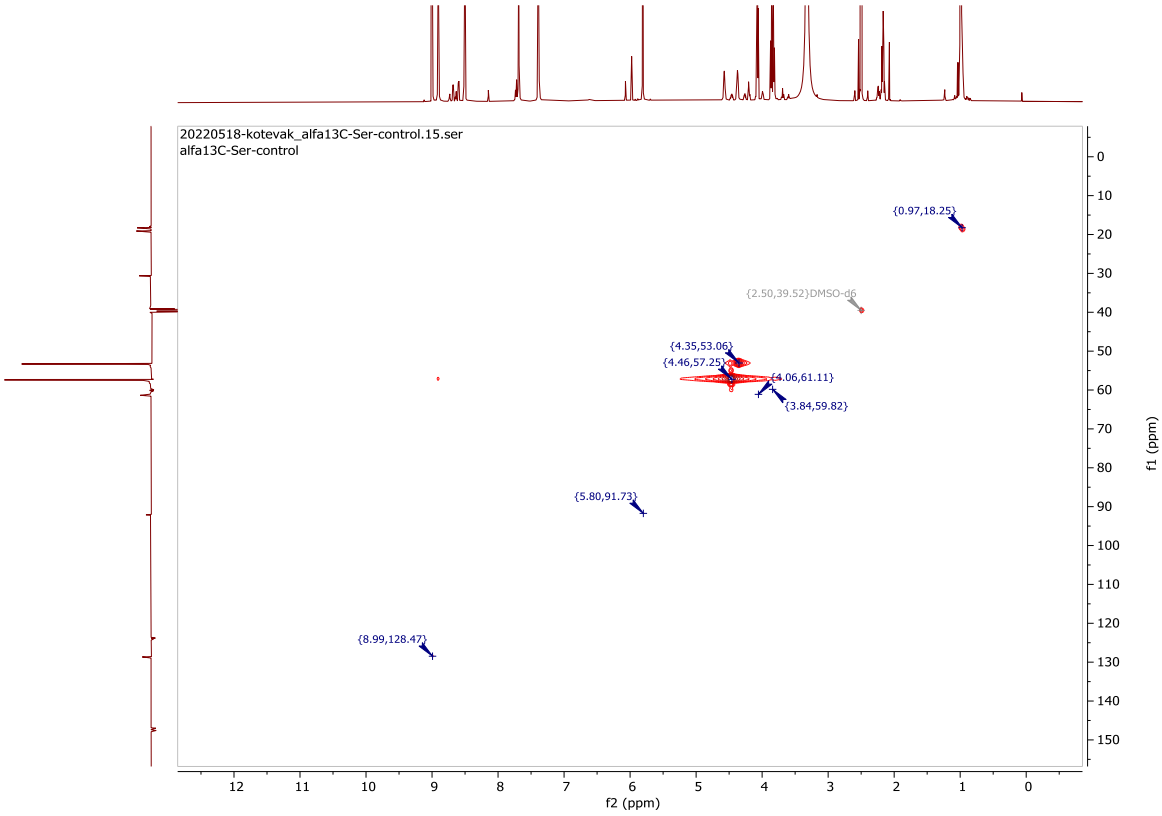

SUPPLEMENTAL FIGURE 7. ^{1}H-^{13}C HSQC spectra of Marfey's labelled L-serine-2-^{13}C in dmso-d_6. There are 2 ^{13}C carbon peaks at 57.3 ppm (major) and at 53.06 ppm (minor). The signal at 57.3 ppm is correlated to the split α-carbon proton. The signal at 53.06 ppm may be due to the presence of D-β-serine in the control.

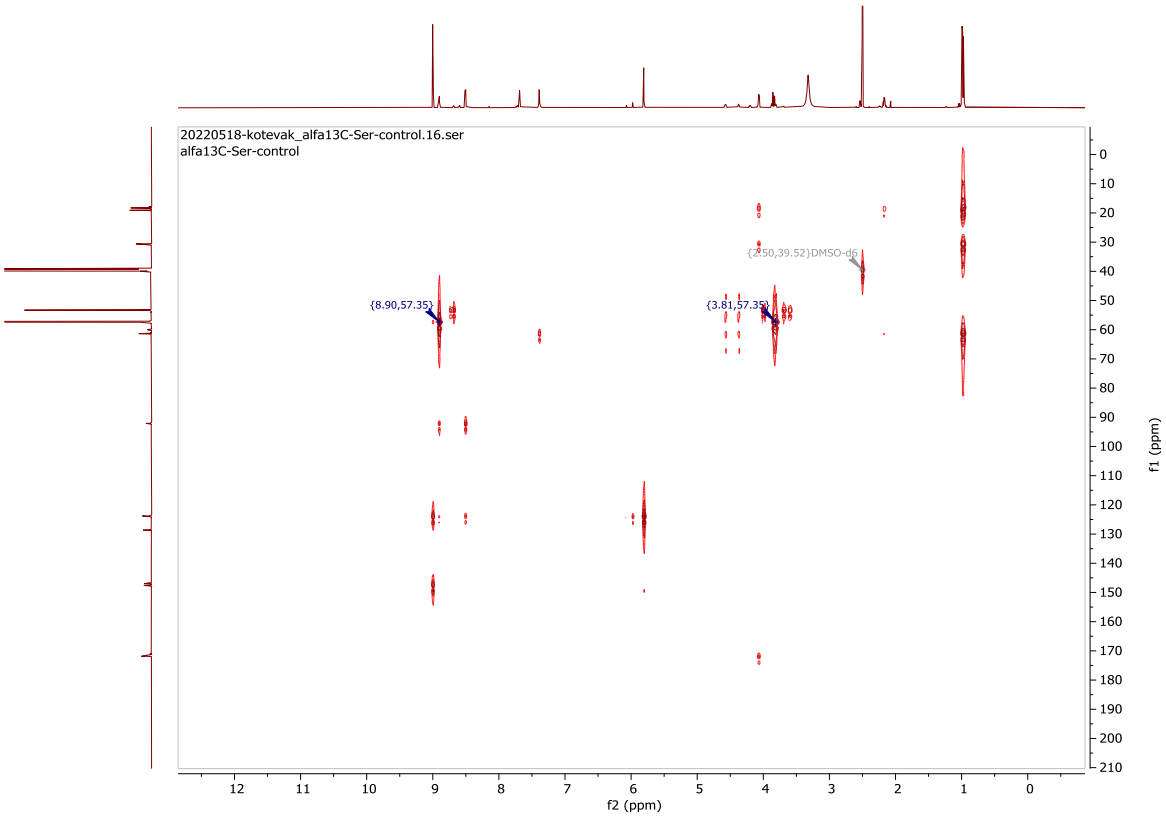

SUPPLEMENTAL FIGURE 8. ^{1}H-^{13}C HMBC spectra of Marfey's labelled L-serine-2-^{13}C in dmso-d_6. The ^{13}C-2-carbon peak at 57.3 ppm is correlated to the α-carbon NH group at 8.90 ppm in addition to the C-3 protons at 3.81 ppm.

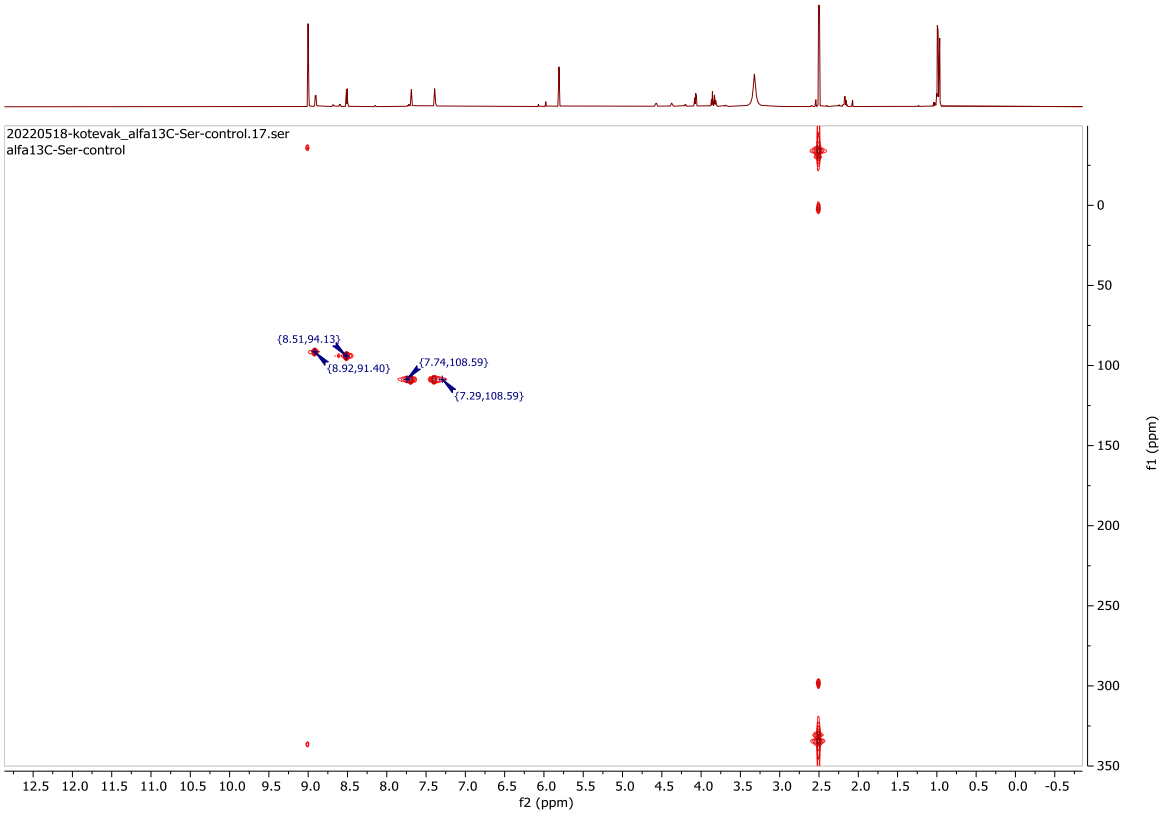

SUPPLEMENTAL FIGURE 9. ^{1}H-^{15}N HSQC spectra of Marfey's labelled L-serine-2-^{13}C in dmso-d_6. The spectra confirmed the chemical shifts of the two α-carbon NH groups at 8.51 ppm (valinamide α-carbon) and 8.92 ppm (serine α-carbon). Two amide carbonyl protons signals are at 7.74 and 7.29 ppm.

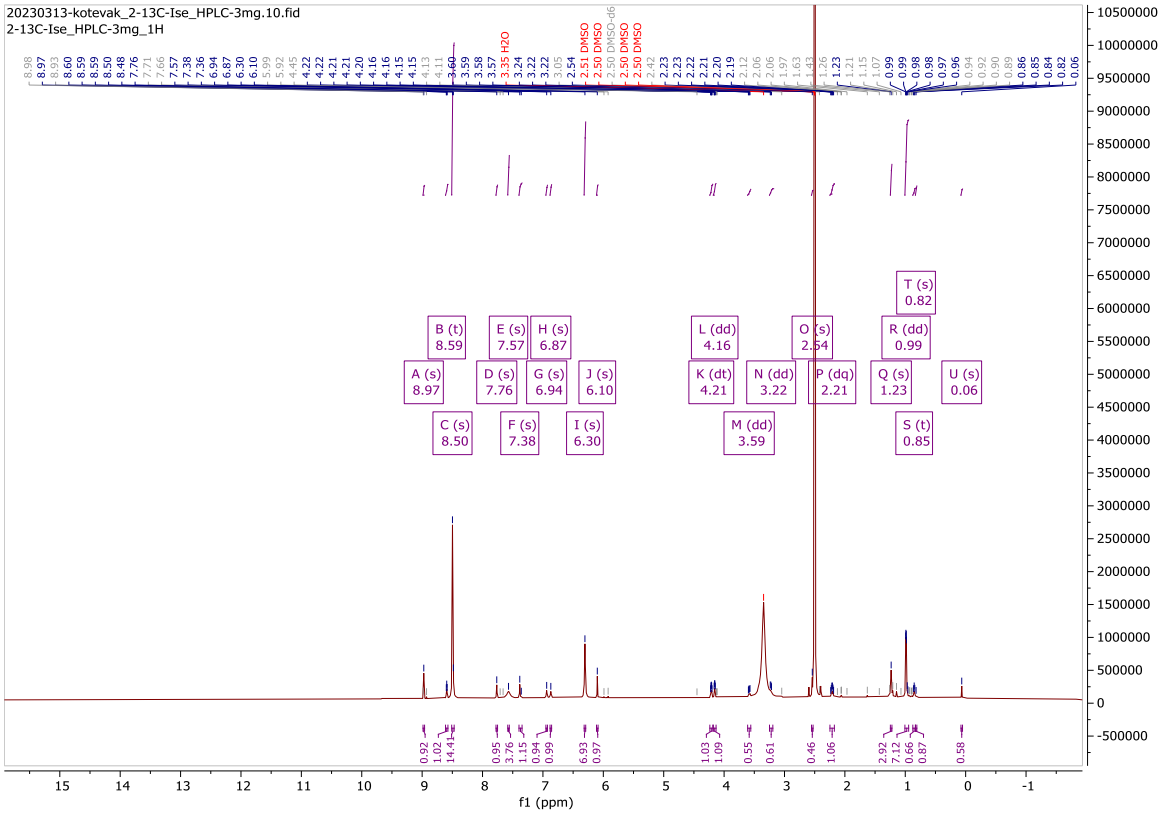

SUPPLEMENTAL FIGURE 10. ^{1}H NMR spectra of Marfey's labelled D-β-serine-3-^{13}C reaction product in dmso-d_6.

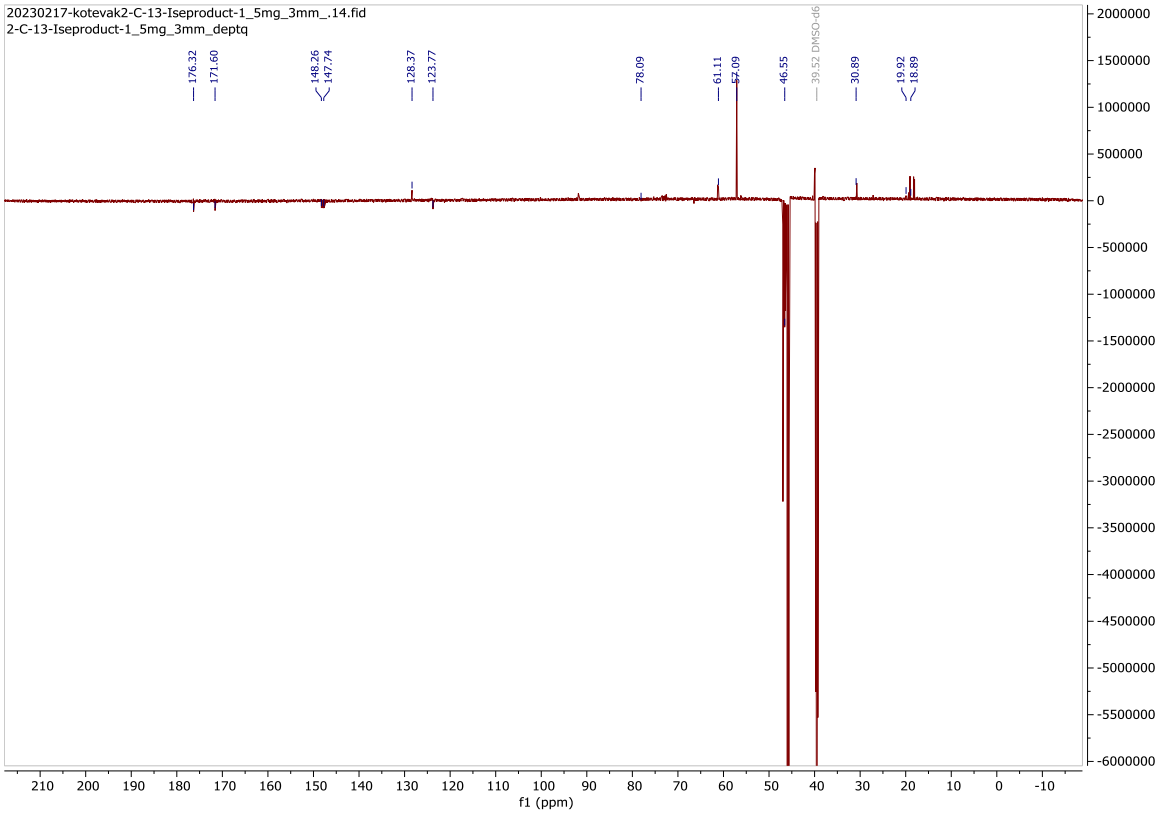

SUPPLEMENTAL FIGURE 11. ^{13}C NMR DEPTQ-135 spectra of Marfey's labelled D-β-serine-3-^{13}C reaction product in dmso-d_6. The carbon bearing the ^{13}C label is now located on the CH_2 group and situated on the opposite plane of CH_3 and CH groups. DEPTQ-135 shows CH/CH3 (methine/methyl) with a positive phase and CH_2 with negative quaternary carbons.

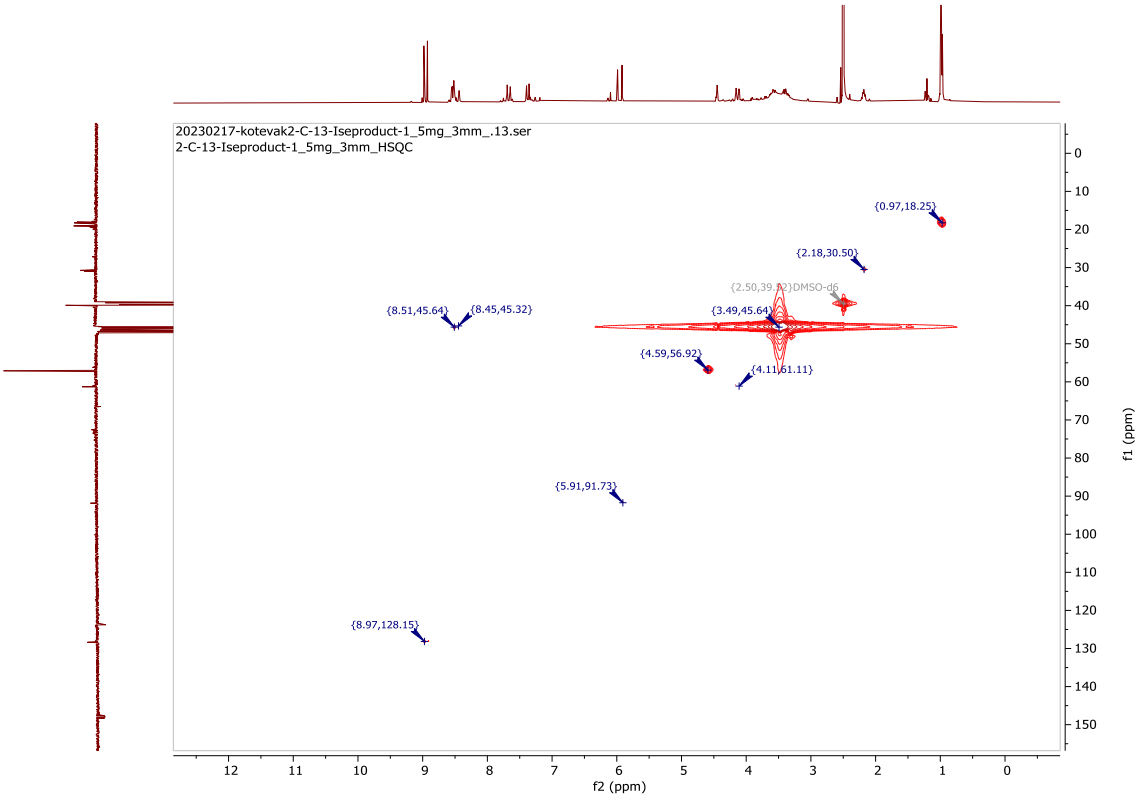

SUPPLEMENTAL FIGURE 12. ^{1}H-^{13}C HSQC spectra of Marfey's labelled D-β-serine-3-^{13}C reaction product in dmso-d_6. The ^{13}C label is at the beta carbon position (^{13}C-3) bound to CH_2 protons split in two with the following chemical shifts: 3.48 (0.5H), 3.3 (1H), and 3.22 (0.5H) ppm.

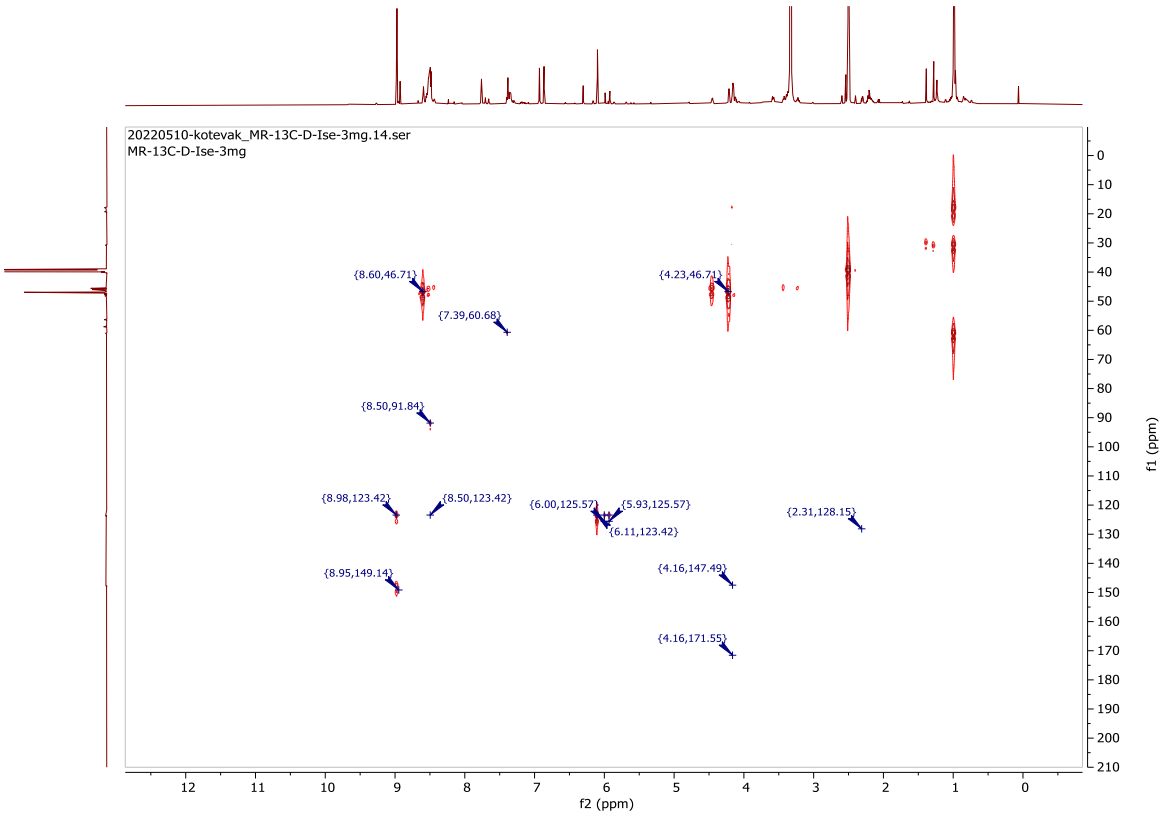

SUPPLEMENTAL FIGURE 13. ^{1}H-^{13}C HMBC spectra of Marfey's labelled D-β-serine-3-^{13}C reaction product in dmso-d_6. The ^{13}C-3 carbon peak at 46.7 ppm are correlated to the NH group at 8.64 ppm in addition to the C-2 protons at 4.23 ppm.

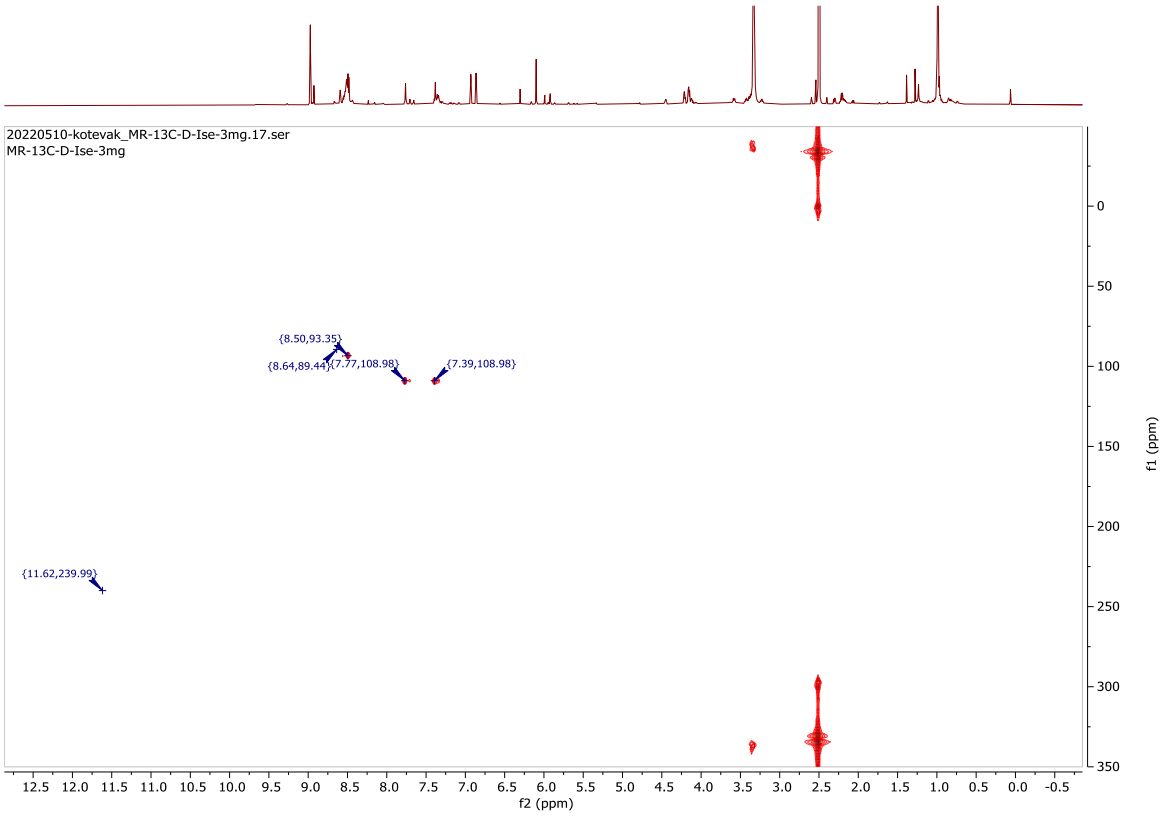

SUPPLEMENTAL FIGURE 14. ^{1}H-^{15}N HSQC spectra of Marfey's labelled D-β-serine-3-^{13}C reaction product in dmso-d_6. The spectra confirmed the chemical shifts of the two α-carbon NH groups at 8.51 ppm (valinamide α-carbon) and 8.64 ppm (D-β-serine).

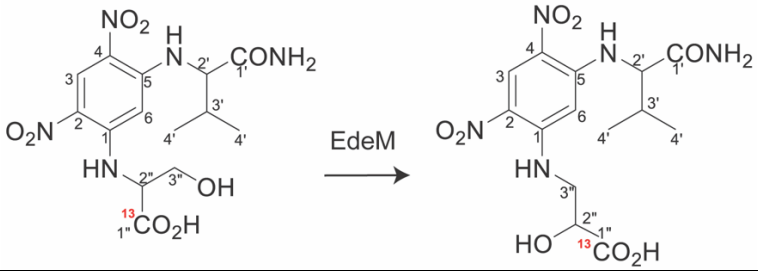

Atom #	^{1}H (Ser)	^{13}C (Ser)	Atom #	^{1}H (D-Ise)	^{13}C (D-Ise)
1	-	146.98	1	-	147.5
2	-	123.99	2	-	123.4
3	9.0 (s, 1H)	128.67	3	8.98 (d, *J* = 6.7 Hz, 1H)	128.15
4	-	123.87	4	-	123.4
5	-	147.53	5	-	148.03
6	5.81 (s, 1H)	91.93	6	6.10 (s, 1H)	92.68
L-Valinamide			L-Valinamide		
NH	8.51 (d, *J* = 7.8 Hz, 1H)	-	NH	8.51	-
1'CONH2	7.68 (d, *J* = 2.1 Hz, 1H) 7.40 (d, *J* = 2.1 Hz, 1H)	169.87	1'CONH2	7.77 7.38	171.60
2'	4.07 (dd, *J* = 7.8, 6.1 Hz, 1H)	61.38	2'	4.15 (dd, *J* = 7.8, 5.6 Hz, 1H)	60.79
3'	2.22 – 2.12 (m, *J* = 6.8 Hz, 1H)	30.62	3'	2.23 – 2.14 (m, 2H)	30.50
4' (CH3)	0.98 (dd, *J* = 15.1, 6.8 Hz, 6H)	19.19 18.37	4' (CH3)	0.99	17.60 18.89
L-Ser			D-Ise		
NH	8.87 (dd, *J* = 7.3, 2.2 Hz, 1H)	-	NH	8.51 (d, *J* = 7.8 Hz, 1H)	-
1" (**^{13}CO$_2$H**)	-	171.15	**1"** (**^{13}CO$_2$H**)	-	**177.24**
2"	4.54 (tt, *J* = 6.5, 2.9 Hz, 1H)	57.09	2"	4.22 (m, 1H)	73.36
3"	3.90 – 3.82 (m, 2H)	59.97	3" (β)	3.64 – 3.47 (m, 2H)	46.61

SUPPLEMENTAL TABLE 3. Complete NMR assignment in dmso-d6 of control L-serine-1-^{13}C and the reaction product D-β-serine-1-^{13}C after derivatization with Marfey's reagent and purification from large-scale EdeM reactions.

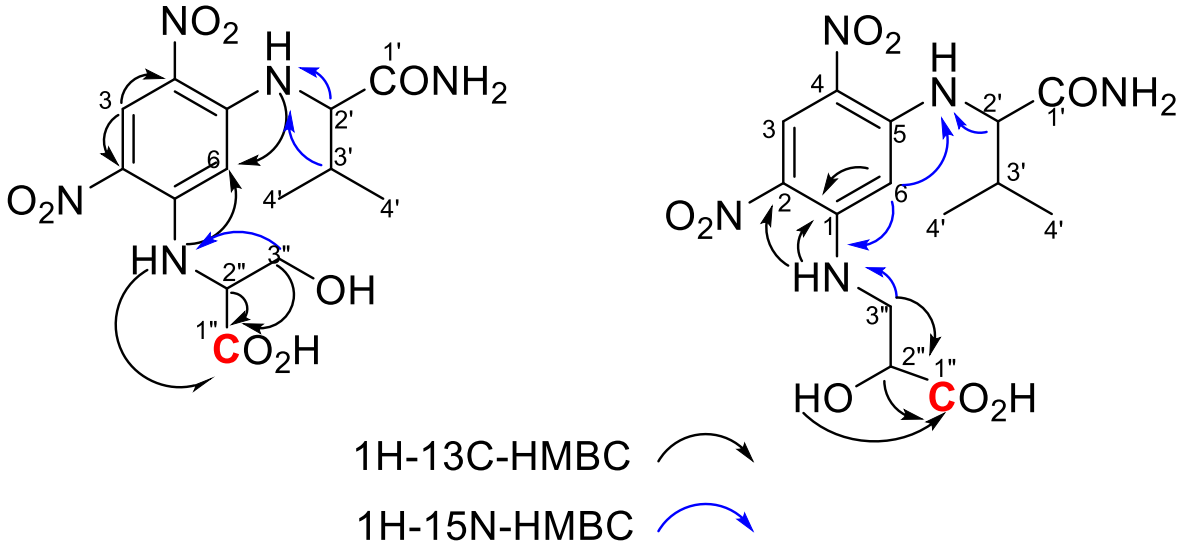

SUPPLEMENTAL FIGURE 15. HMBC diagram of Marfey's labelled L-serine-1-^{13}C control and D-β-serine-1-^{13}C reaction product.

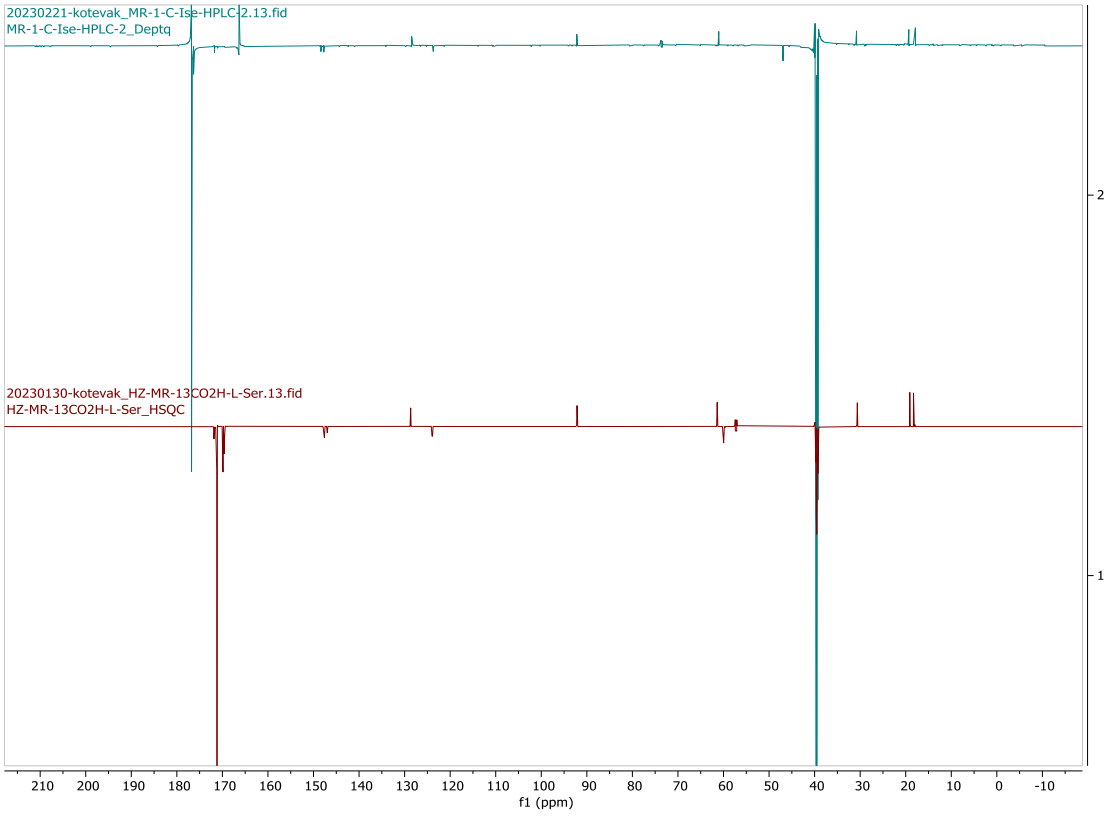

SUPPLEMENTAL FIGURE 16. ^{13}C NMR DEPTQ-135 spectra overlay of Marfey's labelled D-β-serine-1-^{13}C reaction product (top) and L-serine-1-^{13}C control (bottom) in dmso-d_6.

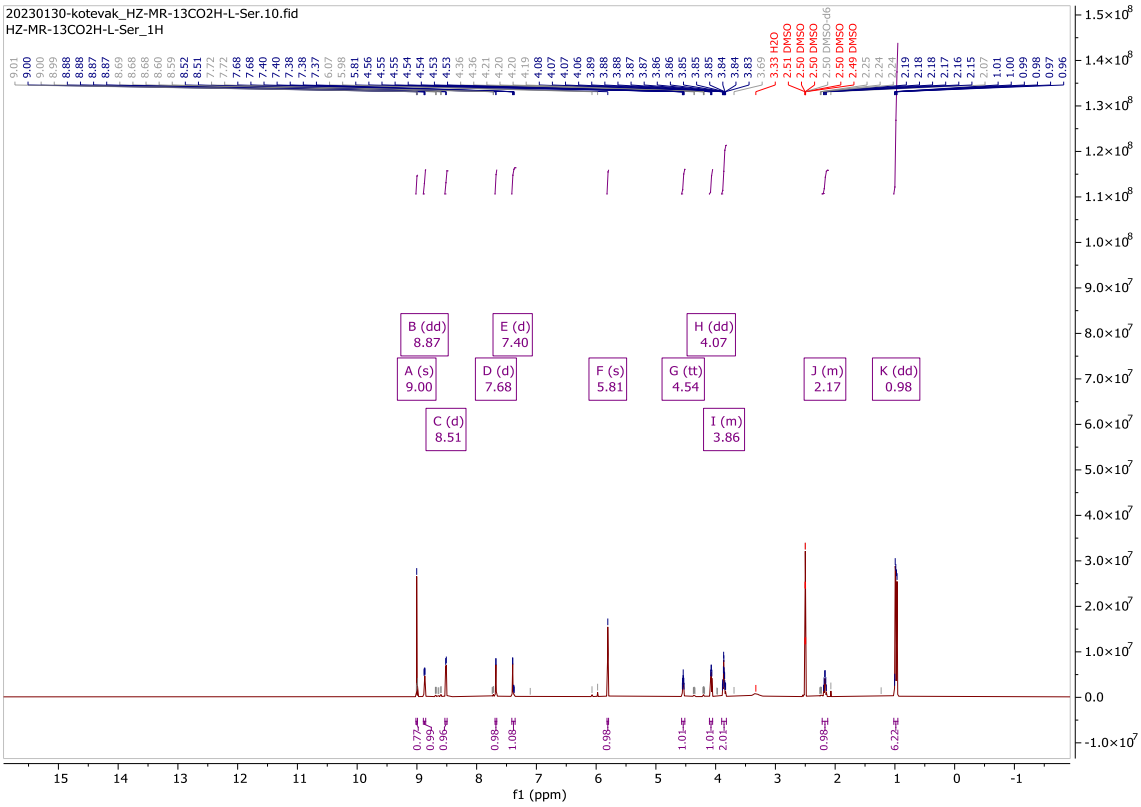

SUPPLEMENTAL FIGURE 17. ^{1}H NMR spectra of L-serine-1-^{13}C control in dmso-d_6.

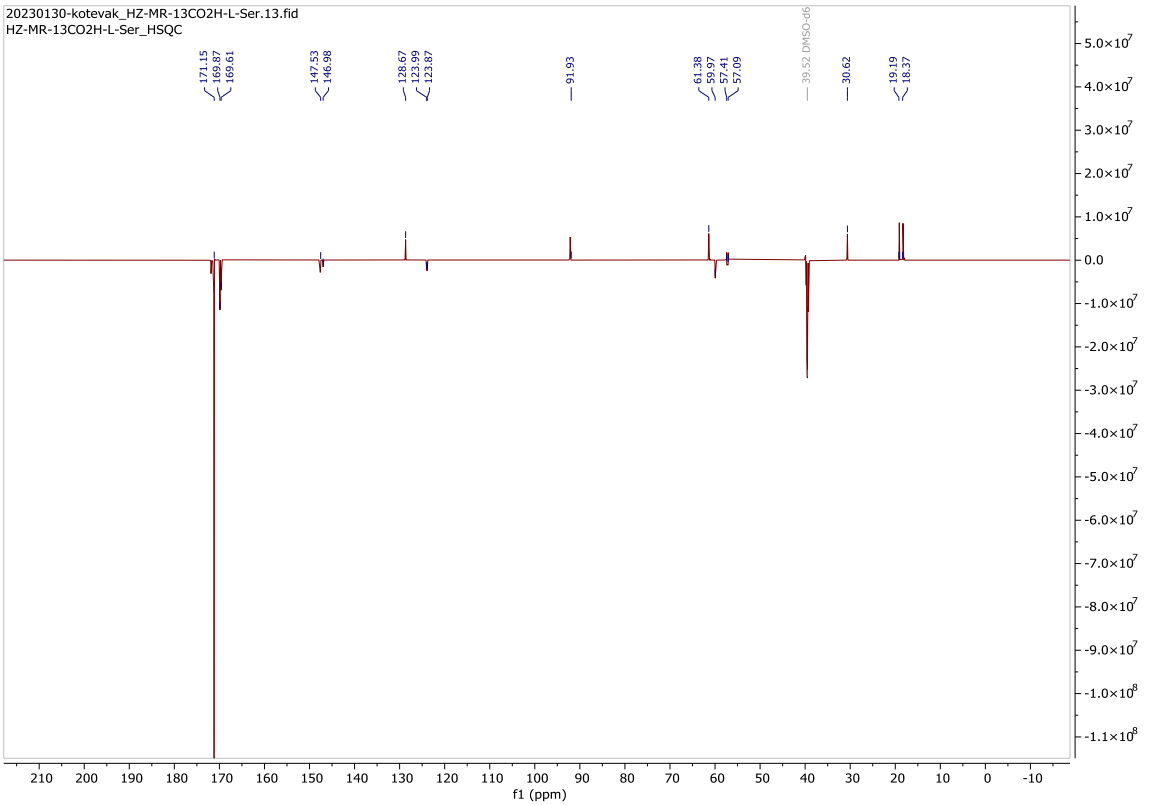

SUPPLEMENTAL FIGURE 18. ^{13}C NMR DEPTQ-135 spectra of L-serine-1-^{13}C control in dmso-d_6.

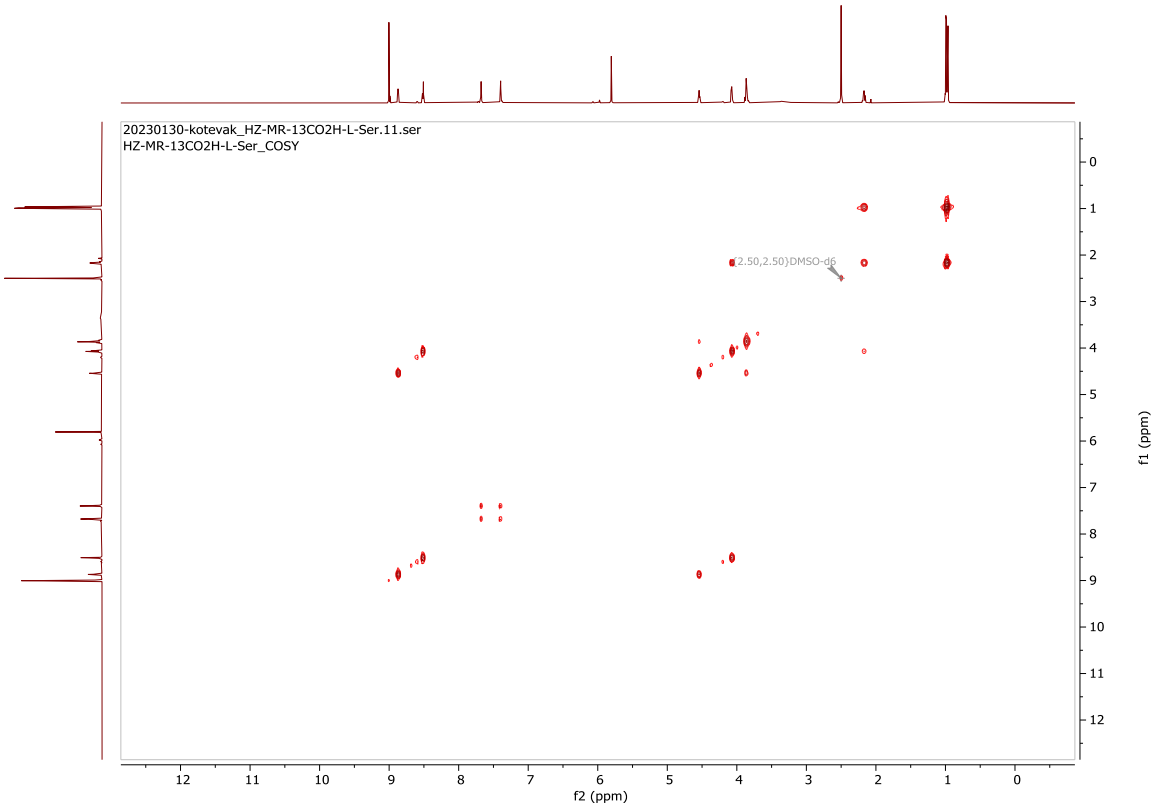

SUPPLEMENTAL FIGURE 19. ^{1}H-^{1}H COSY spectra of L-serine-1-^{13}C control in dmso-d_6.

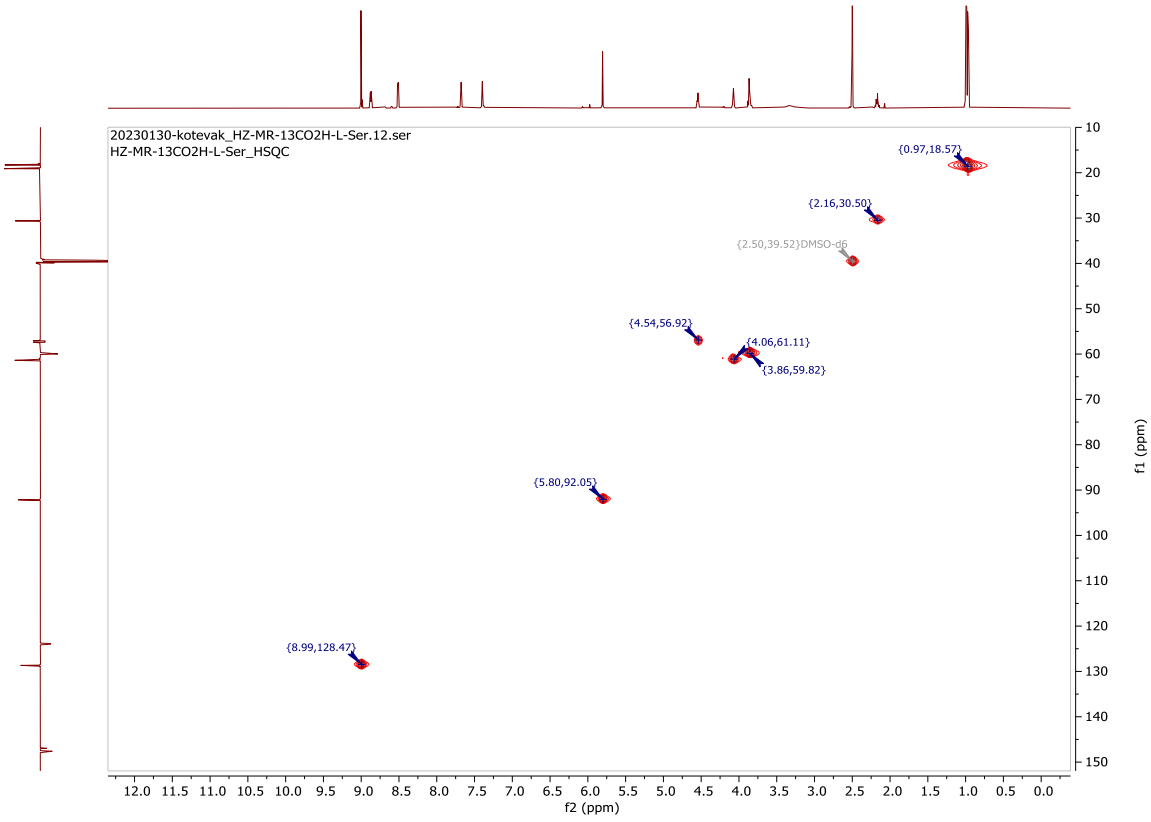

SUPPLEMENTAL FIGURE 20. ^{1}H-^{13}C HSQC spectra of L-serine-1-^{13}C control in dmso-d_6.

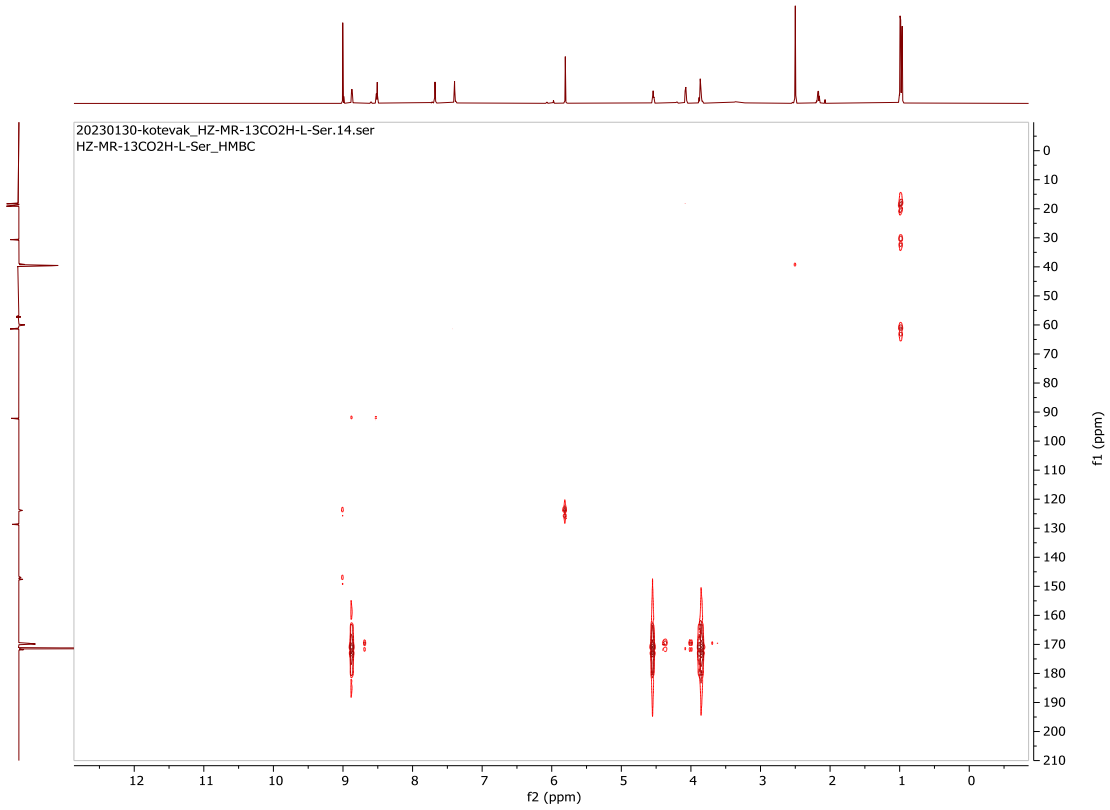

SUPPLEMENTAL FIGURE 21. ^{1}H-^{13}C HMBC spectra of L-serine-1-^{13}C control in dmso-d_6.

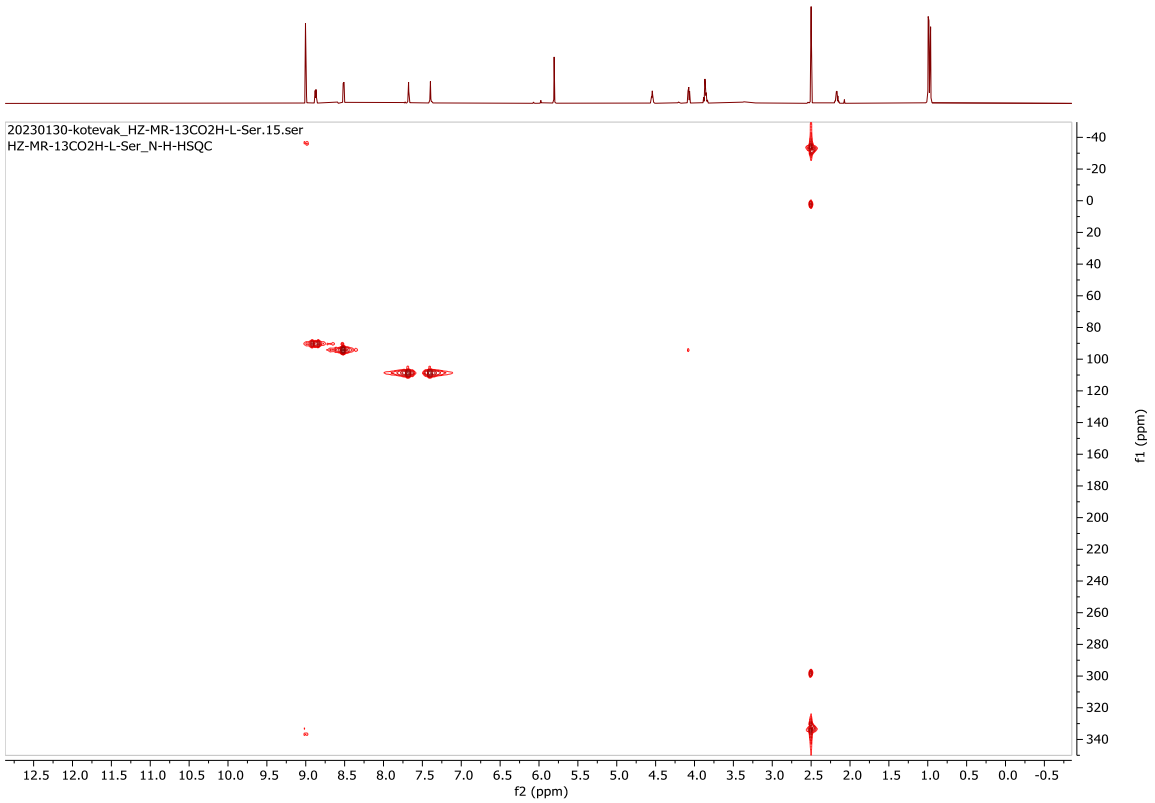

SUPPLEMENTAL FIGURE 22. ^{1}H-^{15}N HSQC spectra of L-serine-1-^{13}C control in dmso-d_6.

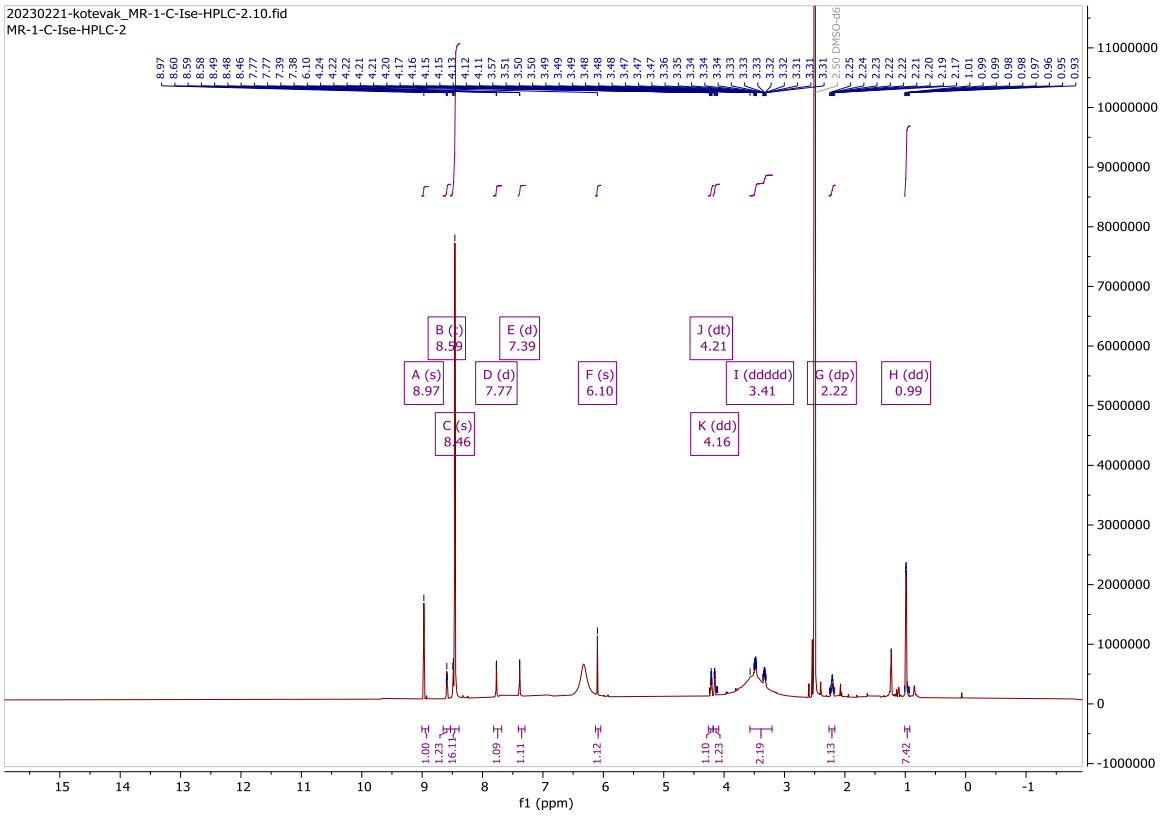

SUPPLEMENTAL FIGURE 23. ^{1}H NMR spectra of D-β-serine-1-^{13}C reaction product in dmso-d_6.

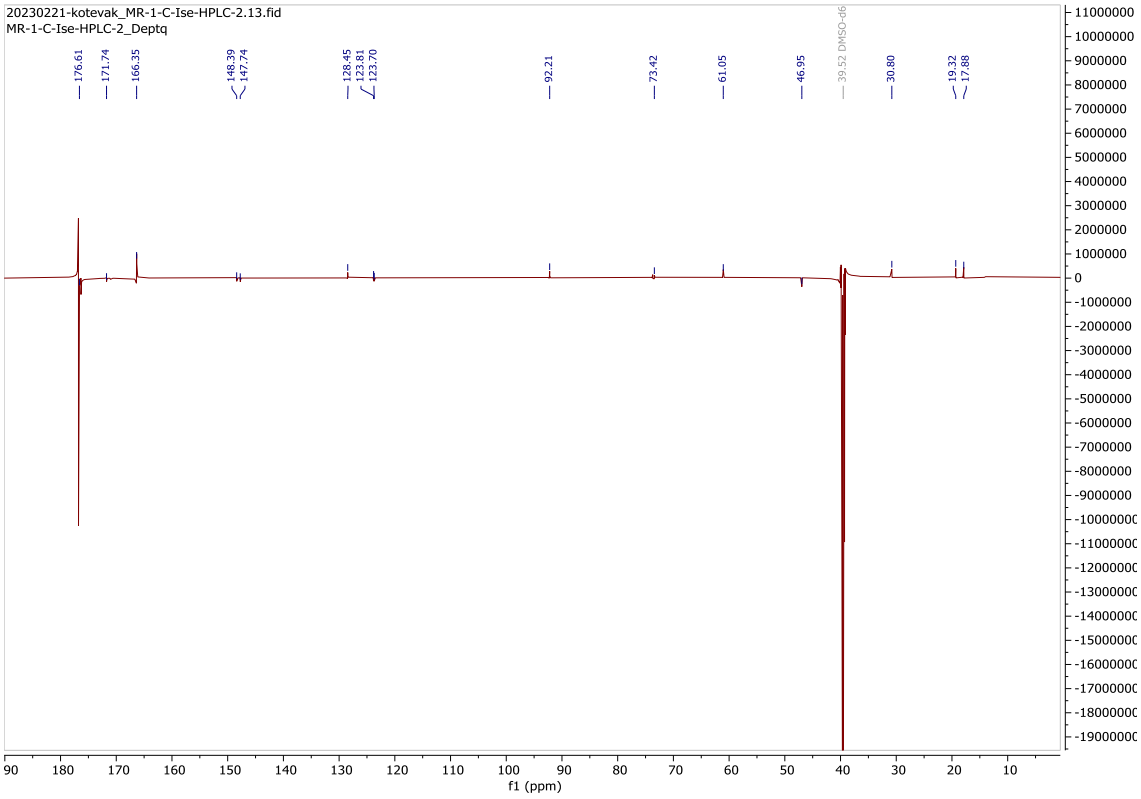

SUPPLEMENTAL FIGURE 24. ^{13}C NMR DEPTQ-135 spectra of D-β-serine-1-^{13}C reaction product in dmso-d_6.

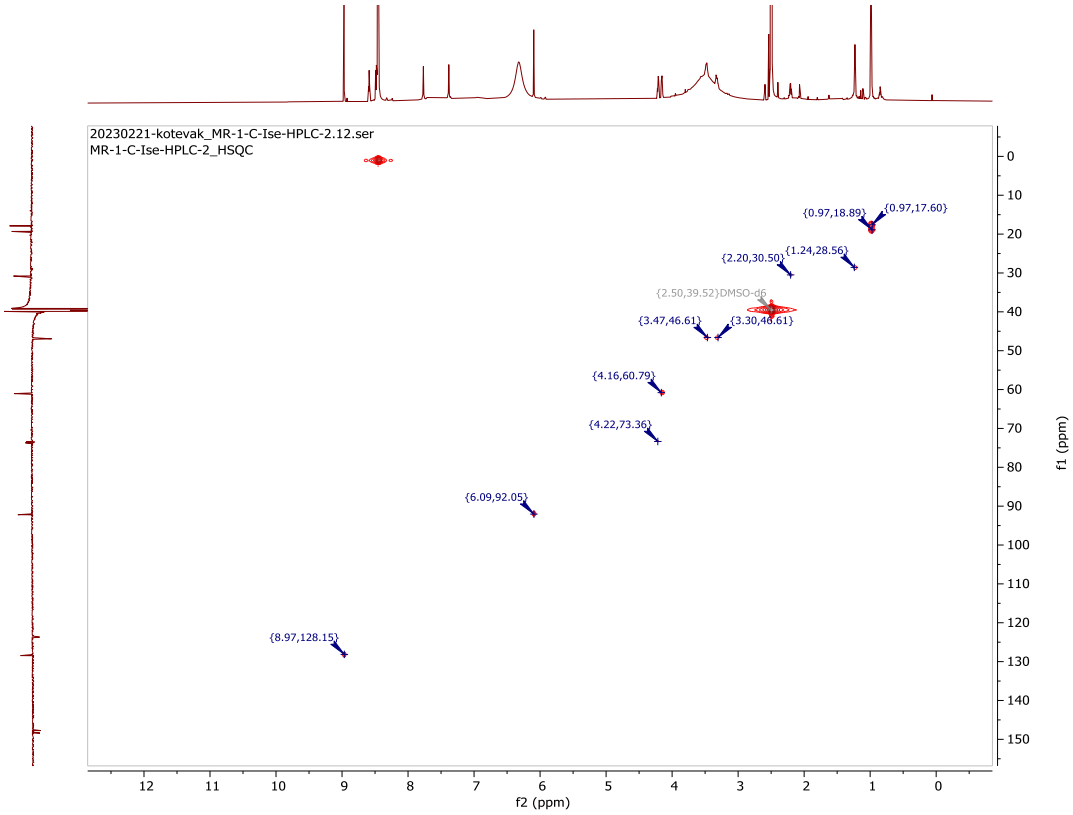

SUPPLEMENTAL FIGURE 25. ^{1}H-^{13}C HSQC spectra of D-β-serine-1-^{13}C reaction product in dmso-d_6.

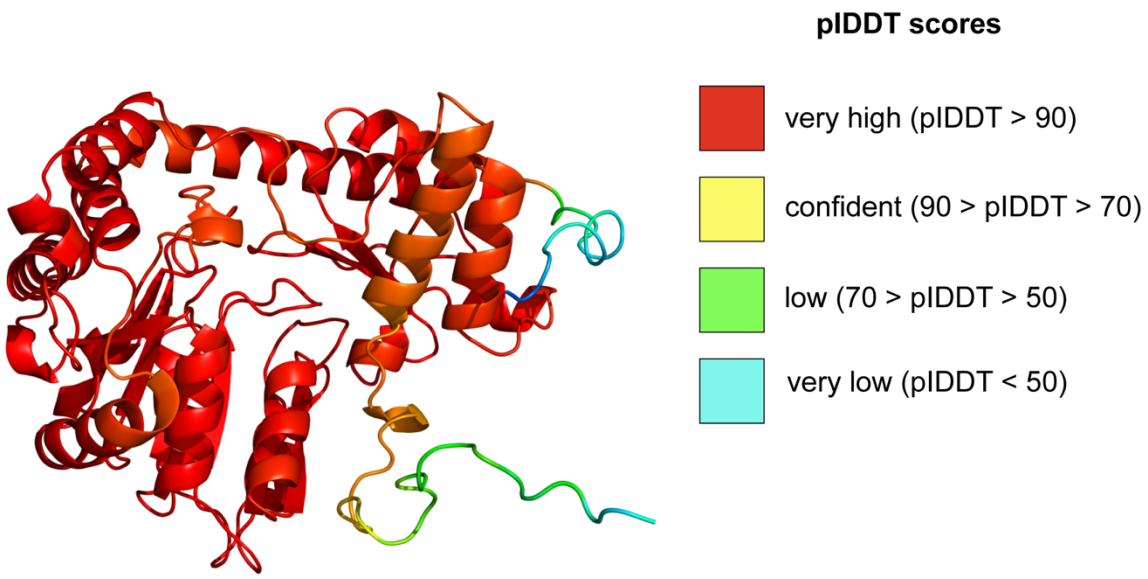

SUPPLEMENTAL FIGURE 26. AlphaFold 3 model of GE-EdeM and associated pIDDT scores.

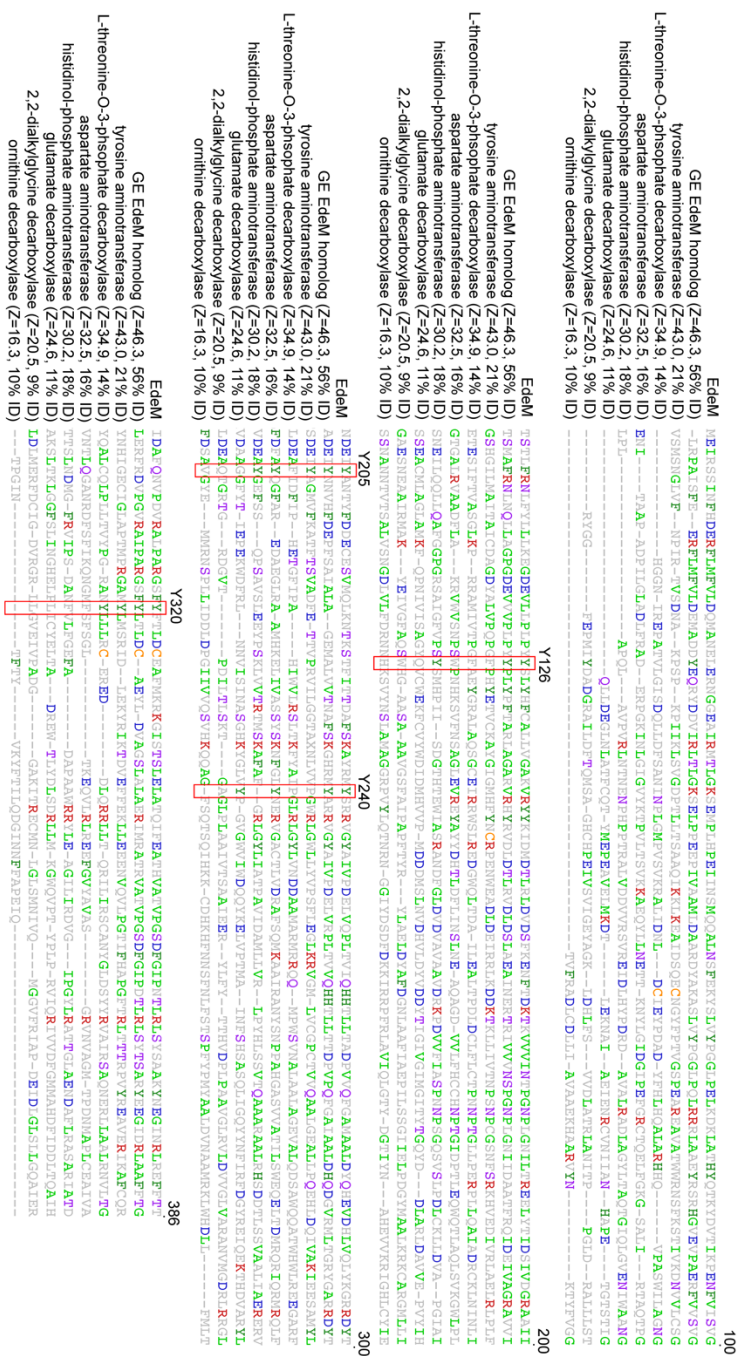

SUPPLEMENTAL FIGURE 27. EdeM Alignments. Full-length structural alignment of EdeM, GE-EdeM (AlphaFold model), tyrosine aminotransferase [PDB 1BW0], L-threonine-*O*-3-phosphate decarboxylase [1LKC], aspartate aminotransferase [1ARG], histidinol-phosphate aminotransferase [4RAE], glutamate decarboxylase [5GP4], 2,2,-dialkylglycine decarboxylase [1M0N], and ornithine decarboxylase [1ORD] completed in DALI.

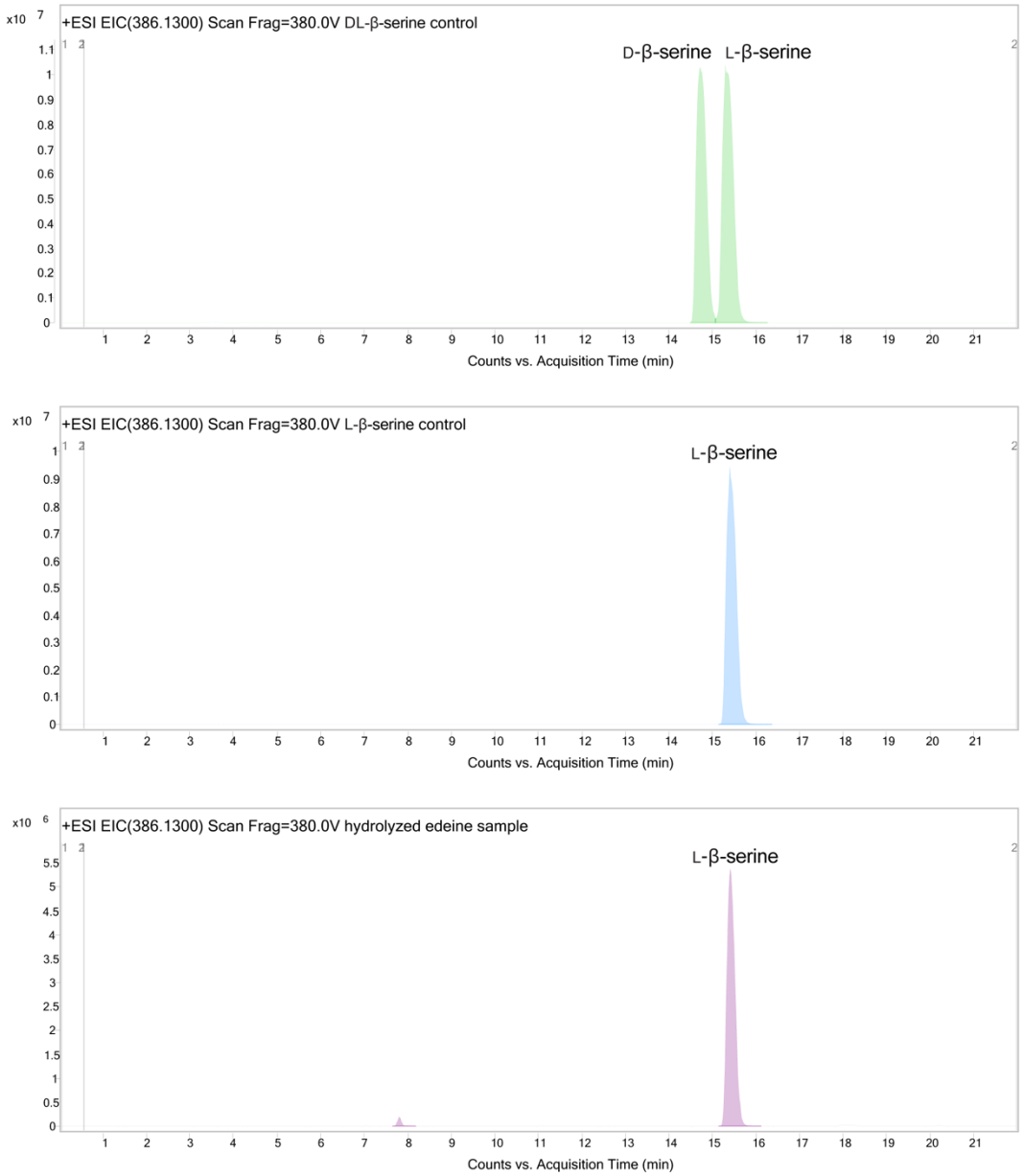

SUPPLEMENTAL FIGURE 28. L-β-serine in edeine. Extracted ion chromatogram in positive mode (+EIC) at 386.13 *m/z* for standards containing a D-/L-β-serine mixture (top) and L-β-serine (middle), and hydrolyzed edeine sample (bottom). D-β-serine has a retention time of ~14.5 minutes, and L-β-serine has a retention time of ~ 15 minutes. Results demonstrate that L-β-serine is present in the hydrolyzed edeine sample.

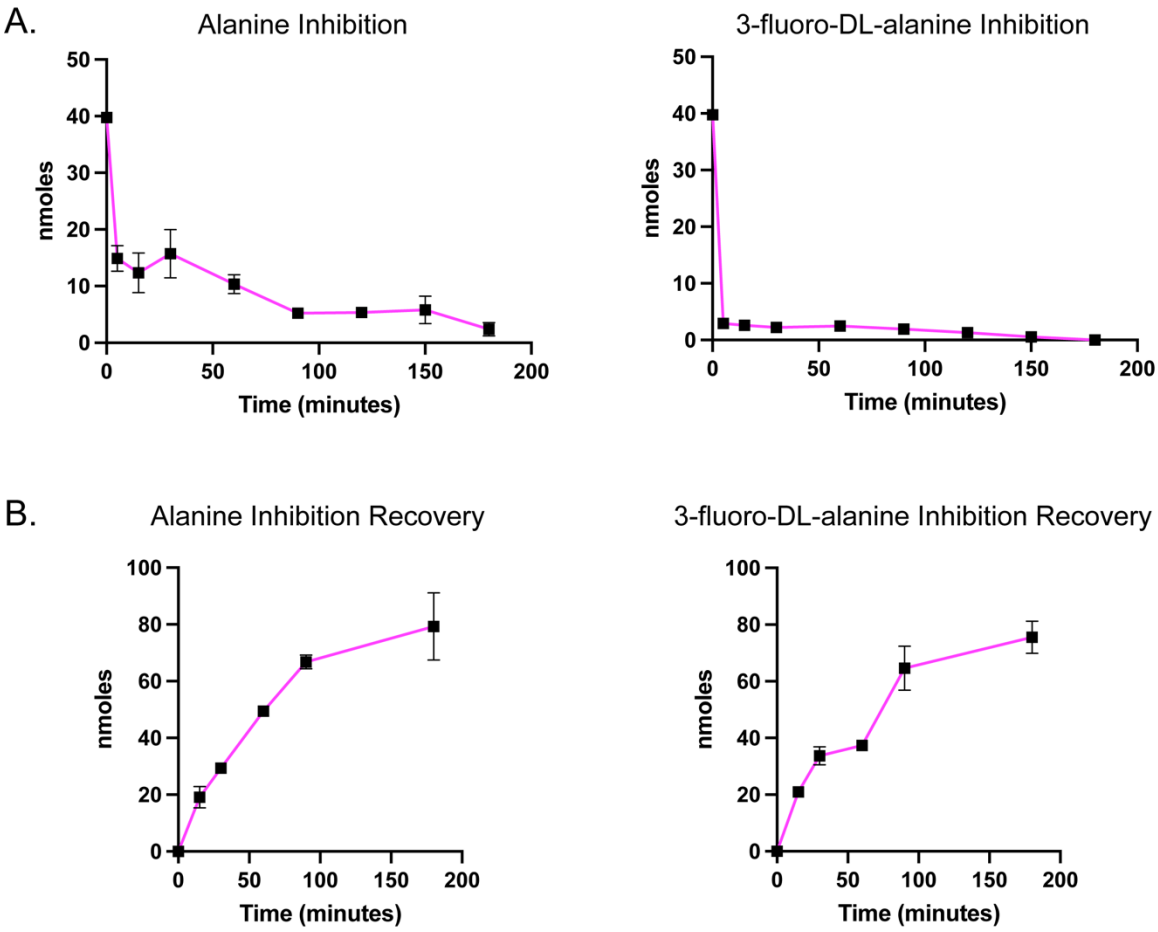

SUPPLEMENTAL FIGURE 29. Inhibitors of EdeM. A. EdeM was incubated with 50 mM of each inhibitor. At each time point, samples of the enzyme were taken and added to a reaction containing L-serine, which was left to react for 15 minutes. The samples were then derivatized with Marfey's reagent and analyzed by HPLC. The amount of D-β-serine produced by EdeM at each time point incubation with the inhibitor is shown in pink. **B.** EdeM was incubated with 50 mM of each inhibitor for 2 hours at room temperature to allow for complete enzyme inhibition. The samples were then processed through a Bio-Gel spin column to remove any unbound inhibitor from the enzyme before being added to a reaction containing L-serine. Time points were taken throughout the incubation to determine the duration required for EdeM to regain its activity by monitoring D-β-serine production (pink).

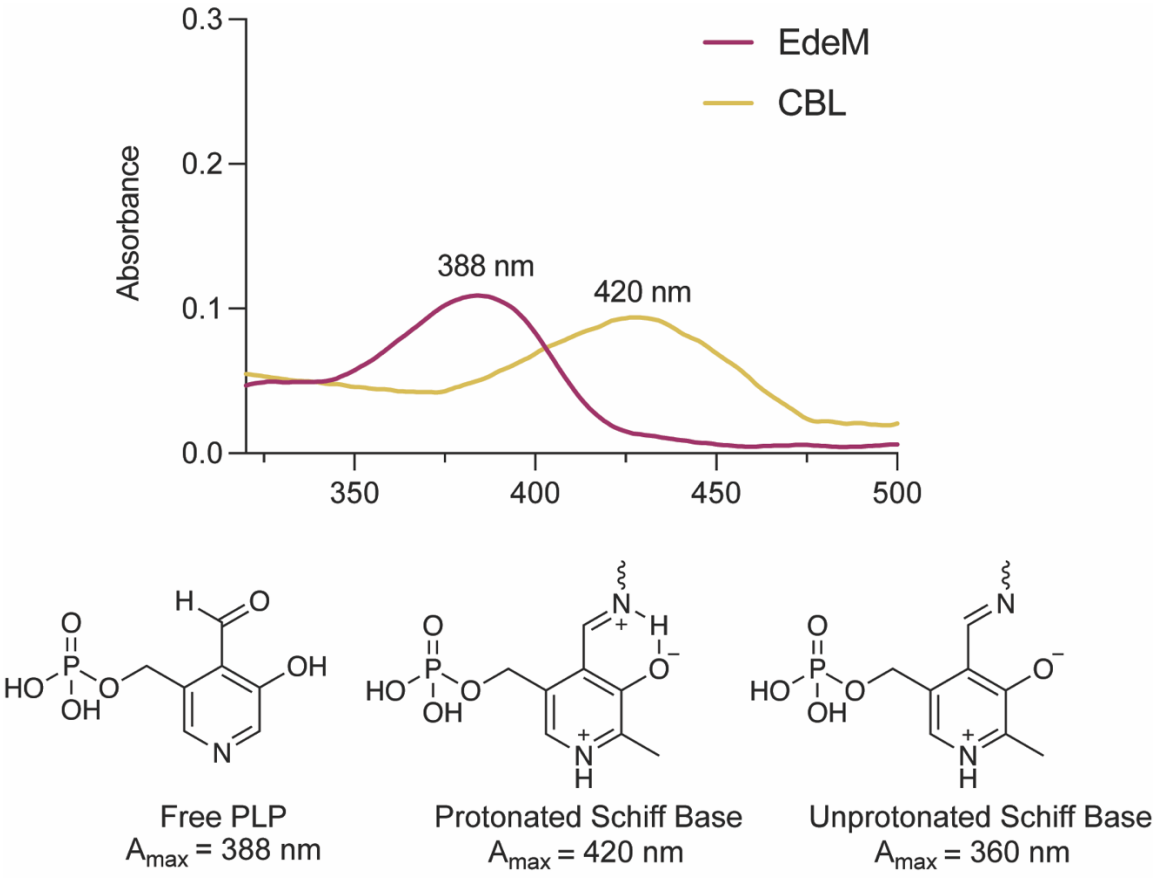

SUPPLEMENTAL FIGURE 30. UV-Vis spectra of EdeM. In PLP-DE, the Schiff base of internal aldimines is conjugated with the PLP π system and has absorption maxima of 420-430 nm when protonated and 360 nm when unprotonated. UV absorbance at 420 nm is detected for the control PLP-DE, cystathionine β-lyase (CBL) (yellow), indicating the formation of protonated Schiff base. When purified, EdeM samples are colourless and have a UV-Vis spectrum with absorbance at 388 nm (maroon), which is indicative of free PLP.

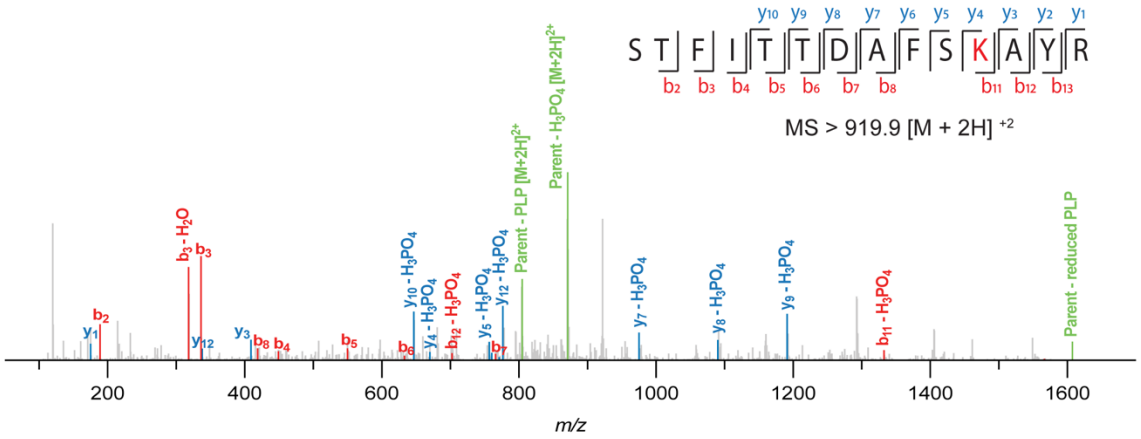

SUPPLEMENTAL FIGURE 31. EdeM Trypsin Digest. To identify the active site lysine residue in EdeM, a trypsin digest was performed on an enzyme sample reduced in the presence of $NaBH_3CN$. Bound PLP could only be detected for the peptide fragment STFITTDAFSKAYR, which contains K235, thereby suggesting that this is the active site lysine residue. Intact protein MS was repeated using a K235A EdeM mutant to verify this finding, and no internal aldimine formation could be detected (data not shown). These results demonstrate that EdeM is a PLP-DE and K235 is the active site lysine residue.

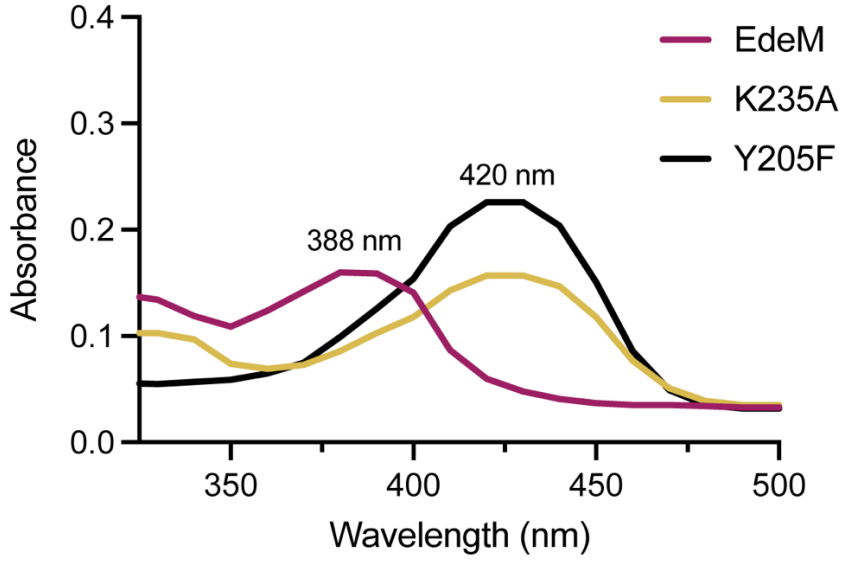

SUPPLEMENTAL FIGURE 32. UV-Vis spectra of EdeM, EdeM K235A, and EdeM Y205F. Wildtype EdeM has an absorbance of 388 nm, which is the same absorbance seen for free PLP. K235A and Y205F have absorbance at 420 nm, indicating the formation of a Schiff base.

CHAPTER 5: Discussion

Summary

At this moment, we find ourselves at a pivotal juncture in history. Our once formidable arsenal of antibiotics, the cornerstone of our battle against infectious bacterial diseases, is threatened. This dangerous situation could potentially plunge us into a post-antibiotic era, where the constraints of pre-modern medicine would once again reign. The urgency of this situation cannot be overstated.

This thesis explores various strategies to aid in prevailing in the arms race against bacteria. First, we must thoroughly understand how bacteria resist antibiotics by fully grasping all known resistance mechanisms. This knowledge prepares us to anticipate and respond to resistance as it emerges in clinical settings. Additionally, it is crucial to continually search for new, previously unidentified resistance mechanisms to stay ahead of emerging threats. **Chapter 2** of this thesis focuses on these efforts, specifically through my research on ciprofloxacin-inactivating enzymes and the investigation of CrpP's efficacy, enhancing our comprehension of the threats to the fluoroquinolone class of antibiotics.

Complementing the understanding of existing resistance mechanisms, leveraging nature's blueprint for bacterial resistance is crucial for discovering novel antibiotics to mitigate the threat of antibiotic resistance. **Chapter 3** discusses this approach using the Antibiotic Resistance Platform (ARP), a library of resistance genes expressed in *E. coli*. This platform streamlines the antibiotic dereplication process, making drug discovery more accessible and reducing the time and financial costs. By lowering these initial barriers to entry, more researchers can participate in the search for new antibiotics, thus bolstering our efforts in the ongoing arms race against bacteria.

Lastly, **Chapter 4** highlights the significance of understanding antibiotic biosynthesis to enhance our grasp of bacterial drug development strategies. This knowledge can be applied through synthetic biology to develop novel antibiotics or optimize existing natural product antibiotics. By investigating the mechanism of EdeM β-serine biosynthesis for edeine, we pave the way for creating optimized edeine analogues that can be produced biosynthetically. This research also opens possibilities for using EdeM in future synthetic biology applications to develop new natural products. These products would not only feature increased structural diversity with β-amino acids but also show decreased susceptibility to proteases.

Ciprofloxacin-Inactivating Enzymes

Although the research presented in this thesis indicates that discovering a novel ciprofloxacin-inactivating enzyme is difficult, it is crucial to recognize that it is not impossible. As highlighted in the introduction, one of the key differences between natural product antibiotics and synthetic ones, aside from their origins, is their duration of existence. Over time, as bacteria are exposed to synthetic antibiotics like ciprofloxacin for extended periods, the likelihood of a housekeeping protein evolving to inactivate ciprofloxacin increases. While AAC(6')-Ib-cr did not specifically evolve to inactivate ciprofloxacin, its adaptation demonstrates bacteria's capacity to adjust to their environments (Robicsek et al. 2006). Given enough time, it is probable that enzymes capable of inactivating ciprofloxacin will emerge.

This likelihood is heightened by the environmental presence of ciprofloxacin, notably in wastewater and river water, where it persists due to its stability (Giebułtowicz et al. 2020; Turiel et al. 2004). Studies have shown that ciprofloxacin and other fluoroquinolones remain stable in these conditions, with water samples at ambient temperature stable for at least two weeks and significantly longer at lower temperatures (Turiel et al. 2004). Moreover, the current resistance mechanisms to ciprofloxacin do not include any enzymes that inactivate the drug, allowing it to remain intact in the environment and providing more opportunities for bacteria to develop resistance through evolutionary pressure. Therefore, the search for ciprofloxacin-inactivating enzymes should continue.

Additionally, fluoroquinolones share structural similarities with quinoline and its congeners, which are present in various bioactive natural products, including anticancer agents like Lophocereine from *Lophocereus schotti* and Lavendamycin from *Streptomyces levendulae* (**Figure 1**) (Jain et al. 2019). Given the natural biosynthesis of quinoline scaffolds, it is plausible that enzymes capable of inactivating quinoline-based antibiotics already exist, and these might be adapted to target fluoroquinolones.

One strategy to potentially curb the development of ciprofloxacin-inactivating enzymes is bioremediation. This method uses living microorganisms, such as bacteria, to remove contaminants and toxins from environments like soil and water. By clearing highly stable synthetic antibiotics from these settings, we can diminish the selective pressure exerted on bacteria. Although there have been no studies on the effectiveness of the strain CI36, discussed in **Chapter 2**, in the bioremediation of ciprofloxacin, employing a bacterial strain

that can remove ciprofloxacin from its environment could be an effective way to reduce the presence of these drugs in natural settings.

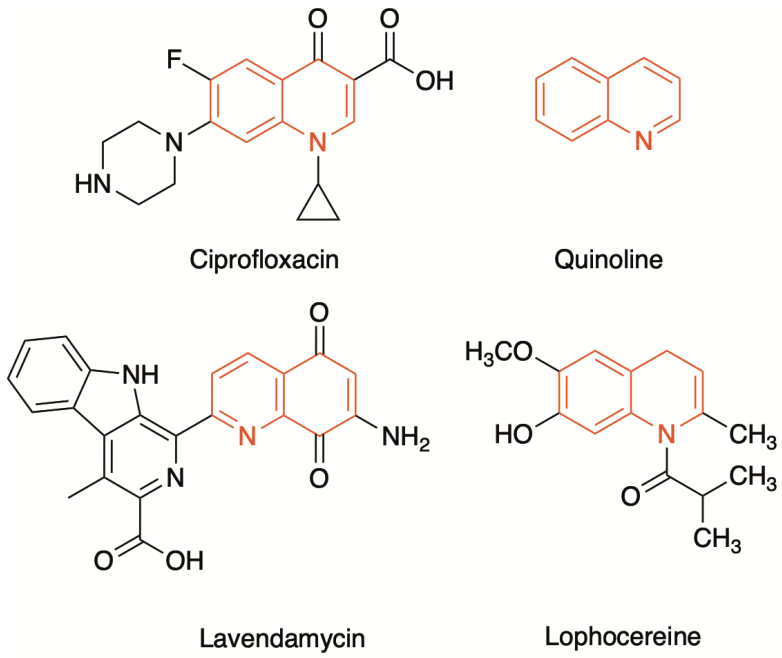

Figure 1. Ciprofloxacin shares structural similarities with quinoline and its congeners, including Lavendamycin and Lophocereine. Quinoline-like scaffolds are highlighted in red.

Antibiotic Dereplication for Natural Product Discovery

A key takeaway from this chapter is that success in drug discovery does not necessarily require the most expensive or high-tech equipment. Often, the most effective methods are accessible, affordable, and straightforward. The Antibiotic Resistance Platform (ARP) exemplifies this principle in the context of antibiotic dereplication for natural product drug discovery. Designed to be a "living document," the ARP is

continuously updated and refined to keep pace with the latest scientific developments in studying antibiotic resistance.

The ongoing improvement of the ARP is crucial. The development of the minimal ARP, for example, aimed to eliminate redundancy and simplify the platform's use. By making the minimal ARP available through Addgene and the *Journal of Visualized Experiments*, we have enhanced its accessibility, though, in the Wright lab, our efforts towards further enhancement continue.

As discussed in **Chapter 3**, the ARP does face certain limitations. Notably, bacteria that produce natural products often generate multiple compounds simultaneously. The complexity of these mixtures can make it challenging to use the ARP effectively when applied directly to media containing secondary metabolites from these organisms. Each strain of *E. coli* in the ARP expresses only one resistance gene, which can be problematic if multiple known antibiotics are present simultaneously.

Several strategies are proposed to address the challenges of detecting antimicrobial activity in the presence of multiple antibiotics. One approach is the use of agar plug assays, as detailed in the discussion section of **Chapter 3**. Another method is prefractionation, which involves dividing crude extracts into several fractions prior to primary screening. This technique isolates compounds that might interfere with each other during the dereplication process using the ARP. Separating these compounds allows each fraction to be independently tested against the ARP using methods like the Kirby Bauer disk diffusion assays. This approach enhances the detection of antimicrobial activity against each strain

in the minimal ARP, potentially yielding positive dereplication IDs for multiple natural products once they are separated from their original mixtures.

Additionally, a viable solution for managing the presence of multiple antibiotics involves developing *E. coli* strains that harbour a combination of resistance genes active against the most common antibiotics. Creating a library of *E. coli* strains with varied gene combinations allows for crude extract activity to be compared against these strains, enabling the deduction of which combinations of natural products are present in an extract.

Another challenge associated with the current overlay method of antibiotic dereplication using the ARP is the risk of contamination. As discussed in **Chapter 3**, working with a library of *E. coli* strains alongside an antibiotic-producing organism over a six-day incubation period presents numerous opportunities for contamination. To mitigate this, members of the Wright lab are exploring an innovative approach involving *E. coli* strains transformed with plasmids expressing different fluorescent proteins, pooled according to various markers. This technique aims to streamline dereplication in liquid media using natural product extracts rather than the producing organism itself, reducing the potential for contamination.

In this revised method, when the various pools of *E. coli* are exposed to natural product extracts, only the strains expressing the appropriate resistance gene will proliferate, emitting a strong fluorescent signal. In contrast, non-resistant strains will not grow. Dereplication is then assessed by correlating each pool's most intense fluorescent signals to the corresponding resistant *E. coli* strain, thus identifying the specific antibiotic being produced. This approach circumvents the issues related to slow-growing, sporulating

bacteria and reduces the common contamination problems associated with the ARP, such as the MHB agar overlay contamination.

Moreover, by employing fluorescently labelled *E. coli* strains grouped by specific markers, we can further mitigate the risk of cross-contamination on the ARP pinning plate. Ultimately, this work underscores the importance of continually re-evaluating scientific methods and striving for improvement. To effectively combat antibiotic resistance, we must persistently reassess our approaches and ensure we leverage the most suitable modern technologies available.

Elucidating the Mechanism of β-serine Biosynthesis in Edeine

The study of edeine in the Wright lab has been a multigenerational endeavour initiated in 1994. Investigating the biosynthesis of β-serine in edeine has uncovered significant insights into the previously unknown biosynthetic pathways of this β-amino acid, the complexities of PLP-dependent enzyme chemistry, and the enigmatic process of edeine synthesis.

While **Chapter 4** highlights numerous advancements in understanding β-serine biosynthesis, several mysteries remain to be explored. A primary focus should be on elucidating the molecular mechanism of β-serine biosynthesis by EdeM. The capability of an enzyme to catalyze the intramolecular transfer of a carboxyl group is highly novel, offering rich insights into PLP-dependent enzymes—a family previously thought to be well understood. Future studies should investigate the prevalence of EdeM homologs or similar proteins, potentially illuminating other unknown enzyme mechanisms.

More research is needed to understand the entire interaction between EdeM and its PLP cofactor. Several peculiarities require clarification, such as why EdeM is colourless when purified, why PLP does not seem to form a Schiff base in the active site with EdeM, and why mutations in essential PLP-interacting residues cause EdeM mutants to turn yellow and display UV absorbance at 420 nm, indicative of a Schiff base formation. Understanding this interaction could provide crucial insights into the enzyme's mechanism. To further complete the narrative, identifying the enzyme responsible for the epimerization of D-β-serine to L-β-serine before its incorporation into edeine is essential. While this component may not be critical for understanding the mechanisms of EdeM and D-β-serine biosynthesis, it is pivotal in elucidating the edeine biosynthetic pathway and possibly explaining why *B. brevis* utilizes EdeM over an enzyme that converts L-serine to L-β-serine.

Finally, a comprehensive understanding of edeine biosynthesis requires elucidating how the DAHAA building block of edeine is produced. With the EdeM pathway nearly completed, DAHAA remains the only component of this peptide antibiotic without a known biosynthetic route. Once assembled, the entire biosynthetic pathway of edeine should be validated to confirm that each gene involved is accurately characterized. This thorough understanding could lead to developing non-toxic edeine analogues via synthetic biology and applying individual biosynthesis enzymes to develop novel antibiotics.

Concluding Remarks

This thesis integrates three critical aspects of natural product drug discovery: understanding antibiotic resistance mechanisms, dereplicating known antibiotics to facilitate drug discovery, and exploring natural product biosynthesis for drug development. By tackling the challenges within these areas, we enhance our potential to prevail in the arms race against antibiotic-resistant bacteria.

In concluding this work, I want to share lessons learned from each chapter beyond the scientific insights gained. **Chapter 2** taught me the importance of every research story, even those that may seem minor. Completing a narrative that involved publishing primarily negative data underscored the high burden of proof required for making robust scientific claims. This experience also highlighted the crucial role of safeguarding primary literature in science, as our entire platform as researchers rests on the foundation of peer-reviewed work.

My work with the Antibiotic Resistance Platform (ARP) proved extremely rewarding. **Chapter 3** showed me that not all scientific success stems directly from publishing papers. While my article in the *Journal of Visualized Experiments* (JoVE) has reached academic institutions worldwide, developing the minimal ARP and depositing this collection of strains into Addgene has been equally impactful, further facilitating global research.

Lastly, the study of EdeM and edeine biosynthesis in **Chapter 4** has taught me that significant discoveries often come in small packages. Initially perceived as a straightforward project, the complexity of EdeM's mechanisms unfolded gradually,

revealing deeper and more intricate layers of knowledge. This experience resonates with Uri Alon's TED talk (https://youtu.be/F1U26PLiXjM?si=5sfKUhLmI3KtEVsT), "Why truly innovative science demands a leap into the unknown," where he describes the concept of "The Cloud." In this metaphor, "A" represents the questions, "B" the answers, and "C," the cloud, is where unexpected solutions are discovered. This project frequently led me into this cloud, highlighting the value of venturing into the unknown. Pursuing questions without known answers and devising seemingly impossible solutions, such as those involving an intramolecular transcarboxylase, are essential. These leaps into the unknown are crucial for advancing our understanding of the world.

REFERENCES

Giebułtowicz, Joanna, Grzegorz Nałęcz-Jawecki, Monika Harnisz, Dawid Kucharski, Ewa Korzeniewska, and Grażyna Płaza. 2020. "Environmental Risk and Risk of Resistance Selection Due to Antimicrobials' Occurrence in Two Polish Wastewater Treatment Plants and Receiving Surface Water." *Molecules* 25 (6). https://doi.org/10.3390/molecules25061470.

Jain, Shweta, Vikash Chandra, Pankaj Kumar Jain, Kamla Pathak, Devendra Pathak, and Ankur Vaidya. 2019. "Comprehensive Review on Current Developments of Quinoline-Based Anticancer Agents." *Arabian Journal of Chemistry* 12 (8): 4920–46.

Robicsek, Ari, Jacob Strahilevitz, George A. Jacoby, Mark Macielag, Darren Abbanat, Chi Hye Park, Karen Bush, and David C. Hooper. 2006. "Fluoroquinolone-Modifying Enzyme: A New Adaptation of a Common Aminoglycoside Acetyltransferase." *Nature Medicine* 12 (1): 83–88.

Turiel, Esther, Antonio Martín-Esteban, Guy Bordin, and Adela R. Rodríguez. 2004. "Stability of Fluoroquinolone Antibiotics in River Water Samples and in Octadecyl Silica Solid-Phase Extraction Cartridges." *Analytical and Bioanalytical Chemistry* 380 (1): 123–28.